

# **SYNTHESIS, STRUCTURE-ACTIVITY RELATIONSHIP AND SOLUBILITY PROFILING OF ANTIMYCOBACTERIAL AMINOQUINAZOLINONES**

Dissertation presented for the degree of Master of Science in  
the Department of Chemistry, University of Cape Town

by

**Jessica Nicole Akester**



**Supervisor: Prof. Kelly Chibale**

Department of Chemistry  
University of Cape Town  
Rondebosch, 7700  
South Africa

*March 2017*

The copyright of this thesis vests in the author. No quotation from it or information derived from it is to be published without full acknowledgement of the source. The thesis is to be used for private study or non-commercial research purposes only.

Published by the University of Cape Town (UCT) in terms of the non-exclusive license granted to UCT by the author.

## DECLARATION

---

I declare that *Synthesis, Structure-Activity Relationship and Solubility Profiling of Antimycobacterial Aminoquinazolinones* is my original work and has not been presented for the award of any degree at any university. I know the meaning of plagiarism and declare that all of the work in the dissertation, except for that which is properly acknowledged, is my own.

Signed by candidate

\_\_\_\_\_  
Signature Removed

Jessica N. Akester

March 2017

## ACKNOWLEDGEMENTS

---

First and foremost, I would like to sincerely thank Prof. Kelly Chibale for providing this opportunity and for his constant guidance, advice, encouragement and support throughout this journey. Thank you for expanding my knowledge and enhancing my abilities in medicinal chemistry and for being an incredible inspiration.

A special thank you goes to Paul Njaria for his time and patience in mentoring and teaching me the finer details of synthesis techniques and skills in writing and presentation. Most of all, thank you for setting an example of what dedication and diligence can accomplish. I also wish to thank Dr. Mathew Njoroge and John Okombo for providing advice, guidance and knowledge in terms of solubility assays and interpretation.

I would also like to thank Elaine Rutherford-Jones, Saroja Naicker and Deirdre Brooks for attending to administrative arrangements and always doing so with a smile. To Deidre Kruger, Duane Knowles and Eddy Kativu thank you for ensuring a good, working laboratory and for maintaining analytical equipment.

A huge thank you goes to Ronnett Seldon, Dale Taylor, Sergio Wittlin (STPH), Mathew Njoroge and Christel Brunschwig for the *in vitro* testing of my compounds. To Pete Roberts for assistance with spectroscopic NMR experiments. I would also like to thank Colorado State University and Helena Boschoff at NIAID for further *in vitro* testing of analogues in this project.

Many thanks to fellow members in Kelly Chibale's research group for the support, ideas, and creating an enjoyable working environment. Especially to my fellow Health and Safety representative and friend, Linley Barnard, for being by my side through this process, conquering all administrative and H&S duties together.

To my parents, Corinne and Steve Akester, and my sister Nadia, your unconditional love and support is unwavering. Finally, to my partner, Jaryd Raizon, thank you for continuously encouraging, supporting and motivating me to be the best that I can possibly be.

## CONFERENCES

---

### **International Conference on Pure and Applied Chemistry (ICPAC) 2016**

Hotel Sofitel Mauritius Impérial Resort And Spa, Flic en Flac, Mauritius

18 – 22 July 2016

Attended the ICPAC 2016 conference whereby I participated in MMV-UCT-MRC's drug discovery workshop on *“Assay Development to Candidate Drug: How to progress small molecule hits from screening efforts.”*

### **H3D Symposium 2016**

Goudini Spa, Western Cape, South Africa

15 – 18 November 2016

Attended the 2016 H3D symposium whereby I presented a poster on *Synthesis, Structure-Activity Relationship and Solubility Profiling of Antimycobacterial Aminoquinazolinones.*

## ABSTRACT

---

Tuberculosis (TB) is a communicable disease caused by an infectious bacterial pathogen called *Mycobacterium tuberculosis* (*Mtb*), which is acquired through the inhalation of bacilli-containing droplets. With the emergence of resistant strains (multidrug-resistant TB (MDR-TB), extensively drug-resistant TB (XDR-TB) and totally drug-resistant TB (TDR-TB)), co-infection with human immunodeficiency virus (HIV), the existence of latent TB infection (LTBI) and the extensive treatment regimen resulting in poor patient compliance, there is therefore a need to develop novel antimycobacterial agents to address these limitations. Within this context, 2-aminoquinazolinone compounds with potent antimycobacterial activity were previously identified. Poor solubility was recognized as a major issue requiring improvement. To this end, structure-activity relationship (SAR) studies were performed around the 2-aminoquinazolinone core in order to optimize these potential antimycobacterial agents with respect to solubility and potency. Various structural modification strategies aimed at improving solubility were explored. These included reducing lipophilicity by introduction of hydrophilic substituents as well as disruption of molecular planarity and/or symmetry of the molecule through removal of aromaticity or increase in the dihedral angle.

Several analogues displayed promising *in vitro* antimycobacterial activity against the H37Rv strain of *Mtb* in glycerol-containing media along with high microsomal metabolic stability. However, the same compounds, with the exception of one phenolic intermediate, were inactive in subsequent assay media that did not contain glycerol as a carbon source. On this basis, the mechanism of action of the 2-aminoquinazolinone series was postulated to be glycerol-dependent. On the other hand, structural modifications, guided by solubility-enhancing strategies, generally resulted in compounds with markedly improved solubility. Saturated ring analogues displayed the most improvement in solubility, which was also reflected in the lower melting points. Additionally, the relationships between solubility and physicochemical parameters (ClogP, tPSA and melting point) were deduced. Melting point was found to be the most strongly correlated with aqueous solubility.

## TABLE OF CONTENTS

---

<i>Declaration</i> .....	<i>ii</i>
<i>Acknowledgements</i> .....	<i>iii</i>
<i>Conferences</i> .....	<i>iv</i>
<i>Abstract</i> .....	<i>v</i>
<i>Table of Contents</i> .....	<i>vi</i>
<i>List of Abbreviations</i> .....	<i>ix</i>
<i>List of Figures</i> .....	<i>xii</i>
<i>List of Tables</i> .....	<i>xv</i>
<i>List of Schemes</i> .....	<i>xv</i>
<b>CHAPTER 1: INTRODUCTION AND LITERATURE REVIEW</b> .....	<b>1</b>
1.1. Tuberculosis .....	1
1.1.1. Epidemiology and Aetiology.....	1
1.1.2. Current Treatment .....	3
1.1.3. Advances in the Development of New Anti-TB Drugs.....	5
1.2. Properties of Drug Candidates in Drug Discovery .....	9
1.2.1. Solubility Improvement Strategies.....	10
1.3. Pharmacological Activity of Aminoquinazolinones .....	15
1.4. Aims and Objectives .....	18
1.4.1. Objective .....	18
1.4.2. Hypothesis.....	18
1.4.3. Specific Aims.....	18
<b>CHAPTER 2: DESIGN, SYNTHESIS AND PHARMACOLOGICAL EVALUATION OF 2-AMINOQUINAZOLINONE ANALOGUES</b> .....	<b>19</b>
2.1. Introduction.....	19
2.1.1. Background Information .....	19
2.2. Design and Rationale of 2-Aminoquinazolinone Derivatives .....	21
2.3. Synthesis and Spectroscopic Characterization of 2-Aminoquinazolinones .....	23
2.3.1. Synthesis of SAR 1 Target Compounds.....	23
2.3.2. Mechanistic Details and Spectroscopic Analyses of SAR 1 Intermediates and Target Compounds .....	25
2.3.3. Synthesis of SAR 2 Target Compounds.....	30

2.3.4.	Mechanistic Details and Spectroscopic Analyses of SAR 2 Intermediates and Target Compounds .....	33
2.4.	Pharmacological Evaluation of Target Compounds .....	38
2.4.1.	<i>In vitro</i> Antimycobacterial Activity and Cytotoxicity .....	39
2.4.2.	Microsomal Metabolic Stability .....	41
2.4.3.	Evaluation of Glycerol Dependency .....	43
2.4.3.1.	<i>Glycerol-Free in vitro Assays</i> .....	43
2.5.	Conclusions.....	45
<b>CHAPTER 3: SYNTHESIS AND PHARMACOLOGICAL EVALUATION OF ACTIVE AMINOQUINAZOLINONE INTERMEDIATE ANALOGUES .....</b>		<b>46</b>
3.1.	Background Information .....	46
3.2.	Target Aminoquinazolinone Intermediate Analogues .....	46
3.3.	Synthesis And Spectroscopic Characterization of Aminoquinazolinone Intermediates .....	47
3.3.1.	SAR 3 Target Compounds.....	47
3.3.2.	SAR 4 Target Compounds.....	51
3.3.3.	SAR 5 Target Compounds.....	52
3.4.	Pharmacological Evaluation Of Synthesized Compounds .....	57
3.4.1.	<i>In vitro</i> Antimycobacterial Activity.....	57
3.5.	Conclusions.....	60
<b>CHAPTER 4: SOLUBILITY STUDIES .....</b>		<b>61</b>
4.1.	Introduction.....	61
4.1.1.	Turbidimetric Solubility Assay.....	63
4.1.2.	HPLC-Based Solubility Assay.....	64
4.2.	Solubility Results .....	65
4.2.1.	SPR 1 Solubility Studies .....	67
4.2.2.	SPR 2 Solubility Studies .....	69
4.2.3.	SPR 3 – 5 Solubility Studies .....	70
4.3.	Physicochemical Properties.....	74
4.4.	Conclusions.....	77
<b>CHAPTER 5: SUMMARY AND FUTURE PROSPECTS .....</b>		<b>79</b>
5.1.	General Summary and Conclusions.....	79
5.2.	Future Outlook and Recommendations.....	82

<b>CHAPTER 6: EXPERIMENTAL RESULTS</b> .....	<b>83</b>
6.1. Materials and Equipment.....	83
6.2. Synthesis and Characterization .....	84
6.2.1. General Procedures and Characterization for SAR 1 Intermediate Compounds 1 – 4 ..	84
6.2.2. General Procedure for Suzuki-Miyaura Coupling Reaction in the Synthesis of the Target Compounds <b>5.1 – 5.11</b> .....	86
6.2.3. General Procedure for the Synthesis of Intermediates <b>6.1 – 6.3</b> .....	92
6.2.4. General Procedure for the Synthesis of Compounds <b>7.1 – 7.9</b> .....	94
6.2.5. General Procedure for the Synthesis of Compounds <b>8.1 – 8.4</b> .....	98
6.2.6. General Procedure for the Synthesis of Compounds <b>8.5 – 8.7</b> .....	100
6.2.7. General Procedure of Suzuki-Miyaura Coupling in the Synthesis of the Target Compounds <b>9.1 – 9.6</b> .....	102
6.2.8. General Procedure for the Synthesis of Compounds <b>12.3 – 12.4</b> .....	108
6.3. Biological Studies.....	109
6.3.1. <i>In vitro</i> Antimycobacterial Assay .....	109
6.3.1.1. <i>7H9 Media Preparation</i> .....	110
6.3.1.2. <i>ADC Enrichment Media Preparation</i> .....	110
6.3.1.3. <i>Casitone 7H9-Based Medium (BSA-Free) Preparation</i> .....	110
6.3.2. <i>In vitro</i> Cytotoxicity Assay .....	110
6.3.3. <i>In vitro</i> Antiplasmodial Assay .....	111
6.3.4. <i>In vitro</i> Metabolic Stability Studies .....	111
6.3.5. Kinetic Solubility Studies .....	112
<b>CHAPTER 7: REFERENCES</b> .....	<b>111</b>

## LIST OF ABBREVIATIONS

---

°C	Degrees Celsius
ADC	Albumin, dextrose and catalase
ADME	Absorption, Distribution, Metabolism and Excretion
AQQI	Amodiaquine quinoneimine
ART	Antiretroviral therapy
ATP	Adenosine triphosphate
AUC	Area under curve
BSA	Bovine serum albumin
CFU	Colony forming units
CHO	Chinese Hamster Ovarian
Cl	Clearance
ClogP	Calculated Log P
COSY	Correlation spectroscopy
CSU	Colorado State University
Da	Daltons
DCM	Dichloromethane
DFT	Density functional theory
DIPEA	<i>N,N</i> -Diisopropylethylamine
DMF	<i>N,N</i> -Dimethylformamide
DMPK	Drug metabolism and pharmacokinetics
DMSO	Dimethyl sulfoxide
DMSO- <i>d</i>	Deuterated dimethyl sulfoxide
DOTS	Directly Observed Therapy Short Course
DST	Drug-Susceptibility Testing
EDCI	<i>N</i> -(3-dimethylaminopropyl)- <i>N'</i> -ethylcarbodiimide
EMB	Ethambutol
Et <sub>2</sub> O	Diethyl ether
Et <sub>3</sub> N	Triethylamine
EtOAc	Ethyl acetate
F	Bioavailability

FDA	Food and Drug Administration
EMA	European Medicines Agency
GAST Fe	Glycerol-alanine-salts with Tween-80 and Iron
GSH	Glutathione
HBA	Hydrogen-bond acceptor
HBD	Hydrogen-bond donor
HCl	Hydrochloric acid
HCV	Hepatitis C Virus
HIV	Human immunodeficiency virus
HLM	Human liver microsomes
HPLC	High Performance Liquid Chromatography
HSQC	Heteronuclear single quantum correlation
ESI	Electron Spray Ionization
IC <sub>50</sub>	Half-maximal inhibitory concentration
INH	Isoniazid
LCMS	Liquid chromatography mass spectrometry
LHS	Left-hand side
LTBI	Latent TB infection
LXR	Liver X Receptors
<i>m/z</i>	Mass-to-charge ratio
MDR-TB	Multidrug-resistant TB
MeOH	Methanol
MHz	Megahertz
MIC	Minimum inhibitory concentration
MLM	Mouse liver microsomes
MP	Melting point
MS	Mass spectrometry
<i>Mtb</i>	<i>Mycobacterium tuberculosis</i>
MTT	3-(4,5-dimethylthiazol-2-yl)-2,5- diphenyltetrazoliumbromide
MW	Microwave
MW	Molecular weight
NaHCO <sub>3</sub>	Sodium bicarbonate

ND	Not determined
NIAID	National Institute of Allergy and Infectious Diseases
NITD	Novartis Institute of Tropical Diseases
NMR	Nuclear Magnetic Resonance
NOESY	nuclear Overhauser effect spectroscopy
NR- <i>Mtb</i>	Non-replicating <i>Mtb</i>
PBS	Phosphate buffered saline
PCl <sub>5</sub>	Phosphorous pentachloride
PdCl <sub>2</sub> (PPh <sub>3</sub> ) <sub>2</sub>	Bis(triphenylphosphine)palladium(II) dichloride
PK	Pharmacokinetics
POCl <sub>3</sub>	Phosphorous (V) oxychloride
PSA	Polar surface area
PZA	Pyrazinamide
RHS	Right-hand side
RIF	Rifampicin
RLM	Rat liver microsomes
RO5	Rule of 5
SAR	Structure-activity relationship
S <sub>N</sub> Ar	Nucleophilic aromatic substitution
TB	Tuberculosis
TDR-TB	Totally drug-resistant TB
TFA	Trifluoroacetic acid
TLC	Thin layer chromatography
tPSA	Topological polar surface area
WHO	World Health Organization
XDR-TB	Extensively drug-resistant TB
δ	Delta (NMR chemical shift)
μM	Micromolar

## LIST OF FIGURES

---

<b>Figure 1:</b> Pictorial diagram representing the annual number of incident TB cases relative to population size (incidence rate) for 2015 .....	1
<b>Figure 2:</b> Pictorial diagram representing the proportion of TB cases coinfecting with HIV .....	2
<b>Figure 3:</b> Chemical structures of first-line anti-TB drugs .....	3
<b>Figure 4:</b> Chemical structures of second-line anti-TB drugs .....	4
<b>Figure 5:</b> Summary of current TB drug treatment regime indicating first-line and second-line drugs .....	4
<b>Figure 6:</b> Chemical structures of various repurposed drugs for the use in TB treatment .....	6
<b>Figure 7:</b> Chemical structures of new, potential anti-TB drugs that are currently in clinical trials .....	7
<b>Figure 8:</b> Global TB drug pipeline summarizing current clinical trial candidates.....	8
<b>Figure 9:</b> Examples of structures incorporating ionizable groups to improve solubility .....	11
<b>Figure 10:</b> Craig plot showing electronic ( $\sigma$ ) and hydrophilic ( $\pi$ ) properties of specific substituents .....	11
<b>Figure 11:</b> Examples of introducing various H-bonding groups to improve solubility of lead compound <b>A</b> .....	12
<b>Figure 12:</b> Example of removal of aromaticity to enhance solubility of a TRPV1 antagonist.....	13
<b>Figure 13:</b> Examples of polychlorinated biphenyls to show the effect of dihedral angles on solubility ...	14
<b>Figure 14:</b> Examples of some quinazolinone scaffolds with various therapeutic effects. ....	15
<b>Figure 15:</b> Representative 2-aminoquinazolin-4(3 <i>H</i> )-one derivatives with therapeutic effects .....	16
<b>Figure 16:</b> Quinazolinone analogues that have shown to possess antimycobacterial activity effects.....	17
<b>Figure 17:</b> General structure of the 2-aminoquinazolinone core scaffold.....	19
<b>Figure 18:</b> Chemical structure, biological activity and solubility data for the hit aminoquinazolinone compound <b>5.1</b> .....	20
<b>Figure 19:</b> Chemical structure, biological activity and solubility data for the sulfoxide- containing aminoquinazolinone compound <b>5.2</b> .....	20
<b>Figure 20:</b> Chemistry design for planning the synthesis of aminoquinazolinone derivatives with two points of diversity, <b>Ar</b> and <b>R<sub>1</sub></b> , around the core incorporating various solubility improvement strategies .....	21
<b>Figure 21:</b> Proposed reaction mechanism for the formation of quinazolinone intermediate <b>1</b> .....	25
<b>Figure 22:</b> Assigned <sup>1</sup> H NMR spectrum confirming the successful synthesis of intermediate <b>1</b> .....	26
<b>Figure 23:</b> Proposed reaction mechanism for the chlorination reaction using POCl <sub>3</sub> (right) and PCl <sub>5</sub> (left).....	26
<b>Figure 24:</b> <sup>1</sup> H NMR spectrum of chlorinated intermediate <b>2</b> .....	27
<b>Figure 25:</b> Proposed mechanism for the S <sub>N</sub> AR reaction in the formation of intermediate <b>3</b> .....	27
<b>Figure 26:</b> <sup>1</sup> H NMR spectrum for the methoxybenzylamine intermediate <b>3</b> .....	28

<b>Figure 27:</b> Proposed mechanism for the deprotection reaction using TFA. ....	<b>28</b>
<b>Figure 28:</b> <sup>1</sup> H NMR spectrum for deprotected intermediate <b>4</b> .....	<b>29</b>
<b>Figure 29:</b> <sup>1</sup> H NMR spectrum of final target compounds, using <b>5.1</b> as an illustrative example .....	<b>30</b>
<b>Figure 30:</b> Proposed mechanism for step ii, amide coupling and intramolecular cyclization reaction .....	<b>33</b>
<b>Figure 31:</b> Proposed mechanism for the hydrolysis of the carbamate moiety in the formation of the 2- aminoquinazolinone intermediates ( <b>8.1 – 8.4</b> ) .....	<b>34</b>
<b>Figure 32:</b> <sup>1</sup> H NMR spectrum of <b>SAR 2</b> compounds, using intermediate <b>8.1</b> as an illustrative example...	<b>35</b>
<b>Figure 33:</b> <i>Cis-trans</i> isomerism of 1,4-disubstituted cyclohexanes upon chair interconversion at equilibrium showing relative stereochemistry of substituents .....	<b>35</b>
<b>Figure 34:</b> Chair conformation of the favoured <i>trans</i> isomer with substituents in equatorial position showing coupling interactions of the axial protons (red) and equatorial protons (blue) .....	<b>36</b>
<b>Figure 35:</b> Extract from NOESY experiment of <b>8.1</b> to establish relative through-space interactions of the substituted protons to determine their <i>cis</i> or <i>trans</i> relationship .....	<b>37</b>
<b>Figure 36:</b> Screening cascade outlining the criteria for progression of work-flow from synthesis to <i>in vivo</i> efficacy studies .....	<b>38</b>
<b>Figure 37:</b> General structure of <b>SAR 1</b> analogues with varying <b>Ar</b> substituents.....	<b>44</b>
<b>Figure 38:</b> General structures of intermediates <b>7 – 8</b> and target compounds <b>9.1 – 9.5</b> that were evaluated for <i>in vitro</i> antimycobacterial activity in glycerol-free media .....	<b>44</b>
<b>Figure 39:</b> Chemistry design for planning the synthesis of quinazolinone analogues derived from <b>7.7</b> with three points of diversity around the core .....	<b>47</b>
<b>Figure 40:</b> <sup>1</sup> H NMR spectrum of new hit compound <b>7.7</b> .....	<b>49</b>
<b>Figure 41:</b> <sup>1</sup> H NMR spectrum of saturated phenol derivative <b>7.2</b> .....	<b>50</b>
<b>Figure 42:</b> <sup>1</sup> H NMR spectrum of saturated <b>SAR 3</b> analogue <b>7.3</b> .....	<b>51</b>
<b>Figure 43:</b> Stacked <sup>1</sup> H NMR spectra of <b>SAR 4</b> intermediates, <b>6.2</b> (2) and <b>6.3</b> (3), indicating key structural changes to the quinazolinone core in comparison to <b>6.1</b> (1).....	<b>52</b>
<b>Figure 44:</b> Stacked <sup>1</sup> H NMR spectra of <b>SAR 5</b> compounds, <b>12.1</b> (2) and <b>12.2</b> (3) indicating key changes in comparison to <b>7.7</b> (1) .....	<b>54</b>
<b>Figure 45:</b> Proposed dehydration/dehydrogenation reaction mechanism for the formation of arylquinazolinone derivatives <b>12.3</b> and <b>12.4</b> .....	<b>55</b>
<b>Figure 46:</b> <sup>1</sup> H NMR spectrum of arylquinazolinone analogues, using <b>12.4</b> as an illustrative example .....	<b>56</b>
<b>Figure 47:</b> Mechanism by which amodiaquine undergoes metabolism to form a reactive metabolite, which under high doses, can result in toxicity effects .....	<b>59</b>
<b>Figure 48:</b> Proposed mechanism by which analogue <b>7.7</b> undergoes metabolic oxidation to a toxic fragment resulting in apparent antimycobacterial growth inhibition .....	<b>60</b>
<b>Figure 49:</b> General outline of <b>SPR 1 – 5</b> structures used in the following solubility studies .....	<b>62</b>

<b>Figure 50:</b> Absorbance versus concentration curve of the highly soluble control, hydrocortisone.....	<b>64</b>
<b>Figure 51:</b> Absorbance versus concentration curve of the insoluble control, reserpine.....	<b>64</b>
<b>Figure 52:</b> Graph comparing solubility results using the turbidimetric assay (low range values shown) and the HPLC-based assay (pH 7.4) across all compounds in the series.....	<b>65</b>
<b>Figure 53:</b> Computational models of <b>5.1</b> and <b>11</b> indicating calculated dihedral angles (centre) with 90° angle views (right) using Maestro .....	<b>68</b>
<b>Figure 54:</b> Computational models of <b>SAR 3</b> analogues showing the calculated dihedral angle between the phenol moiety and the quinazolinone core.....	<b>73</b>
<b>Figure 55:</b> Relationship between solubility and ClogP data of <b>SAR 1 – 5</b> .....	<b>74</b>
<b>Figure 56:</b> Relationship between solubility and tPSA data of <b>SAR 1 – 5</b> .....	<b>75</b>
<b>Figure 57:</b> Relationship between solubility and melting point data of <b>SAR 1 – 5</b> .....	<b>76</b>
<b>Figure 58:</b> Summary of aqueous solubility trends observed for <b>SPR 1</b> and <b>SPR 2</b> series' based on values obtained using the HPLC-method .....	<b>77</b>
<b>Figure 59:</b> Summary of aqueous solubility trends observed for <b>SPR 3 – 5</b> based on values obtained using the HPLC-method .....	<b>78</b>
<b>Figure 60:</b> Summary of antimycobacterial activity trends observed for <b>SAR 1</b> derivatives in GAST Fe media.....	<b>79</b>
<b>Figure 61:</b> General structure of inactive <b>SAR 1</b> and <b>SAR 2</b> derivatives tested in glycerol-free media.....	<b>80</b>
<b>Figure 62:</b> Summary of antimycobacterial SAR 3 – 5 results tested in glycerol-free media displaying inactivity, except for compound <b>7.7</b> .....	<b>80</b>
<b>Figure 63:</b> Solubility results of <i>ortho</i> -substituted analogue <b>11</b> compared to frontrunner compound <b>5.1</b> .....	<b>81</b>
<b>Figure 64:</b> Structures of highly soluble <b>SPR 2</b> analogues incorporating saturated ring substituents.....	<b>81</b>
<b>Figure 65:</b> Structure of <i>ortho</i> -phenol analogue displaying high solubility compared to <b>7.7</b> owing to disruption of molecular symmetry.....	<b>82</b>

## LIST OF TABLES

---

<b>Table 1:</b> Isolated percentage yields for <b>SAR 1</b> target compounds <b>5.1 – 5.11</b> .....	<b>24</b>
<b>Table 2:</b> Isolated percentage yields for <b>SAR 2</b> intermediates and target compounds. ....	<b>32</b>
<b>Table 3:</b> Pharmacological activity and cytotoxicity of <b>SAR 1</b> compounds .....	<b>39</b>
<b>Table 4:</b> Microsomal metabolic stability results of selected <b>SAR 1</b> compounds, reported as percentage of concentration remaining.....	<b>41</b>
<b>Table 5:</b> <i>In vitro</i> MIC results for compound <b>5.2</b> from CSU using glycerol-containing and glycerol-free media with different strains, Erdman and H37Rv.....	<b>43</b>
<b>Table 6:</b> <i>In vitro</i> antimycobacterial activity results for intermediate <b>7.7</b> against <i>Mtb</i> (H37Rv) in a variety of media .....	<b>46</b>
<b>Table 7:</b> Isolated percentage yields for <b>SAR 3</b> target compounds.....	<b>48</b>
<b>Table 8:</b> <i>In vitro</i> antimycobacterial activity results for <b>SAR 3 - 5</b> against <i>Mtb</i> (H37Rv) in glycerol-free media .....	<b>57</b>
<b>Table 9:</b> Apparent aqueous solubility results and physicochemical parameters for <b>SPR 1</b> target compounds .....	<b>67</b>
<b>Table 10:</b> Apparent aqueous solubility results and physicochemical parameters for <b>SPR 2</b> target compounds .....	<b>69</b>
<b>Table 11:</b> Apparent aqueous solubility results and physicochemical parameters for aminoquinazolinone intermediates <b>SPR 3 – SPR 5</b> .....	<b>71</b>

## LIST OF SCHEMES

---

<b>Scheme 1:</b> General synthetic protocol towards <b>SAR 1</b> target compounds <b>5.1 – 5.11</b> .....	<b>23</b>
<b>Scheme 2:</b> General synthetic protocol towards target compounds for <b>SAR 2</b> .....	<b>31</b>
<b>Scheme 3:</b> General synthetic protocol towards <b>SAR 3</b> compounds <b>7.1 – 7.4</b> and <b>7.7</b> .....	<b>48</b>
<b>Scheme 4:</b> General synthetic protocol towards <b>SAR 4</b> compounds <b>7.8</b> and <b>7.9</b> .....	<b>51</b>
<b>Scheme 5:</b> General synthetic protocol towards <b>SAR 5</b> compounds <b>12.1</b> and <b>12.2</b> .....	<b>53</b>
<b>Scheme 6:</b> General synthetic protocol towards <b>SAR 5</b> compounds <b>12.3</b> and <b>12.4</b> .....	<b>54</b>

## CHAPTER 1: INTRODUCTION AND LITERATURE REVIEW

### 1.1. TUBERCULOSIS

#### 1.1.1. EPIDEMIOLOGY AND AETIOLOGY

Tuberculosis (TB) is a communicable disease caused by an infectious bacterial pathogen called *Mycobacterium tuberculosis* (*Mtb*), which typically replicates in the lungs (pulmonary TB) but can affect other areas too (extrapulmonary TB).<sup>1</sup> According to the World Health Organization (WHO), 10.4 million people developed TB in 2015 (Figure 1) with 1.8 million deaths occurring worldwide making it the leading cause of death from a curable infectious disease. Six countries, India, Indonesia, China, Nigeria, Pakistan and South Africa accounted for 60% of new cases. TB has thus been recognized as one of three priority diseases for drug research and development.<sup>2</sup>

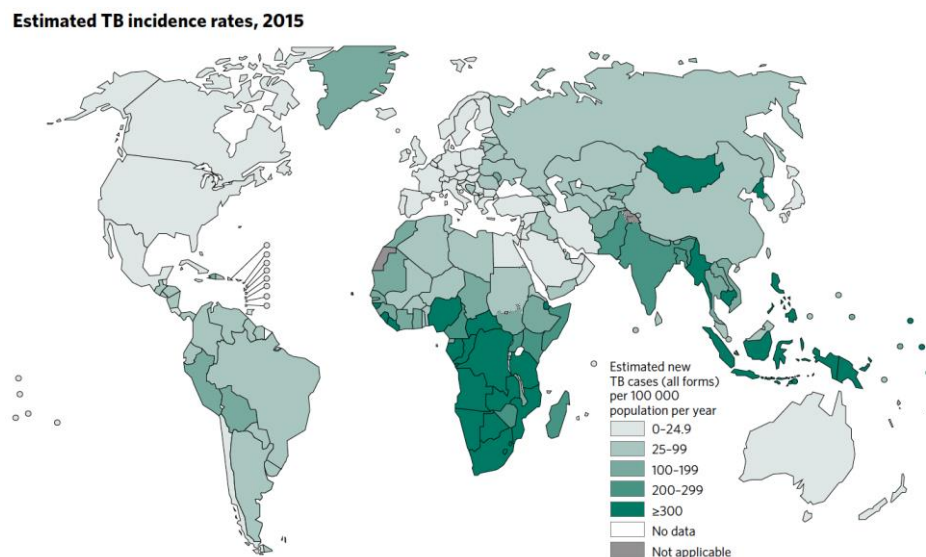


**Figure 1:** Pictorial diagram representing the annual number of incident TB cases relative to population size (incidence rate) for 2015.<sup>1</sup>

A variety of species of mycobacteria that are related to *Mtb*, which includes *M. bovis*, *M. tuberculosis*, *M. africanum*, *M. microti* and *M. canettii* are referred to as the mycobacterial complex.<sup>3</sup> Mycobacteria appear as slightly curved or straight rods that are 1 – 4  $\mu\text{m}$  in length and 0.3 – 0.6  $\mu\text{m}$  in width and are characterized as non-sporulating, non-motile, weakly gram-positive and acid-fast bacilli. The waxy cell wall of mycobacteria has many unique characteristics that enable survival in its host such as hydrophobicity, resistance to drying, acid-fastness against staining and resistance to varying acidic/alkaline environments.<sup>4</sup>

*Mtb* infection is acquired through the inhalation of bacilli-containing droplets, mainly from patients with active pulmonary TB, and develops as a consequence of failed immune regulation in the host. However, the majority of people infected with *Mtb* acquire it as an asymptomatic latent TB infection (LTBI). Approximately 2-3 billion people have LTBI and are therefore at risk of reactivation of the disease, with 10% of those progressing into active TB.<sup>5,6</sup> This can be prevented through effective treatment. The development of novel vaccines that may prevent TB disease reactivation by containing the pathogen in a latent state in LTBI persons is being investigated. About 13 of these vaccine candidates have entered clinical trials in the past few years.<sup>1</sup> A shortcoming of these vaccines is that they do not eradicate the pathogen but rather prevent or delay the reactivation of the dormant infection.<sup>3</sup>

The probability of developing TB is much higher among people infected with human immunodeficiency virus (HIV) whereby TB is the leading cause of morbidity and mortality among HIV-infected people. This could be attributed to the enhancement of the HIV replication process by the host’s immune response to *Mtb* and possibly leading to acceleration of the natural progression of the HIV infection. 1.2 Million people of the 10.4 million who developed TB in 2015 were HIV positive resulting in 400 000 deaths. The African region accounts for the highest proportion of HIV-positive TB cases (31%) and exceeds 50% in parts of Southern Africa (Figure 2), as a result of the TB epidemic being fuelled by the HIV epidemic in this region.<sup>2,7</sup>

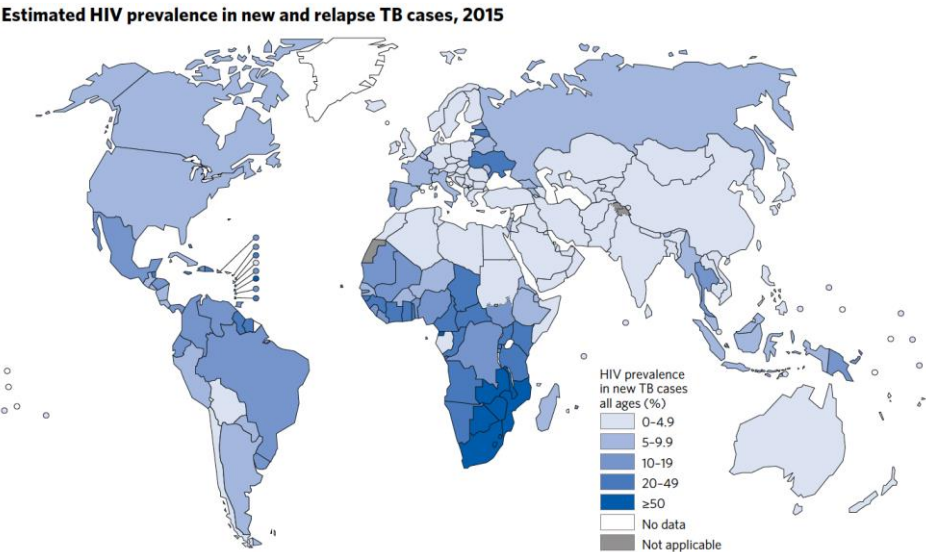


**Figure 2:** Pictorial diagram representing the proportion of TB cases coinfecting with HIV.<sup>1</sup>

### 1.1.2. CURRENT TREATMENT

The current anti-TB drugs can be divided into first-line drugs and second-line drugs. First-line drugs include isoniazid (INH), rifampicin (RIF), ethambutol (EMB), pyrazinamide (PZA) and streptomycin (Figure 3). Second-line drugs include injectables such as amikacin, kanamycin, capreomycin; ciprofloxacin and ofloxacin as fluoroquinolones; as well as ethionamide, cycloserine and *p*-aminosalicylic acid (Figure 4).<sup>3,8</sup>

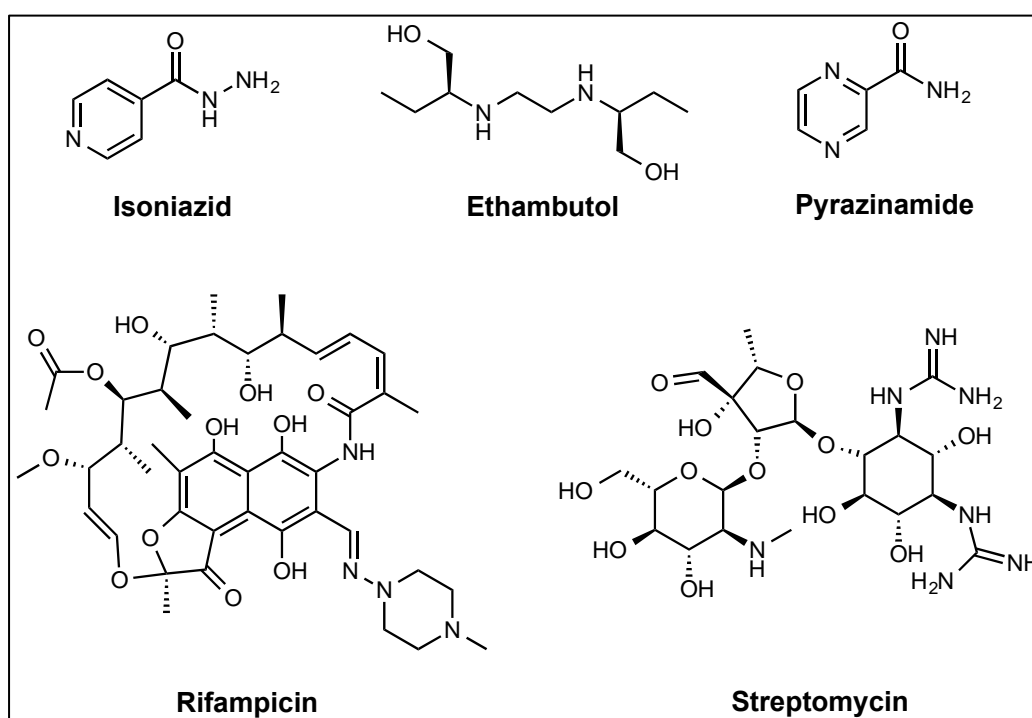


**Figure 3:** Chemical structures of first-line anti-TB drugs.

The current chemotherapy regime outlined in Figure 5 involves a 2 – 4 month intensive phase whereby the first-line drugs are administered followed by a continuation phase for 4 – 18 months with isoniazid and rifampicin in combination with some second-line drugs, should they be required.<sup>5,8</sup> The WHO recommended a TB control strategy involving Directly Observed Therapy Short Course (DOTS) wherein the above treatment regimen is directly observed by a healthcare worker for at least the first 2 months of treatment as this is the period when the emergence of drug resistance is at its greatest.<sup>7,3</sup>

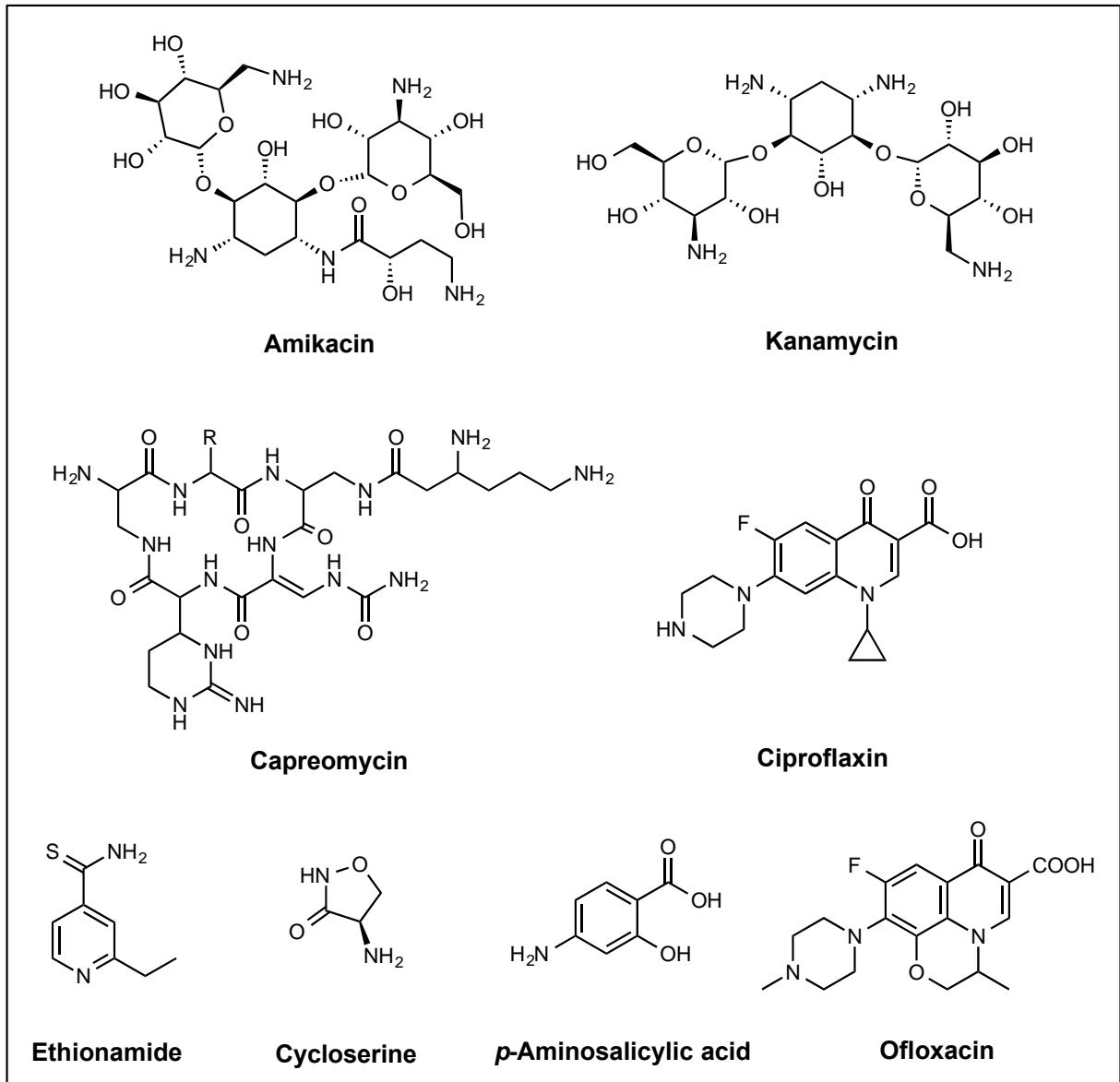


Figure 4: Chemical structures of second-line anti-TB drugs.

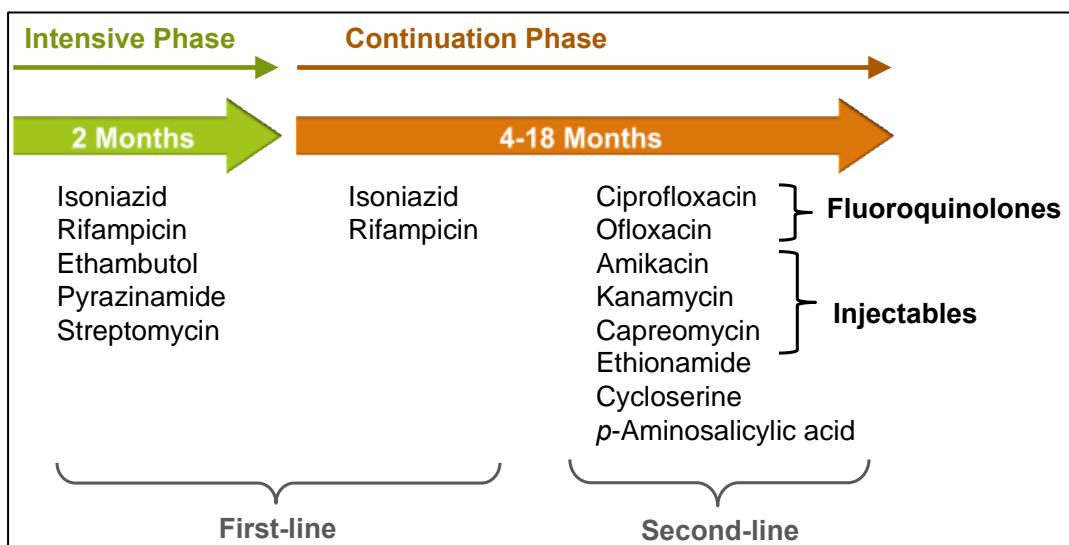


Figure 5: Summary of current TB drug treatment regime indicating first-line and second-line drugs.

Challenges of the current therapy include drug intolerance and toxicities, pharmacokinetics (PK), patient adherence and drug-drug interactions, specifically with antiretroviral therapy (ART) drugs in patients co-infected with TB and HIV.<sup>5</sup> The prolonged treatment duration could possibly be attributed to the presence of subpopulations of bacteria that are non-replicating (NR-*Mtb*) and this contributes to poor patient compliance, high incidence of side effects and the emergence of drug resistant *Mtb* strains.<sup>9</sup> These strains have been termed multidrug-resistant TB (MDR-TB), extensively drug-resistant TB (XDR-TB) and totally drug-resistant TB (TDR-TB).<sup>10</sup> MDR-TB occurs when the strain is resistant to isoniazid and rifampicin and accounted for approximately half a million new cases to the total TB incidences in 2015, 9.5% of which had XDR-TB.<sup>1</sup> XDR-TB occurs when the strain is resistant to isoniazid and rifampicin as well as to any of the aforementioned fluoroquinolones and to at least one of three of the second-line injectable drugs, whilst strains that are resistant to all available first-line and second-line TB drugs are termed TDR-TB.<sup>2,5</sup>

Treatment for MDR-TB ideally requires individualized programs based on *in vitro* drug-susceptibility testing (DST) for each patient, resulting in a more complicated and time-consuming treatment with increased patient compliance. MDR-TB patients should undergo the intensive phase for 8 months with incorporation of at least four of the second-line drugs in combination with pyrazinamide.<sup>5,11</sup> The total treatment duration amounts to 20 months in patients with no previous treatment and 28 months in those who have had previous treatment with patients being monitored using sputum smear microscopy as well as culture. ART is recommended for all patients with HIV and drug-resistant TB requiring second-line anti-TB drugs irrespective of CD4 cell count, as early as possible (first 8 weeks) following initiation of anti-TB treatment.<sup>5,11</sup>

### **1.1.3. ADVANCES IN THE DEVELOPMENT OF NEW ANTI-TB DRUGS**

With the emergence of resistant strains, co-infection with HIV, the existence of LTBI and the extensive treatment regimen; the future of drug design in the development of new anti-TB drugs should aim to:

- Shorten the duration of treatment by developing more potent drugs than existing drugs
- Target MDR and XDR strains of *Mtb*<sup>5</sup>

- Simplify treatment by reducing the pill burden and dosing frequency
- Decrease drug-drug interactions with no antagonism to other TB drugs and ARTs
- Kill *Mtb* in its different physiological states, including LTBI.<sup>12,13</sup>

Many drug candidates currently in clinical trials are drugs that were developed to treat other infectious diseases and have since been repurposed for the treatment of TB (Figure 6).<sup>5</sup> Specifically, some compounds that have been repurposed for TB include the fluoroquinolones, gatifloxacin and moxifloxacin, which are currently in phase III clinical trials, and were originally used in the treatment of respiratory tract infections. Metronidazole is a nitromidazole that is used in the treatment of infections caused by anaerobic bacteria and protozoa and is now in phase II clinical trials as a potential anti-TB drug. Additionally, the oxazolidinone, linezolid was previously used to treat infections caused by gram-positive pathogens and has since been repurposed for TB and is in phase II of clinical trials.<sup>5,14</sup>

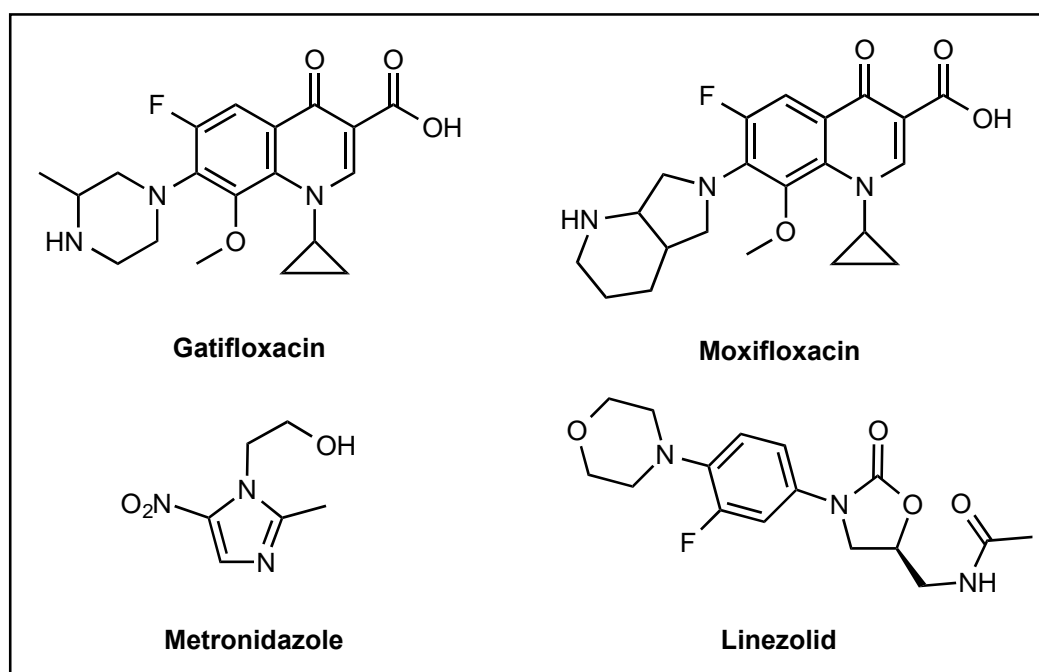


**Figure 6:** Chemical structures of various repurposed drugs for the use in TB treatment.

A number of new drug candidates based on known chemotypes have advanced to clinical trials (Figure 8). Examples of such are depicted in Figure 7 and include other oxazolidinone derivatives, AZD-5847 and sutezolid (PNU-100480) which are in phase II clinical trials. Additional phase II drug candidates include SQ-109, an analog of ethambutol containing a substituted ethylene diamine, and pretomanid (PA-824) a



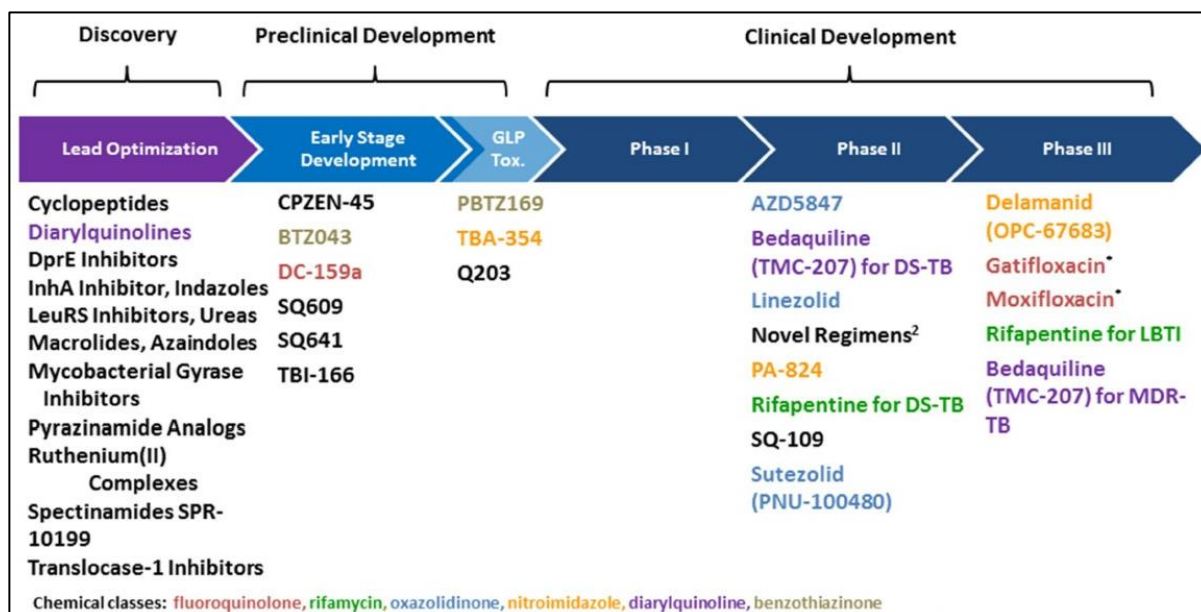


Figure 8: Global TB drug pipeline summarizing current clinical trial candidates.<sup>19</sup>

These advances in anti-TB drugs are a promising development but there is still an ongoing need to develop potent drugs that can combat the various limitations of current regimens.

## 1.2. PROPERTIES OF DRUG CANDIDATES IN DRUG DISCOVERY

There are a number of physiological barriers that exist *in vivo*, which reduce the amount of dosed compound that reaches the target. Therefore, a drug candidate should possess properties that enable good absorption, distribution, metabolism, elimination (ADME) properties and low toxicity in order to reach these targets. Good absorption is attributed to dissolution rate and solubility in the gastrointestinal tract. First pass metabolism occurs here followed by metabolism in the liver. Distribution happens when the compound permeates into the tissues from the blood capillaries, with elimination occurring simultaneously by removal of the compound from the bloodstream by the liver and kidneys.<sup>20,21</sup>

Various properties determine the effectiveness of a drug candidate. In order for a drug-like compound to survive through the completion of human clinical trials, this compound would need to possess sufficiently acceptable ADME and toxicity properties. Improvement of these properties early on in drug discovery is important in saving time and resources on failed drug candidates. Efficient ADME processes can be determined by physicochemical (solubility, permeability, lipophilicity, chemical stability), PK (clearance, half-life, bioavailability, drug-drug interactions, LD<sub>50</sub>) and biochemical (metabolism, protein and tissue binding, and transport) properties.<sup>22,23</sup> Improvement of these properties is most often performed by modification of the chemical structure, usually at sites in the molecule which have been shown by structure-activity relationship (SAR) studies to not be crucial for therapeutic target binding.<sup>20</sup>

These various properties are most often influenced by structural properties such as hydrogen bonding, lipophilicity, molecular weight,  $pK_a$ , polar surface area (PSA), shape and reactivity. Therefore, modifications of these structural parameters will allow for improved ADME properties. In this regard, a set of guidelines, known as the Lipinski's rule of 5 (RO5), was established. The RO5 states that drug likeness is more likely when the number of hydrogen-bond donors (HBD) (sum of OH and NH) is < 5; the number of hydrogen-bond acceptors (HBA) (sum of O and N atoms) is < 10; the molecular weight (MW) is < 500 Daltons (Da); and when ClogP (the calculated 1-octanol/water partition coefficient) is < 5.<sup>20,24</sup>

Optimization of the physicochemical, PK and biochemical characteristics using these various strategies and guidelines should enable improved ADME processes to allow for the synthesis of effective potential drug candidates active *in vivo*.

### 1.2.1. SOLUBILITY IMPROVEMENT STRATEGIES

Poor absorption of drug candidates can result due to poor solubility despite the possibility of having a high permeation rate.<sup>25</sup> Solubility is the maximum dissolved concentration under given solution conditions and is a major determinant of intestinal absorption and oral bioavailability and therefore plays a major role in the effectiveness of the drug.<sup>20</sup> Many drug development failures are a result of poor solubility.<sup>25</sup>

There are a variety of methods that can be implemented to improve the solubility of a compound. This could be through physical methods such as utilizing different polymorphs, solid dispersion of hydrophobic drugs with a hydrophilic carrier or through the formation of salts.<sup>20,26,27</sup> The application of supramolecular techniques for instance, the formation of inclusion complexes (eg. cyclodextrins) or cocrystal formation, can be formulated to provide a more soluble drug.<sup>26,27</sup>

Additionally, various chemical modification strategies enable solubility improvement. Some of the strategies involve the addition of an ionizable group, reducing ClogP (lipophilicity), addition of hydrogen-bonding, adding a polar group, reducing the molecular weight, constructing a prodrug, or disruption of molecular planarity and symmetry to reduce crystal packing.<sup>20</sup>

The addition of ionizable groups such as basic amines and carboxylic acids results in improved solubility, as ionized molecules are more soluble in aqueous media than the neutral molecule as they are more polar.<sup>20</sup> An example of such is the incorporation of an amine side chain onto the antimalarial agent artemisinin, which resulted in enhanced solubility (Figure 9).<sup>28</sup> Furthermore, the protease inhibitor L-685,434 possessed good potency *in vitro* but lacked *in vivo* activity, owing to poor solubility. Introduction of an ionizable centre resulted in improved solubility, allowing for better absorption and thus improved activity of indinavir *in vivo*, as well as enhanced bioavailability (Figure 9).<sup>20,29</sup>

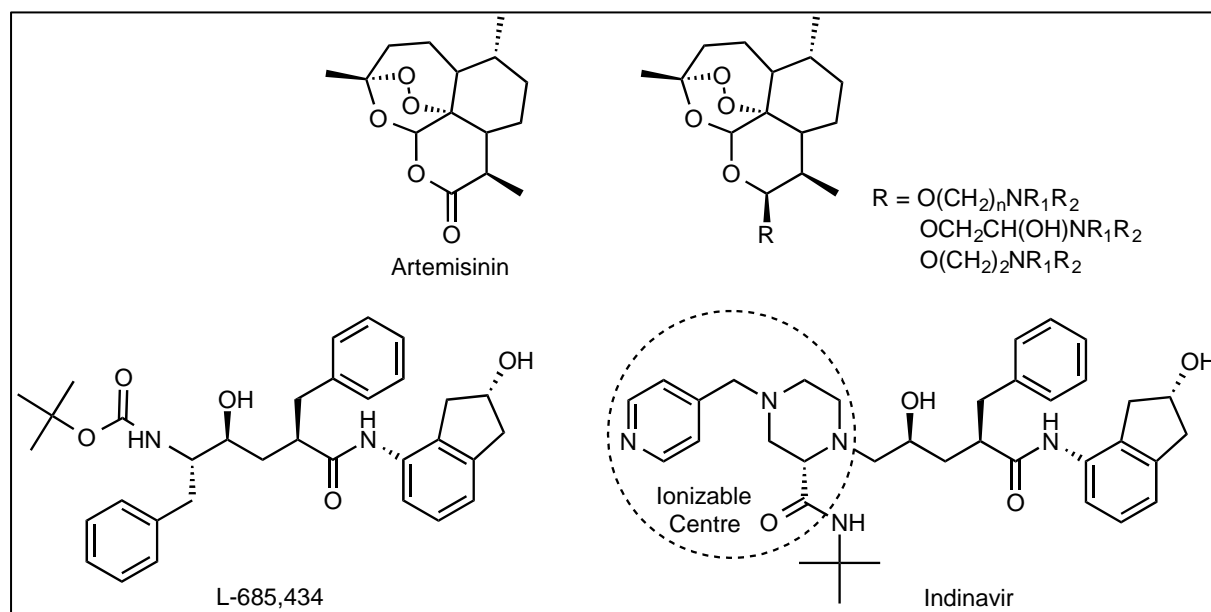


**Figure 9:** Examples of structures incorporating ionizable groups to improve solubility.

A general approach to improving solubility is through the reduction of lipophilicity since the aqueous solubility of a molecule is generally dependent on their hydrophobicity (logP). LogP is defined using the equation:<sup>20</sup>

$$\log P = \log \frac{(\text{solute in } n\text{-octanol})}{(\text{solute in water})}$$

Therefore, as solubility in aqueous media increases, the logP value decreases. This can be accomplished by introducing hydrophilic groups. Hydrophilic groups may, however, interfere with the necessary hydrophobic target protein – drug interactions.<sup>25</sup> Examples of hydrophilic substituents are represented in the two left-hand side (LHS) quadrants ( $-\pi$ ) of the Craig plot (Figure 10).<sup>25,30</sup>

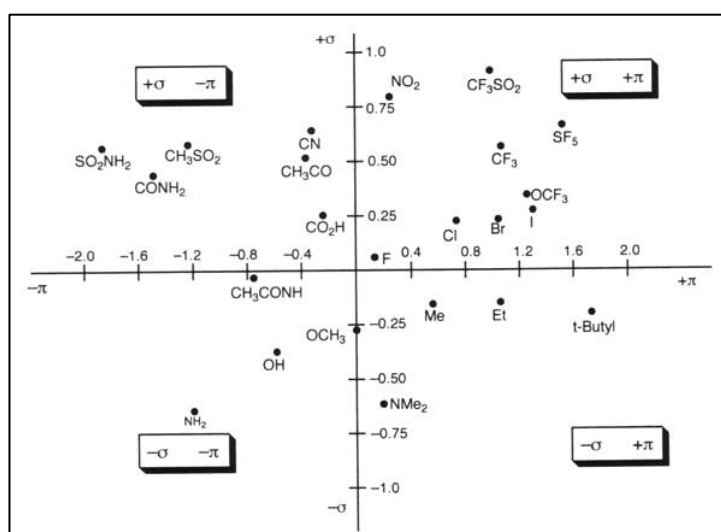


**Figure 10:** Craig plot showing electronic ( $\sigma$ ) and hydrophilic ( $\pi$ ) properties of specific substituents.

Introducing water solubilizing H-bonding groups, HBD and HBA, such as hydroxyl or amino groups has been shown to improve solubility. For example studies reported by Le Manach et al. focused on the synthesis and evaluation of antiplasmodial compounds, specifically on the improvement of solubility and efficacy properties of the lead compound, 3,6-diarylimidazopyridazine (**A**) (Figure 11). Substitution of one of the sulfone moieties for a more H-bonding hydroxyl-containing amide (**B**) or a piperazine sulfonamide group (**C**) resulted in enhanced solubility whilst maintaining activity. Replacement of the sulfone for the more strongly H-bonding sulfoxide substituent as in compound (**D**) was shown to significantly improve solubility.<sup>30</sup>

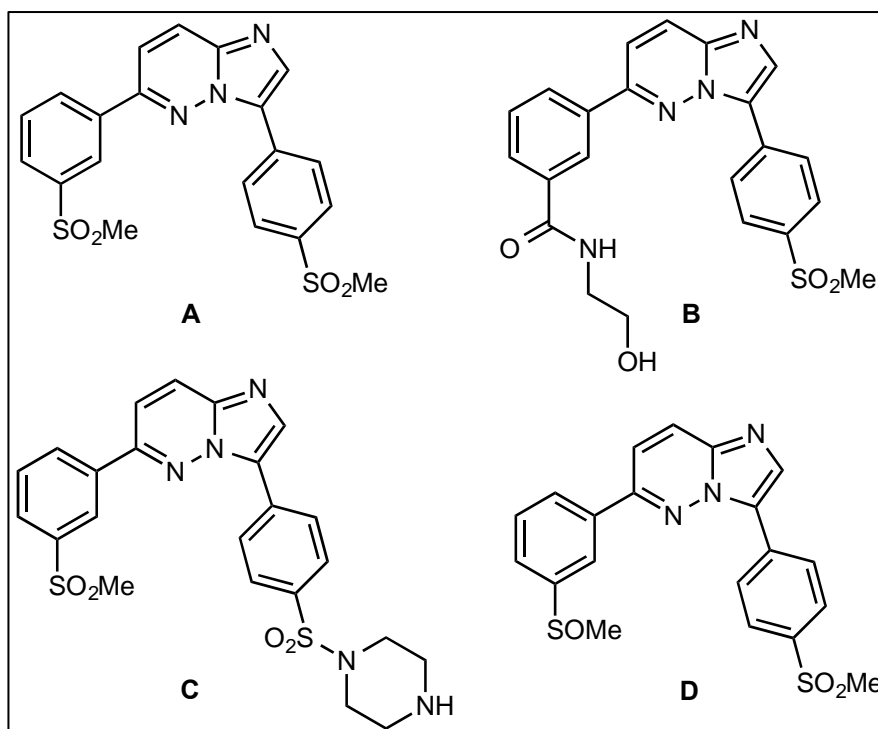


**Figure 11:** Examples of introducing various H-bonding groups to improve solubility of lead compound **A**.<sup>30</sup>

The solubility of a solid solute in water depends on the crystallinity of the solute and the ability of the solute to interact with water. Therefore disruption of crystal packing would be a method for improving aqueous solubility. However, few modifications based on crystal packing have been reported. What is known though is that melting point is related to crystal lattice and crystal packing energies and that molecular symmetry and planarity are known to influence crystal packing. Therefore, upon disruption of the molecular planarity, a decrease in the efficiency of crystal packing would be expected resulting in a decrease of the melting point, which provides a reasonable strategy to improve solubility. To reiterate this principle, Gavezzotti stated that “a very old rule of

thumb says that symmetrical molecules pack in a three-dimensional periodic lattice more easily than less symmetrical ones therefore forming more stable, higher-melting and less soluble crystals.”<sup>25</sup>

Various strategies for the reduction of crystal packing can be achieved either by removal of aromaticity, increasing the dihedral angle, introduction of substituents into the benzylic position and/or by twisting of fused rings. Disruption of molecular symmetry enables an increase in aqueous solubility without an increase of molecular weight, which could negatively affect PK.<sup>25</sup>

Removal of aromaticity results in distortion of the ring conformation away from planarity therefore disturbing the crystal-stacking ability of the compound. For example, Wang et al. identified vanilloid receptor 1 (TRPV1) antagonists (**E**) that were thermodynamically insoluble and therefore introduced partial saturation to the 4-(trifluoromethyl)phenyl ring substituent (**F**) to reduce structural planarity (Figure 12).<sup>31</sup>

The new derivative depicted in Figure 12 (**F**) showed a 13-fold improvement in solubility, but a decrease in potency was observed. Looking at the calculated parameters, a decrease in melting point suggests solubility improvement can be partly attributed to the disruption of planarity as well as to increased hydrophilicity (lower ClogP), which could also contribute to the decrease in activity.<sup>25</sup>

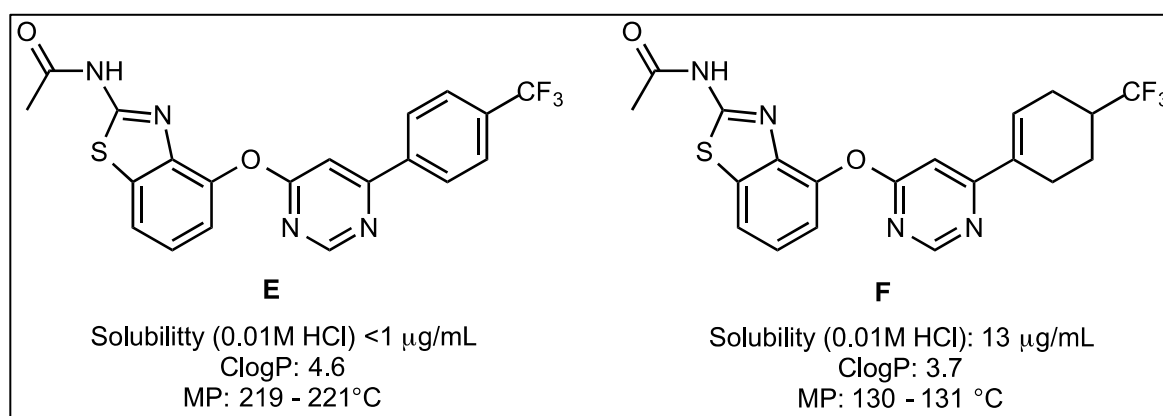


**Figure 12:** Example of removal of aromaticity to enhance solubility of a TRPV1 antagonist.

Little is known about the effect of increased dihedral angles on solubility but an example is illustrated in the case of polychlorinated biphenyls. It was found that *ortho*-substituted biphenyls, which have larger dihedral angles, showed increased solubility. Specifically, *ortho* derivative 2,2'-dichlorobiphenyl (**G**) exhibited a greater aqueous

solubility of 900  $\mu\text{g/mL}$  than 2,4'-dichlorobiphenyl (**H**) and 4-chlorobiphenyl (**I**), which obtained solubility values of 637  $\mu\text{g/mL}$  and 400  $\mu\text{g/mL}$ , respectively (Figure 13).<sup>25,32</sup> The dihedral angle is a convenient numerical parameter that can be obtained by calculation or by X-ray crystal structure analysis and therefore makes it a suitable means for improving solubility.<sup>25</sup>

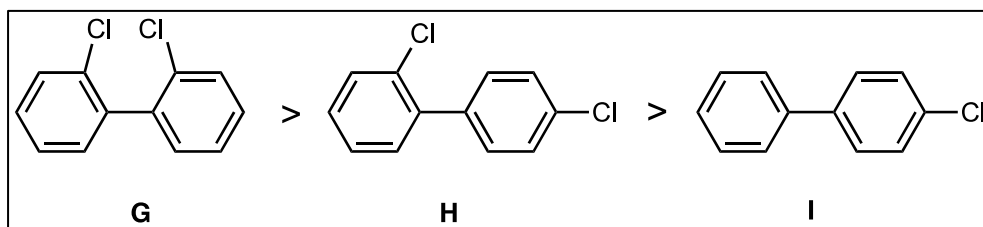


**Figure 13:** Examples of polychlorinated biphenyls to show the effect of dihedral angles on solubility.

This research project partly focuses on reduction of lipophilicity by means of introducing hydrophilic substituents as well as the disruption of molecular planarity and symmetry through removing aromaticity and increasing dihedral angles to improve solubility. Incorporation of a combination of approaches was also explored.

### 1.3. PHARMACOLOGICAL ACTIVITY OF AMINOQUINAZOLINONES

2-Aminoquinazolin-4(3H)-ones are derived from a class of compounds called quinazolinones. Quinazolinones have been extensively explored in a variety of therapeutic areas, with studies showing antitumor,<sup>33</sup> antifungal,<sup>34</sup> antibacterial,<sup>35</sup> anticancer,<sup>36,37</sup> antimalarial,<sup>38</sup> antihypertensive,<sup>39</sup> anti-inflammatory,<sup>40</sup> antimicrobial<sup>41-43</sup> and sedative hypnotic<sup>44</sup> effects of these compounds (Figure 14). On the other hand, literature on the 2-aminoquinazolin-4(3H)-ones derivatives as therapeutic entities is relatively scarce.

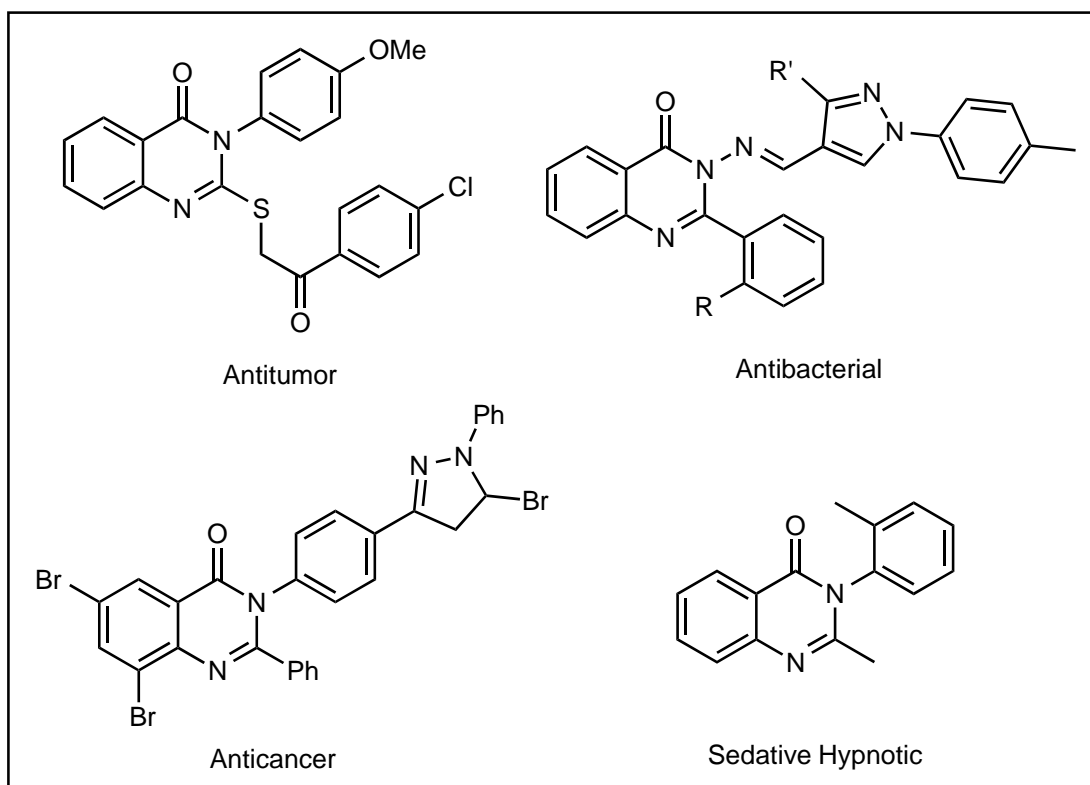


**Figure 14:** Examples of some quinazolinone scaffolds with various therapeutic effects.

However, recently Lievers et al. identified 2-aminoquinazolinone (**J**) in Figure 15, through various optimizational strategies, as a potent inhibitor of Hepatitis C virus (HCV) replication *in vitro* as a result of **J** inhibiting the lipid kinase P14K111 $\alpha$ , a host cellular protein, which is essential for HCV replication. Inhibition of this protein will halt further progression of the virus, making compound **J** a potent host inhibitor candidate for HCV.<sup>45</sup>

On the other hand, research by Deuschle and colleagues established various aminoquinazolinone derivatives possessing partial agonistic properties upon binding to liver X receptors (LXR). LXRs play an important role in the control of cholesterol homeostasis in intestinal mucosa cells and macrophages. Therefore, these LXR nuclear receptor protein-binding compounds (**K**) were patented towards further development as treatments for cholesterol-related conditions or diseases and/or lipid-associated disorders (Figure 15).<sup>46</sup>

Recently, Jirgensons and coworkers patented 2-aminoquinazolin-4(3*H*)-one derivatives containing a tetrahydrofuran moiety in the 3-position and a 7-phenyl substituent as a novel class of nonpeptidomimetic inhibitors of malarial aspartic proteases, specifically digestive plasmepsins I, II and IV. These plasmepsins are involved in the degradation of haemoglobin to amino acids making them promising targets for antimalarial drugs. Compound **L** was discovered using nuclear magnetic resonance (NMR) spectroscopy-based fragment screening against Plm II.<sup>47</sup>

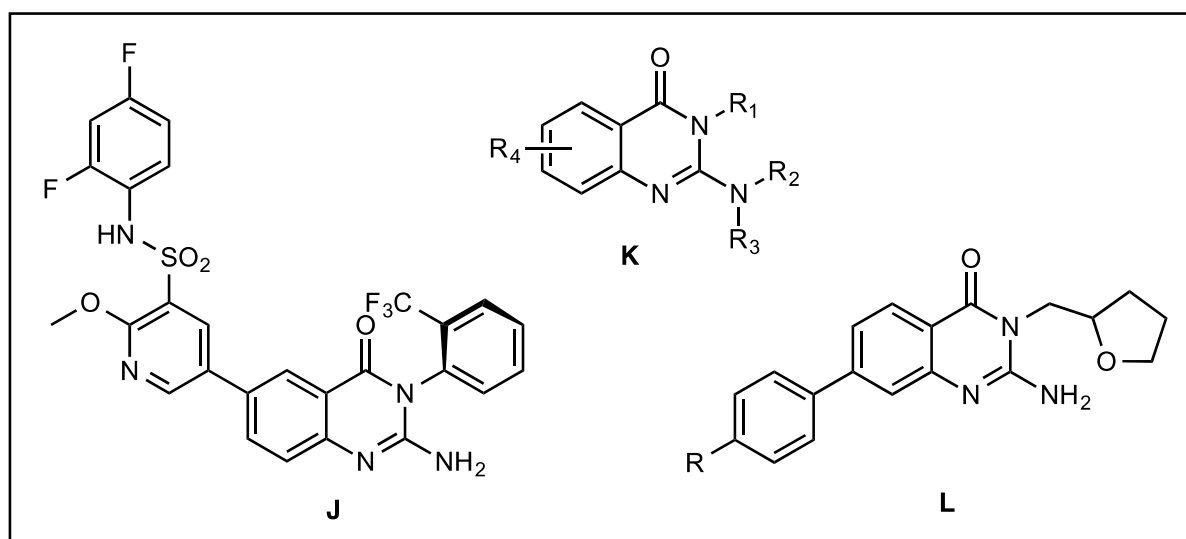


**Figure 15:** Representative 2-aminoquinazolin-4(3*H*)-one derivatives with therapeutic effects.

Within the context of TB, some research has explored the incorporation of quinazolinones as anti-TB agents (Figure 16). Particularly, Pattan and co-workers identified various *N*-3-(4-(4-chlorophenylthiazole-2-yl)-(2-(amino)methyl)-quinazolin-4(3*H*)-one derivatives (**M**) (Figure 16), as potential growth inhibitors of H<sub>37</sub>Rv strain of *Mtb*.<sup>48</sup> Omar and Alafeefy synthesized 2-alkylthio-6-iodo-3-substitued-quinazolin-4-one analogues (**N**) (Figure 16) with three compounds showing more than 95% growth inhibition at a minimum inhibitory concentration (MIC) of less than 6.25 µg/mL of *Mtb* strain H<sub>37</sub>Rv.<sup>49</sup>

A series of novel compounds involving the conjugation of a substituted-quinazolin-4(3*H*)-one moiety as a side arm onto a fullerene scaffold were reported by Patel et al. This class of quinazolinone-fullerene conjugates were evaluated for *in vitro* antimycobacterial activity against *Mtb* (H<sub>37</sub>Ra) with compound **O** (Figure 16) showing effective growth inhibition at MIC 1.562 mg/mL with an inhibition of 98.83%.<sup>50</sup> Additionally, studies by Reddy and co-workers produced compound **P** exhibiting 97% inhibition of *Mtb* (H<sub>37</sub>Ra) at 25 µg/mL.<sup>51</sup>

More recently, Couturier and colleagues identified quinazolinone **Q** (Figure 16) by high throughput phenotypic screening against *Mycobacterium smegmatis* as potential anti-TB agents. Optimization of **Q** led to more potent, yet poorly soluble *Mtb* growth inhibitors, three of which advanced to *in vivo* efficacy studies. These derivatives displayed favourable PK profiles but insignificant *in vivo* efficacy.<sup>52</sup>

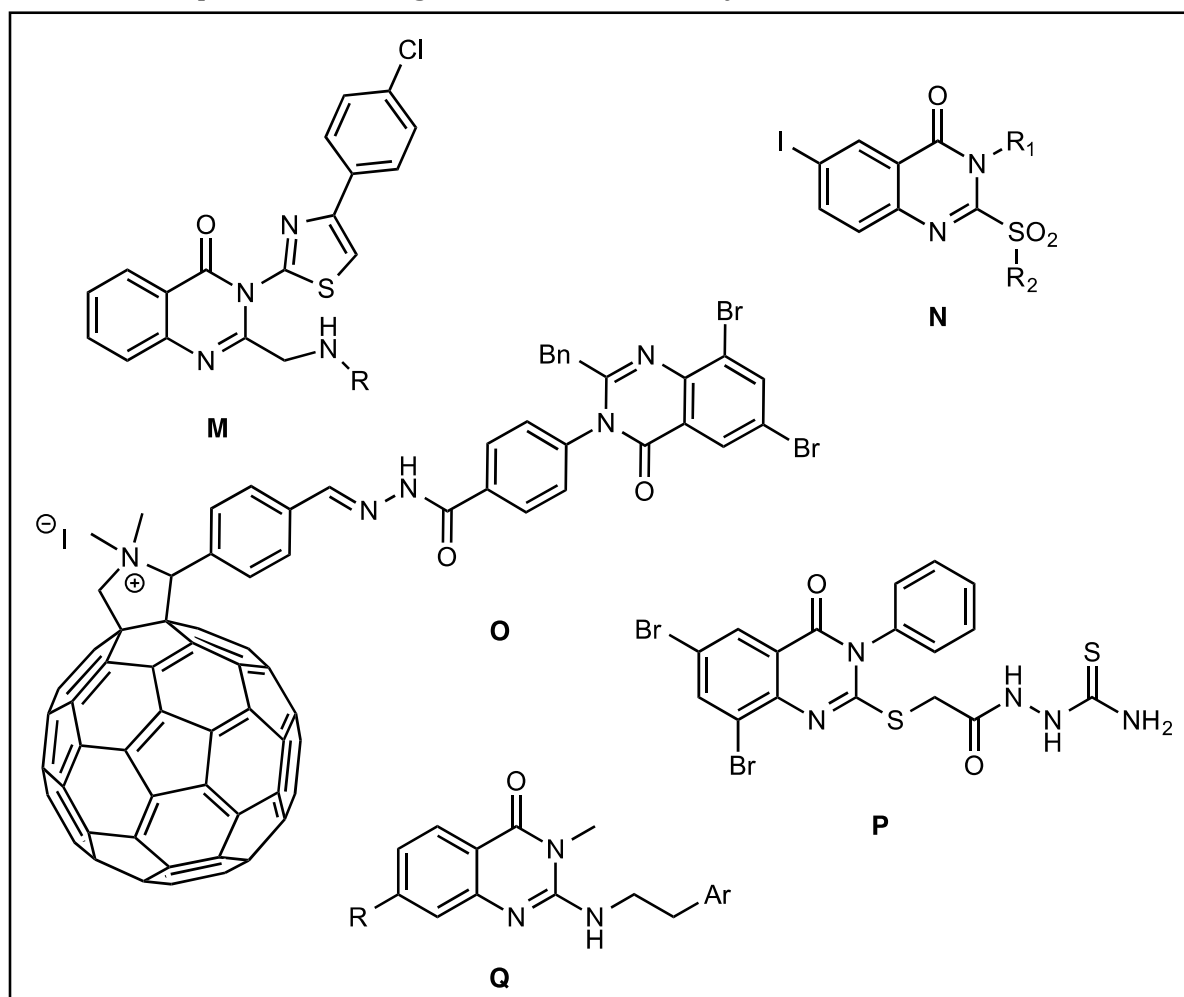


**Figure 16:** Quinazolinone analogues that have shown to possess antimycobacterial activity effects.

The above examples provide insight into the current medicinal applications of quinazolinone-based compounds, including the significance in their recent antimycobacterial activity.

#### **1.4. AIMS AND OBJECTIVES**

##### **1.4.1. OBJECTIVE**

The main objective of this research was to perform SAR studies around the 2-aminoquinazolin-4(3*H*)-one core towards optimization of these potential antimycobacterial agents with respect to solubility and potency.

##### **1.4.2. HYPOTHESIS**

The hypothesis was whether it would be possible to identify novel aminoquinazolinone-based antituberculosis drug leads with favorable solubility, potency and metabolic stability.

##### **1.4.3. SPECIFIC AIMS**

- i. Synthesis and *in vitro* antimycobacterial SAR studies of various aminoquinazolinones.
- ii. Profiling with respect to solubility and metabolic stability.
- iii. Confirmation of the factors responsible for any improved solubility and deducing relationships.

## CHAPTER 2: DESIGN, SYNTHESIS AND PHARMACOLOGICAL EVALUATION OF 2-AMINOQUINAZOLINONE ANALOGUES

---

### 2.1. INTRODUCTION

This chapter reports on the design, synthesis and spectroscopic characterization of compounds based on the 2-aminoquinazolinone structure (Figure 17). Modifications around the core in positions 3 and 6 of the quinazolinone moiety incorporating aryl and saturated ring substituents were explored in an attempt to improve solubility. Adapted synthetic schemes were employed to achieve the desired target molecules. Some of the synthesized compounds were initially tested for *in vitro* antimycobacterial activity in media containing glycerol-alanine-salts with Tween-80 and iron (GAST Fe) as well as media that comprises of 7H9 broth with a growth supplement containing bovine albumin, dextrose and catalase (7H9 ADC).<sup>53</sup> Samples were tested against the virulent human *Mtb* strain, H37Rv,<sup>54</sup> whereby the most active derivatives were profiled with respect to cytotoxicity and microsomal metabolic stability. Aminoquinazolinone intermediates and target compounds were subsequently reevaluated in glycerol-free media. The apparent solubility of all target compounds was also measured using kinetic solubility assays, as described in Chapter 4.

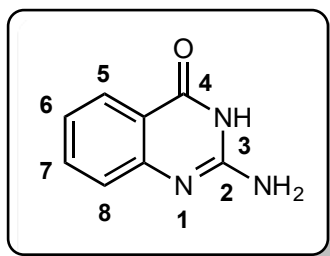


**Figure 17:** General structure of the 2-aminoquinazolinone core scaffold.

#### 2.1.1. BACKGROUND INFORMATION

On the basis of the structural similarity shared with previous antimalarial 2-aminopyridines,<sup>55</sup> 2-aminoquinazolinones were synthesized for evaluation against the human malaria parasite *Plasmodium falciparum*, but were found to be inactive. Subsequent phenotypic whole-cell screening of this series against *Mtb* identified the aminoquinazolinone **5.1** with favourable antimycobacterial potency, but low solubility (Figure 18). Towards improving the solubility of **5.1**, preliminary SAR studies were

conducted. These studies led to the sulfoxide **5.2**, which showed to improve solubility, Figure 19.

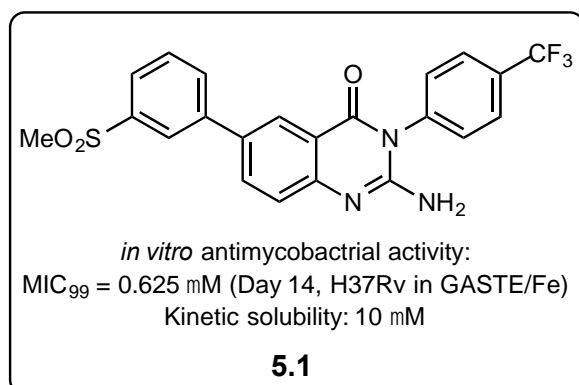


**Figure 18:** Chemical structure, biological activity and solubility data for the hit aminoquinazolinone compound **5.1**.

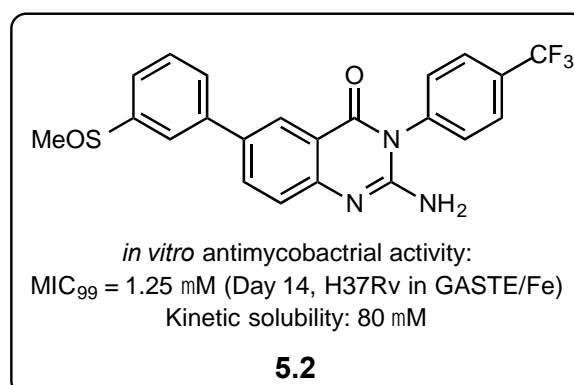


**Figure 19:** Chemical structure, biological activity and solubility data for the sulfoxide-containing aminoquinazolinone compound **5.2**.

Further profiling of frontrunner compounds **5.1** and **5.2** was ongoing in parallel to the research described in this dissertation, whose main focus was to apply the various solubility improvement approaches to the hit compound **5.2** whilst also expanding the SAR.

## 2.2. DESIGN AND RATIONALE OF AMINOQUINAZOLINONE DERIVATIVES

In order to explore the SAR for this class of compounds, various structural changes around the aminoquinazolinone core would need to be implemented. Therefore, a variety of analogues were selected for synthesis based on this, resulting in two points of diversity, **SAR 1** and **SAR 2**, whilst the aminoquinazolinone core scaffold remained fixed (Figure 20).

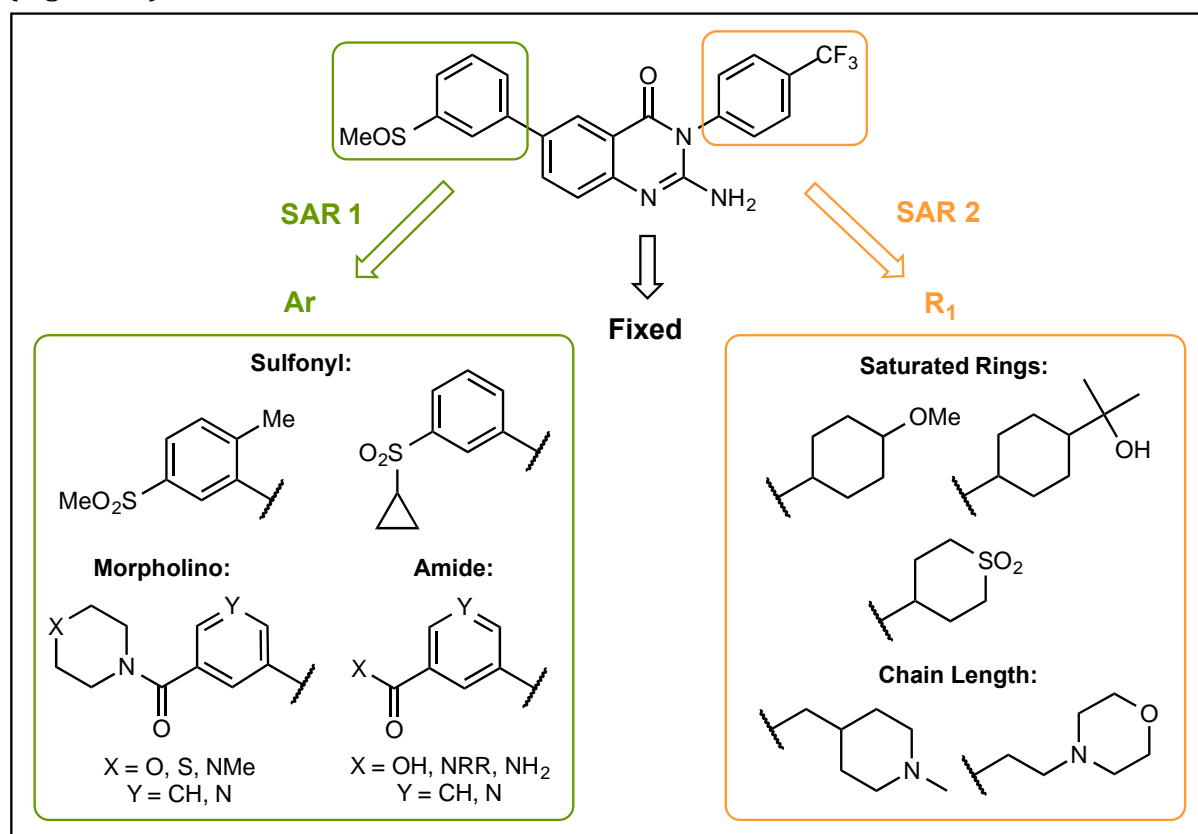


**Figure 20:** Chemistry design for planning the synthesis of aminoquinazolinone derivatives with two points of diversity, **Ar** and **R<sub>1</sub>**, around the core incorporating various solubility improvement strategies.

**SAR 1** was initially explored with structural modifications occurring at **Ar** whereas the right hand side (RHS) **R<sub>1</sub>** remained fixed. Previous studies revealed that the presence of the sulfone moiety in the *ortho*- and *para*-positions resulted in inactive ( $MIC_{99} > 160\mu M$ ) compounds. This confirmed the *meta*-position as optimal for activity in respect of **Ar** groups of **SAR 1**. Substituents were selected not only to create structural diversity and expand the SAR, but also to potentially improve solubility properties. Subsequently, a number of the aforementioned solubility improvement strategies were considered in designing **SAR 1** analogues for synthesis, which can be divided into three categories: sulfonyl, morpholino and amide derivatives (Figure 20).

Specifically, sulfonyl analogues investigated the reduction of crystal packing through the addition of a substituent in the *ortho*-position to increase the dihedral angle as well as interchange of the sulfonylmethyl moiety for a cyclopropyl substituent. The morpholino group of compounds incorporates a combination of hydrophilic, polar substituents as well as saturated rings to disrupt planarity. Introduction of an ionizable group was explored through the addition of a pyridinyl analogue. This was also introduced into the amide series whereby the main strategy was to reduce lipophilicity by including polar, hydrophilic substituents.

The choice of **Ar** substituents was also determined by the commercial availability of the appropriate arylboronic acids or esters necessary for the introduction of **Ar** substituents.

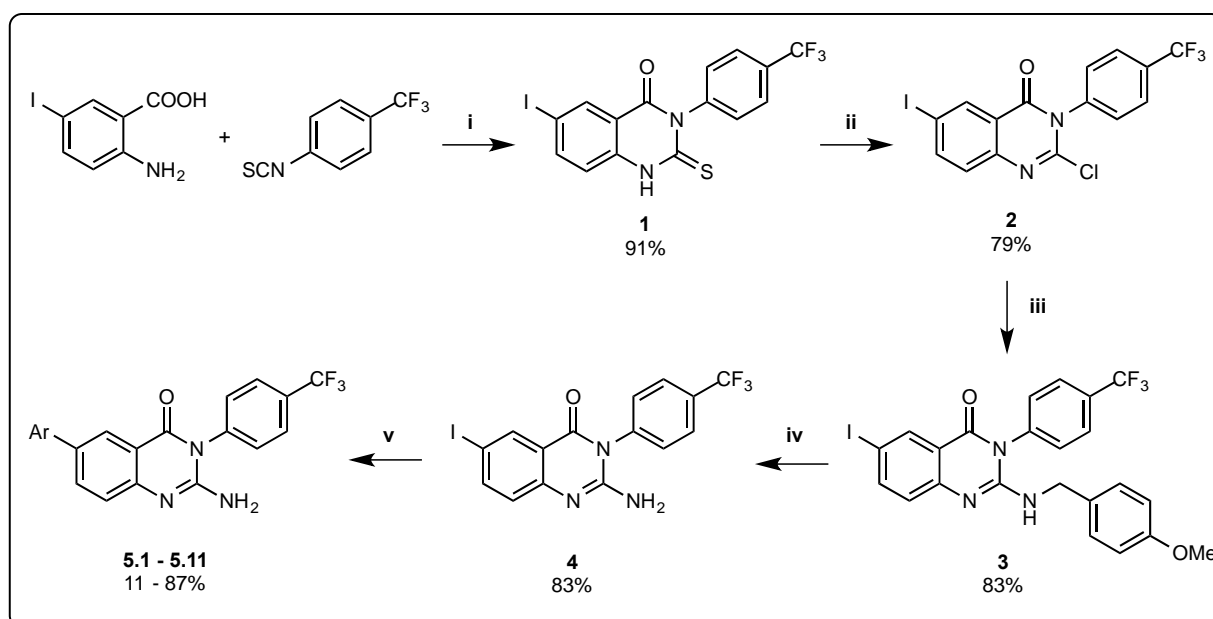
In order to explore **SAR 2**, various substituents were selected for **R<sub>1</sub>** using the solubility improvement approaches, while the **Ar** and aminoquinazolinone core remained unchanged. Previously synthesized analogues of the **R<sub>1</sub>** moiety in which the trifluoromethyl group was in the *meta*- and *ortho*-positions displayed moderate to poor activity, respectively, thereby confirming the necessity of the aromatic substituent to be in the *para*-position for **SAR 2** derivatives.

The main focus for selection of substituents for **SAR 2** analogues was the removal of aromaticity as a strategy to improve solubility (Figure 20). Variations in chain length as well as the incorporation of hydrophilic substituents were additionally explored. Commercial availability of appropriate amines was also a consideration for **SAR 2** derivatives.

## 2.3. SYNTHESIS AND SPECTROSCOPIC CHARACTERIZATION OF 2-AMINOQUINAZOLINONES

### 2.3.1. SYNTHESIS OF SAR 1 TARGET COMPOUNDS

Literature on the synthesis of 2,3-disubstituted quinazolinone compounds, particularly for the 2-amino derivatives, is rare as much of the literature is dominated by unsubstituted quinazolinone-based compounds.<sup>56,57</sup> However, Leivers and coworkers recently described a synthetic procedure for the formation of 2-aminoquinazolinones as anti-HCV agents acting through the inhibition of P14KIII $\alpha$ .<sup>45</sup>



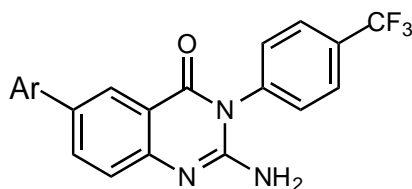
**Scheme 1:** General synthetic protocol towards target compounds **5.1 – 5.11**. *Reagents and conditions:* (i) Dioxane, Et<sub>3</sub>N, reflux (110 °C), 4 h; (ii) POCl<sub>3</sub>, PCl<sub>5</sub>, N<sub>2</sub>, 110 °C, 6-12 h; (iii) DMF, 4-methoxybenzylamine, DIPEA, 80 °C, 4 h; (iv) TFA, reflux, 48 h or MW (110 °C) 20 min, (v) Dioxane/water, ArB(OH)<sub>2</sub>, PdCl<sub>2</sub>(PPh<sub>3</sub>)<sub>2</sub>, K<sub>2</sub>CO<sub>3</sub>, 80 °C, 1-5 h.

The **SAR 1** target compounds were therefore synthesized using the synthetic procedure outlined in Scheme 1, adapted from work reported by Leivers and coworkers. Briefly, the synthesis involved commercially available 2-amino-5-iodobenzoic acid and 4-(trifluoromethyl)phenyl isothiocyanate, which undergo a cyclization reaction to afford intermediate **1**.

Chlorination of the thioxo intermediate was achieved using phosphorous oxychloride (POCl<sub>3</sub>) in the presence of phosphorous pentachloride (PCl<sub>5</sub>) to give the 2-chloro intermediate **2**. The amino group was then installed using 4-methoxybenzylamine in a substitution reaction to yield intermediate **3**, followed by subsequent deprotection using

trifluoro acetic acid (TFA) to afford the 2-aminoquinazolinone **4**. The desired **Ar** substituent was then incorporated via a Suzuki-Miyaura cross-coupling reaction between the penultimate iodo compound **4** and the appropriate boronic acid or ester to form target compounds **5.1 – 5.11** in low to high yields (Table 1).

**Table 1:** Isolated percentage yields for **SAR 1** target compounds **5.1 – 5.11**.



Compound (Code)	Ar	Variables	Percentage Yield (%)
<b>5.1</b> (JA025)			46
<b>5.2</b> (JA010)			40
<b>5.3</b> (JA013)			71
<b>5.4</b> (JA018)		Y = CH, X = O	87
<b>5.5</b> (JA019)		Y = CH, X = S	83
<b>5.6</b> (JA020)		Y = CH, X = NMe	32
<b>5.7</b> (JA021)		Y = N, X = O	50
<b>5.8</b> (JA017)		Y = CH, R = R' = H	25
<b>5.9</b> (JA022)		Y = CH, R = H, R' = Me	27
<b>5.10</b> (JA023)		Y = N, R = H, R' = Me	45
<b>5.11</b> (JA016)		Y = CH, R = R' = Me	45

### 2.3.2. MECHANISTIC DETAILS AND SPECTROSCOPIC ANALYSES OF SAR 1 INTERMEDIATES AND TARGET COMPOUNDS

The proposed mechanism for step (i) is initiated by a nucleophilic attack of the amino nitrogen of 2-amino-5-iodobenzoic acid on the electron deficient isothiocyanate carbon (Figure 21). This is followed by a proton transfer step between the two nitrogens on the thiourea intermediate to allow for intramolecular cyclization to occur. This is achieved via an attack at the acyl centre, which is hypothesized to be activated through interaction of the carbonyl oxygen with triethylammonium ion, to afford the quinazolinone intermediate **1**.

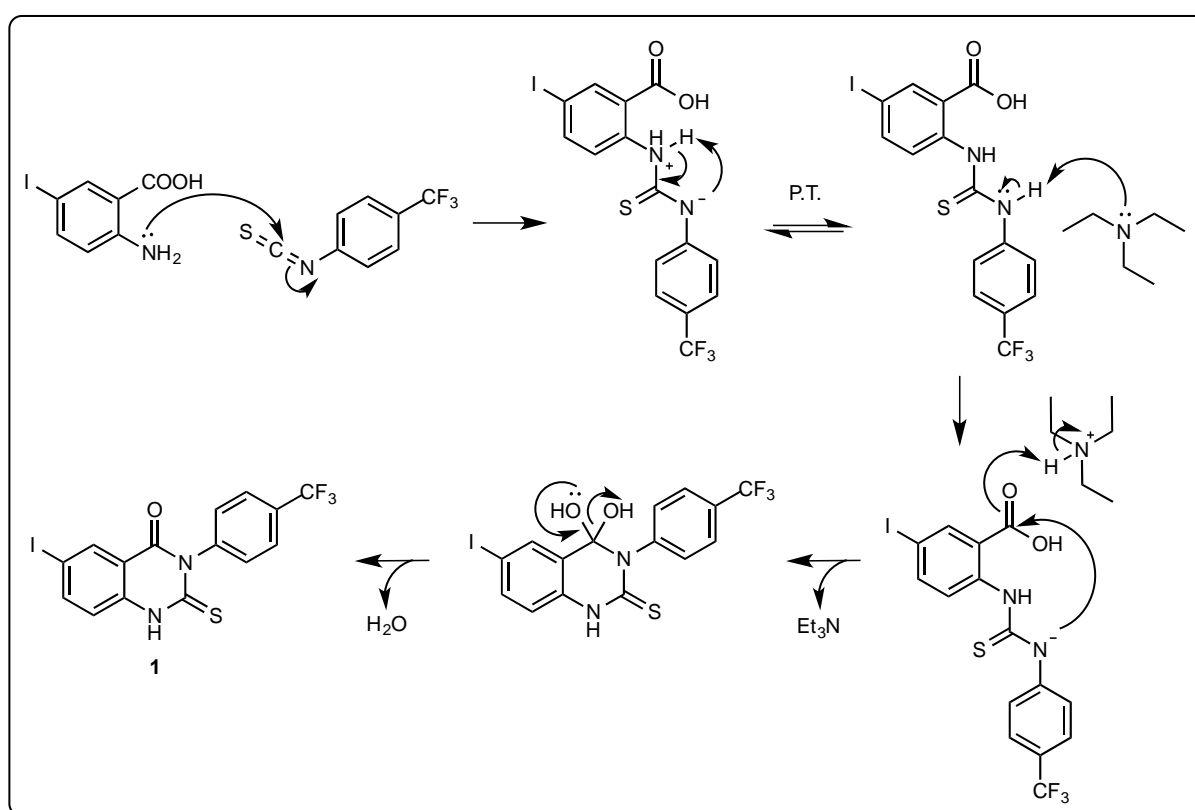


**Figure 21:** Proposed reaction mechanism for the formation of quinazolinone intermediate **1**.

The structure of compound **1** was confirmed by 1D <sup>1</sup>H NMR (Figure 22), consisting of a broad, highly deshielded, singlet proton signal resonating at  $\delta$  13.18, which is characteristic of the quinazolinone proton (H-6). The structure is further confirmed by the conserved coupling pattern observed in the aromatic region including a diagnostic long-range coupling ( $^4J$  = 1.92 Hz) between H-1 ( $\delta$  8.20) and H-2 ( $\delta$  8.10) as well as the presence of two, symmetrical doublets corresponding to the disubstituted 4-(trifluoromethyl)phenyl group protons at  $\delta$  7.88 and  $\delta$  7.56.

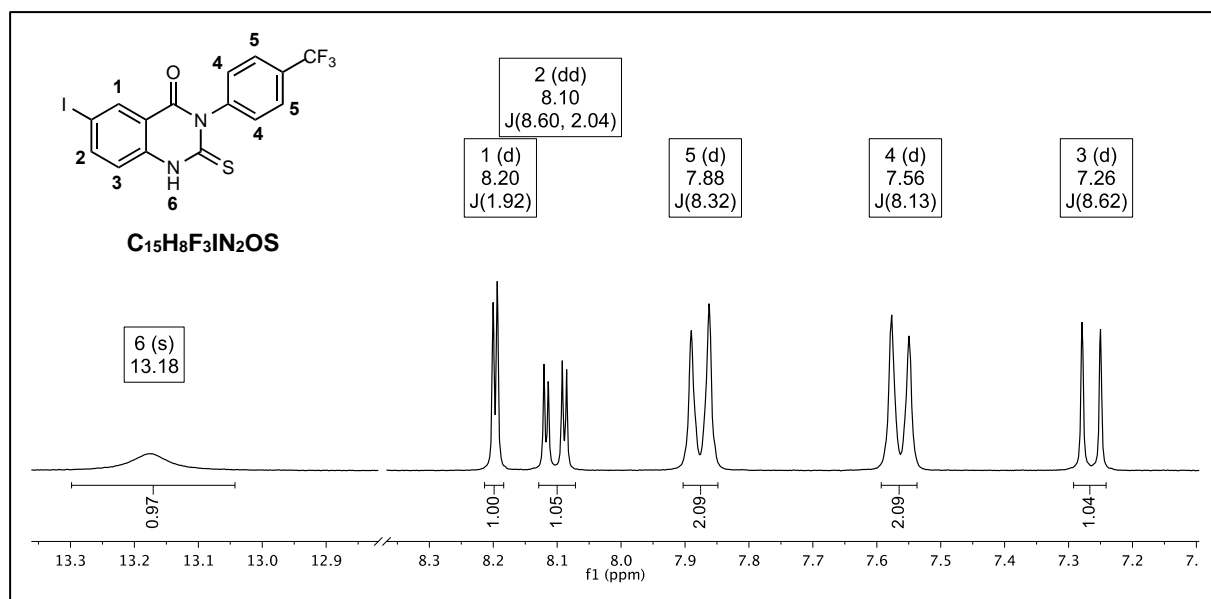


**Figure 22:** Assigned  $^1\text{H}$  NMR spectrum confirming the successful synthesis of intermediate **1**.

The chlorination reaction (ii) is proposed to proceed via an attack of the 2-thioxo center on the phosphorous of  $\text{POCl}_3/\text{PCl}_5$  with the loss of a chloride ion. The chloride then attacks the electrophilic thiocarbonyl carbon resulting in elimination of phosphenothioic chloride and the release of hydrochloric acid (HCl) to afford the 2-chloro intermediate **2**.  $\text{POCl}_3$  is used in conjunction with  $\text{PCl}_5$ , as previous attempts with using only  $\text{POCl}_3$  as the chlorinating agent produced low yields (Figure 23).

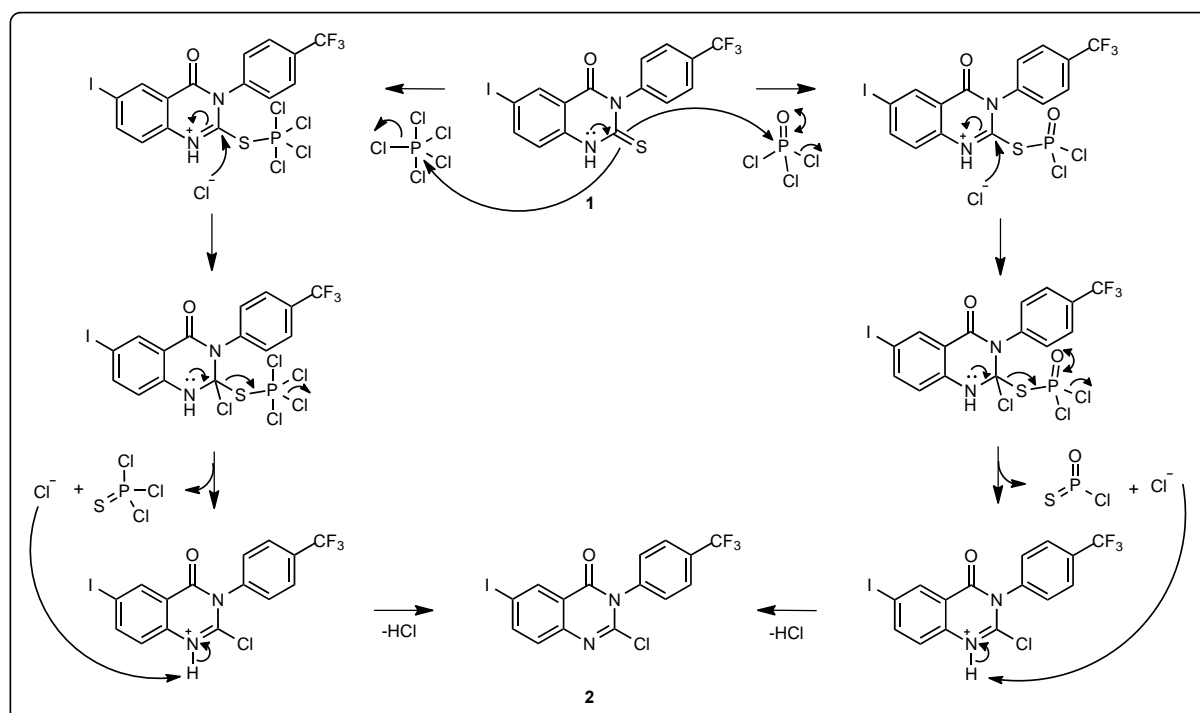


**Figure 23:** Proposed reaction mechanism for the chlorination reaction using  $\text{POCl}_3$  (right) and  $\text{PCl}_5$  (left).

$^1\text{H}$  NMR confirmed successful chlorination due to the absence of the key diagnostic quinazolinone amino proton signal in intermediate **2** that was previously observed in intermediate **1**, whilst the quinazolinone core proton signals ( $\text{H}^1$ ,  $\text{H}^2$ ,  $\text{H}^3$ ) remain intact (Figure 24).

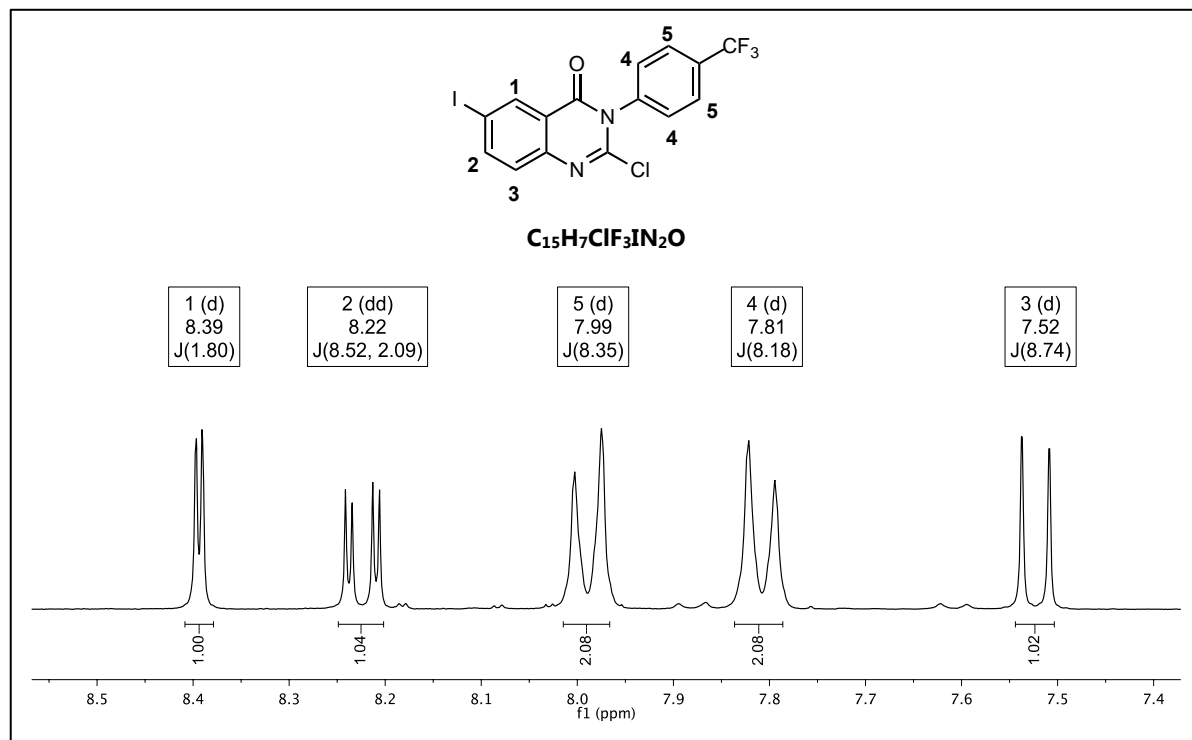


**Figure 24:**  $^1\text{H}$  NMR spectrum of chlorinated intermediate **2**.

With a good leaving group in the 2-position, the 4-methoxybenzylamino group is introduced via a nucleophilic aromatic substitution reaction ( $\text{S}_{\text{N}}\text{Ar}$ ) of the chloro group, which is assisted by the push of electrons through the conjugated ring system of the quinazolinone core (Figure 25).

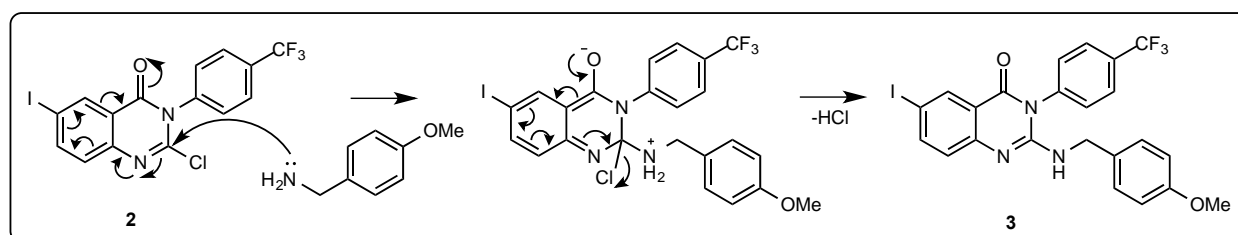


**Figure 25:** Proposed mechanism for the  $\text{S}_{\text{N}}\text{Ar}$  reaction in the formation of intermediate **3**.

The appearance of new proton signals corresponding to the aminobenzyl in the  $^1\text{H}$  NMR spectrum (Figure 26) confirmed that successful nucleophilic substitution had occurred. Characteristic signals include the broad NH triplet at  $\delta$  6.68, the benzylic methylene doublet ( $\delta$  4.44) and the methoxy singlet ( $\delta$  3.71).

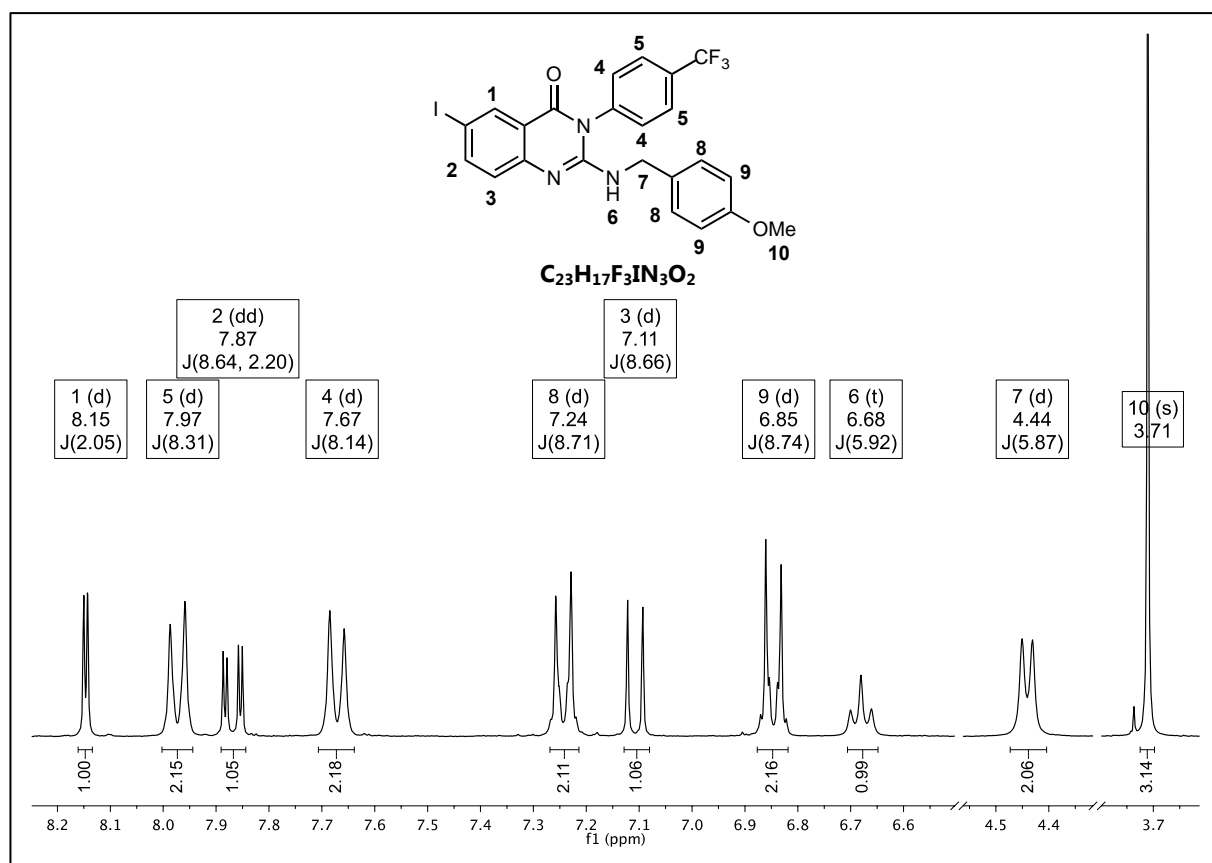


**Figure 26:** <sup>1</sup>H NMR spectrum for the methoxbenzylamine intermediate **3**.

The key 2-aminoquinazolinone intermediate **4** was generated via a deprotection reaction catalyzed by TFA and assisted by the push of electrons through the benzyl ring to afford the desired free amino group, as mechanistically shown in Figure 27.

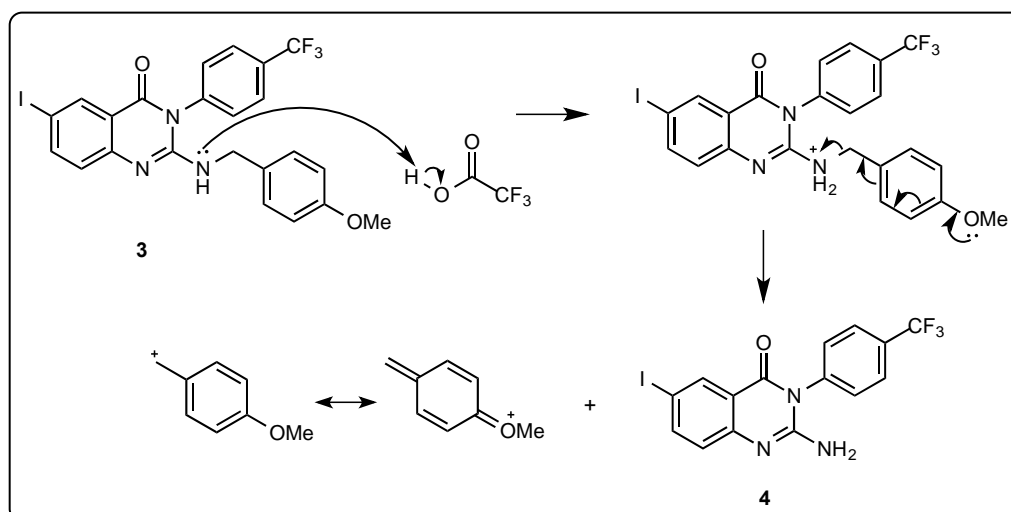


**Figure 27:** Proposed mechanism for the deprotection reaction using TFA.

<sup>1</sup>H NMR confirmed successful deprotection with the presence of a broad singlet at  $\delta$  6.60 corresponding to the free primary amine of the 2-aminoquinazolinone (Figure 28).

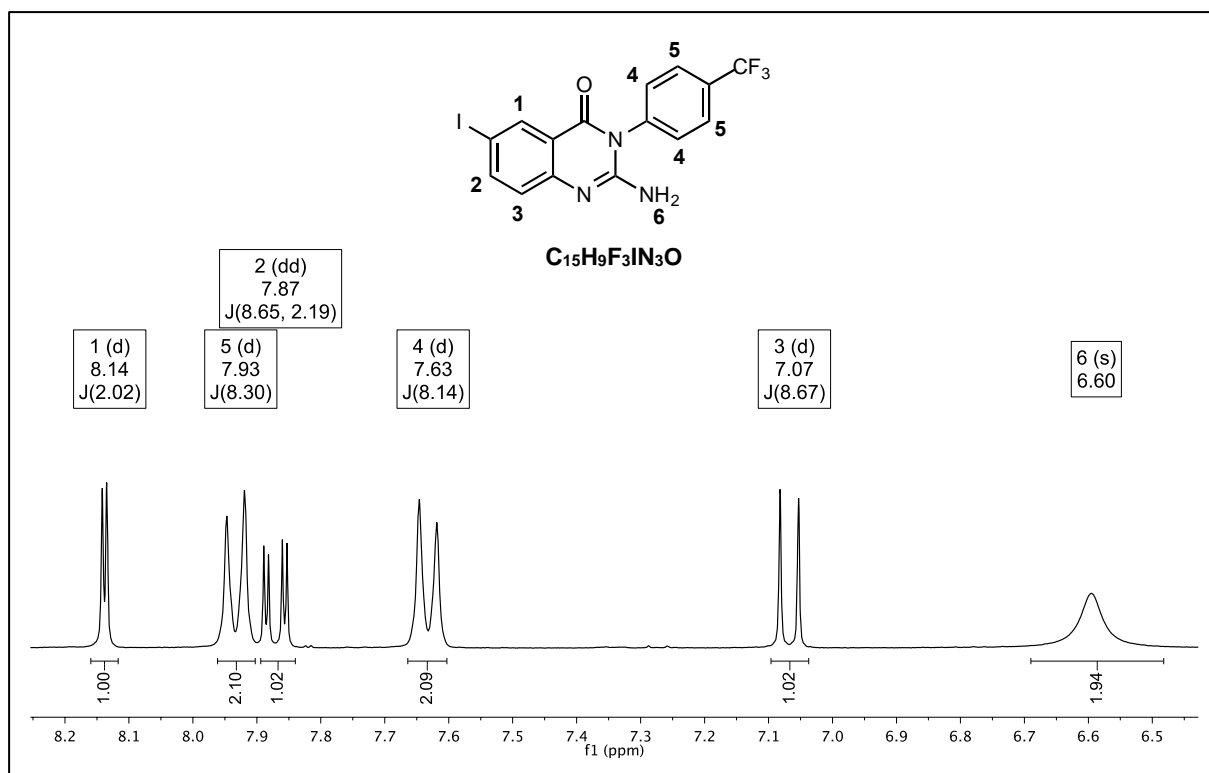


**Figure 28:** <sup>1</sup>H NMR spectrum for deprotected intermediate **4**.

The final step in synthetic Scheme 1 introduces the structural diversity of **Ar** substituents via a Suzuki-Miyaura cross-coupling reaction, which is a palladium-catalyzed reaction between an aryl halide and an aryl boronic acid or ester to form biaryl systems. The mechanism was first published by Suzuki in 1985 and proceeds *via* a catalytic cycle incorporating three major steps; oxidative addition, transmetalation and reductive elimination.<sup>58</sup>

Structural assignments for final target compounds (**5.1** – **5.11**) were assisted by 2D heteronuclear single quantum correlation (HSQC) and correlation spectroscopy (COSY) NMR experiments. For characterization purposes compound **5.1** is used as an illustrative example of the coupling pattern observed for the target compounds, with the addition of signals relating to the **Ar** substituents (Figure 29). For example, a highly deshielded triplet ( $\delta$  8.20) is observed with a small coupling constant ( $^4J \sim 1.81$ ) owing to long range coupling from H-7 to H-8 and to H-10. This is reflected in the splitting pattern for these two protons, which are additionally coupled to H-9 ( $^3J = 7.81$ ) as well as to each other, therefore a doublet of doublet of doublets (ddd) or doublet of triplets is observed for these two protons, with a corresponding triplet correlating to H-9 at  $\delta$  7.75. This coupling pattern is observed for most of the *meta*-substituted aromatic substituents with slight deviations.

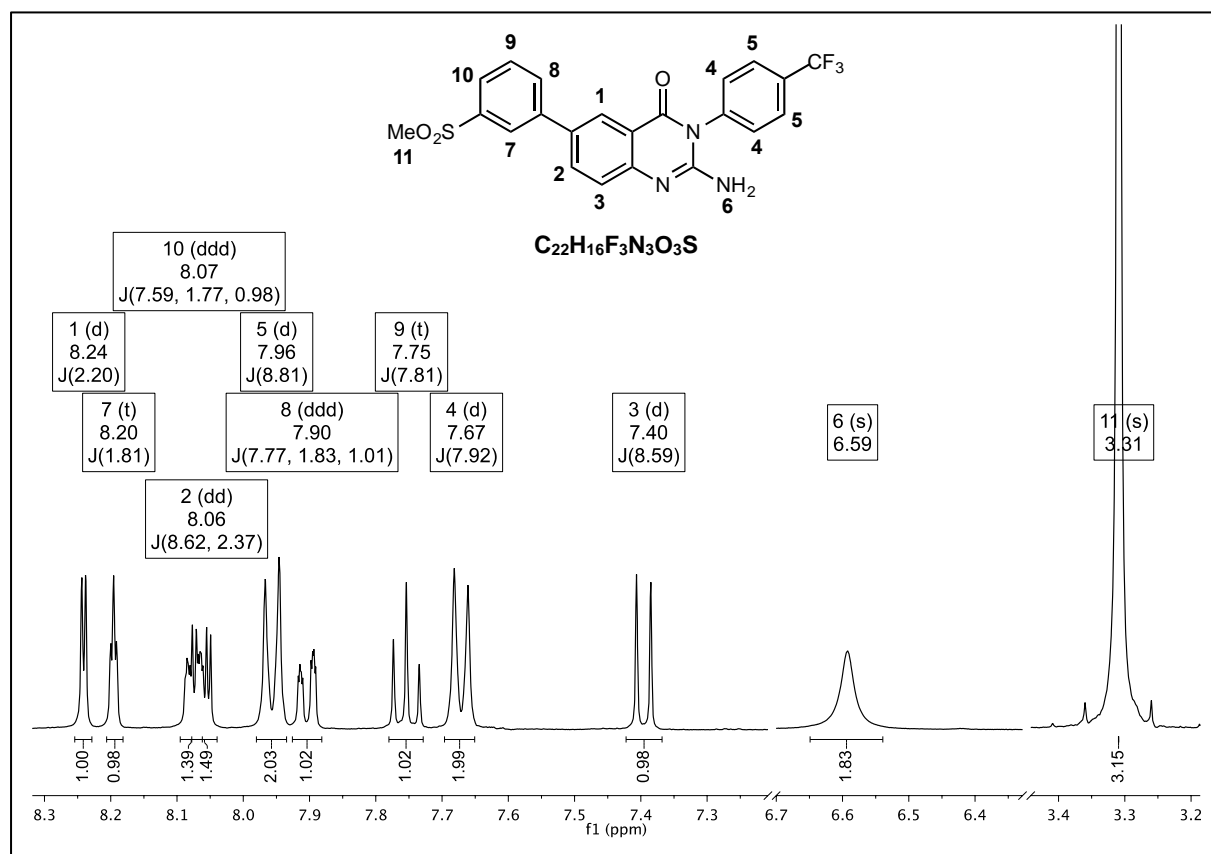
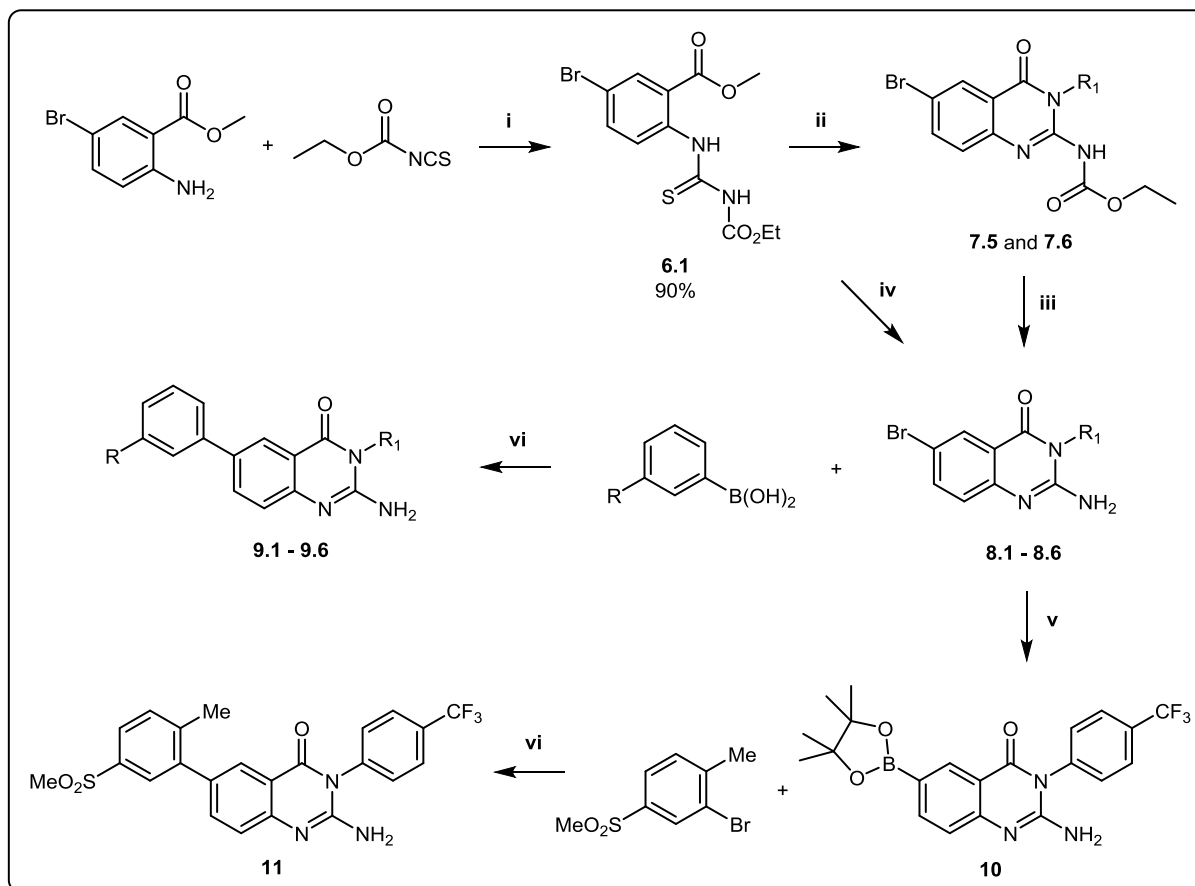


**Figure 29:** <sup>1</sup>H NMR spectrum of final target compounds, using **5.1** as an illustrative example.

### 2.3.3. SYNTHESIS OF SAR 2 TARGET COMPOUNDS

In order to create structural diversity for **SAR 2** using synthetic Scheme 1, different **R<sub>1</sub>** substituents would need to be introduced using various arylisothiocyanates. However, these have limited commercial availability and therefore, alternative synthetic procedures were explored.

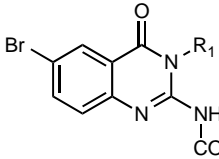
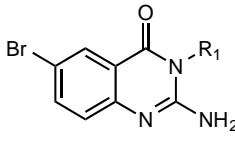
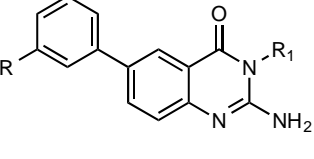
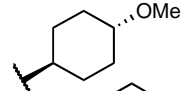
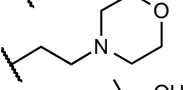
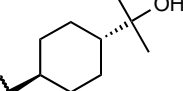
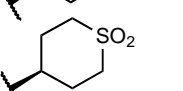
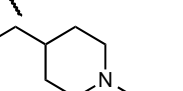
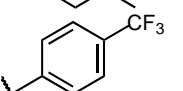
Work reported by Lecoutey and coworkers describing a one-pot synthesis of 2-aminoquinazolinones using methyl anthranilate as the starting material and incorporating structural diversity in the 3-position using commercially available primary aromatic amines (anilines) was considered.<sup>59</sup> However, previous attempts by our research group using methyl 2-amino-5-bromobenzoate as a starting material failed, as intermediate **6.1** precipitated out of solution and had to be isolated prior to cyclization.



**Scheme 2:** General synthetic protocol towards target compounds for **SAR 2**. *Reagents and conditions:* (i) Acetonitrile, rt (24.4°C), 10 min; (ii) DCM, EDCl, R<sub>1</sub>NH<sub>2</sub>, rt (24°C), 18 h; (iii) TFA, MW, 110°C, 20 min; (iv) DMF, EDCl, R<sub>1</sub>NH<sub>2</sub>, rt (5h) → 100°C (18–22h); (v) Dioxane, B<sub>2</sub>pin<sub>2</sub>, PdCl<sub>2</sub>(dppf), KOAc, 80 °C, 2 h; (vi) Dioxane/water, PdCl<sub>2</sub>(PPh<sub>3</sub>)<sub>2</sub>, K<sub>2</sub>CO<sub>3</sub>, 80 °C, 5 h.

Briefly, the modified synthetic protocol involves an initial reaction between methyl 2-amino-5-bromobenzoate and ethoxycarbonyl isothiocyanate to form the isolated thioureido intermediate (**6.1**). This intermediate then undergoes cyclization and a simultaneous amide coupling reaction with the appropriate amine using *N*-(3-dimethylaminopropyl)-*N'*-ethylcarbodiimide hydrochloride (EDCI) as a coupling agent in dichloromethane (DCM) at 24°C to yield carbamate intermediates **7.5** and **7.6**. The methyl ester was then cleaved in an acid-catalyzed reaction to afford the 2-aminoquinazolinones **8.5** and **8.6** in quantitative yield (Table 2).

**Table 2:** Isolated percentage yields for **SAR 2** intermediates and target compounds.

					
	R <sub>1</sub>	7	8	9	R
1 (JA045)			55 %	11 %	SOMe
2 (JA051)			69 %	17 %	SOMe
3 (JA055)			40 %	22 %	SOMe
4 (JA056)			42 %	17 %	SOMe
5 (JA049)		98 %	96 %	20 %	SOMe
6 (JA039)		69 %	83 %	11 %	COOH

It was found that some intermediates underwent coupling to the amine but subsequent cyclization was not observed. Therefore, upon substitution of DCM for *N,N*-dimethylformamide (DMF), and allowing the reaction to proceed at 24 – 26°C for 5 hours to form the uncyclised intermediate, the temperature was raised to 100°C under pressure and stirred for 18 – 22 hours. This allowed for intramolecular cyclization and deprotection of the ester to take place resulting in the aminoquinazolinone intermediates **8.1** – **8.4** in one step (iv).

Finally, the **Ar** substituent of the parent compound was incorporated using 3-methylsulfinylphenylboronic acid *via* the Suzuki-Miyaura cross-coupling reaction to obtain final **SAR 2** target compounds **9.1** – **9.5**. The yields of intermediates and target compounds are summarized in Table 2.

Previous attempts at synthesizing **SAR 1** compounds **9.6** and **11** using Scheme 1 were unsuccessful. For this reason, Scheme 2 was adopted in the synthesis of these compounds by incorporating the (trifluoromethyl)aniline at step ii for both **9.6** and **11**.

The carboxylic acid moiety was installed for target compound **9.6** by reacting **8.6** with 3-carboxyphenylboronic acid at step vi. The synthesis of **11** was slightly different in that intermediate **8.6** was transformed into a boronic acid pinacol ester (**10**) using bis(pinacolato)diboron, to which the **Ar** substituent was installed by reacting **10** with 2-bromo-1-methyl-4-(methylsulfonyl)benzene as the aryl halide, under Suzuki-Miyaura cross-coupling conditions to afford target compound **11**.

### 2.3.4. MECHANISTIC DETAILS AND SPECTROSCOPIC ANALYSES OF SAR 2 INTERMEDIATES AND TARGET COMPOUNDS

The key difference between **SAR 1** and **SAR 2** synthetic protocols occurs at step ii in Scheme 2. The proposed mechanism for step ii proceeds via an attack on the electrophilic carbon of EDCI by the nucleophilic quinazolinone sulfur to form an activated thiourea complex. This enables coupling of the appropriate amine at the methylene centre to allow for intramolecular cyclization to occur at the acyl centre, to afford the quinazolinone intermediates **7**, with the loss of methanol (Figure 30).

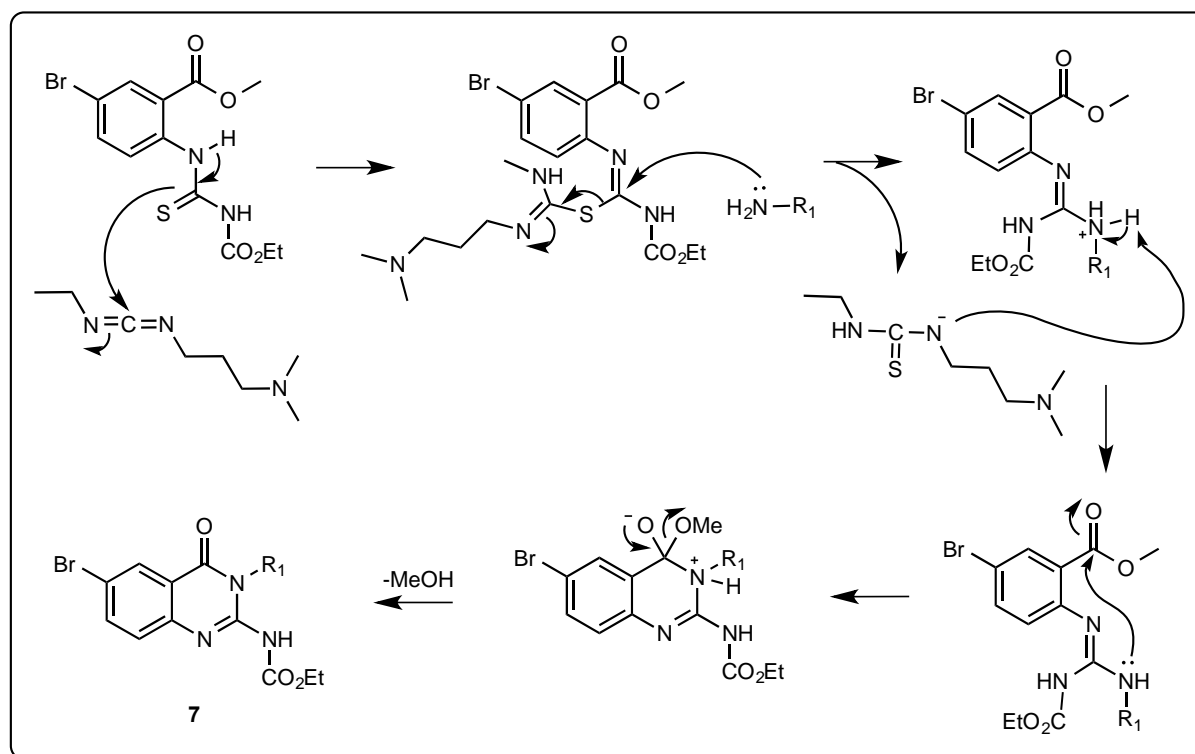


**Figure 30:** Proposed mechanism for step ii, amide coupling and intramolecular cyclization reaction.

Deprotection of the carbamate moiety in DMF at high temperatures in step iv is postulated to be facilitated by the thiourea byproduct formed previously to furnish the corresponding primary amine intermediates (**8**), through a reaction mechanism shown

in Figure 31. The carbamate ester is lost as an ethyl carbocation and the reaction is driven by release of carbon dioxide gas. The anion intermediate formed is resonance stabilized by the conjugation of electrons within the quinazolinone ring.

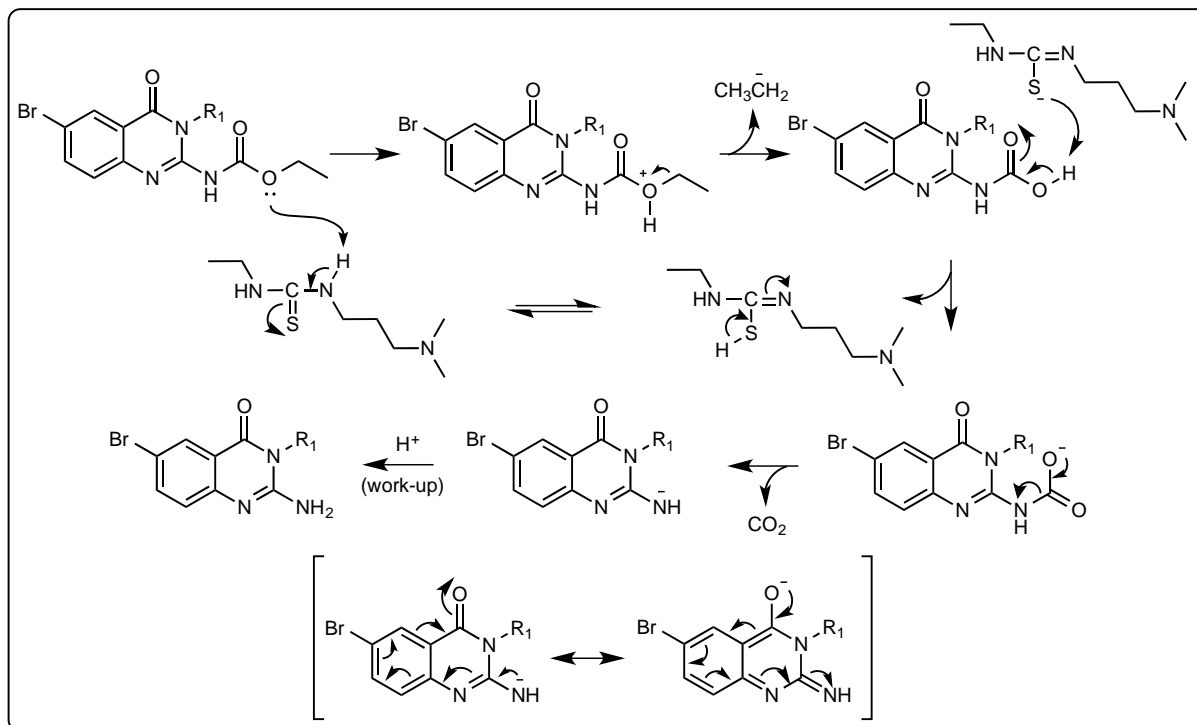


**Figure 31:** Proposed mechanism for the hydrolysis of the carbamate moiety in the formation of the 2-aminoquinazolinone intermediates (**8.1** – **8.4**).

The structures of the **SAR 2** target compounds and their relevant intermediates were confirmed by 1D and 2D NMR experiments. Using intermediate **8.1** as an illustrative example (Figure 32), it is evident that the  $^1\text{H}$  NMR spectra are slightly more complex, particularly in the aliphatic region due to the saturated ring system of the **R**<sub>1</sub> substituents. The splitting pattern observed is due to *cis-trans* isomerism, which occurs in 1,4-disubstituted cyclohexanes due to the relative conformational relationship between substituents on the ring in the chair conformations.

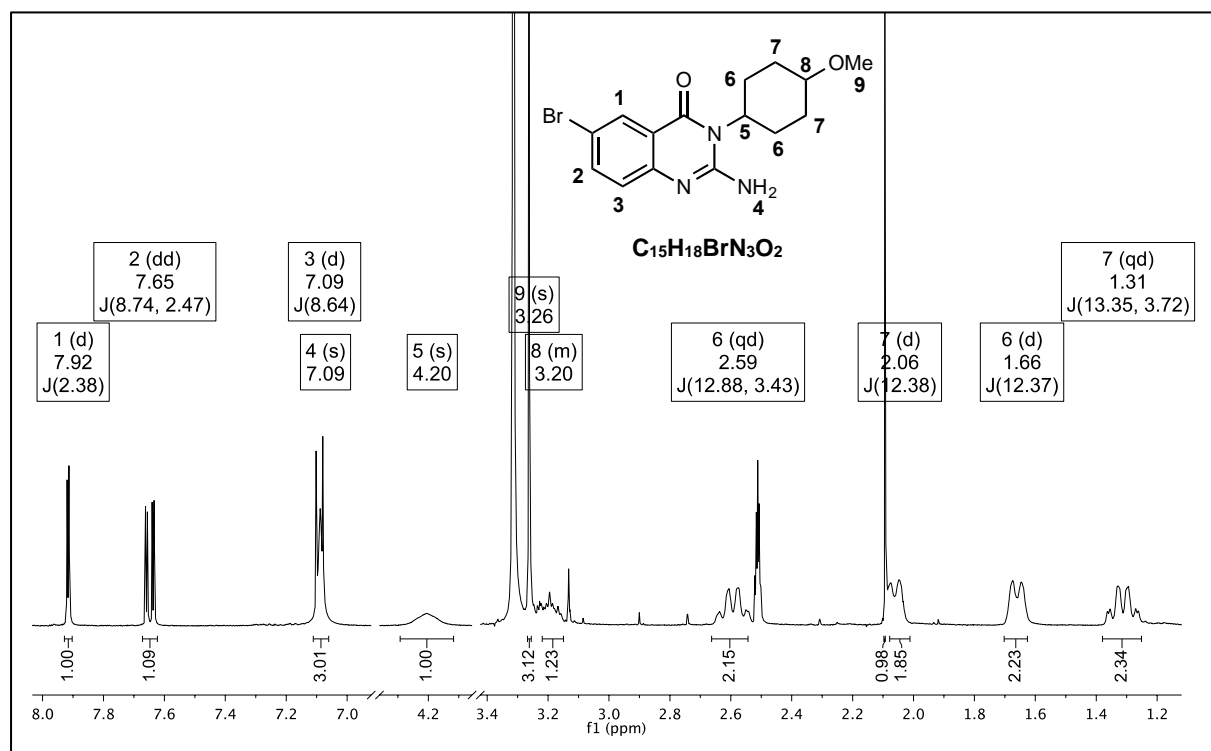


**Figure 32:** <sup>1</sup>H NMR spectrum of SAR 2 compounds, using intermediate 8.1 as an illustrative example.

*Cis*-isomers have substituents pointing in the same direction with both conformational diastereomers having an axial-equatorial relationship at equilibrium (Figure 33.i). Conversely, *trans*-isomers have both substituents either in the axial or in the equatorial positions and pointing in opposite directions (Figure 33.ii). The conformations with substituents in the equatorial position are most energetically favoured and therefore, upon chair-interconversion, the *trans*-isomer with both substituents equatorial is the favoured conformation.

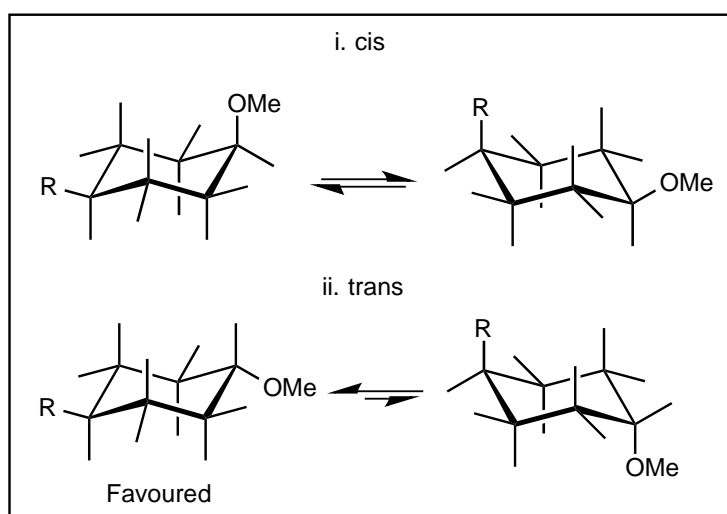


**Figure 33:** *Cis-trans* isomerism of 1,4-disubstituted cyclohexanes upon chair interconversion at equilibrium showing relative stereochemistry of substituents.

The starting materials used to introduce these substituents contained only one isomer and therefore various analytical experiments were performed to confirm the conformation of these 1,4-disubstituted compounds. Liquid chromatography-mass spectroscopy (LCMS) showed the presence of only one isomer as one peak was observed in the chromatogram and this was substantiated by the  $^1\text{H}$  NMR experiment with signals correlating to one compound present. Assignments of axial and equatorial protons on the non-substituted carbons were established from the splitting pattern of these signals in the  $^1\text{H}$  NMR spectra, assisted by HSQC, COSY and (nuclear Overhauser effect spectroscopy) NOESY experiments.

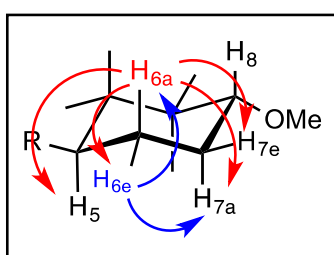


**Figure 34:** Chair conformation of the favoured *trans* isomer with substituents in equatorial position showing coupling interactions of the axial protons (red) and equatorial protons (blue).

Using the favoured *trans*-isomer with substituents in the equatorial positions (Figure 34), axial protons (H-6<sub>ax</sub>) exhibit large coupling values to the neighbouring axial protons (H-7<sub>ax</sub> and H-5) as well as to its geminal proton (H-6<sub>eq</sub>), resulting in a quartet with a *J*-value of 12-13 Hz, as illustrated in Figure 34 in red. Additionally, these axial protons can sometimes experience a small coupling (~3-4 Hz) to the vicinal, equatorial proton (H-7<sub>eq</sub>), resulting in the quartet to split into a quartet of doublets ( $\delta$  2.59) if the resolution of the spectrum is good enough. The equatorial protons (H-6<sub>eq</sub>) therefore exhibit large coupling to its geminal axial protons (H-6<sub>ax</sub>), forming a doublet ( $\delta$  1.66), which can sometimes split into a doublet of doublets if coupling to the vicinal axial proton (H-7<sub>ax</sub>) occurs (Figure 34 in blue).

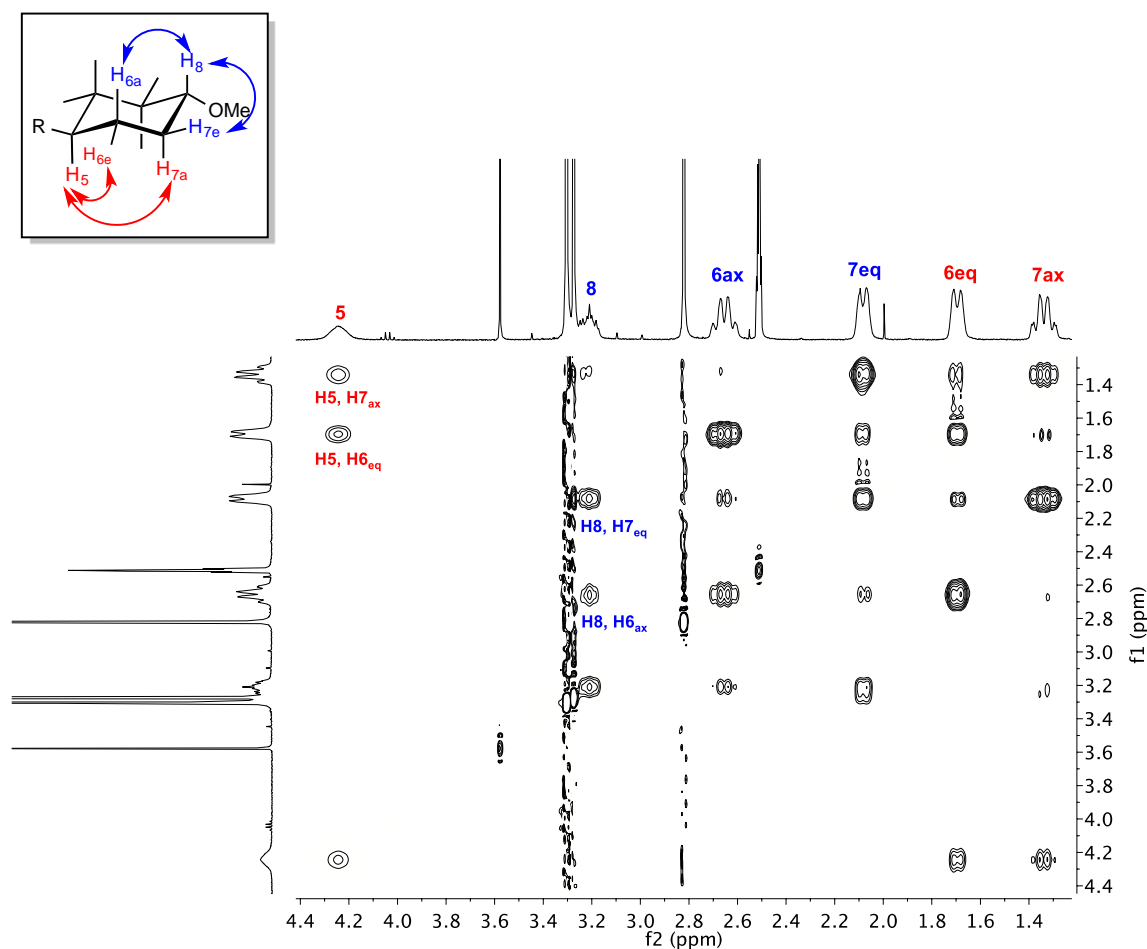


**Figure 35:** Extract from NOESY experiment of **8.1** to establish relative through-space interactions of the substituted protons to determine their *cis* or *trans* relationship.

In order to establish the relative relationships between substituents, NOESY experiments were used as this technique determines through-space correlations between protons. Looking at the signals for the protons on the substituted carbons (H-5 and H-8) in Figure 35, it can be observed that they exhibit through-space correlations with different pairs of protons, suggesting that they point in opposite directions i.e. *trans*-isomer. Using the favoured *trans*-isomer with substituents in the equatorial positions, through-space interactions of H-5 with H-6<sub>eq</sub> and H-7<sub>ax</sub> are observed, whereas H-8 experiences correlations with H-6<sub>ax</sub> and H-7<sub>eq</sub>. This confirms that the *trans*-isomer with both substituents in the equatorial position as the product.

## 2.4. PHARMACOLOGICAL EVALUATION OF TARGET COMPOUNDS

The biological evaluation of synthesized target compounds were determined using various assessments as outlined in the screening cascade depicted in Figure 36. Once synthesized, all compounds were submitted for antimycobacterial evaluation as well as solubility studies using turbidimetric and kinetic solubility assays. Potent analogues that inhibit *Mtb* growth with 99% inhibition at a minimum concentration ( $MIC_{99}$ ) of  $10\mu M$  or less were further evaluated for cytotoxicity against the mammalian Chinese Hamster Ovarian (CHO) cell line. If found to have an acceptable cytotoxicity profile, they were assessed for microsomal metabolic stability whereby analogues with more than 75% of its parent compound present after 30 minutes are deemed metabolically stable. Compounds that fulfill these criteria would be further screened for *in vivo* pharmacokinetics to establish properties such as bioavailability (F), exposure (AUC) and clearance (Cl) for the eventual efficacy studies in a mouse model. However, these assays were not carried out in this research as it was beyond the scope of the project.

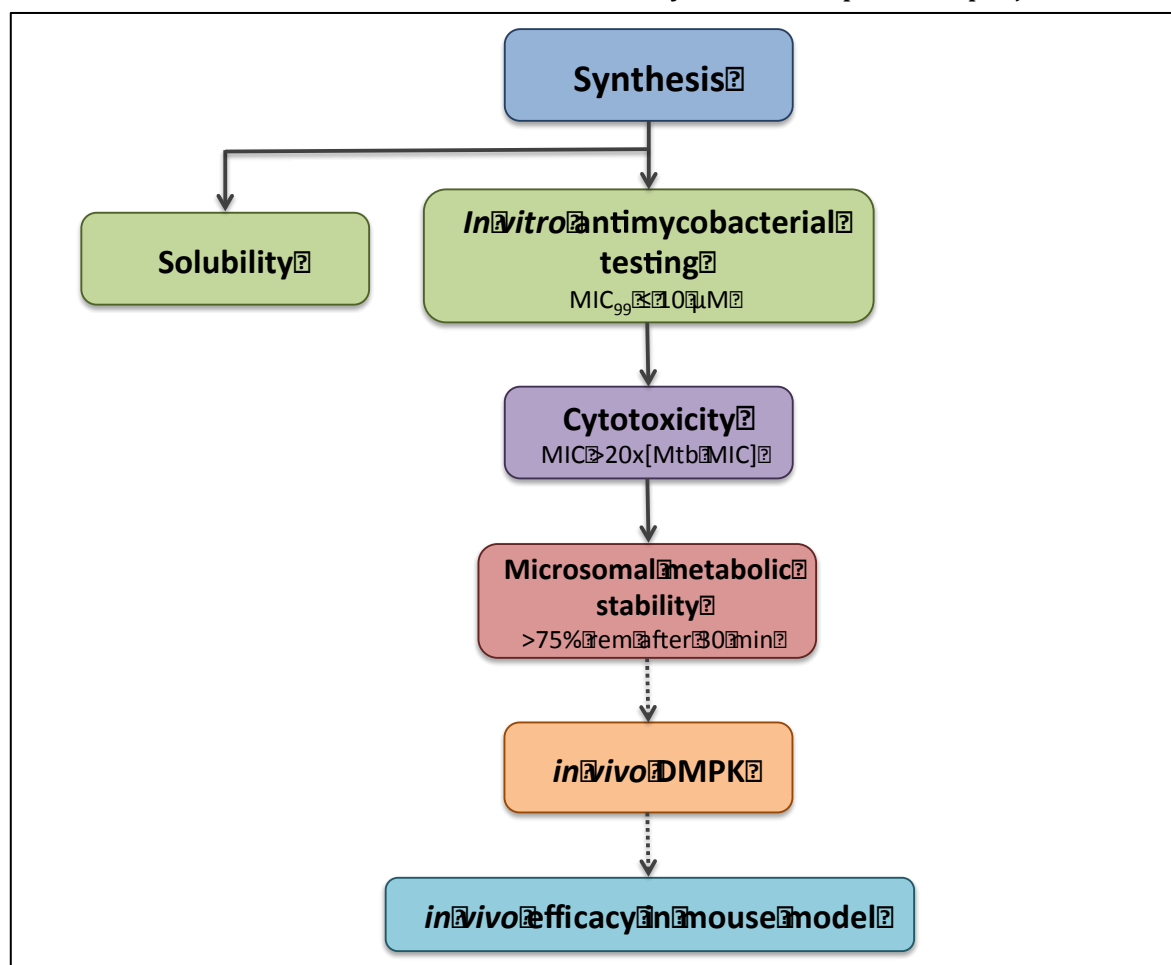


**Figure 36:** Screening cascade outlining the criteria for progression of work-flow from synthesis to *in vitro* microsomal metabolic stability.

### 2.4.1. *IN VITRO* ANTIMYCOBACTERIAL ACTIVITY AND CYTOTOXICITY

Synthesized **SAR 1** target compounds were submitted for antimycobacterial activity evaluation against the H37Rv strain of *Mtb*. Studies were performed in both GAST Fe and 7H9 ADC media and reported as MIC<sub>99</sub> values at day 14 (Table 3).

**Table 3:** Pharmacological activity and cytotoxicity of **SAR 1** compounds.

Compound (Code)	Ar	Variables	<i>In vitro</i> antimycobacterial activity MIC <sub>99</sub> (μM)		Cytotoxicity CHO: IC <sub>50</sub> (μM)
			GAST Fe Day 14	7H9 ADC Day 14	
5.1 (JA025)			<0.244	2.28	190
5.2 (JA010)			0.64	1.36	>226
5.3 (JA013)			2.35	1.28	0.021 ± 0.0048
11 (JA038)			4.22	0.19	>100
5.4 (JA018)		Y = CH, X = O	4.93	1.73	8.77 ± 1.08
5.5 (JA019)		Y = CH, X = S	0.656	0.351	>50
5.6 (JA020)		Y = CH, X = NMe	1.57	1.54	>50
5.7 (JA021)		Y = N, X = O	83	69.5	ND
5.8 (JA017)		Y = CH, R = R' = H	0.92	< 0.244	>236
5.9 (JA022)		Y = CH, R = H, R' = Me	0.78	< 0.244	96.3 ± 1.05
5.10 (JA023)		Y = N, R = H, R' = Me	9.22	4.13	ND
5.11 (JA016)		Y = CH, R = R' = Me	2.15	3.41	0.64 ± 0.12
9.6 (JA039)			112	8.1	>50
<b>Control</b>			Rifampicin		Emetine
			0.00213	0.00218	0.018 ± 0.004

ND = Not Determined

The *in vitro* antimycobacterial activity results depicted in Table 3 generally indicate comparable MIC<sub>99</sub> values across all compounds (<10 μM), exhibiting promising inhibitory effects on the H37Rv strain of *Mtb*, with the exception of **5.7** and **9.6**. Upon observation of trends within different groups of compounds, the addition of the cyclopropyl moiety (**5.3**) in the sulfone series, as well as the introduction of a methyl substituent in the *ortho*-position of the biaryl moiety (**11**), resulted in compounds with comparable activity to the sulfone **5.1** and sulfoxide **5.2** parent compounds, in the 7H9 media in particular.

Comparing the activity of heterocyclic amides **5.4** – **5.7**, excellent inhibitory effects were shown by thiomorpholine **5.5**, followed by the methylpiperazine **5.6** in both media. The pyridinyl derivative (**5.7**) was found to be the least active of this series.

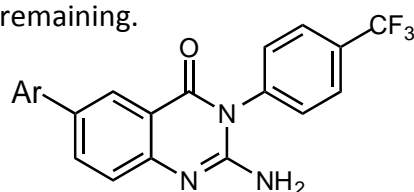
The amide analogues followed the trend of NMe<sub>2</sub> (**5.11**) > NH<sub>2</sub> (**5.8**) > NHMe (**5.9**) in GAST Fe media, with the secondary amine (**5.9**) displaying the most promising activity of the amide series. However, a slight loss of activity was observed for **5.10** upon replacement of the phenyl ring (Y = C) with a pyridinyl ring (Y = N) in both media. Moving from the amides to the carboxylic acid derivative (**9.6**) resulted in relatively poor activity, especially in the GAST Fe media.

According to the screening cascade in Figure 36, compounds that exhibited promising antimycobacterial activity (MIC<sub>99</sub> ≤ 10 μM) were selected for cytotoxicity evaluation against a mammalian cell-line, CHO, using Emetine as a reference control. With the exception of compounds **5.3**, **5.4** and **5.11**, all other target compounds displayed low cytotoxicity (Table 3).

## 2.4.2. MICROSOMAL METABOLIC STABILITY

The *in vitro* microsomal metabolic stability of a selected sample of **SAR 1** compounds with *in vitro* antimycobacterial activity of MIC<sub>99</sub> less than 10 µM, was determined in human liver microsomes (HLM), rat liver microsomes (RLM) and mouse liver microsomes (MLM). Samples were incubated for 30 minutes and analysed by high performance liquid chromatography-mass spectrometry (HPLC-MS/MS) to determine the percentage remaining.

**Table 4:** Microsomal metabolic stability results of selected **SAR 1** compounds, reported as a percentage of concentration remaining.



Compound	Ar	Variable	Metabolic Stability (% Remaining)		
			HLM	RLM	MLM
5.1 (JA025)			97.0	100	92.0
5.2 (JA010)			73.0	ND	ND
5.3 (JA013)			85.0	97.6	97.1
11 (JA038)			64.8	85.8	89.9
5.4 (JA018)		Y = CH, X = O	71.0	76.9	77.6
5.5 (JA019)		Y = CH, X = S	83.0	22.9	22.0
5.6 (JA020)		Y = CH, X = NMe	96.6	85.5	93.8
5.8 (JA017)		Y = CH, R = R' = H	88.0	ND	ND
5.9 (JA022)		Y = CH, R = H, R' = Me	97.6	100	100
5.11 (JA016)		Y = CH, R = R' = Me	85.0	86.3	88.5
9.6 (JA039)			98.7	97.0	98.4

ND = Not Determined

A value of more than 75% concentration of tested compound remaining is within acceptable limits, based on the screening cascade in Figure 36. Therefore, results obtained in Table 4 suggest good metabolic stability of **SAR 1** compounds in liver microsomes across the three species.

The morpholine derivatives **5.4** and **5.6** were moderately stable across all species. However, thiomorpholine **5.5** shows high metabolic stability in HLM but displays substantial instability in RLM and MLM. This difference may be due to differences in CYP enzymes across species that are responsible for specific reactions. Metabolite identification studies would need to be performed to ascertain precise metabolic reactions, and where they are occurring on the molecule.

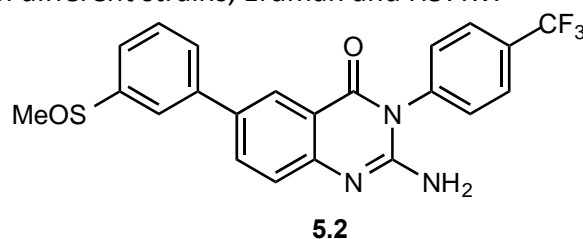
Suffice to conclude that several compounds could be evaluated *in vivo* as they would be expected to have good exposure in mice based on the metabolic stability data in MLM.

### 2.4.3. EVALUATION OF GLYCEROL DEPENDENCY

#### 2.4.3.1. Glycerol-Free *in vitro* Assays

Despite exhibiting favourable *in vitro* potency and PK properties, compound **5.2** failed to show *in vivo* efficacy in the acute mouse TB model. As a result, further studies into the *in vitro* assays were explored in an effort to understand the lack of *in vivo* efficacy. One possible hypothesis for the lack of *in vivo* efficacy might be due to differences in carbon sources for *Mtb* under *in vitro* conditions and *in vivo* in mice. For this reason, collaborators at Colorado State University (CSU) subsequently retested compound **5.2** in different carbon source media, which contained 7H12 broth media, casitone, palmitic acid, bovine serum albumin (BSA), catalase and Tween-80, as well as two different *Mtb* strains were explored, Erdman and H37Rv (Table 5).

**Table 5:** *In vitro* MIC results for compound **5.2** from CSU using glycerol-containing and glycerol-free media with different strains, Erdman and H37Rv.



Strain	Media	MIC in mg/L for:		
		5.2	Rifampin	Isoniazid
Erdman	7H9 + glycerol + ADC	1	0.03	0.016
H37Rv	7H9 + glycerol + ADC	0.5	0.016	0.016
Erdman	7H12 + casitone + palmitic acid + BSA + catalase + Tween-80	>16	<0.008	0.016
H37Rv	7H12 + casitone + palmitic acid + BSA + catalase + Tween-80	>16	<0.008	0.016

MIC assays repeated in 7H9, glycerol and ADC media revealed similar activity to those reported from UCT, with **5.2** shown to be active only in glycerol-containing media.

To further substantiate these findings, collaborators at the National Institute of Allergy and Infectious Diseases (NIAID) performed further *in vitro* assays on 11 additional

“active” **SAR 1** aminoquinazolinones (Figure 37) in media containing glucose as the carbon source in 7H9 broth with BSA or casitone as the amino acid source and tyloxapol as the surfactant component. Consistent with data obtained at CSU, these were also found to lack activity ( $MIC_{99} > 50 \mu M$ ) in the absence of glycerol in the culture medium.

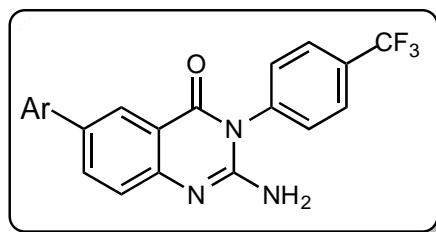


**Figure 37:** General structure of **SAR 1** analogues with varying **Ar** substituents.

Whilst *in vivo* studies were being investigated, some **SAR 2** compounds were simultaneously synthesized and tested for *in vitro* antimycobacterial activity utilizing new media (GAST Fe and 7H9 Glu ADC) containing glucose as the carbon source. All intermediates and target compounds of the **SAR 2** series (Figure 38) exhibited poor activity ( $MIC_{99} > 50 \mu M$ ), possibly suggesting dependency on glycerol in the media for inhibition of *Mtb* growth.

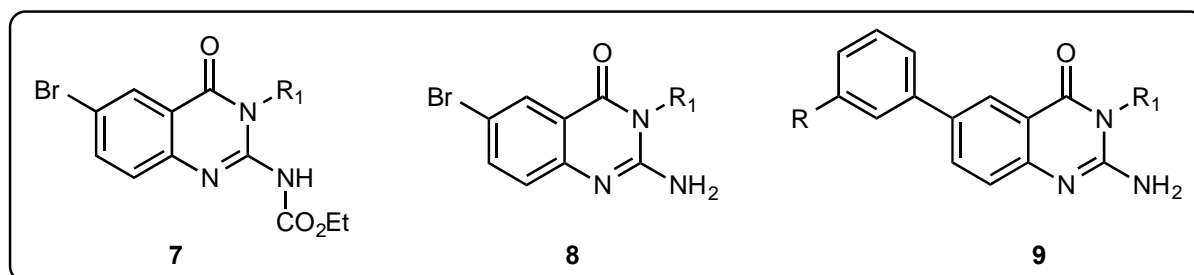


**Figure 38:** General structures of intermediates **7 – 8** and target compounds **9.1 – 9.5** that were evaluated for *in vitro* antimycobacterial activity in glycerol-free media.

There are many factors that contribute to the growth of *Mtb* *in vitro* and *in vivo*, one of which is the presence of a suitable carbon source as carbon metabolism plays a major role in the ability of *Mtb* to replicate and persist in the host. Therefore, it is able to metabolically adapt to the host’s environments depending on the nutrients available, as *Mtb* is capable of oxidizing multiple carbon sources. This ability is key to the pathogenicity of *Mtb*.<sup>60</sup>

Despite *Mtb* being able to grow on a variety of carbon sources *in vitro*, glycerol has long been the preferred source of energy and carbon for *Mtb* under *in vitro* conditions and is therefore present in most standard growth media.<sup>61</sup>

The discrepancy between the *in vitro* activity and *in vivo* efficacy of the aminoquinazolinone series was explained by a major difference in carbon metabolism between bacteria replicating in a standard broth medium as compared to an infected host.<sup>61</sup> The lack of *in vivo* efficacy of aminoquinazolinone compound **5.2** suggests that glycerol is not a carbon source either readily available, or primarily used by *Mtb* in mouse lungs and that the aminoquinazolinone series exert their inhibitory effect *in vitro* by dysregulating the glycerol dissimilation pathway.<sup>62</sup> This data is consistent with that reported by researchers at the Novartis Institute of Tropical Diseases (NITD) in 2010.<sup>61</sup>

The presence of glycerol in the media leads to the build up of glycerol-3-phosphate (G3P) and dihydroxyacetone phosphate (DHAP) by these compounds which induces toxic consequences to *Mtb* as accumulation of sugar phosphates is known to be highly toxic for most bacteria.<sup>61</sup> Previous studies showed that compounds with glycerol-specific activity promote the accumulation of G3P resulting in a rapid depletion of adenosine triphosphate (ATP) utilized for phosphorylation of glycerol essentially leading to self-poisoning of *Mtb*.<sup>61,63</sup>

These results highlight the importance of validating the relevance of *in vitro* assay conditions to reproduce the environment encountered by *Mtb* in the infected host.<sup>61,62</sup>

## 2.5. CONCLUSIONS

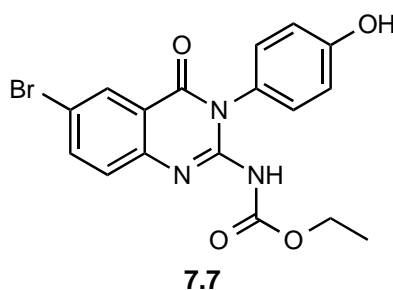
In summary, 18 aminoquinazolinone target compounds were successfully synthesized and characterized. Of these, 13 **SAR 1** compounds were evaluated for antimycobacterial activity in glycerol-containing media with 11 of them showing promising activity. These were subsequently evaluated for cytotoxicity and microsomal metabolic stability. Retesting of **SAR 1** and **SAR 2** intermediates and target compounds in glycerol-free media revealed inactivity of all target compounds, suggesting glycerol-dependency of the aminoquinazolinone series.

## CHAPTER 3: SYNTHESIS AND BIOLOGICAL EVALUATION OF ACTIVE AMINOQUINAZOLINONE INTERMEDIATE ANALOGUES

### 3.1. BACKGROUND INFORMATION

Approximately 90 aminoquinazolinone analogues were collectively synthesized by other members of our team. Of these, 35 analogues showed moderate to excellent *in vitro* antimycobacterial activity in various glycerol-containing media. All intermediates and target compounds were subsequently retested in glycerol-free *in vitro* assays with all, but one intermediate **7.7** (Table 6), displaying complete loss of activity ( $MIC_{99} > 50$ ).

**Table 6:** *In vitro* antimycobacterial activity results for intermediate **7.7** against *Mtb* (H37Rv) in a variety of media.



<i>In vitro</i> antimycobacterial activity, $MIC_{99}$ ( $\mu M$ )			
GAST Fe	7H9 ADC	7H9/glucose/BSA/ tyloxapol	7H9/glucose/ casitone/tyloxapol
Day 7/Day 14	Day 7/Day 14	Day 7/Day 14	Day 7/Day 14
1.2 / 1.56	1.2 / 1.56	6.25 / 3.13	2.3 / 4.7

This chapter therefore describes the synthesis and characterization of derivatives of **7.7**, exploring variations in regioisomers and hydrogen-bonding properties towards establishing whether or not antimycobacterial activity can be retained in glycerol-free media.

### 3.2. TARGET AMINOQUINAZOLINONE INTERMEDIATE ANALOGUES

Structural modifications were envisaged on **7.7** focusing on three points of diversity (**SAR 3**, **SAR 4** and **SAR 5**) for the synthesis of new analogues (Figure 39).

Analogues for **SAR 3** involved structural modifications at  $R_2$  whilst the carbamate and bromo substituents of the quinazolinone core remained fixed. From the previous results,

it was observed that the phenol group was essential for activity. Therefore regioisomers with the hydroxyl moiety in the *ortho*- and *meta*-positions around the ring were targeted. Additionally, alternative HBD substituents were employed (eg. NH<sub>2</sub>). Since compound **7.7** possessed poor solubility (kinetic solubility at pH 7.4 <5) the solubility improvement strategy of removing aromaticity was again investigated. In **SAR 4**, bromo regioisomers were explored.

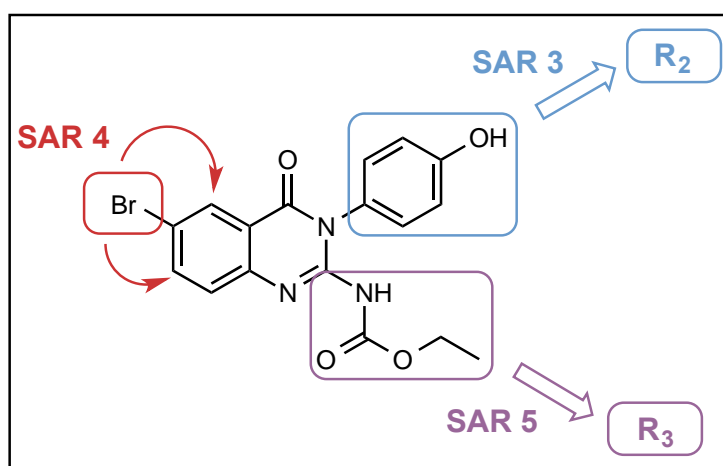


**Figure 39:** Chemistry design for planning the synthesis of quinazolinone analogues derived from **7.7** with three points of diversity around the core.

**SAR 5** explored variations of the carbamate moiety. Upon reviewing the literature on quinazolinones, work reported by Khadka and coworkers describe the synthesis of 2-arylquinazolinones as potential inhibitors of topoisomerases for the treatment of cancer.<sup>64</sup> These structures were therefore incorporated into **SAR 5** to determine whether replacement of R<sub>2</sub> substituents into the R<sub>3</sub> position would have any antimycobacterial effects. Feasibility of the synthesis of such derivatives was also considered for all **SAR 5** analogues.

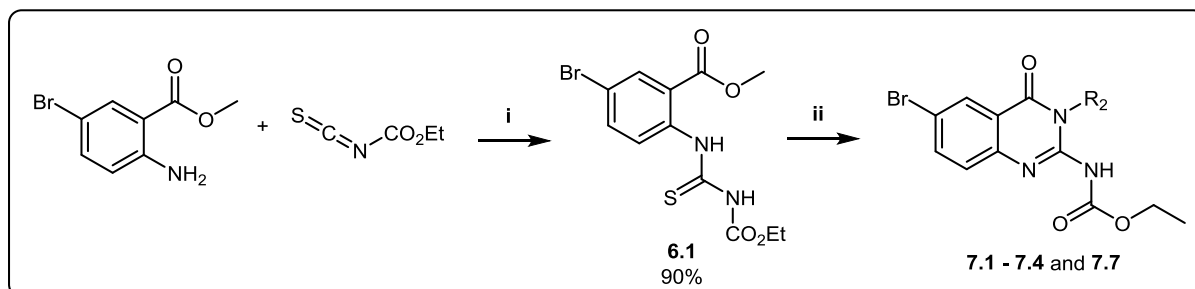
### 3.3. SYNTHESIS AND SPECTROSCOPIC CHARACTERIZATION OF AMINOQUINAZOLINONE INTERMEDIATES

#### 3.3.1. SAR 3 TARGET COMPOUNDS

The synthesis of **SAR 3** and **SAR 4** derivatives were adapted from the protocol outlined in synthetic Scheme 3. Since the carbamate moiety was to remain fixed, only the first two steps of the synthesis were required.

Essentially, the synthesis involved the formation of a thioureido intermediate **6.1**, as described previously, which precipitates out of the acetonitrile solution. Once isolated,

this intermediate and the appropriate amine were dissolved in either DCM or DMF, depending on their solubilizing ability, and were subsequently treated with the coupling agent, EDCI, to produce the desired cyclic target compounds **7.1** – **7.4** and **7.7** in low to high yields (Table 7).



**Scheme 3:** General synthetic protocol towards **SAR 3** compounds **7.1** – **7.4** and **7.7**. *Reagents and conditions:* (i) Acetonitrile, 24°C, 30 min; (ii) DCM/DMF, R<sub>2</sub>NH<sub>2</sub>, EDCI, 21 – 25°C, 18 h.

**Table 7:** Isolated percentage yields for **SAR 3** target compounds.

Compound	R <sub>2</sub>	Percentage Yield (%)
<b>7.1</b> <b>(JA060)</b>		38
<b>7.2</b> <b>(JA059)</b>		31
<b>7.3</b> <b>(JA057)</b>		47
<b>7.4</b> <b>(JA062)</b>		81
<b>7.7</b> <b>(JA061)</b>		62

The NMR spectra of **SAR 3** analogues have key diagnostic signals occurring in the aromatic region due to changes in the R<sub>2</sub> position, with the appearance of aliphatic signals for **7.3** as a result of the introduction of a saturated ring. The core quinazolinone and carbamate signals remain constant as shown by new hit compound **7.7** (Figure 40). Analogues with *para*-substituted R<sub>1</sub> substituents (**7.4** and **7.7**) exhibited an AB splitting of signals corresponding to H-7 and H-8 in the aromatic region as seen with **SAR 1** derivatives.

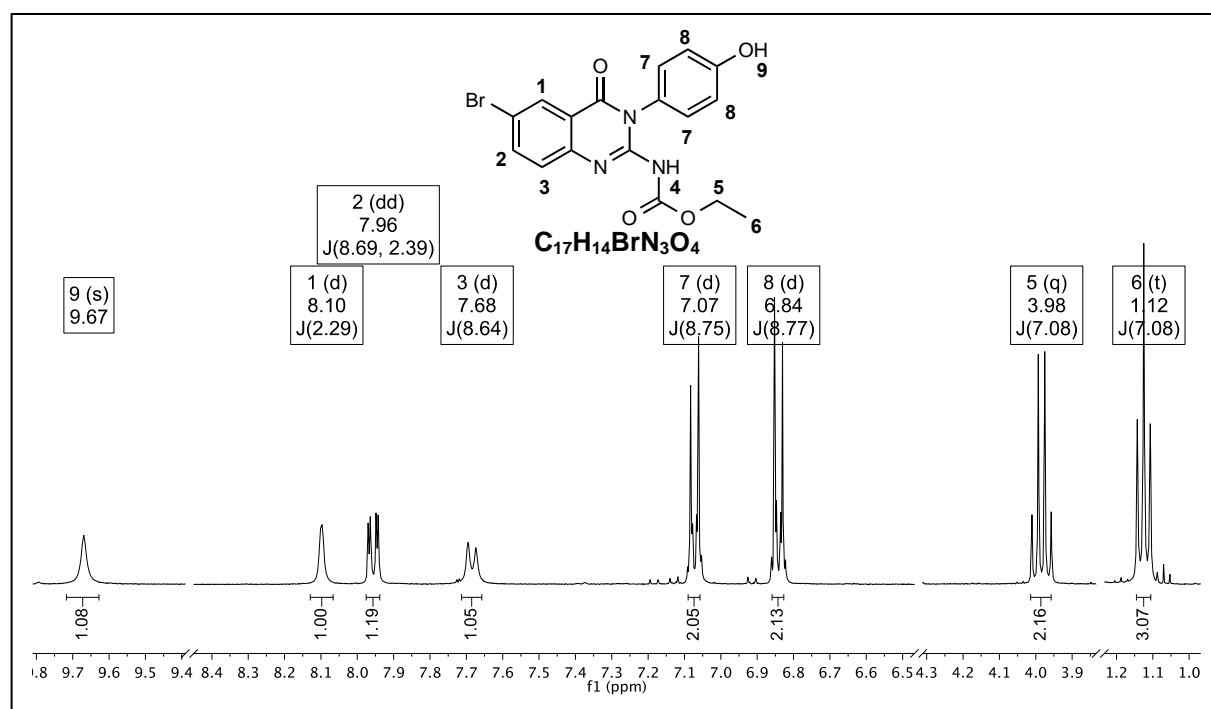


**Figure 40:** <sup>1</sup>H NMR spectrum of new hit compound **7.7**.

Displacement of the hydroxyl group around the ring for analogues **7.1** (*ortho*) and **7.2** (*meta*) resulted in a change in the characteristic aromatic signals due to removal of the axis of symmetry. Using **7.2** as an example (Figure 41), four proton signals appear in the  $\delta$  6.7 – 7.3 region, with long-range coupling (<sup>4</sup>J) being observed between H-7, H-9 and H-10. Assignment of H-7 and H-9 was established from 2D HMBC NMR experiments.

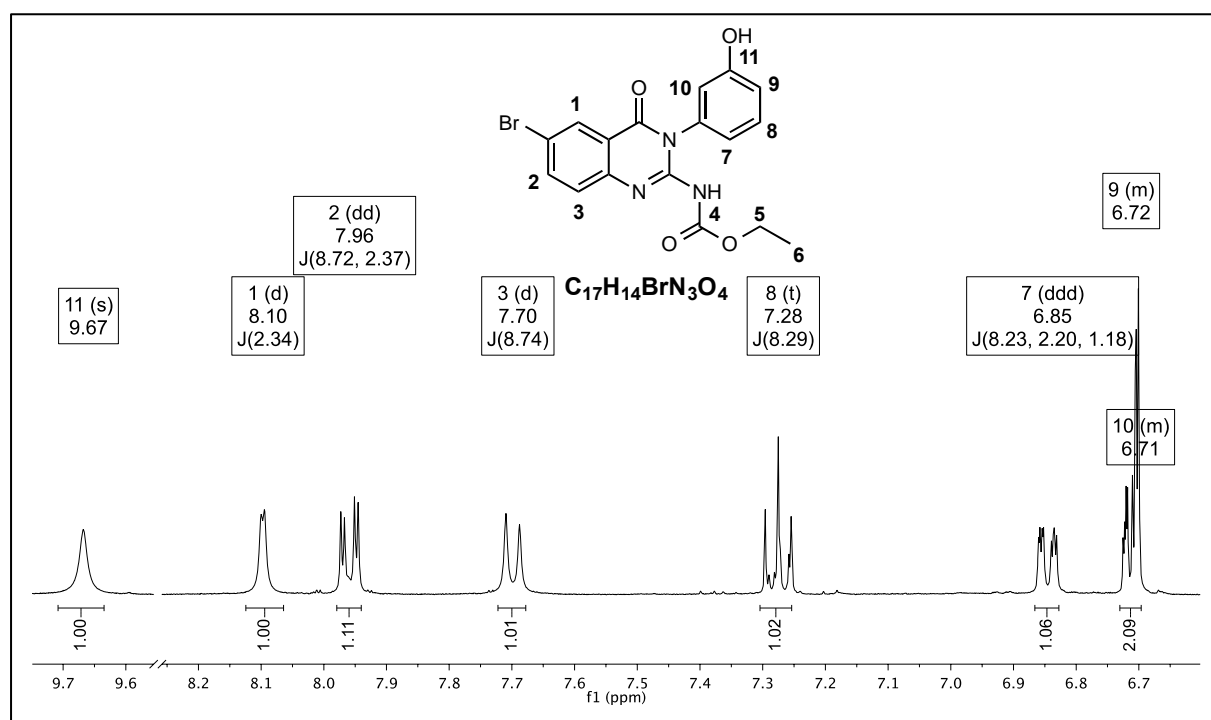


**Figure 41:**  $^1H$  NMR spectrum of saturated phenol derivative **7.2**.

Removal of aromaticity for **7.3** resulted in the appearance of axial-equatorial coupling pattern for H-8 and H-9 in the aliphatic region due to *cis-trans* isomerism, as observed for **SAR 2** compounds. Interestingly, a triplet of doublets is observed for H-10 at  $\delta$  3.44 due to large coupling to neighboring H-9<sub>ax</sub> protons ( $^3J = 10.99$ ) to form a triplet with additional coupling to the hydroxyl proton, which results in the splitting of the triplet into doublets to form a td splitting pattern (Figure 42). Relative stereochemistry was established by the amine starting material used with confirmation of axial/equatorial proton signals determined from 2D NMR, specifically NOE spectroscopy, as described previously in Chapter 2 (Figure 35).

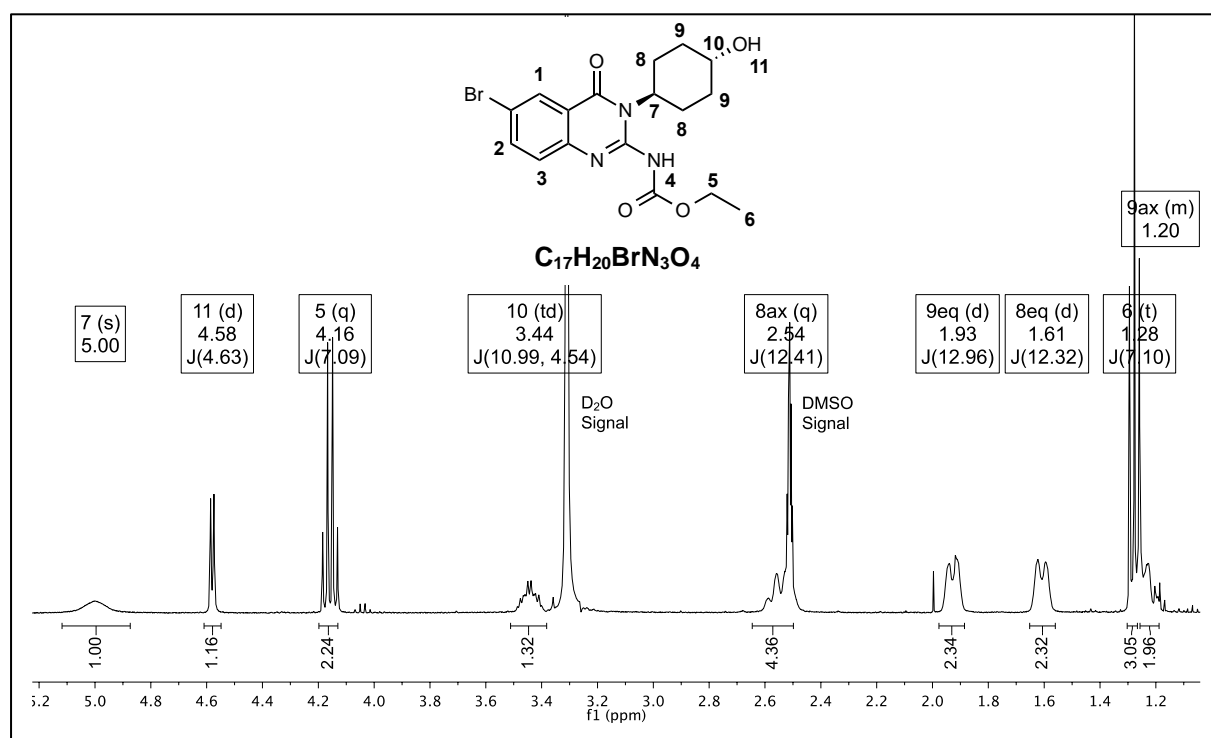
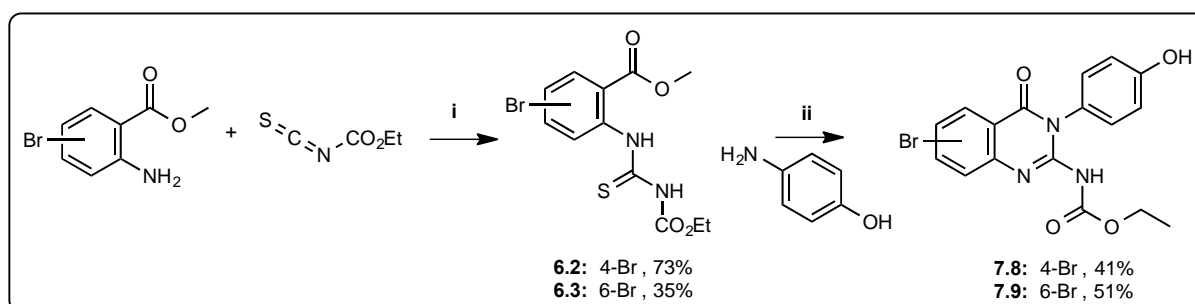


**Figure 42:** <sup>1</sup>H NMR spectrum of saturated **SAR 3** analogue **7.3**.

### 3.3.2. SAR 4 TARGET COMPOUNDS

The synthesis of **SAR 4** analogues differs from that previously described for **SAR 2** and **SAR 3** as it utilizes methyl 2-amino-4-bromobenzoate and methyl 2-amino-6-bromobenzoate as starting materials. Compounds **7.8** and **7.9** were formed by reacting the resulting thioureido intermediates **6.2** and **6.3** with 4-aminophenol in a cyclization and amide coupling reaction with moderate yields (Scheme 4). The synthesis of **SAR 3** and **SAR 4** compounds follow closely to the first two steps of **SAR 2**, and the mechanism for such compounds was described previously in Figure 30.



**Scheme 4:** General synthetic protocol towards **SAR 4** compounds **7.8** and **7.9**. *Reagents and conditions:* (i) Acetonitrile, 24°C, 30 min; (ii) DCM, EDCl, 21 - 25°C, 18-22 h.

Key structural changes to the quinazolinone core brought about by **SAR 4** analogues can be illustrated using  $^1\text{H}$  NMR spectra of intermediates **6.2** and **6.3**. Using **6.1** as a reference in Figure 43, the order of chemical shift signals in the aromatic region remain relatively the same with varying splitting patterns, depending on its neighboring protons.

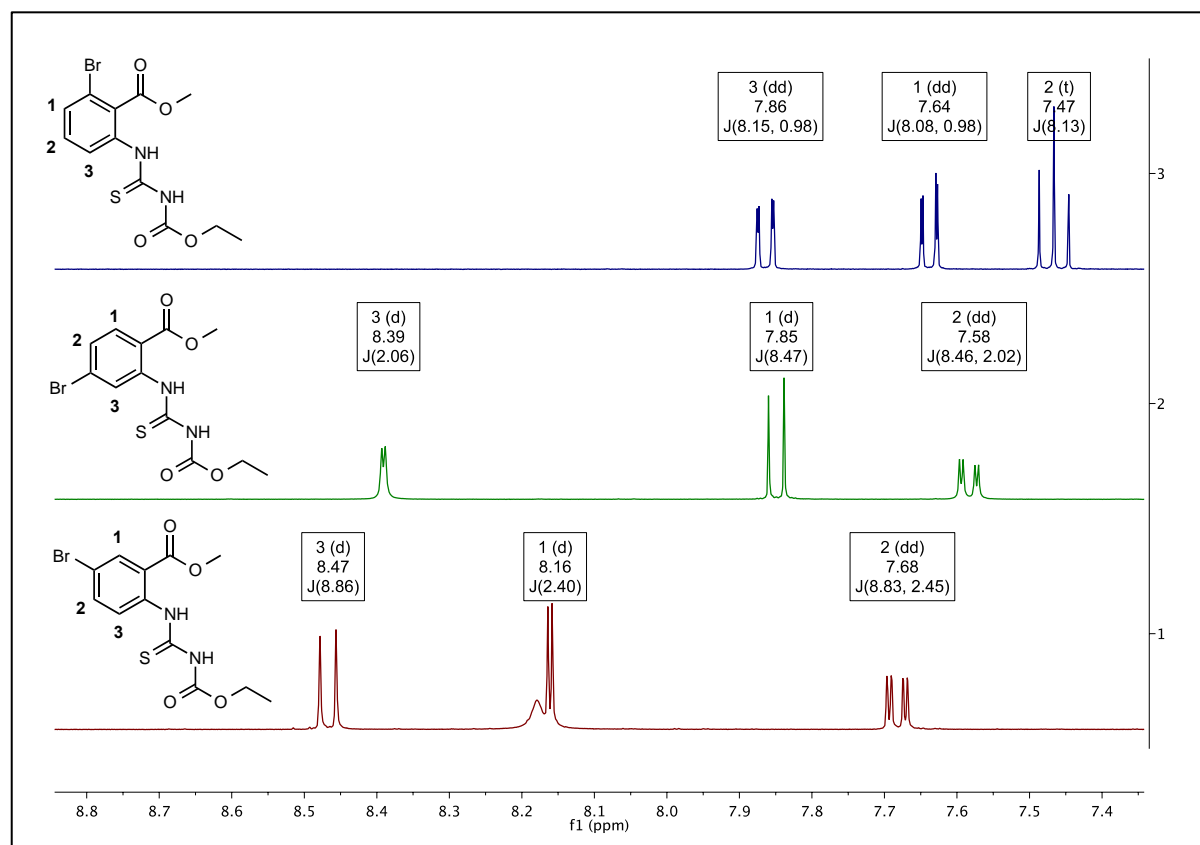
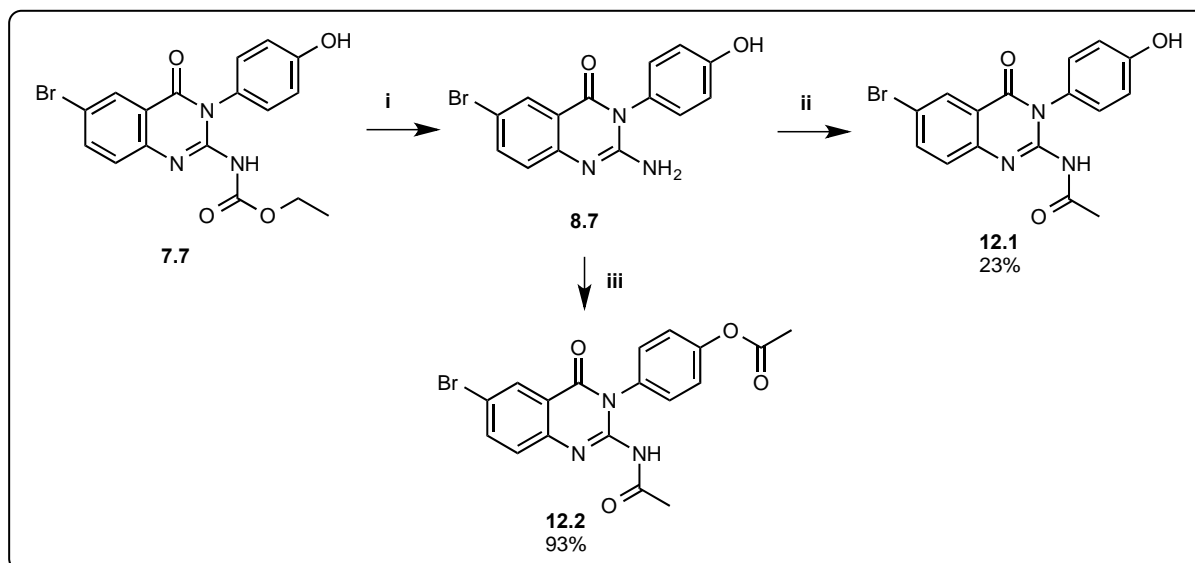


**Figure 43:** Stacked  $^1\text{H}$  NMR spectra of **SAR 4** intermediates, **6.2** (2) and **6.3** (3), indicating key structural changes to the quinazolinone core in comparison to **6.1** (1).

### 3.3.3. SAR 5 TARGET COMPOUNDS

The synthesis of compounds **12.1** and **12.2** utilizes compound **7.7** (Scheme 5) and further diversifies the carbamate moiety by initially cleaving the methyl ester off via an acid catalyzed reaction with TFA to form the 2-aminoquinazolinone intermediate **8.7**. The intermediate was then heated in acetic anhydride to 100°C to acetylate the amine in the 2-position. It was found that upon heating the solution to reflux, acetylation also occurred at the phenol moiety (**12.1**) and the diacetylated byproduct **12.2** was subsequently isolated and incorporated into **SAR 5**.



**Scheme 5:** General synthetic protocol towards SAR 5 compounds **12.1** and **12.2**. Reagents and conditions: (i) TFA, MW 110 °C, 60 min; (ii) Ac<sub>2</sub>O (1.1 Eq.), 100 °C; 2 h (iii) Ac<sub>2</sub>O (2.0 Eq.), 140 °C, 20 h.

Replacement of the carbamate moiety resulted in changes in the aliphatic region. Initial addition of a single acetyl group to the more susceptible amine was confirmed by the appearance of a singlet at  $\delta$  1.87 (Figure 44-2), whilst the OH signal ( $\delta$  9.76) remained in place. Two methyl singlets at  $\delta$  2.20 and  $\delta$  2.31, with the disappearance of the hydroxyl proton signal (Figure 44-3) provided evidence for the diacetylated product. The phenol proton signal patterns differ in that when the hydroxyl group is in place (Figure 44-1 and 44-2), H-6's and H-7's are chemically equivalent but magnetically non-equivalent, resulting in distorted doublet of doublets. The addition of the acetyl group results in overlap of H-6 and H-7 signals due to chemical and magnetic equivalence, forming a distorted singlet.

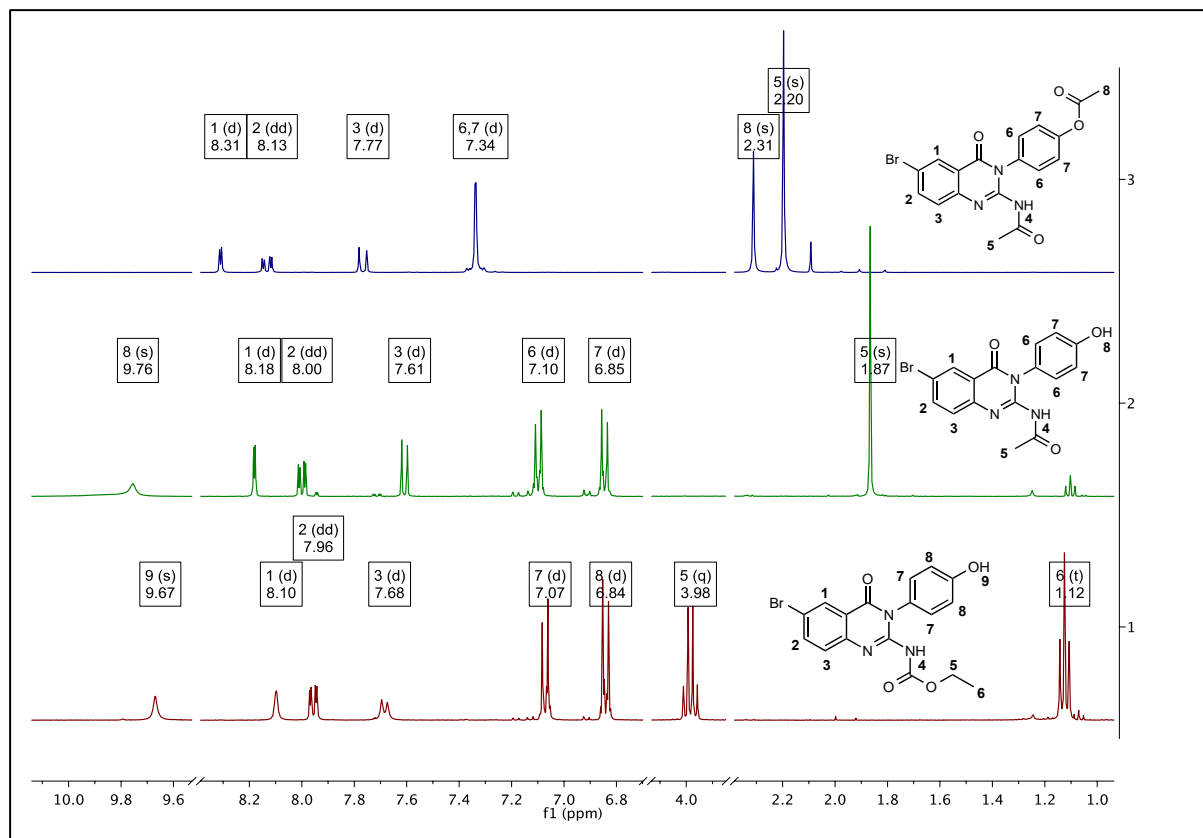
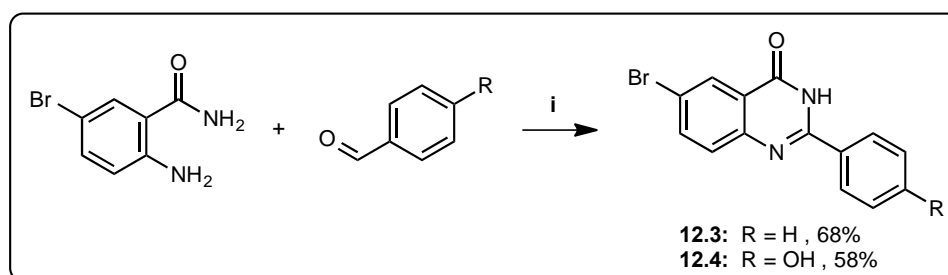


**Figure 44:** Stacked  $^1\text{H}$  NMR spectra of SAR 5 compounds, **12.1** (2) and **12.2** (3) indicating key changes in comparison to **7.7** (1).

The synthesis of 2-arylquinazolinone analogues **12.3** and **12.4** outlined in Scheme 6 involves a thermal cyclodehydration/dehydrogenation reaction between bromo-substituted anthranilamides and different benzaldehydes in the presence of *N,N*-dimethylacetamide and sodium bisulfate.



**Scheme 6:** General synthetic protocol towards SAR 5 compounds **12.3** and **12.4**. Reagents and conditions: (i) *N,N*-dimethylacetamide,  $\text{NaHSO}_4$ ,  $150\text{ }^\circ\text{C}$ , 3 h.

The mechanism for the cyclodehydration/dehydrogenation reactions is initiated by the protonation of the aldehyde by NaHSO<sub>4</sub> to activate the carbonyl moiety and make it more susceptible to attack by the neutral amine nucleophile. Following nucleophilic addition to the electrophilic carbonyl carbon, proton transfer allows for the formation of a better leaving group, enabling attack of the amide nitrogen to the electrophilic acyl centre in a dehydration step. Dehydrogenation by NaSO<sub>4</sub><sup>-</sup> and water provides the desired 2-arylquinazolinone products **12.3** and **12.4** (Figure 45).

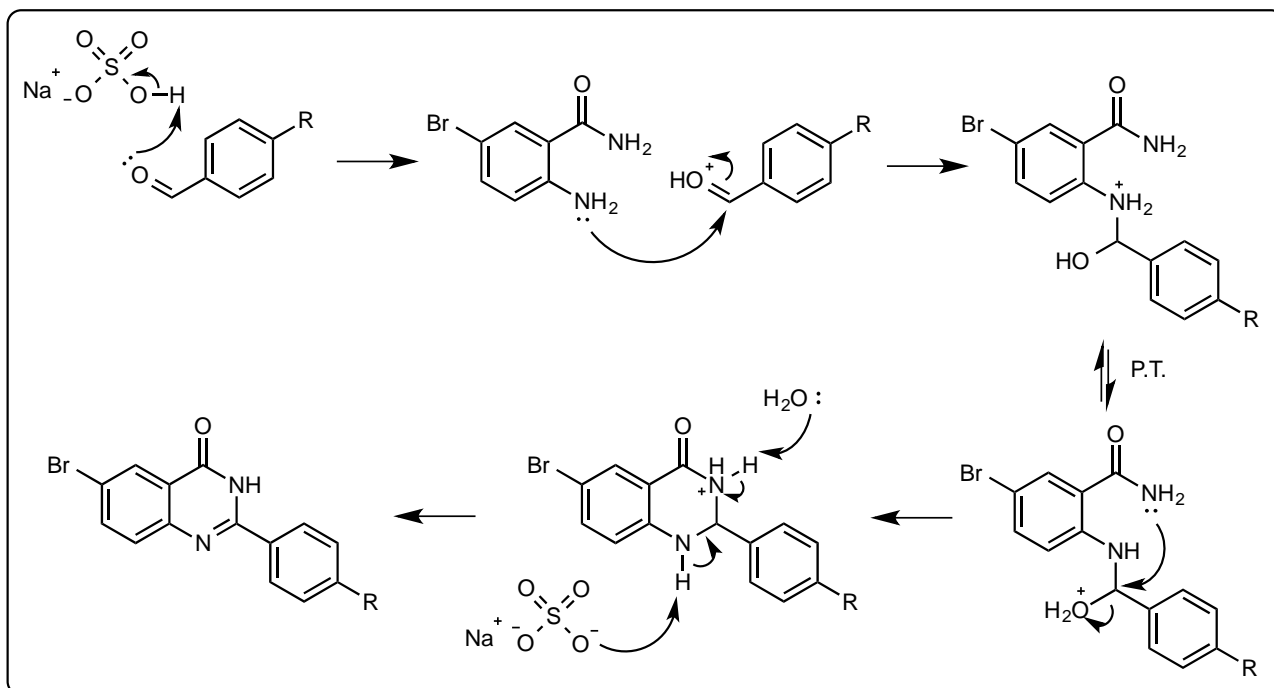


**Figure 45:** Proposed dehydration/dehydrogenation reaction mechanism for the formation of arylquinazolinone derivatives **12.3** and **12.4**.

The <sup>1</sup>H NMR spectra of the 2-arylquinazolinone derivatives (Figure 46) varied as characteristic signals for the phenol moiety shifted. The aromatic H-5 signal was greatly deshielded as evidenced by the shift from ~ δ 7.10 in **7.7** to δ 8.80 in **12.4**, owing to the electron donating effects of the hydroxyl substituent.

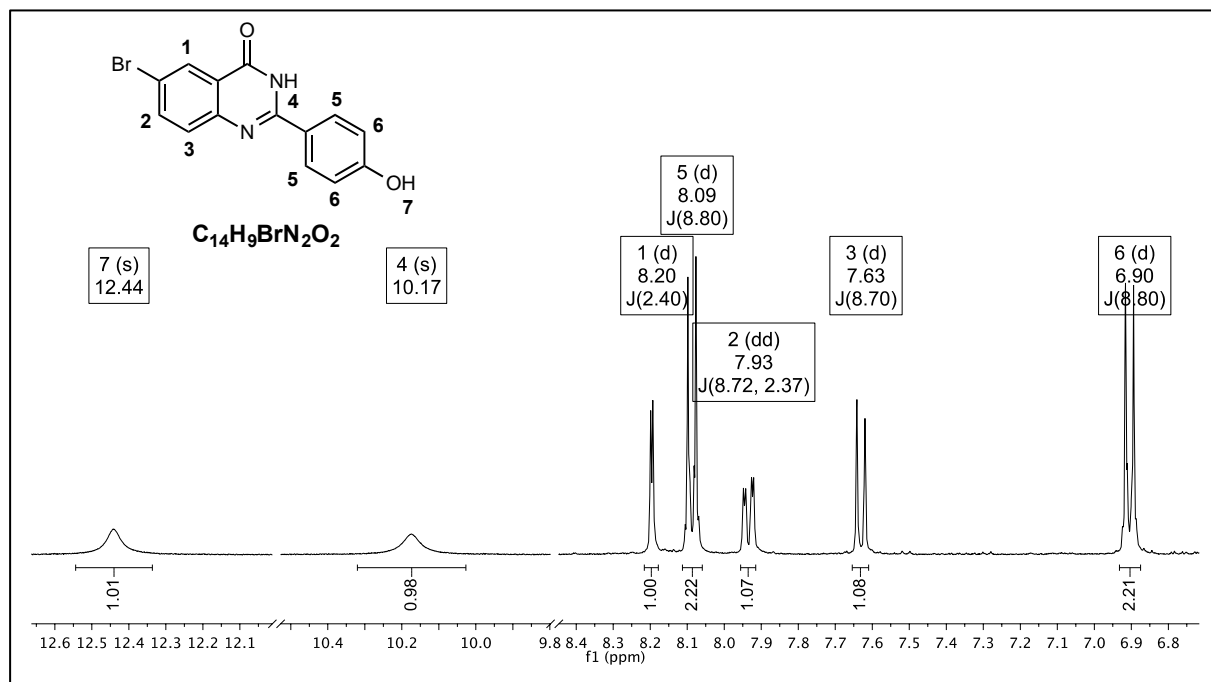


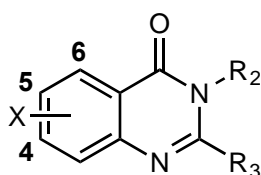
**Figure 46:**  $^1H$  NMR spectrum of arylquinazolinone analogues, using **12.4** as an illustrative example.

### 3.4. PHARMACOLOGICAL EVALUATION OF SYNTHESIZED COMPOUNDS

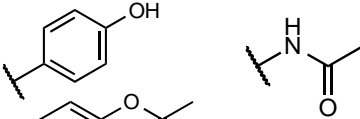
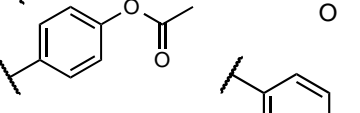
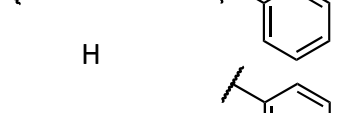
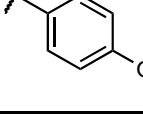
#### 3.4.1. *IN VITRO* ANTIMYCOBACTERIAL ACTIVITY

The synthesized derivatives were evaluated for their *in vitro* antimycobacterial activity against the H37Rv strain of *Mtb* using modified assay protocols, without glycerol as the carbon source, in order to establish SAR. Results reported in Table 8 as MIC<sub>90</sub> and MIC<sub>99</sub> at day 14.

**Table 8:** *In vitro* antimycobacterial activity results for SAR 3 - 5 against *Mtb* (H37Rv) in glycerol-free media.



Compound	X	R <sub>2</sub>	R <sub>3</sub>	<i>In vitro</i> antimycobacterial activity (Day 14)			
				MIC <sub>90</sub> (μM)		MIC <sub>99</sub> (μM)	
				GAST Fe	7H9 GLU ADC	GAST Fe	7H9 GLU ADC
<b>SAR 3</b>							
7.7 (JA061)				4.87	1.18	49	4.67
7.1 (JA060)				77	> 125	> 125	> 125
7.2 (JA059)	5-Br			> 125	> 125	> 125	> 125
7.3 (JA057)				> 125	> 125	> 125	> 125
7.4 (JA062)				> 125	> 125	> 125	> 125
<b>SAR 4</b>							
7.8 (JA065)	4-Br			> 125	> 125	> 125	> 125
7.9 (JA069)	6-Br			> 125	> 125	> 125	> 125

SAR 5						
<b>12.1</b> <b>(JA066)</b>		> 125	> 125	> 125	> 125	> 125
<b>12.2</b> <b>(JA063)</b>		44.2	> 125	69.6	> 125	> 125
<b>12.3</b> <b>(JA072)</b>	5-Br 	> 125	> 125	> 125	> 125	> 125
<b>12.4</b> <b>(JA073)</b>		> 125	> 125	> 125	> 125	> 125
<b>Control</b>	Rifampicin	0.011	0.00561	0.118	0.0537	
	Glycerol dependent control			1.19	> 125	

Evidently, having the hydroxyl group in the *para*-position is vital for activity since derivatives with the substituent in the *ortho* (7.1) and *meta* (7.2) positions displayed complete loss of activity. Replacement of the hydroxyl with an amino group (7.4) and removal of aromaticity (7.3) were both detrimental to activity.

On the other hand, having the bromo substituent in the 5-position of the quinazolinone core is necessary for activity as the other regioisomers (7.8 and 7.9) were inactive. When the carbamate moiety was replaced by an amide group, the resulting compound (12.1) was inactive. However, the diacetylated compound (12.2) displayed some modest potency against *Mtb* in the GAST Fe media (MIC<sub>90</sub> = 44.2 μM and MIC<sub>99</sub> = 69.6 μM). Both 2-arylquinazolinone derivatives (12.3 and 12.4) were inactive (MIC values > 125 μM).

Evidently, the initial intermediate (7.7) that displayed activity even in glycerol-free media incorporated substituents, which were necessary for *Mtb* growth inhibition in ideal positions around the quinazolinone core. This is hypothesized to be due to the formation of a reactive metabolite on the phenol moiety attached to a nitrogen as is known for amodiaquine.<sup>65,66</sup>

Amodiaquine undergoes metabolic oxidation by cytochrome P450 enzymes *in vivo* to form toxic amodiaquine quinoneimine (AQQI) metabolites. The antioxidant glutathione (GSH) acts as a nucleophile and detoxifies AQQI's by extracting the new species from the

system. However, glutathione levels in the cell get depleted at high doses resulting in reactive toxic metabolites of AQQI analogues reacting with thiol-containing human proteins, which form drug-protein adducts that are fatal to the liver cells (Figure 47). This can lead to toxic effects such as hepatotoxicity and agranulocytosis.<sup>65,67</sup>

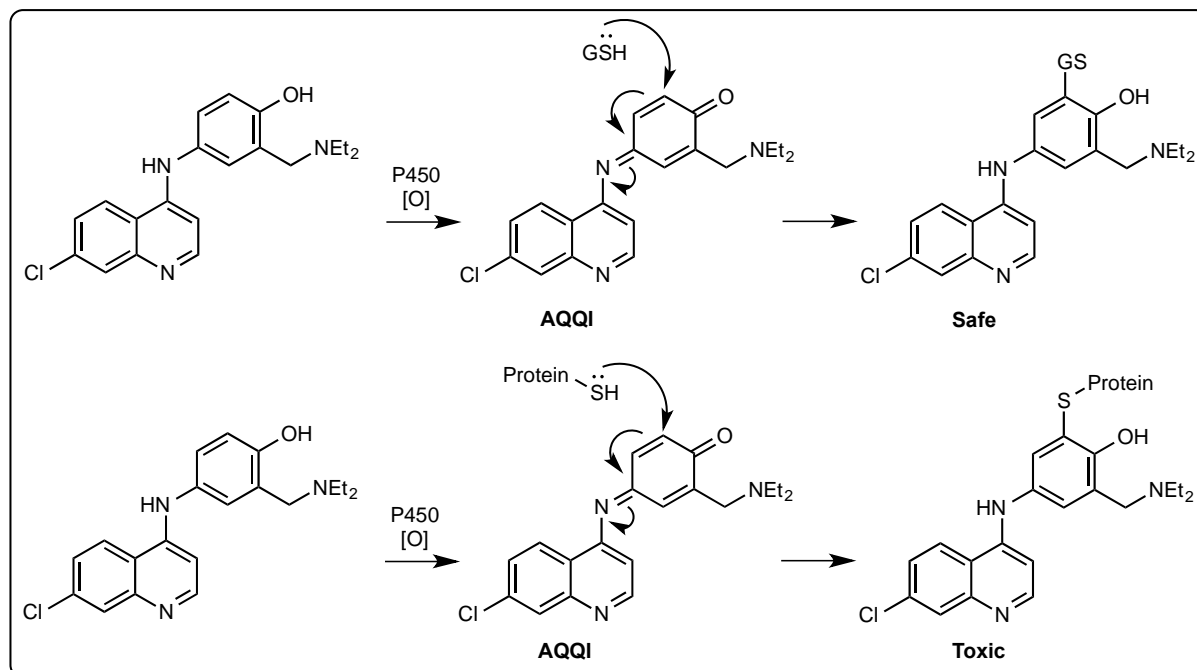


**Figure 47:** Mechanism by which amodiaquine undergoes metabolism to form a reactive metabolite, which under high doses, can result in toxicity effects.

It is therefore hypothesized that this phenomenon could be occurring with **7.7**, resulting in a toxic fragment, which could be responsible for the observed *in vitro* antimycobacterial activity in glycerol-free media. Since the nitrogen does not have a proton attached, the mechanism of such metabolism is proposed to proceed via an initial enzyme-mediated nucleophilic attack at the acyl centre, resulting in the opening of the quinazolinone ring. This would render the compound susceptible to electrochemical oxidation by P450 enzymes forming a reactive metabolite (Figure 48).

Studies by O'Neill and coworkers showed that interchange of the 3-hydroxyl and 4-Mannich base side chain in the synthesis of isoquine derivatives inhibits the formation of the toxic quinoneimine metabolite of amodiaquine.<sup>65</sup> Therefore, the loss of activity observed for *ortho*- (**7.1**) and *meta*- (**7.2**) phenol substituents in **SAR 3** may be further substantiated by this finding, as this phenomenon is only possible for *para*-phenols. Further reactive metabolite generation, trapping and identification studies would need to be performed to confirm this possibility.

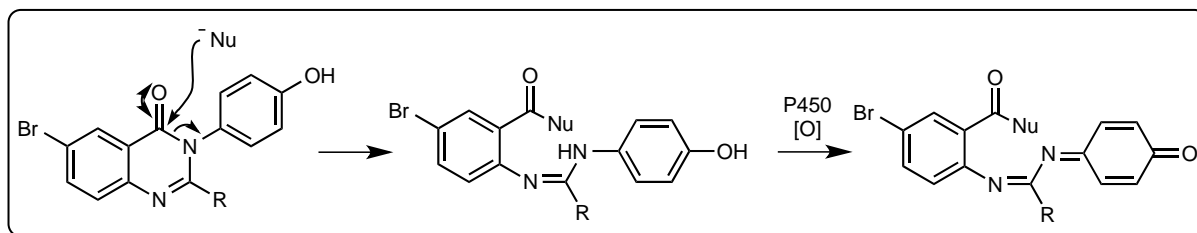


**Figure 48:** Proposed mechanism by which analogue **7.7** undergoes metabolic oxidation to a toxic fragment resulting in apparent antimycobacterial growth inhibition.

### 3.5. CONCLUSIONS

The aminoquinazolinone intermediate **7.7** found to possess antimycobacterial activity in glycerol-free media formed a basis for structural modifications aimed at preliminary SAR exploration. To this end, 11 new analogues were successfully synthesized, characterized and evaluated for antimycobacterial activity. All synthesized analogues were found to be inactive. This could be explained by the toxic phenol fragment attached to the nitrogen, which could undergo metabolic oxidation to form a reactive metabolite resulting in apparent activity observed in the assay. These findings therefore suggest that the 2-aminoquinazolinone scaffold is not a suitable chemotype for anti-TB agents.

## CHAPTER 4: SOLUBILITY STUDIES

---

### 4.1. INTRODUCTION

Solubility plays a major role in biological assays, formulation for *in vivo* dosing and intestinal absorption. It is therefore important to establish the solubility of potential drug candidates early on in the drug discovery process.<sup>27,68</sup> This enables a determination of how feasible it is to perform subsequent *in vitro* assays as well as detecting possible absorption, distribution, metabolism and excretion (ADME) problems early.<sup>69</sup> Poorly soluble compounds may precipitate out of solution during biological testing leading to poorly reproducible and unreliable *in vitro* and *in vivo* results.<sup>26</sup> Solubility is a measurable parameter. However, the reported values obtained are not finite as they are dependent on solvent factors (pH, temperature, ionic composition, co-solvent effects) and experimental conditions (time, detection method, assay materials) at the time of measurement.<sup>68,70</sup>

Different solubility assays have been implemented in drug discovery, each with its own strengths and limitations. These assays can be classified as either thermodynamic or kinetic solubility. The thermodynamic solubility method follows the addition of aqueous solution directly to a solid sample of a compound, therefore the crystal form is important as crystal energy must be overcome for dissolution.<sup>68,70,71</sup> Incubation times are longer (72 hours) to allow equilibrium to be established. Thermodynamic solubility is known as the 'gold standard' of solubility measurement but it has lower throughput and therefore is used later on in drug discovery, typically before First-in-Man studies whereby the crystalline form is determined before and after the assay.<sup>68,71</sup> In contrast to thermodynamic solubility, the kinetic method involves initially dissolving the solid compound in an organic solvent [eg. Dimethyl sulfoxide (DMSO)] prior to adding to aqueous buffer, which mimics conditions used in biological studies. Since the compounds are already dissolved, no crystal energy needs to be overcome. Incubation times are shorter (2-4 hours), therefore equilibrium is not established with kinetic solubility and the presence of DMSO results in co-solvent effects. Both of these factors lead to generally higher solubility values compared to the thermodynamic method but results in a higher throughput.<sup>68,70,72</sup>

Two types of solubility experiments were performed on the aminoquinazolinone series, both of which were kinetic solubility in nature with the major difference being the detection method. The first relies on the appearance of turbidity in solution once a compound exceeds its solubility limit in the assay (turbidimetric solubility method). In contrast, the alternative method measures the amount of material that has dissolved into solution as quantified using HPLC-UV analysis.<sup>68,70</sup> The latter approach was adapted by our research group as a hybrid method between thermodynamic and kinetic solubility whereby DMSO is evaporated off prior to the addition of aqueous buffer to the amorphous solid. Removal of DMSO eliminates possible solubility enhancement effects (co-solvent effects).<sup>73</sup> For the purpose of this discussion, this approach will be termed “HPLC-based method”.

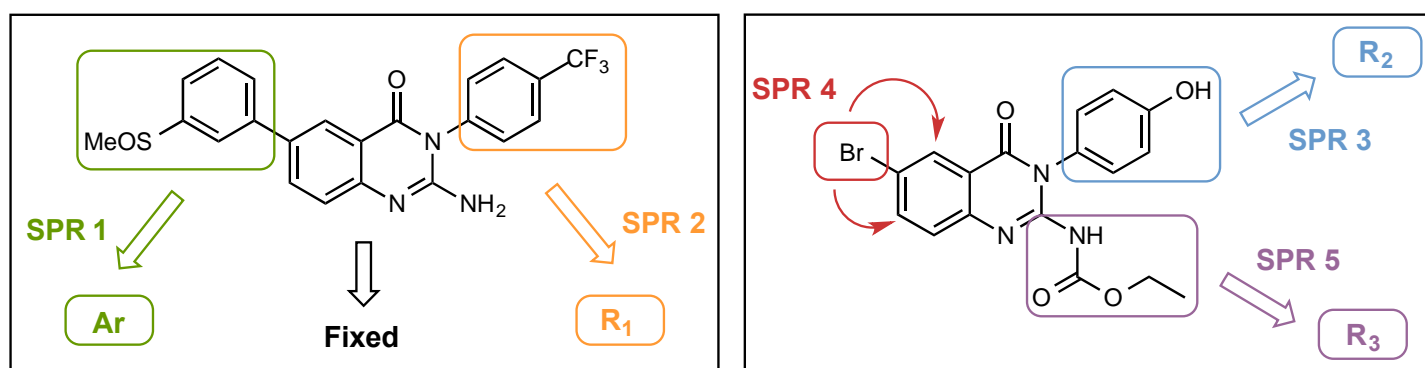


**Figure 49:** General outline of **SPR 1 – 5** structures used in the following solubility studies.

With the intention of fulfilling the aims and objectives of this work, solubility studies were performed on all target compounds in order to deduce structural property relationships (SPR) with respect to solubility. SPR compounds were selected based on **SAR 1 – 5** structures as outlined in Figure 49. This chapter therefore describes the results of turbidimetric- and HPLC-based solubility methods for synthesized aminoquinazolinone derivatives in order to determine whether or not chemical modifications aimed at reducing lipophilicity, disrupting molecular planarity/symmetry or a combination of strategies enabled optimization of this series with regard to solubility. Changes in physicochemical parameters such as ClogP, topological polar surface area (tPSA), melting point and calculated dihedral angles were examined in order to determine the factors responsible for any improved solubility and deduce relationships.

#### 4.1.1. TURBIDIMETRIC SOLUBILITY ASSAY

Turbidimetric solubility assays were performed in 96-well microtiter plates and involved dissolving the target compounds in DMSO to obtain stock solutions of 10 mM, from which serial dilutions were prepared in a pre-dilution plate with DMSO to obtain concentrations from 0 – 10  $\mu$ M in triplicate. Secondary dilutions were made in both DMSO and phosphate buffered saline (PBS) (pH 7.4) solutions to achieve final concentrations ranging from 0 to 200  $\mu$ M and allowed to incubate at room temperature for 2 hours. As the concentration of the testing compound increases in the PBS media, precipitation should increase accordingly and causes turbidity, as most organic compounds are not freely soluble in aqueous media. Turbidity was detected by measuring the absorbance at 620 nm and the approximate solubility determined by plotting concentration against corrected absorbance. The limit of solubility was then indicated by the concentration value at which the absorbance in the PBS solution rises above the DMSO baseline, and reported as a range.<sup>74,75</sup>

Two controls are used to validate the turbidimetric solubility assay, a highly soluble control (hydrocortisone) and an insoluble control (reserpine). This is indicated by the corrected absorbance versus concentration plots of these compounds whereby hydrocortisone appears to be soluble across the entire test concentration range (Figure 50) in contrast to reserpine which displays poor solubility with the PBS curve deviating from the DMSO baseline in the 1 – 5  $\mu$ M range (Figure 51).

The general classification of solubility ranges for organic compounds using the turbidimetric solubility assay is defined as follows:<sup>75</sup>

- High: > 100  $\mu$ M
- Moderate: 20 – 100  $\mu$ M
- Low: < 20  $\mu$ M

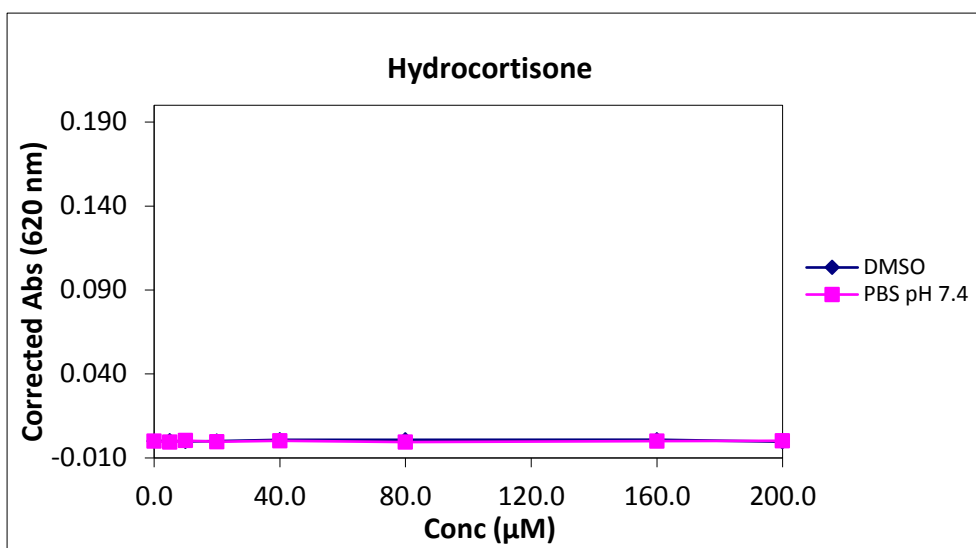


**Figure 50:** Absorbance versus concentration curve of the highly soluble control, hydrocortisone.

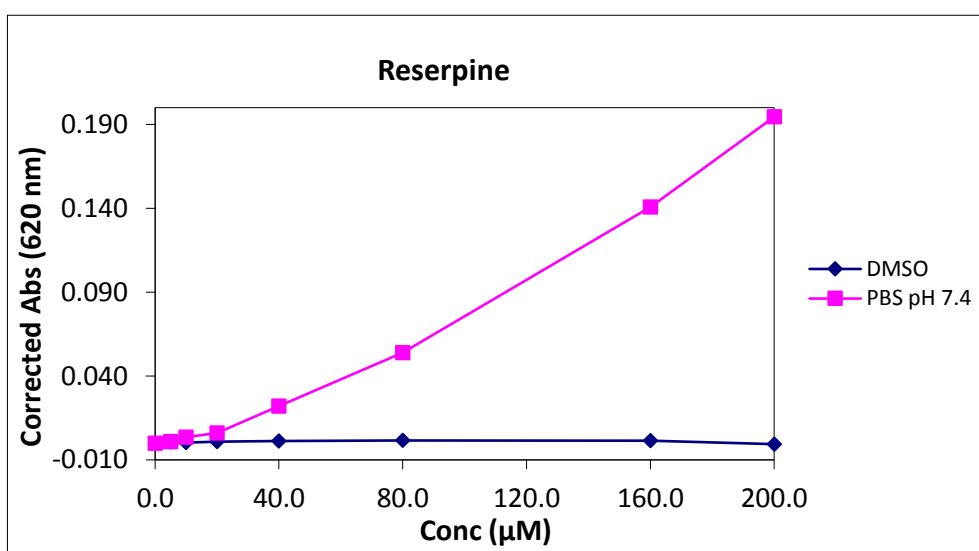


**Figure 51:** Absorbance versus concentration curve of the insoluble control, reserpine.

#### 4.1.2. HPLC-BASED SOLUBILITY ASSAY

An alternative, more accurate method was additionally used to determine the aqueous solubility of compounds, which incorporates elements of kinetic and thermodynamic solubility in a hybrid method. This involved using the DMSO-dry down method, adapted from Zhou et al.<sup>69</sup> Briefly, the high and medium calibration standards (220µM, 100µM) in duplicate, as well as the samples (200µM) in triplicate, were added to a 96-well plate, from a 10mM stock solution in DMSO. DMSO was then evaporated from the samples for 2 hours. DMSO was added to the standards and after vortexing the plate, the high standard was used to prepare a low (11µM) calibration standard in DMSO. Phosphate buffered saline (pH 7.4) was added to the sample wells and the plate was incubated for 32 hours at 25°C with shaking. The plate was then centrifuged at 2500g for 30 minutes

and the supernatants transferred to another plate for analysis. Aqueous solubility was determined from UV peak areas of the samples relative to the standards using best-fit calibration curves.<sup>73</sup>

The general classification of solubility ranges for organic compounds using the kinetic solubility method is defined as follows:

- High: > 150  $\mu\text{M}$
- Moderate: 50 – 150  $\mu\text{M}$
- Low: 11 – 50  $\mu\text{M}$
- Very Low: < 11  $\mu\text{M}$

Since calibration standards are used in the kinetic solubility assay at concentrations of 11, 100 and 220  $\mu\text{M}$ , values below 11  $\mu\text{M}$  and above 220  $\mu\text{M}$  are not well defined and therefore compounds outside of these ranges should be considered poorly or highly soluble, respectively. If the difference in solubility between two compounds were below 15% then their solubilities are comparable. However, solubility values between two compounds may be distinguished if they have a significant difference above 15%.

## 4.2. SOLUBILITY RESULTS

Upon overall observation of the differences in results between the turbidimetric and HPLC-based methods across the aminoquinazolinone series in Figure 52, it is evident that the turbidimetric assay tended to give higher solubility values than the HPLC-method.

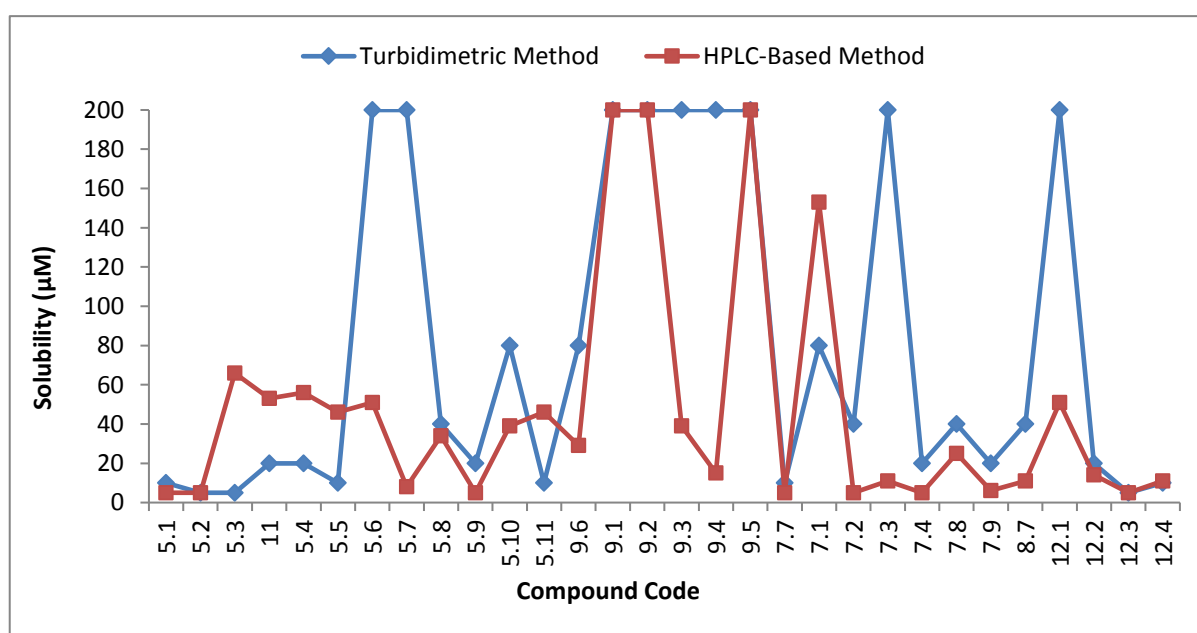


**Figure 52:** Graph comparing solubility results using the turbidimetric assay (low range values shown) and the HPLC-based assay (pH 7.4) across all compounds in the series.

Using the lower limit of the turbidimetric solubility range, 18 of the 30 tested compounds exhibited higher values than the HPLC method. This discrepancy could be due to the shorter incubation period of the turbidimetric method, which means that measurements are performed on a saturated solution rather than a solution that has reached equilibrium.<sup>68,70</sup> Additionally, turbidimetric and HPLC-assays differ in the identity of the precipitate formed at equilibrium (amorphous or crystalline) as solubility is influenced by the solid state form of a compound. The turbidimetric method tends to favour amorphous precipitates due to the presence of DMSO whereas the longer incubation time and absence of DMSO in the HPLC-based assay favours the form that is more energetically favoured. If an amorphous solid is precipitated in the HPLC-based assay, then the results are likely to be closer to the turbidimetric method than if a crystalline precipitate is formed.<sup>72</sup> The large differences between the assays for these compounds may therefore suggest that crystalline material is being formed in the HPLC-assay. Further investigation into this phenomenon would need to be carried out. Since the HPLC-method is more rigorous, the following SPR analysis of the aminoquinazolinone series will be deduced using the HPLC-based solubility results.

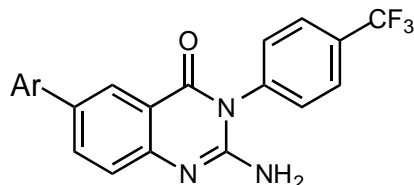
Various calculated and/or measured structural parameters can be used to explain the factors responsible for any improved solubility. As mentioned previously, ClogP is a measure of lipophilicity whereby addition of hydrophilic groups reduces lipophilicity, therefore lowering the ClogP value.<sup>26</sup> tPSA is defined as the sum of polar atoms in a molecule. This property is commonly used to predict intestinal absorption, blood-brain barrier penetration and Caco-2 monolayer permeation but is used as a relative estimation of polarity to determine the influence of this property on aqueous solubility for this chapter.<sup>76</sup> The measured melting point property is indicative of crystal lattice energy, wherein more stable, tightly packed crystal structures will have higher melting points and generally decrease the solubility of the compound.<sup>25</sup> Where appropriate, dihedral angles between biaryl moieties were obtained by means of density functional theory (DFT) calculations (B3LYP) using the software Maestro to determine the degree of distortion away from planarity.

The above parameters are incorporated in the following discussion to aid in the interpretation of the solubility data and to determine whether or not the theoretical solubility improvement strategies are experimentally validated.

#### 4.2.1. SPR 1 SOLUBILITY STUDIES

SPR analysis of **SPR 1** compounds can be divided into three general groups of compounds based on their **Ar** substituents: the sulfones, morpholino and amide derivatives (Table 9).

**Table 9:** Apparent aqueous solubility results and physicochemical parameters for **SPR 1** target compounds.



Cmpd. (Code)	Ar	Variables	Turbidimetric Solubility Range ( $\mu\text{M}$ )	HPLC-based Solubility pH 7.4 ( $\mu\text{M}$ )	ClogP <sup>a</sup>	tPSA <sup>b</sup>	MP ( $^{\circ}\text{C}$ ) <sup>c</sup>
5.1 (JA025)			5 – 10	<5	3.54	92.83	246.3 – 250.4
5.2 (JA010)			10 – 20	<5	3.58	75.76	325.5 – 328.3
5.3 (JA013)			5 – 10	66	4.13	92.83	245.1 – 248.2
11 (JA038)			20 – 40	53	3.74	92.83	278.0 – 282.2
5.4 (JA018)		Y = CH, X = O	20 – 40	56	3.81	88.23	273.0 – 277.9
5.5 (JA019)		Y = CH, X = S	10 – 20	46	4.54	79.00	263.5 – 271.2
5.6 (JA020)		Y = CH, X = NMe	>200	51	4.37	82.24	232.1 – 236.3
5.7 (JA021)		Y = N, X = O	>200	8	2.71	100.59	239.0 – 246.8
5.8 (JA017)		Y = CH, R = H, R' = H	40 – 80	34	3.69	101.78	295.5 – 299.9
5.9 (JA022)		Y = CH, R = H, R' = Me	20 – 40	<5	3.90	87.79	292.5 – 298.0
5.10 (JA023)		Y = N, R = H, R' = Me	80 – 160	39	3.15	100.15	310.5 – 313.5
5.11 (JA016)		Y = CH, R = R' = Me	10 – 20	46	3.64	79.00	286.0 – 288.9
9.6 (JA039)			80 – 160	29	4.92	95.99	319.1 – 323.6

<sup>a</sup> Calculated Log P, determined using ChemBioDraw Ultra 14.0

<sup>b</sup> Topological polar surface area, calculated using ChemBioDraw Ultra 14.0

<sup>c</sup> Melting point, recorded on Stuart SMP40 automatic melting point apparatus

Analysis of the sulfonyl analogues generally depicts data in the low to moderate solubility range, which is to be expected since the frontrunner compounds previously showed low solubility. Transformation of the sulfone **5.1** to the more strongly H-bonding sulfoxide group **5.2** resulted in no improvement in aqueous solubility. However, replacement of the sulfonylmethyl substituent for a cyclopropyl moiety (**5.3**) resulted in a 13-fold solubility enhancement using the HPLC-based method. The addition of a methyl substituent in the *ortho*-position (**11**) resulted in moderate improvement in solubility owing to disruption of planarity through the increase of the dihedral angle between the biaryl systems of **11** (50.6°) compared to the parent analogue **5.1** (33.9°), as indicated in the computational models depicted in Figure 53. The results obtained were not as significant as expected possibly due to the introduction of a hydrophobic methyl substituent as indicated by the increase in ClogP.

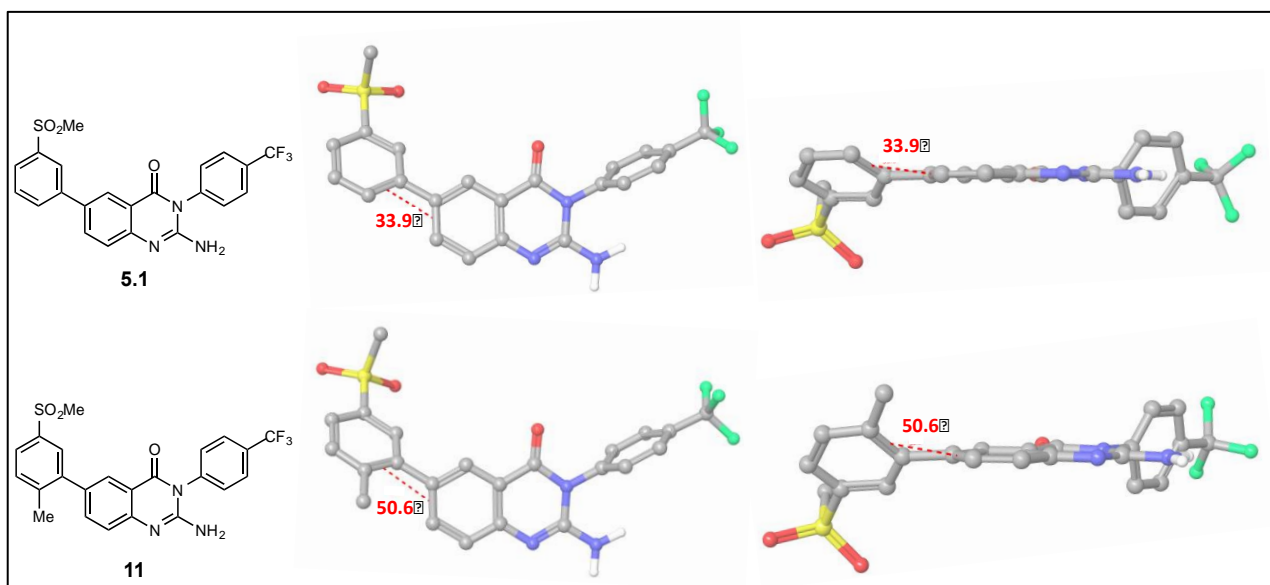


**Figure 53:** Computational models of **5.1** and **11** indicating calculated dihedral angles (centre) with 90° angle views (right) using Maestro.

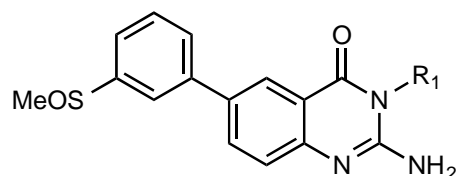
The introduction of morpholino-type structures was beneficial, with an overall improvement in solubility observed compared to the parent sulfinyl compound **5.2**. This could be attributed to the introduction of water solubilizing H-bonding groups as well as the incorporation of saturated ring systems to reduce molecular planarity and disrupt crystal-stacking capability as indicated by the decrease in melting points relative to **5.2**. Of the phenyl analogues, the morpholino-derivative **5.4** displayed the most improved aqueous solubility (56  $\mu$ M). The thiomorpholine (**5.5**) and methylpiperazine (**5.6**) derivatives displayed comparable, moderate solubility whilst incorporation of an ionizable centre as in the pyridinyl analogue (**5.7**) resulted in poor solubility (8  $\mu$ M).

The amide analogues generally displayed low solubility. The strategy for this series was the addition of ionizable, hydrophilic groups to reduce lipophilicity. The solubility trend follows NMe<sub>2</sub> (**5.11**) > NH<sub>2</sub> (**5.8**) > NHMe (**5.9**), which is reflected in the order of increasing lipophilicity (ClogP). Transition from the phenyl secondary amide **5.9** to the pyridinyl derivative **5.10** resulted in significant enhancement of aqueous solubility owing to the reduction in lipophilicity (from ClogP = 3.90 to ClogP = 3.15). Transformation to the carboxylic acid moiety made no significant improvement, maintaining values in the low solubility range. The melting points across the amide derivatives are relatively similar to the frontrunner compounds. This suggests that the apparent improvements in solubility are due to lipophilic properties and not disruption of molecular planarity and symmetry for this series of compounds

#### 4.2.2. SPR 2 SOLUBILITY STUDIES

The main strategy for **SPR 2** analogues was the incorporation of saturated rings in the R<sub>1</sub> position in order to reduce crystal-packing capabilities, which in turn, should result in improved solubility (Table 10).

**Table 10:** Apparent aqueous solubility results and physicochemical parameters for **SPR 2** target compounds.



Compound (Code)	R <sub>1</sub>	Turbidimetric Solubility Range (μM)	HPLC-based Solubility pH 7.4 (μM)	ClogP <sup>a</sup>	tPSA <sup>b</sup>	MP (°C) <sup>c</sup>
<b>9.1</b> (JA045)		>200	>200	1.91	84.99	221.3 – 223.6
<b>9.2</b> (JA051)		>200	>200	0.85	88.23	214.2 – 217.2
<b>9.3</b> (JA055)		>200	39	1.96	95.99	232.0 – 237.2
<b>9.4</b> (JA056)		>200	15	1.06	101.78	328.1 – 333.2
<b>9.5</b> (JA045)		>200	>200	1.36	79.00	235.7 – 237.8

<sup>a</sup> Calculated Log P, determined using ChemBioDraw Ultra 14.0

<sup>b</sup> Topological polar surface area, calculated using ChemBioDraw Ultra 14.0

<sup>c</sup> Melting point, recorded on Stuart SMP40 automatic melting point apparatus

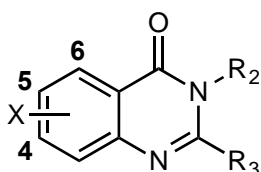
The anticipated improvements were observed, particularly for compounds **9.1**, **9.2** and **9.5**, displaying high solubility (>200  $\mu\text{M}$ ) in both assays. Table 10 indicates that the HPLC-method results differ from those of the turbidimetric assay in that compounds **9.3** and **9.4** showed values in the low solubility range (39.3  $\mu\text{M}$  and 15.3  $\mu\text{M}$ , respectively). Comparing **9.3** to **9.5**, **9.3** was predicted to be relatively more lipophilic (ClogP = 1.96) relative to **9.5** (ClogP = 1.36). Therefore it was expected to have a lower solubility than **9.5** albeit the two compounds have melting points in the same range. Whereas with **9.4**, despite the lowered lipophilicity, the melting point is the highest of this series suggesting tighter packing.

To confirm the factors contributing to improved solubility for the saturated analogues, ClogP, tPSA and melting point were examined. All compounds showed reduced hydrophobicity (ClogP) and melting point parameters compared to **5.2** with increased polarity (tPSA). Therefore, improvement of solubility can be ascribed to 2 factors in this case: decrease of lipophilicity and disruption of molecular planarity to reduce crystal packing ability, which results in lower melting, more soluble compounds.

### 4.2.3. SPR 3 – 5 SOLUBILITY STUDIES

Upon exploring the aminoquinazolinone intermediates for *in vitro* antimycobacterial activity in glycerol-free media, 12 new intermediate derivatives were synthesized and subsequently tested for their solubility. Table 11 summarizes the solubility results obtained for **SPR 3 – 5**.

**Table 11:** Apparent aqueous solubility results and physicochemical parameters for aminoquinazolinone intermediates **SPR 3 – SPR 5**.



Cmpd. (Code)	X	R <sub>2</sub>	R <sub>3</sub>	Turbidimetric Solubility Range (μM)	HPLC-based Solubility pH 7.4 (μM)	ClogP <sup>a</sup>	tPSA <sup>b</sup>	MP (°C) <sup>c</sup>
<b>SPR 3</b>								
7.7 (JA061)				10 – 20	<5	4.03	91.23	317.8 – 322.4
7.1 (JA060)				80 – 160	153	3.86	91.23	186.1 – 190.1
7.2 (JA059)	5-Br			40 – 80	<5	4.03	91.23	350.9 – 356.9
7.3 (JA057)				>200	11	2.18	91.23	310.0 – 317.7
7.4 (JA062)				20 – 40	<5	3.44	97.02	331.2 – 339.4
<b>SPR 4</b>								
7.8 (JA065)	4-Br			40 – 80	25	4.03	91.23	193.4 – 200.1
7.9 (JA069)	6-Br			20 – 40	6	4.03	91.23	314.8 – 319.9

SPR 5

8.7 (JA062)		NH <sub>2</sub>	40 – 80	11	3.05	78.92	310.1 – 318.2
12.1 (JA066)			>200	51	3.21	82.00	231.4 – 234.6
12.2 (JA063)	5-Br 		20 – 40	14	2.86	88.07	228.0 – 234.6
12.3 (JA072)	H 		5 – 10	<5	3.32	41.46	306.2 – 310.4
12.4 (JA073)	H 		10 – 20	11	2.88	61.69	314.6 – 318.1

<sup>a</sup> Calculated Log P, determined using ChemBioDraw Ultra 14.0

<sup>b</sup> Topological polar surface area, calculated using ChemBioDraw Ultra 14.0

<sup>c</sup> Melting point, recorded on Stuart SMP40 automatic melting point apparatus

Overall, a slight improvement in aqueous solubility was observed across all three series compared to the parent compound **7.7**, which was poorly soluble (<5 μM). Exploring the different regioisomers of the phenol moiety in **SPR 3**, the *ortho*-derivative (**7.1**) was found to be highly soluble, with a 30-fold increase in solubility, whilst the *meta*-isomer (**7.2**) showed no improvement in solubility. Calculated dihedral angles for the three derivatives (Figure 54) revealed comparable distortions from planarity (approximately 70°). Therefore disruption of molecular planarity is not likely to be the reason for improved solubility. However, compound **7.1** did display reduced lipophilicity (ClogP = 3.86) as well as lowered melting point (MP = 186.1 – 190.1°C) than those of corresponding *meta*- and *para*-derivatives. These results suggest that disruption of molecular symmetry accounts for the decrease in crystal packing energy and lowered melting point, leading to increased solubility.

The removal of aromaticity approach was additionally explored in this series with compound **7.3**. This saturated ring derivative displayed poor solubility with no significant decrease in melting point. These results suggest that the crystal packing in this molecule is dramatically different despite expecting **7.3** to be more soluble; the melting point suggests that it remains tightly packed.

Substitution of the hydroxyl moiety (7.7) for an amino group (7.4) resulted in no change in solubility. All **SPR 3** derivatives, except 7.1, displayed poor solubility in the HPLC-method, with values comparable to the parent compound (<11  $\mu\text{M}$ ) and is reflected in the melting point parameter of this series.

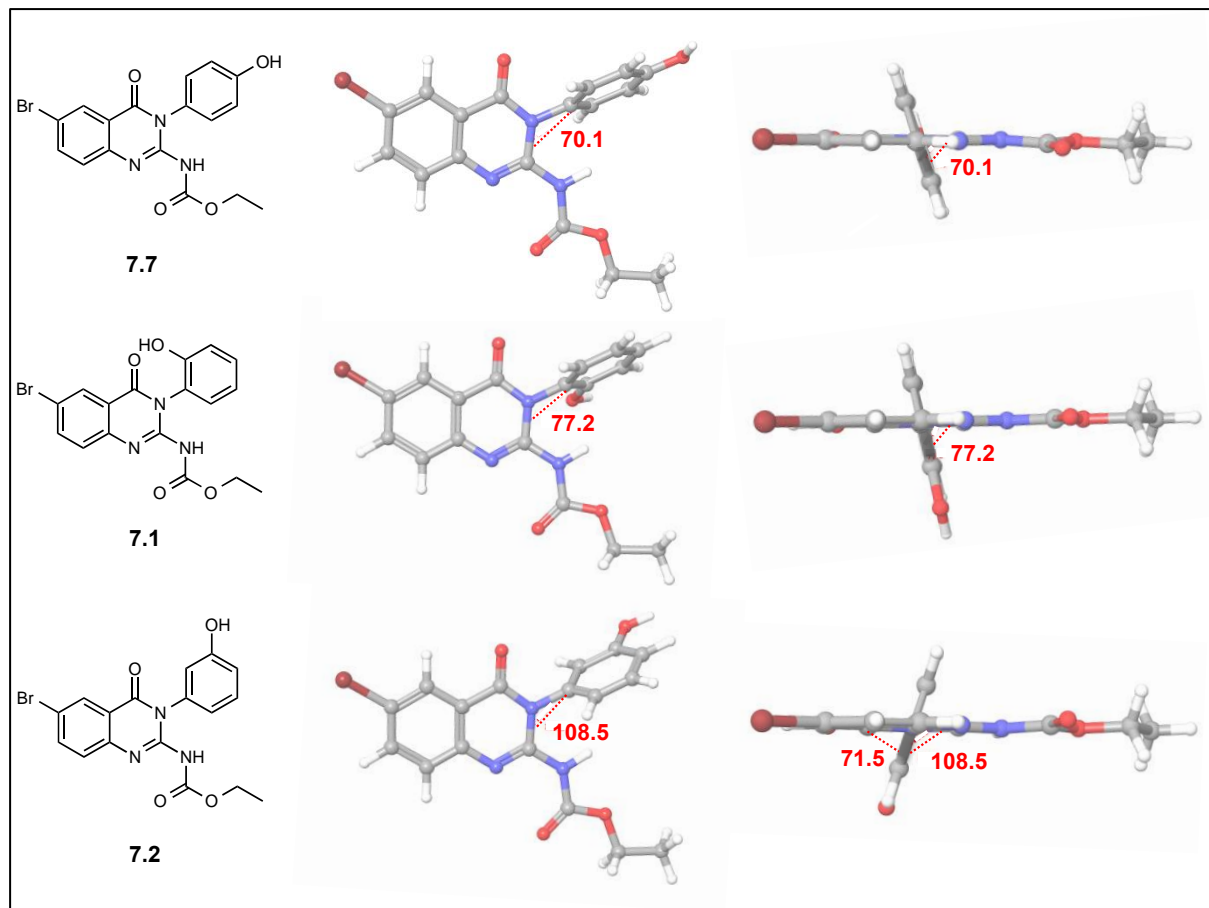


**Figure 54:** Computational models of **SAR 3** analogues showing the calculated dihedral angle between the phenol moiety and the quinazolinone core.

The exploration of regioisomers of the bromo substituent on the aminoquinazolinone core in the **SPR 4** series revealed moderate improvement when the bromo substituent was placed in the 4-position (7.8). Derivation of the structural parameters (Table 11) of 7.8 and 7.9 reveals similar values across properties as the parent compound 7.7, except the melting point of 7.8 is marginally lower. This suggests that the bromo substituent in the 4-position contributes to disruption of the crystal packing ability to produce a lower melting, more soluble compound.

In the final series, **SPR 5** (Figure 49), wherein the  $R_3$  position was explored, the mono-acetylated derivative 12.1 exhibited the most improvement in solubility using the HPLC-based assay (51.1  $\mu\text{M}$ ) and turbidimetric assay (>200  $\mu\text{M}$ ). However, the diacetylated

product (**12.2**) showed low solubility whilst all other **SPR 5** derivatives displayed no significant improvement in aqueous solubility. Both acetylated products, **12.1** and **12.2**, have reduced lipophilicity and melting point parameters compared to **7.7**.

Attempts at including aryl substituents into the R<sub>3</sub> position proved to be detrimental to solubility as compounds **12.3** and **12.4** exhibited poor solubility in both assays, presumably due to the low polarity observed for these compounds (tPSA = 41.46 and 61.69).

### 4.3. PHYSICOCHEMICAL PROPERTIES

In an attempt to understand the factors responsible for improved aqueous solubility, the physicochemical parameters and log (HPLC-based solubility) in Tables 9 – 11 were plotted. Evan's guidelines were used to determine the degree of correlation strength (R<sup>2</sup> value):<sup>77</sup>

- 0.0 – 0.19: Very weak
- 0.2 – 0.39: Weak
- 0.4 – 0.59: Moderate
- 0.6 – 0.79: Strong
- 0.8 – 1.00: Very strong

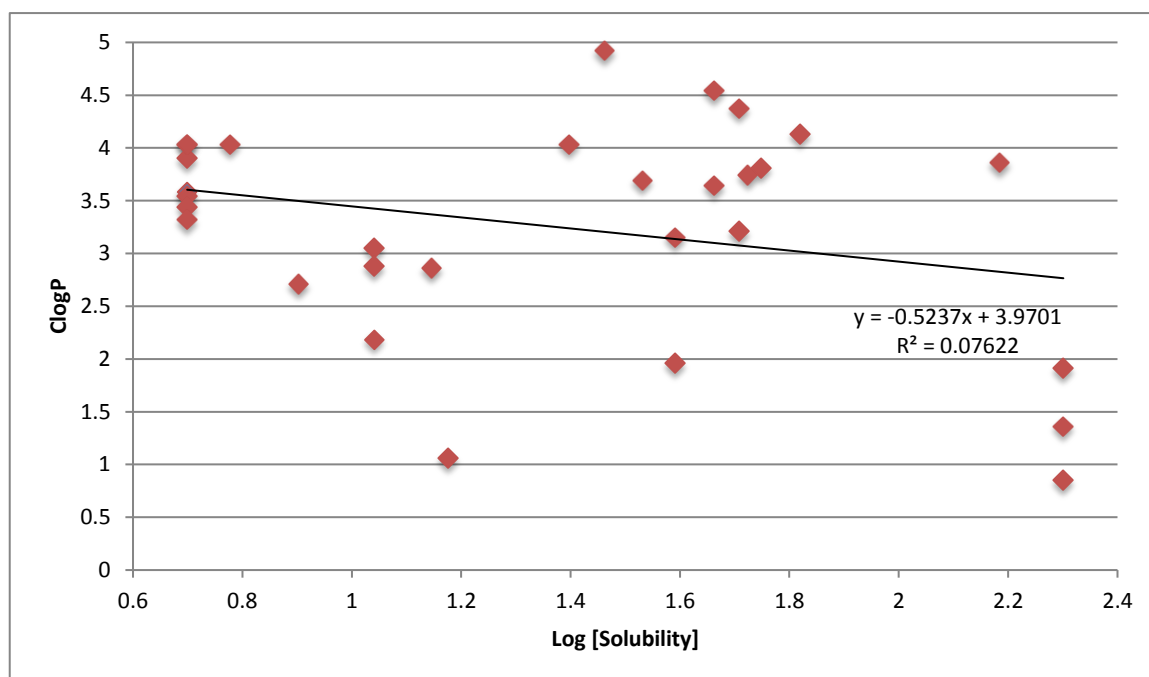
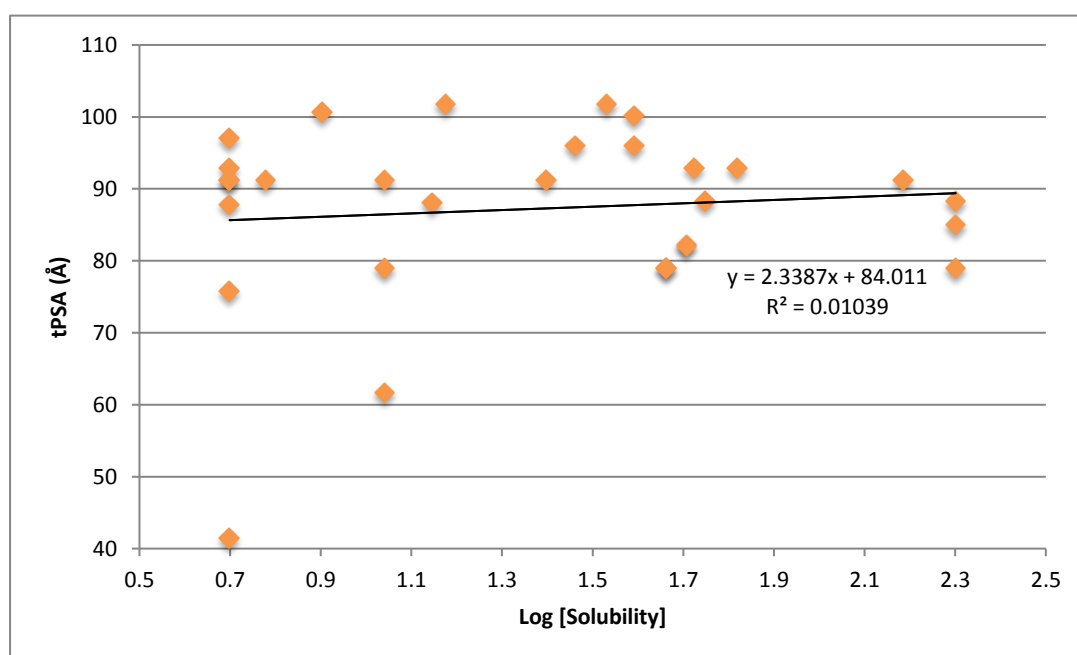


Figure 55: Relationship between solubility and ClogP data of SPR 1 - 5.

As shown in Figure 55, ClogP was very weakly but negatively correlated to log (solubility) with an  $R^2$  value of 0.07. As expected, the relationship between ClogP and solubility is not direct because for these compounds, the changes in dihedral angle and crystal packing especially have a greater influence than a simple reduction or increase in ClogP. However, it was noted that of the five least lipophilic compounds, three were in the most soluble class and therefore is indicative that reduced lipophilicity is a parameter for solubility improvement for this aminoquinazolinone series.



**Figure 56:** Relationship between solubility and tPSA data of **SAR 1 - 5**.

Figure 56 shows that tPSA was found to have little to no correlation with solubility ( $R^2 = 0.01$ ). There are many drastic structural changes around the aminoquinazolinone core scaffold across **SPR 1- 5**. As such, a combination of factors contributes to the apparent reduction or enhancement of solubility.

In contrast to the limitations of the aforementioned physicochemical correlations, the melting point parameter was found to be the most strongly correlated with aqueous solubility ( $R^2 = 0.43$ ).

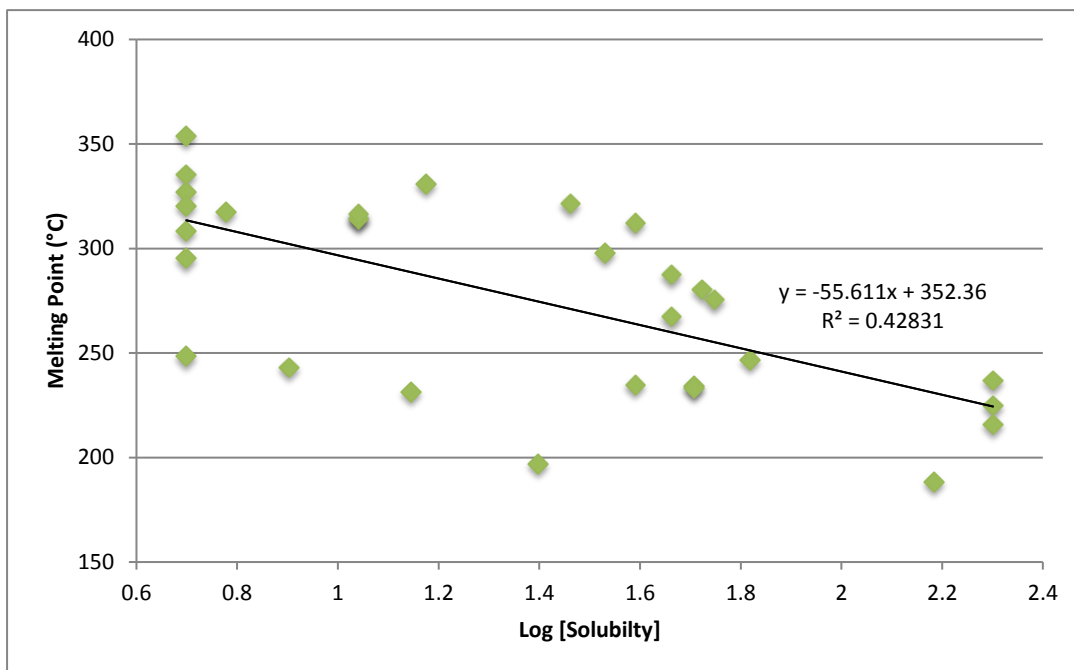


**Figure 57:** Relationship between solubility and melting point data of **SAR 1 - 5**.

The moderate relationship between melting point and log (solubility) observed in Figure 57 suggests that the crystal packing efficiency of the compounds in its crystal lattice is more dominant than changes in lipophilicity or polarity. These results imply that disruption of molecular planarity and/or symmetry by removal of aromaticity or introduction of substituents in the *ortho*-position decreases crystal packing energy so as to lower the melting point, leading to increased solubility. This strong, negative correlation between melting point and solubility is supported by previous reports wherein high solubility was shown to be associated with reduced melting points.<sup>71,78-80</sup>

Overall, log (solubility) was most correlated with melting point than ClogP and tPSA factors. In other words, these analyses suggest that melting point can be considered as an applicable parameter for aqueous solubility of aminoquinazolinone compounds described above.

#### 4.4. CONCLUSIONS

In summary, 30 compounds were synthesized and analysed for their kinetic solubility using turbidimetric and HPLC-based methods. Physicochemical parameters were included in order to deduce the possible factors responsible for any improvement in solubility. Overall, the turbidimetric method was found to be over-estimating solubility compared to the HPLC-based method. However, similar trends were still observed for compounds in relation to one another. The relative aqueous solubility trends of **SPR 1** and **SPR 2** using the HPLC-based method are summarized in Figure 58.

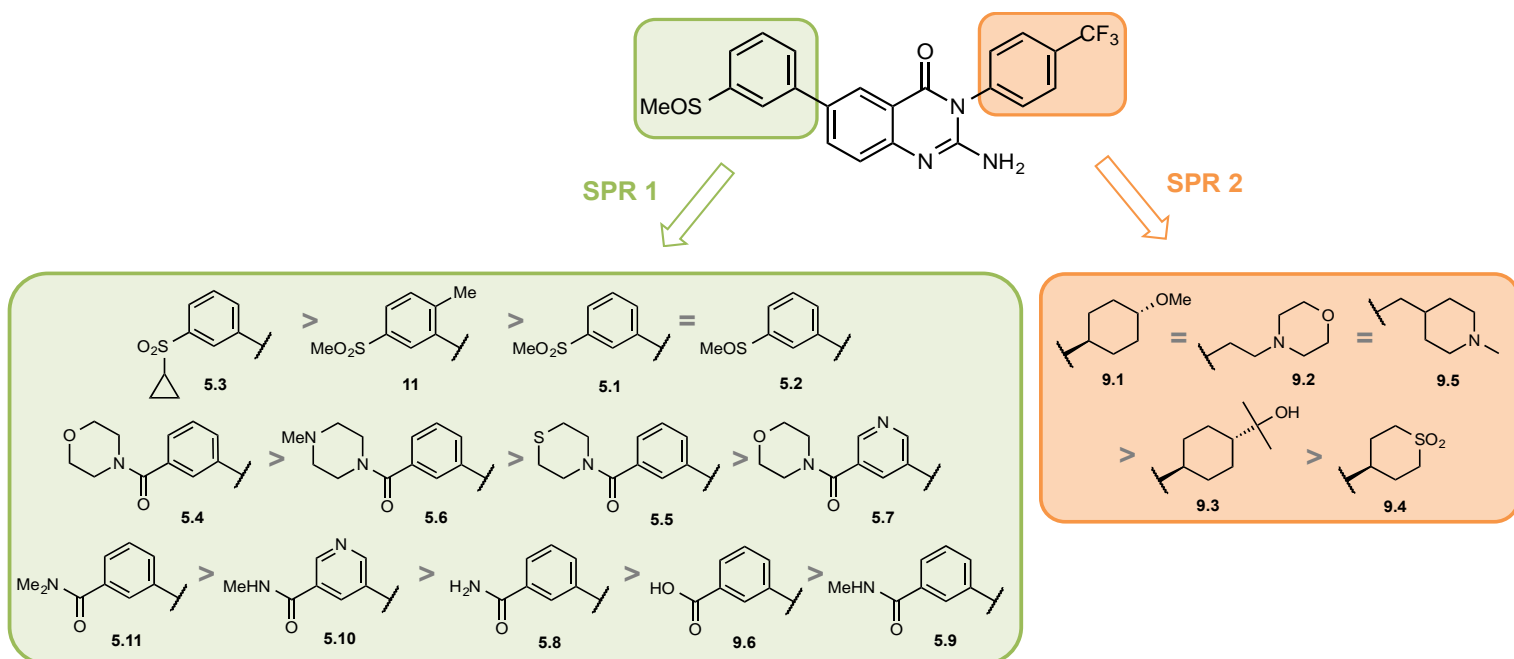


**Figure 58:** Summary of aqueous solubility trends observed for **SPR 1** and **SPR 2** series' based on values obtained using the HPLC-method.

In **SPR 1**, a moderate improvement in solubility was evident for the morpholino and amide series compared to the front-runner compounds **5.1** and **5.2**. Introducing a methyl substituent in the *ortho*-position (**11**) was found to be a successful approach toward increasing the dihedral angle and, in turn, improving aqueous solubility. The strategy of removing aromaticity to disrupt planarity and subsequently disturb the efficiency of crystal packing to improve solubility was explored in **SPR 2**. This resulted in highly soluble (>200  $\mu\text{M}$ ) compounds **9.1**, **9.2** and **9.5**, which was reflected in the lowered melting points of these derivatives.

Figure 59 summarizes the trends observed between structures of **SPR 3 – 5** and aqueous solubility. The new aminoquinazolinone intermediates generally displayed poor to moderate solubility. The most promising analogue, however, was the *ortho*-phenol derivative **7.1**, which was shown to be highly soluble (156  $\mu$ M) owing to the disruption of molecular symmetry.

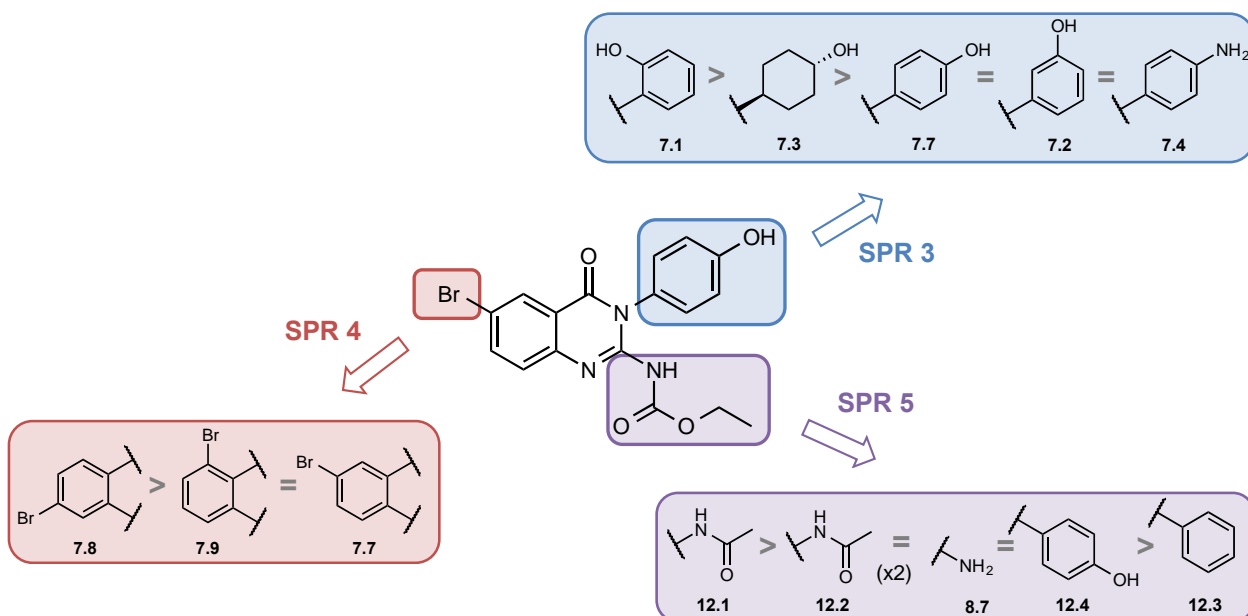


**Figure 59:** Summary of aqueous solubility trends observed for **SPR 3 – 5** based on values obtained using the HPLC-method.

Analysis of the relationships between solubility and physicochemical properties (ClogP, tPSA and MP) were performed. As shown in Figure 57, melting point was most moderately correlated with solubility ( $R^2 = 0.43$ ), suggesting that melting point can be considered as a parameter for the aqueous solubility of 2-aminoquinazolinones that were modified in ways that disrupted molecular symmetry and planarity.

In general, the results obtained suggest that the chemical modifications employed, particularly introduction of substituents to modify the dihedral angle and saturation of aromatic rings to disrupt molecular planarity and symmetry, were effective at improving the aqueous solubility of the aminoquinazolinone series. A combination of these approaches with the conventional approach of reducing lipophilicity may be especially successful.

## CHAPTER 5: SUMMARY AND FUTURE PROSPECTS

### 5.1. GENERAL SUMMARY AND CONCLUSIONS

A series of 2-aminoquinazolinones designed to improve solubility were successfully synthesized. Substituents were selected to reduce lipophilicity by introducing hydrophilic moieties or to disrupt molecular planarity/symmetry by reducing aromaticity or increasing the dihedral angle. Adapted synthetic routes were employed to deliver the desired analogues. All synthesized compounds were characterized by  $^1\text{H-NMR}$ ,  $^{13}\text{C-NMR}$  (1D and 2D), LCMS as well as melting point.

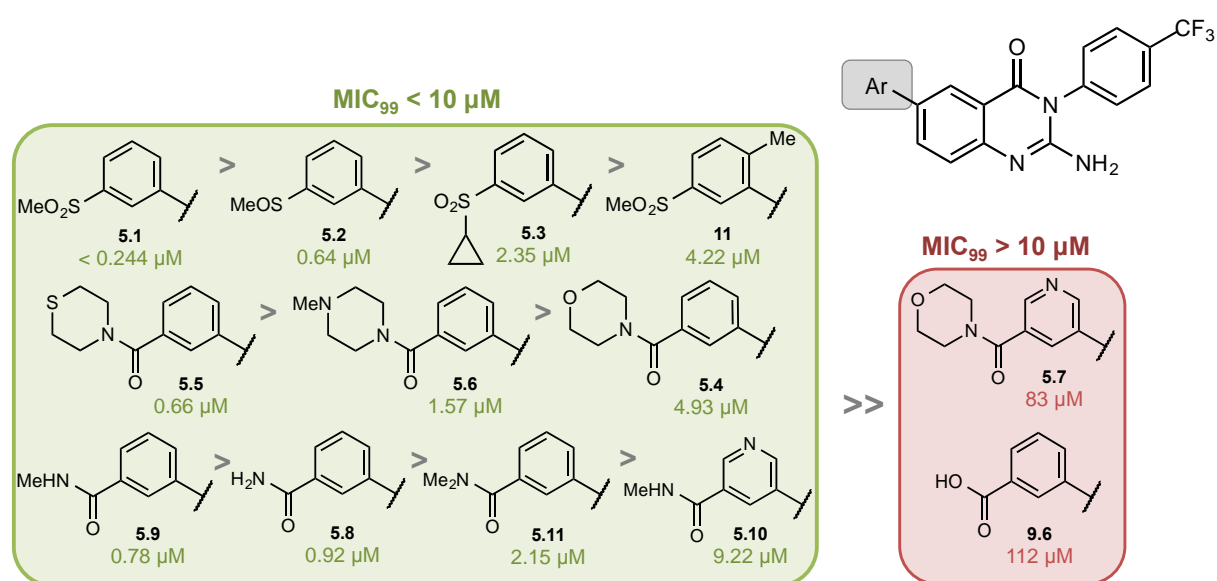


**Figure 60:** Summary of antimycobacterial activity trends observed for **SAR 1** derivatives in GAST Fe media.

**SAR 1** derivatives were evaluated for *in vitro* antimycobacterial activity in GAST Fe and 7H9 ADC media, as well as for cytotoxicity and metabolic stability. The following conclusions from the *in vitro* results were drawn:

- ✓ All compounds, except **5.7** and **9.6**, exhibited promising antimycobacterial activity ( $\text{MIC}_{99} < 10 \mu\text{M}$ ) in glycerol-containing media against the H37Rv strain of *Mtb* (Figure 60).
- ✓ Of the 11 compounds that were evaluated for cytotoxicity, 8 of them displayed low cytotoxicity.
- ✓ Derivatives displayed good metabolic stability in liver microsomes across three species (HLM, RLM, MLM).

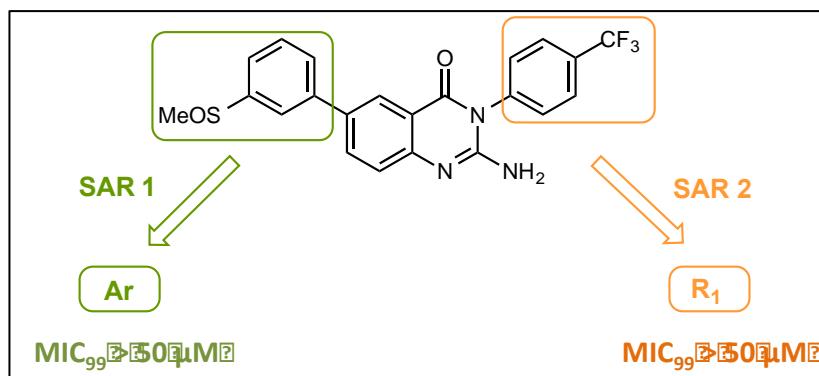


**Figure 61:** General structure of inactive **SAR 1** and **SAR 2** derivatives tested in glycerol-free media.

The disconnect between *in vitro* and *in vivo* results on frontrunner compounds **5.1** and **5.2** was investigated. In this regard, subsequent *in vitro* assays were performed on **SAR 1** and **SAR 2** intermediates and target compounds in glycerol-free media (Figure 61). All derivatives, except one intermediate **7.7**, were inactive. SAR was thus explored around this intermediate but no substantial activity was observed for the new analogues (Figure 62). These results suggest that the activity of 2-aminoquinazolinones on *Mtb* is glycerol-dependent.

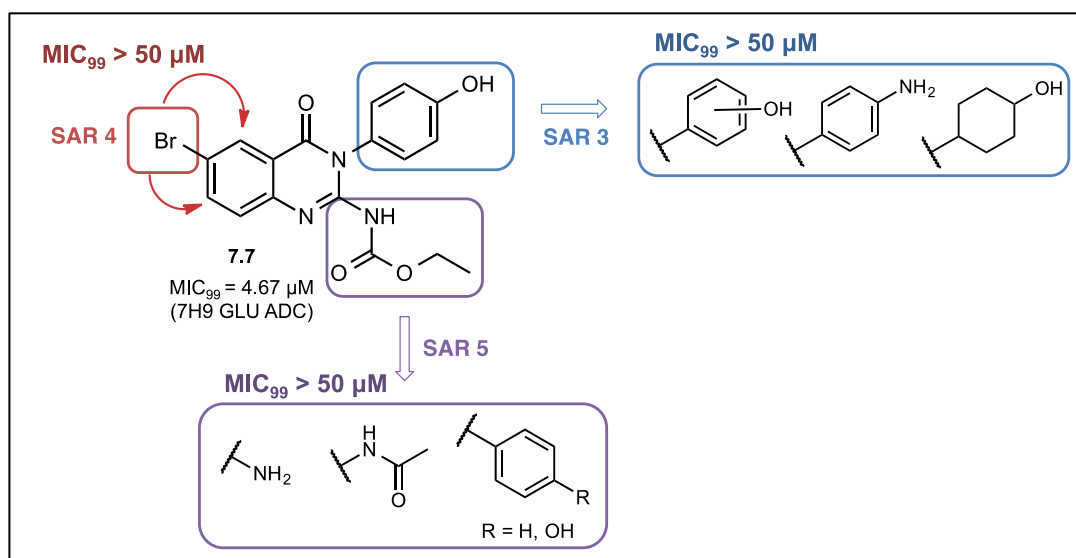


**Figure 62:** Summary of antimycobacterial **SAR 3 – 5** results tested in glycerol-free media displaying inactivity, except for compound **7.7**.

Solubility studies were performed on 30 synthesized target compounds of **SPR 1 - 5**. Turbidimetric and HPLC-based assay methods were used for solubility analysis and the following conclusions were deduced:

- ✓ The turbidimetric assay generally over-estimated solubility.
- ✓ Introduction of hydrophilic **Ar** substituents resulted in moderate improvement in solubility.
- ✓ Introduction of a substituent in the *ortho*-position to disrupt molecular planarity and symmetry resulted in 10-fold improvement in the solubility of **11** relative to the parent analogue **5.1** and was accompanied by an increase in the calculated dihedral angle (Figure 63).

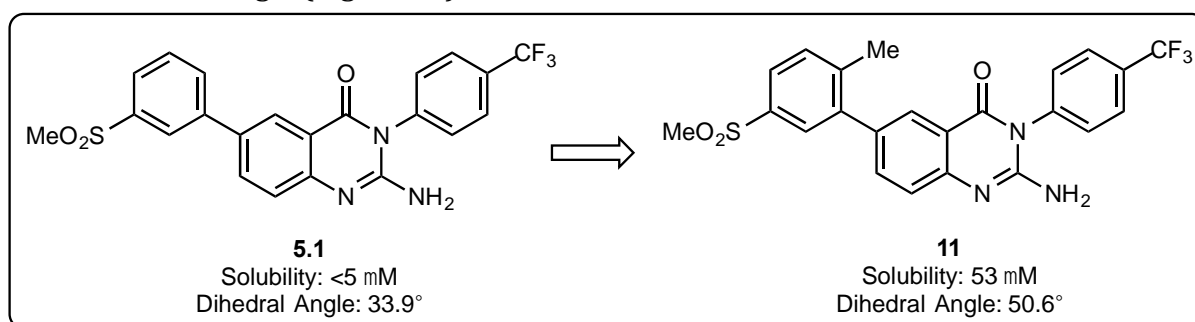


**Figure 63:** Solubility results of *ortho*-substituted analogue **11** compared to frontrunner compound **5.1**.

- ✓ Saturated ring systems of **SPR 2** analogues displayed the most promising results with 3 out of the 5 **SPR 2** compounds showing high solubility (>200  $\mu$ M). Reduction in crystal packing energy due to disruption of planarity was confirmed by the reduction in melting point.

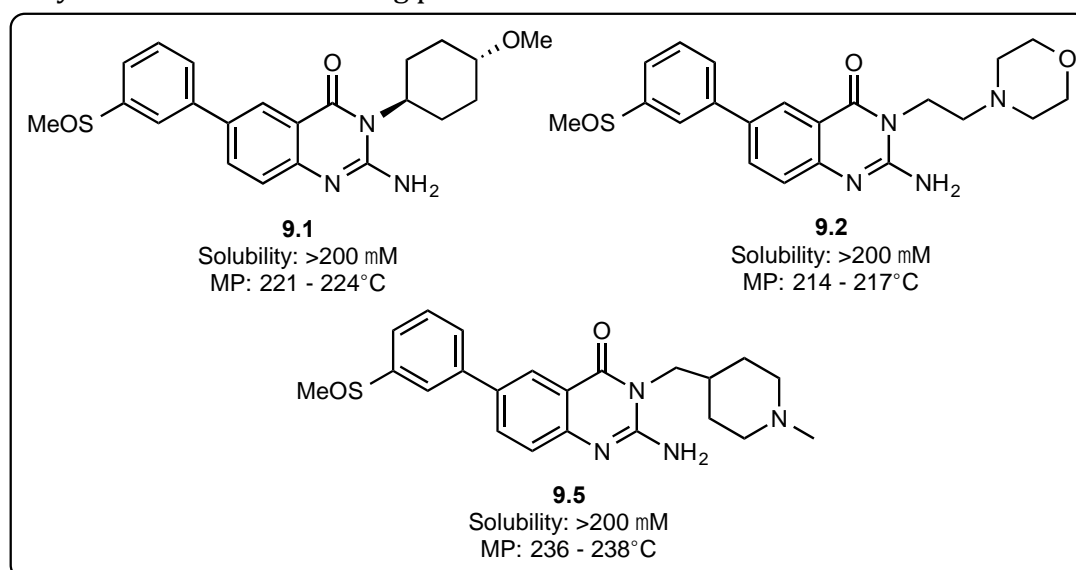


**Figure 64:** Structures of highly soluble **SPR 2** analogues incorporating saturated ring substituents.

- ✓ **SPR 3 – 5** compounds showed poor to moderate solubility albeit the *ortho*-phenol derivative was found to be highly soluble due to disruption of molecular symmetry as shown by the decrease in melting point.

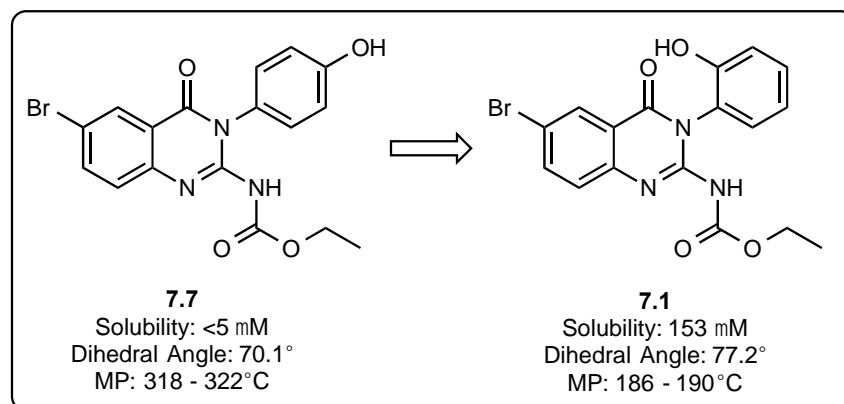


**Figure 65:** Structure of *ortho*-phenol analogue displaying high solubility compared to 7.7 owing to disruption of molecular symmetry.

- ✓ Relationships between solubility and the physicochemical parameters (ClogP, tPSA and melting point) were deduced. Melting point was found to be the most correlated with solubility suggesting that changes in crystal packing efficiency is more dominant than changes in lipophilicity for this series.

## 5.2. FUTURE OUTLOOK AND RECOMMENDATIONS

- Since the mechanism of action of the 2-aminoquinazolinone series was found to be glycerol-dependent, it is recommended that this mechanism be thoroughly investigated.
- Since selected compounds showed good cytotoxicity, metabolic stability and *in vivo* DMPK profiles, they should be explored in other disease models.
- In order to determine whether or not the mechanism of inhibition of the growth of *Mtb* by intermediate **7.7** is occurring via the proposed formation of a reactive metabolite, reactive metabolite generation, trapping and identification studies should be undertaken.
- Further exploration of the X-ray crystal structure of saturated derivatives (**SPR 2**) and *ortho*-substituted analogues (**7.1** or **11**) should be undertaken in order to provide insight into the disruption of crystal packing and reduction of crystal lattice energy.

## CHAPTER 6: EXPERIMENTAL RESULTS

---

### 6.1. MATERIALS AND EQUIPMENT

All commercially available chemicals were purchased from Sigma-Aldrich, Merck or Combi-Blocks Limited and were of analytical grade, thus used without further purification. Reactions were monitored by thin layer chromatography (TLC) using Fluka or Merck F254 aluminium-backed pre-coated silica gel plates and were visualized under ultraviolet light at 254 or 366 nm. Silica gel column chromatography was performed using Merck kieselgel 60: 70-230 mesh by gravity column chromatography or by flash chromatography on a Biotage Isolera™ system (Biotage AB, Uppsala, Sweden).

Reported compounds were characterized using 1D and 2D <sup>1</sup>H NMR, <sup>13</sup>C NMR, HPLC-MS and melting point determination.

<sup>1</sup>H NMR spectra were recorded on a Varian Mercury (300 MHz), a Bruker Ultrashield-Plus (400 MHz) spectrometer or a Bruker (600 MHz). <sup>13</sup>C NMR spectra were recorded on the same instruments at 101 MHz or 151 MHz. NMR samples were dissolved in deuterated dimethylsulfoxide (DMSO-*d*<sub>6</sub>) or chloroform (CDCl<sub>3</sub>). Chemical shifts ( $\delta$ ) are reported in parts per million (ppm) to 2 decimal places. Coupling constants (*J*) are reported in Hertz (Hz) to one decimal place. Abbreviations used in assigning <sup>1</sup>H-NMR signals are: s (singlet), d (doublet), dd (doublet of doublets), ddd (doublet of doublet of doublets), t (triplet), td (triplet of doublets), q (quartet), or m (multiplet).

Target compounds' peak purities and mass spectrometry were determined on an Agilent HPLC system equipped with Agilent 1260® Infinity Binary Pump, Agilent 1260® Infinity Diode Array Detector, Agilent 1290® Infinity Column Compartment, Agilent 1260® Infinity Autosampler, Agilent 6120® Quadrupole LC/MS and Peak Scientific® Genius 1050 Nitrogen Generator. The column used was an X-bridge® C18, 2.5  $\mu$ m, 3.0 mm (ID) x 50 mm (length) maintained at 35 °C. The injection volume was 2  $\mu$ L while the mass spectra were obtained both by positive mode Electron Spray ionization (ESI) and Atmospheric Pressure Chemical Ionization (APCI). The diode array detector was programmed to scan the eluents at an absorption wavelength range of 210-640 nm.

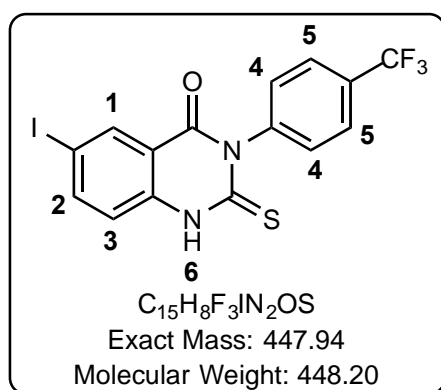
Melting points were determined using a Stuart SMP40 automatic melting point apparatus and are uncorrected.

## 6.2. SYNTHESIS AND CHARACTERIZATION

### 6.2.1. GENERAL PROCEDURES AND CHARACTERIZATION FOR SAR 1 INTERMEDIATE COMPOUNDS 1 – 4

#### **6-Iodo-2-thioxo-3-(4-(trifluoromethyl)phenyl)-2,3-dihydroquinazolin-4(1H)-one (1)**

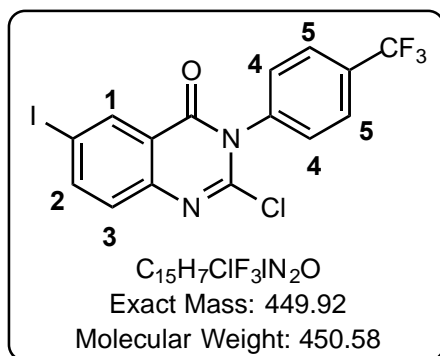
2-amino-5-iodobenzoic acid (5.08 g, 19.30 mmol, 1.0 Eq) and 1-isothiocyanato-4-(trifluoromethyl)benzene (4.12 g, 20.26 mmol, 1.05 Eq) were dissolved in dioxane (74.5 mL) and treated with triethylamine (3.8 mL, 1.5 Eq). The solution was refluxed for 4 hours, cooled to room temperature, and the solids that formed were filtered. The solids were resuspended in diethyl ether (Et<sub>2</sub>O) and filtered again to afford the thioxoquinazolinone intermediate.



White solid (7.84 g, 91%); m.p. 296 – 300°C; R<sub>f</sub> (EtOAc:Hex, 3:7) 0.37; <sup>1</sup>H NMR (300 MHz, DMSO-*d*<sub>6</sub>) δ 13.18 (s, 1H, H<sup>6</sup>), 8.20 (d, *J* = 1.9 Hz, 1H, H<sup>1</sup>), 8.10 (dd, *J* = 8.6, 2.0 Hz, 1H, H<sup>2</sup>), 7.88 (d, *J* = 8.3 Hz, 2H, H<sup>5</sup>), 7.56 (d, *J* = 8.1 Hz, 2H, H<sup>4</sup>), 7.26 (d, *J* = 8.6 Hz, 1H, H<sup>3</sup>); <sup>13</sup>C NMR (101 MHz, DMSO-*d*<sub>6</sub>) δ 176.14, 159.02, 144.21, 143.32, 139.64, 135.69, 130.72 (2C), 126.60 (2C), 126.56, 118.77, 118.54, 88.18, 66.84; HPLC-MS (APCI/ESI): Purity > 99%, t<sub>R</sub> = 4.452 min, m/z [M+H]<sup>+</sup> = 448.9.

#### **2-Chloro-6-iodo-3-(4-(trifluoromethyl)phenyl)quinazolin-4(3H)-one (2)**

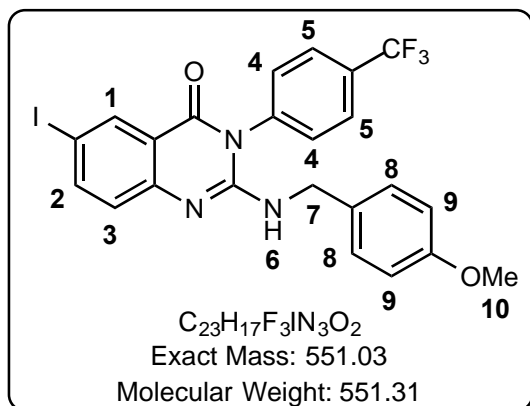
PCl<sub>5</sub> (6.3 g, 30.26 mmol, 1.73 Eq) was added in one portion to a mixture of **1** (7.84 g, 17.5 mmol, 1.0 Eq) in POCl<sub>3</sub> (38.8 mL, 417.7 mmol, 23.88 Eq) at room temperature (24.4°C). The mixture was stirred for 15 minutes at 24.4°C and was subsequently heated at 110°C for 14 hours under nitrogen. The reaction was cooled to room temperature, concentrated *in vacuo* and then diluted with ethyl acetate to be added portionwise to stirred ice – saturated sodium bicarbonate and stirred until all solids dissolved. The organic layer was then separated, washed with brine, dried over magnesium sulphate and concentrated under reduced pressure. The resulting residue was triturated in Et<sub>2</sub>O and filtered to obtain **2**.



Off-white solid (6.26 g, 79%); m.p. 200 – 204°C; R<sub>f</sub> (EtOAc:Hex, 3:7) 0.69; <sup>1</sup>H NMR (300 MHz, DMSO-*d*<sub>6</sub>) δ 8.39 (d, *J* = 1.8 Hz, 1H, H<sup>1</sup>), 8.22 (dd, *J* = 8.5, 2.1 Hz, 1H, H<sup>2</sup>), 7.99 (d, *J* = 8.3 Hz, 2H, H<sup>5</sup>), 7.81 (d, *J* = 8.2 Hz, 2H, H<sup>4</sup>), 7.52 (d, *J* = 8.7 Hz, 1H, H<sup>3</sup>); <sup>13</sup>C NMR (101 MHz, DMSO-*d*<sub>6</sub>) δ 150.20, 143.82, 139.91, 135.86, 135.42, 130.71 (2C), 130.44, 129.22, 127.13 (2C), 126.41, 118.23, 116.99, 85.69; HPLC-MS (APCI/ESI): Purity = 90%, t<sub>R</sub> = 4.567 min, m/z [M+H]<sup>+</sup> = 450.9.

### 6-Iodo-2-((4-methoxybenzyl)amino)-3-(4-(trifluoromethyl)phenyl)quinazolin-4(3H)-one (3)

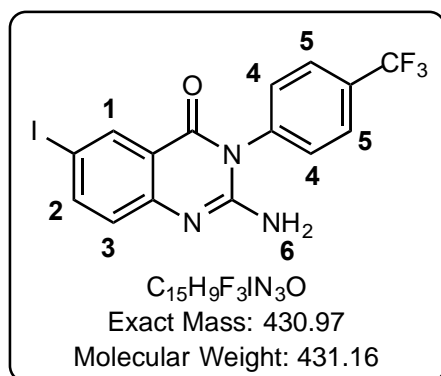
4-Methoxybenzylamine (2.36 mL, 18.06 mmol, 1.3 Eq) and *N,N*-diisopropylethylamine (DIPEA) (4.84 mL, 27.8 mmol, 2.0 Eq) were dissolved in DMF and **2** (6.26 g, 13.9 mmol, 1.0 Eq) was added portionwise. The reaction was stirred for 4 hours at 80°C and allowed to cool to room temperature. The solvent was concentrated under reduced pressure and diluted with ethyl acetate. The organic phase was washed with 5% lithium chloride (x5), brine (x3), dried over magnesium sulphate and concentrated *in vacuo*.



Brown solid (6.36 g, 83%); m.p. 172 – 175°C; R<sub>f</sub> (EtOAc:Hex, 3:7) 0.46; <sup>1</sup>H NMR (300 MHz, DMSO-*d*<sub>6</sub>) δ 8.15 (d, *J* = 2.0 Hz, 1H, H<sup>1</sup>), 7.97 (d, *J* = 8.3 Hz, 2H, H<sup>5</sup>), 7.87 (dd, *J* = 8.6, 2.2 Hz, 1H, H<sup>2</sup>), 7.67 (d, *J* = 8.1 Hz, 2H, H<sup>4</sup>), 7.24 (d, *J* = 8.7 Hz, 2H, H<sup>8</sup>), 7.11 (d, *J* = 8.7 Hz, 1H, H<sup>3</sup>), 6.85 (d, *J* = 8.7 Hz, 2H, H<sup>9</sup>), 6.68 (t, *J* = 5.9 Hz, 1H, H<sup>6</sup>), 4.44 (d, *J* = 5.9 Hz, 2H, H<sup>7</sup>), 3.71 (s, 3H, H<sup>10</sup>); <sup>13</sup>C NMR (101 MHz, DMSO-*d*<sub>6</sub>) δ 161.00, 158.55, 150.59, 149.58, 143.08, 139.05, 134.95, 132.01, 130.97 (2C), 130.70, 130.14 (q, *J* = 32.0 Hz, 1C, C-CF<sub>3</sub>), 128.88 (2C), 124.7 (q, *J* = 272.5 Hz, 1C, C-F<sub>3</sub>), 127.75 (2C), 127.60, 119.49, 114.00 (2C), 84.74, 44.18; HPLC-MS (APCI/ESI): Purity = 96%, t<sub>R</sub> = 4.902 min, m/z [M+H]<sup>+</sup> = 552.0.

### 2-Amino-6-iodo-3-(4-(trifluoromethyl)phenyl)quinazolin-4(3H)-one (4)

Compound **3** (6.35 g, 11.52 mmol, 1.0 Eq) was dissolved in TFA (56.2 mL, 63.7 Eq) and refluxed at 80°C for 72 hours. The reaction was cooled to room temperature and the solvent was concentrated. The residue was resuspended in DCM and added portionwise to a stirred ice – saturated sodium bicarbonate solution. The organic phase was separated, the aqueous phase was extracted with DCM and the combined organic phases were diluted with Et<sub>2</sub>O to a 1:1 ratio DCM/Et<sub>2</sub>O. The solids were filtered, washed with Et<sub>2</sub>O and dried under vacuum to afford the aminoquinazolinone intermediate **4**.

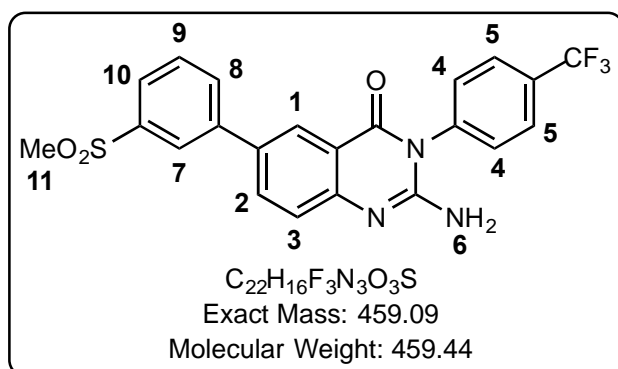


Pale green solid (4.3404 g, 87%); m.p. 265 – 270°C; R<sub>f</sub> (EtOAc:Hex, 1:1) 0.26; <sup>1</sup>H NMR (300 MHz, DMSO-*d*<sub>6</sub>) δ 8.14 (d, *J* = 2.0 Hz, 1H, H<sup>1</sup>), 7.93 (d, *J* = 8.3 Hz, 2H, H<sup>5</sup>), 7.87 (dd, *J* = 8.7, 2.2 Hz, 1H, H<sup>2</sup>), 7.63 (d, *J* = 8.1 Hz, 2H, H<sup>4</sup>), 7.07 (d, *J* = 8.7 Hz, 1H, H<sup>3</sup>), 6.60 (s, 2H, H<sup>6</sup>); <sup>13</sup>C NMR (101 MHz, DMSO-*d*<sub>6</sub>) δ 161.06, 152.21, 150.20, 143.04, 139.51, 135.01, 130.59 (2C), 130.03, 127.59, 127.55 (2C), 126.93, 119.24, 84.35; HPLC-MS (APCI/ESI): Purity = 98%, t<sub>R</sub> = 4.208 min, m/z [M+H]<sup>+</sup> = 432.0.

#### 6.2.2. GENERAL PROCEDURE FOR SUZUKI MIYaura COUPLING REACTION IN THE SYNTHESIS OF THE TARGET COMPOUNDS 5.1 – 5.11

2-Amino-6-iodo-3-(4-(trifluoromethyl)phenyl)quinazolin-4(3H)-one **4** (1.0 Eq) and the appropriate arylboronic acid or ester (1.5 Eq) were dissolved in anhydrous 1,4-dioxane (1.84 mL) and flushed with nitrogen. Bis(triphenylphosphine)palladium(II) dichloride, PdCl<sub>2</sub>(PPh<sub>3</sub>)<sub>2</sub>, (0.1 Eq) was added to the solution, cesium carbonate or potassium carbonate (3.0 Eq) was dissolved in water (0.05 Eq) and subsequently added to the reaction mixture. The solution was heated at 80°C until TLC monitoring showed completion (1-3 hours), allowed to cool to room temperature and diluted with EtOAc to be filtered through celite. The organic phase was washed with water and brine, dried over magnesium sulphate and concentrated under reduced pressure. The resulting crude residue was purified by silica-gel chromatography using the relevant solvent system, combined pure fractions were concentrated *in vacuo*, triturated with Et<sub>2</sub>O, filtered and dried under vacuum to give the relevant target compound **5.1 - 5.11**.

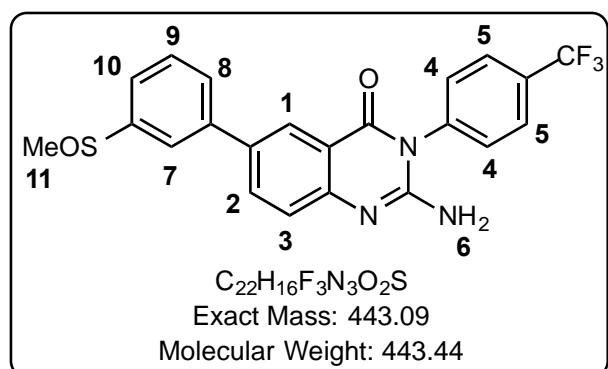
**2-Amino-6-(3-(methylsulfonyl)phenyl)-3-(4-(trifluoromethyl)phenyl)quinazolin-4(3H)-one (5.1)**



Obtained from **4** (236.3 mg, 0.55 mmol, 1.0 Eq), using 3-methylsulfonylphenyl boronic acid (164.4 mg, 0.82 mmol, 1.5 Eq), as a white solid (115.2 mg, 46%); m.p 246.3 – 250.4°C;  $R_f$  (EtOAc:DCM, 6:4) 0.35;  $^1H$  NMR (400 MHz, DMSO- $d_6$ )  $\delta$  8.24 (d,  $J$  = 2.2 Hz, 1H, H<sup>1</sup>), 8.20 (t,  $J$  = 1.8 Hz,

1H, H<sup>7</sup>), 8.07 (ddd,  $J$  = 7.6, 1.8, 1.0 Hz, 1H, H<sup>10</sup>), 8.06 (dd,  $J$  = 8.6, 2.4 Hz, 1H, H<sup>2</sup>), 7.96 (d,  $J$  = 8.8 Hz, 1H, H<sup>5</sup>), 7.90 (ddd,  $J$  = 7.8, 1.8, 1.0 Hz, 1H, H<sup>8</sup>), 7.75 (t,  $J$  = 7.8 Hz, 1H, H<sup>9</sup>), 7.67 (d,  $J$  = 7.9 Hz, 1H, H<sup>4</sup>), 7.40 (d,  $J$  = 8.6 Hz, 1H, H<sup>3</sup>), 6.59 (s, 2H, H<sup>6</sup>), 3.31 (s, 3H, H<sup>11</sup>);  $^{13}C$  NMR (101 MHz, DMSO- $d_6$ )  $\delta$  162.24, 152.18, 150.88, 142.21, 140.96, 139.69, 133.66, 131.86, 131.66, 130.64 (2C), 130.17 (q,  $J$  = 32.0 Hz, 1C,  $\underline{C}$ -CF<sub>3</sub>), 127.61, 127.58 (2C), 125.83, 125.41, 124.96, 124.87, 124.54 (q,  $J$  = 272.5 Hz, 1C,  $\underline{C}F_3$ ), 117.40, 43.95; HPLC-MS (APCI/ESI): Purity = 99%,  $t_R$  = 3.693 min,  $m/z$  [M+H]<sup>+</sup> = 460.0.

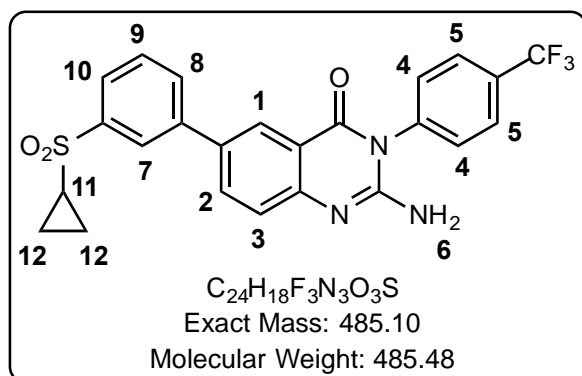
**2-Amino-6-(3-(methylsulfinyl)phenyl)-3-(4-(trifluoromethyl)phenyl)quinazolin-4(3H)-one (5.2)**



Obtained from **4** (210.1 mg, 0.49 mmol, 1.0 Eq), using 3-methylsulfinylphenyl boronic acid (98.6 mg, 0.54 mmol, 1.3 Eq), as an off-white solid (85.9 mg, 40%); m.p 325.5 – 328.3°C;  $R_f$  (MeOH:EtOAc, 1:9) 0.20;  $^1H$  NMR (400 MHz, DMSO- $d_6$ )  $\delta$  8.21 (d,  $J$  = 2.0 Hz, 1H, H<sup>1</sup>), 8.04 (dd,  $J$  = 8.6, 2.4

Hz, 1H, H<sup>2</sup>), 7.98 (t,  $J$  = 2.2 Hz, 1H, H<sup>7</sup>), 7.95 (d,  $J$  = 8.2 Hz, 2H, H<sup>5</sup>), 7.87 (dt,  $J$  = 6.6, 2.2 Hz, 1H, H<sup>10</sup>), 7.72 – 7.64 (m, 4H, H<sup>4</sup>, H<sup>8</sup>, H<sup>9</sup>), 7.38 (d,  $J$  = 8.2 Hz, 1H, H<sup>3</sup>), 6.57 (s, 2H, H<sup>6</sup>), 2.82 (s, 3H, H<sup>11</sup>);  $^{13}C$  NMR (101 MHz, DMSO- $d_6$ )  $\delta$  162.28, 152.08, 150.68, 147.89, 140.82, 139.73, 133.64, 132.55, 130.66 (2C), 130.45, 130.14 (q,  $J$  = 32.0 Hz, 1C,  $\underline{C}$ -CF<sub>3</sub>), 128.86, 127.61, 127.57, 125.34, 124.75, 124.7 (q,  $J$  = 272.48 Hz, 1C,  $\underline{C}F_3$ ), 122.64, 121.49, 117.37, 43.74; HPLC-MS (APCI/ESI): Purity > 99%,  $t_R$  = 4.346 min,  $m/z$  [M+H]<sup>+</sup> = 444.1.

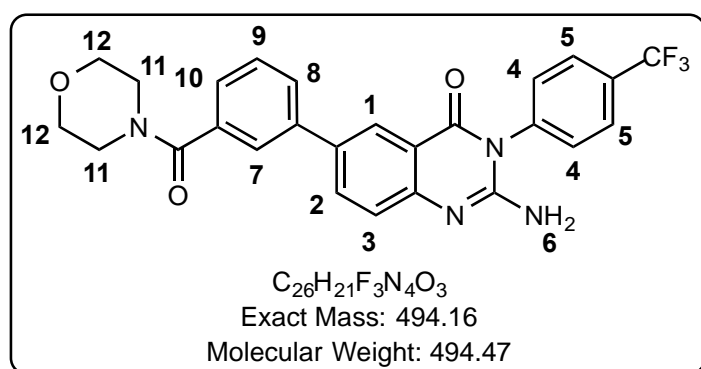
**2-Amino-6-(3-(cyclopropylsulfonyl)phenyl)-3-(4-(trifluoromethyl)phenyl)quinazolin-4(3H)-one (5.3)**



Obtained from **4** (208.7 mg, 0.48 mmol, 1.0 Eq), using 3-(cyclopropylsulfonyl)phenyl boronic acid (120.5 mg, 0.73 mmol, 1.5 Eq), as a pale yellow solid (167.8 mg, 71%); m.p 245.1 – 248.2 °C;  $R_f$  (EtOAc:Hexane, 1:1) 0.13;  $^1H$  NMR (400 MHz, DMSO- $d_6$ )  $\delta$  8.22 (d,  $J = 2.3$  Hz, 1H, H<sup>1</sup>), 8.14 (t,  $J = 1.7$

Hz, 1H, H<sup>7</sup>), 8.10 – 8.06 (m, 1H, H<sup>10</sup>), 8.05 (dd,  $J = 8.6, 2.3$  Hz, 1H, H<sup>2</sup>), 7.96 (d,  $J = 8.3$  Hz, 2H, H<sup>5</sup>), 7.87 (dt,  $J = 7.8, 1.1$  Hz, 1H, H<sup>8</sup>), 7.76 (t,  $J = 7.8$  Hz, 1H, H<sup>9</sup>), 7.67 (d,  $J = 8.2$  Hz, 2H, H<sup>4</sup>), 7.40 (d,  $J = 8.6$  Hz, 1H, H<sup>3</sup>), 6.60 (s, 2H, H<sup>6</sup>), 3.01 (m, 1H, H<sup>11</sup>), 1.21 – 1.15 (m, 2H, H<sup>12</sup>), 1.10 – 1.02 (m, 2H, H<sup>12</sup>);  $^{13}C$  NMR (101 MHz, DMSO- $d_6$ )  $\delta$  162.25, 152.20, 150.90, 141.99, 141.06, 139.70, 133.66, 131.84, 131.66, 130.82, 130.66 (2C), 130.16 (q,  $J = 32.0$  Hz, 1C,  $\underline{C}$ -CF<sub>3</sub>), 127.62, 127.58, 126.15, 125.45, 124.94 (2C), 124.57 (q,  $J = 272.48$  Hz, 1C,  $\underline{C}F_3$ ), 117.41, 32.45, 5.93 (2C); HPLC-MS (APCI/ESI): Purity = 98%,  $t_R = 3.974$  min,  $m/z$  [M+H]<sup>+</sup> = 486.1.

**2-Amino-6-(3-(morpholine-4-carbonyl)phenyl)-3-(4-(trifluoromethyl)phenyl)quinazolin-4(3H)-one (5.4)**

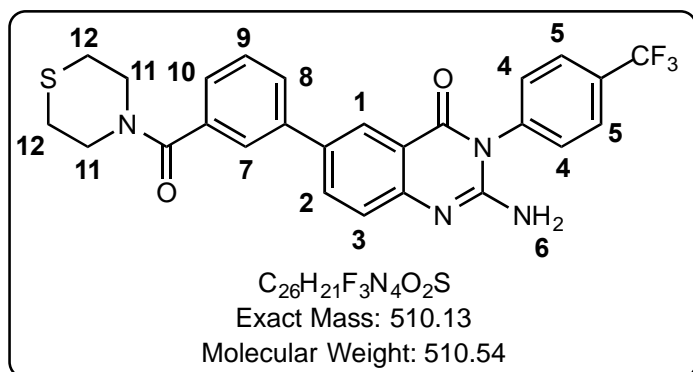


Obtained from **4** (202.6 mg, 0.47 mmol, 1.0 Eq), using 3-(morpholine-4-carbonyl)phenyl boronic acid (165.7 mg, 0.71 mmol, 1.5 Eq), as a pale yellow solid (202.1 mg, 87%); m.p 273.0 – 277.9 °C;  $R_f$  (3% MeOH in EtOAc)

0.4;  $^1H$  NMR (300 MHz, DMSO- $d_6$ )  $\delta$  8.16 (d,  $J = 2.2$  Hz, 1H, H<sup>1</sup>), 8.00 (dd,  $J = 8.6, 2.3$  Hz, 1H, H<sup>2</sup>), 7.95 (d,  $J = 8.3$  Hz, 2H, H<sup>5</sup>), 7.79 (dt,  $J = 7.8, 1.1$  Hz, 1H, H<sup>10</sup>), 7.70 (t,  $J = 1.5$  Hz, 1H, H<sup>7</sup>), 7.66 (d,  $J = 8.1$  Hz, 2H, H<sup>4</sup>), 7.55 (t,  $J = 7.7$  Hz, 1H, H<sup>9</sup>), 7.38 (dt,  $J = 6.4, 1.3$  Hz, 1H, H<sup>8</sup>), 7.36 (d,  $J = 8.6$  Hz, 1H, H<sup>3</sup>), 6.56 (s, 2H, H<sup>6</sup>), 3.62 (m, 4H, H<sup>12</sup>), 3.47 (m, 4H, H<sup>11</sup>);  $^{13}C$  NMR (101 MHz, DMSO- $d_6$ )  $\delta$  169.40, 162.28, 151.99, 150.50, 140.04, 139.75, 136.97, 133.61, 132.91, 130.67 (2C), 130.16 (q,  $J = 32.0$  Hz, 1C,  $\underline{C}$ -CF<sub>3</sub>), 129.70, 127.79, 127.57

(2C), 126.10, 125.28, 125.15, 124.58, 124.57 (q,  $J = 272.48$  Hz, 1C,  $\underline{\text{C}}\text{F}_3$ ), 117.34, 66.54 (4C); HPLC-MS (APCI/ESI): Purity = 98%,  $t_R = 3.824$  min,  $m/z$   $[\text{M}+\text{H}]^+ = 495.1$ .

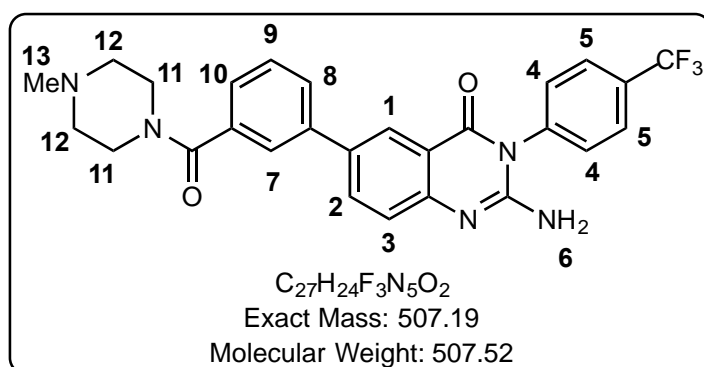
**2-Amino-6-(3-(thiomorpholine-4-carbonyl)phenyl)-3-(4-(trifluoromethyl)phenyl)quinazolin-4(3H)-one (5.5)**



Obtained from **4** (211.3 mg, 0.49 mmol, 1.0 Eq), using 3-(thiomorpholine-4-carbonyl)phenyl boronic acid (184.6 mg, 0.74 mmol, 1.5 Eq), as a pale yellow solid (208.4 mg, 83%); m.p 263.5 – 271.2 °C;  $R_f$  (Hexane:EtOAc, 7:3) 0.15;  $^1\text{H}$  NMR

(400 MHz,  $\text{DMSO}-d_6$ )  $\delta$  8.17 (d,  $J = 1.9$  Hz, 1H,  $\text{H}^1$ ), 8.01 (dd,  $J = 8.6, 2.4$  Hz, 1H,  $\text{H}^2$ ), 7.95 (d,  $J = 8.2$  Hz, 2H,  $\text{H}^5$ ), 7.78 (dt,  $J = 7.9, 1.5$  Hz, 1H,  $\text{H}^{10}$ ), 7.70 (t,  $J = 1.9$  Hz, 1H,  $\text{H}^7$ ), 7.66 (d,  $J = 8.1$  Hz, 2H,  $\text{H}^4$ ), 7.55 (t,  $J = 7.8$  Hz, 1H,  $\text{H}^9$ ), 7.37 (d,  $J = 8.9$  Hz, 1H,  $\text{H}^3$ ), 7.36 (dt,  $J = 7.6, 1.3$  Hz, 1H,  $\text{H}^8$ ), 6.55 (s, 2H,  $\text{H}^6$ ), 3.74 (m, 4H,  $\text{H}^{11}$ ), 2.67 (m, 4H,  $\text{H}^{12}$ );  $^{13}\text{C}$  NMR (101 MHz,  $\text{DMSO}-d_6$ )  $\delta$  169.69, 162.27, 151.98, 150.48, 140.04, 139.74, 137.44, 133.61, 132.88, 130.65 (2C), 130.13 (q,  $J = 32.0$  Hz, 1C,  $\underline{\text{C}}-\text{CF}_3$ ), 129.75, 127.59 (3C), 125.71, 125.26, 124.79, 124.60, 124.54 (q,  $J = 272.48$  Hz, 1C,  $\underline{\text{C}}\text{F}_3$ ), 117.33, 27.24 (4C); HPLC-MS (APCI/ESI): Purity = 97%,  $t_R = 4.213$  min,  $m/z$   $[\text{M}+\text{H}]^+ = 511.1$ .

**2-Amino-6-(3-(4-methylpiperazine-1-carbonyl)phenyl)-3-(4-(trifluoromethyl)phenyl)quinazolin-4(3H)-one (5.6)**

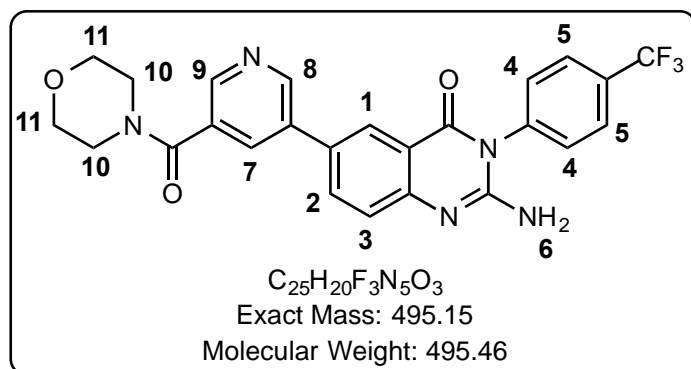


Obtained from **4** (205.3 mg, 0.48 mmol, 1.0 Eq), using 3-(4-methylpiperazine-1-carbonyl)phenyl boronic acid, pinacol ester (235.9 mg, 0.71 mmol, 1.5 Eq), as a brown-white solid (76.8 mg, 32%); m.p 232.1 – 236.3 °C;  $R_f$

(5% MeOH in EtOAc) 0.13;  $^1\text{H}$  NMR (300 MHz,  $\text{DMSO}-d_6$ )  $\delta$  8.15 (d,  $J = 2.3$  Hz, 1H,  $\text{H}^1$ ), 8.00 (dd,  $J = 8.6, 2.4$  Hz, 1H,  $\text{H}^2$ ), 7.95 (d,  $J = 8.3$  Hz, 2H,  $\text{H}^5$ ), 7.78 (dt,  $J = 8.0, 1.2$  Hz, 1H,  $\text{H}^{10}$ ), 7.63 – 7.70 (m, 3H,  $\text{H}^4, \text{H}^7$ ), 7.54 (t,  $J = 7.7$  Hz, 1H,  $\text{H}^9$ ), 7.36 (d,  $J = 8.6$  Hz, 1H,  $\text{H}^3$ ), 7.35 (dt,  $J = 7.6, 1.3$  Hz, 1H,  $\text{H}^8$ ), 6.56 (s, 2H,  $\text{H}^6$ ), 3.51 (m, 4H,  $\text{H}^{11}$ ), 2.34 (m, 4H,  $\text{H}^{12}$ ), 2.20

(s, 3H, H<sup>13</sup>); <sup>13</sup>C NMR (101 MHz, DMSO-*d*<sub>6</sub>) δ 169.26, 162.28, 151.98, 150.49, 139.99, 139.74, 137.32, 133.59, 132.91, 130.66 (2C), 129.71, 127.69 (2C), 127.58, 127.55, 125.99, 125.29, 124.96, 124.55, 117.33, 54.95 (2C), 46.06; HPLC-MS (APCI/ESI): Purity = 99%, t<sub>R</sub> = 3.041 min, m/z [M+H]<sup>+</sup> = 508.2.

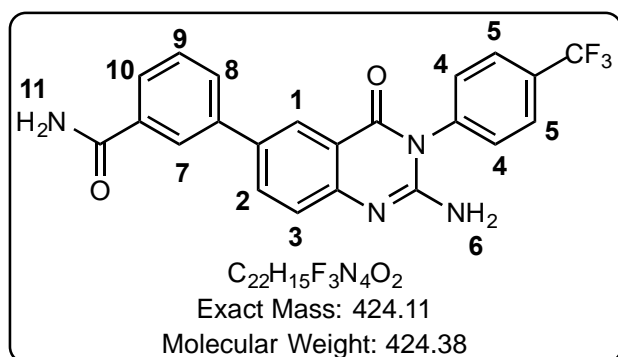
**2-Amino-6-(5-(morpholine-4-carbonyl)pyridin-3-yl)-3-(4-(trifluoromethyl)phenyl)quinazolin-4(3H)-one (5.7)**



Obtained from **4** (206.3 mg, 0.48 mmol, 1.0 Eq), using *N*-(morpholine-4-carbonyl)pyridine-3-boronic acid, pinacol ester (228.4 mg, 0.72 mmol, 1.5 Eq), as a white solid (117.6 mg, 50%); m.p 239.0 – 246.8 °C; R<sub>f</sub> (2% MeOH in EtOAC)

0.2; <sup>1</sup>H NMR (400 MHz, DMSO-*d*<sub>6</sub>) δ 9.00 (d, *J* = 2.3 Hz, 1H, H<sup>8</sup>), 8.59 (d, *J* = 2.0 Hz, 1H, H<sup>9</sup>), 8.23 (d, *J* = 2.3 Hz, 1H, H<sup>1</sup>), 8.14 (t, *J* = 2.1 Hz, 1H, H<sup>7</sup>), 8.06 (dd, *J* = 8.6, 2.3 Hz, 1H, H<sup>2</sup>), 7.96 (d, *J* = 8.7 Hz, 2H, H<sup>5</sup>), 7.67 (d, *J* = 8.6 Hz, 2H, H<sup>4</sup>), 7.39 (d, *J* = 8.6 Hz, 1H, H<sup>3</sup>), 6.61 (s, 2H, H<sup>6</sup>), 3.65 (m, 4H, H<sup>11</sup>), 3.43 (m, 4H, H<sup>10</sup>); <sup>13</sup>C NMR (101 MHz, DMSO-*d*<sub>6</sub>) δ 167.20, 162.16, 152.22, 150.97, 148.46, 146.47, 139.68, 135.07, 133.69, 132.58, 132.17, 130.64 (2C), 130.30, 129.98, 129.73, 127.61, 127.57 (2C), 125.91, 125.44, 125.17, 123.20, 117.46, 66.45; HPLC-MS (APCI/ESI): Purity = 96%, t<sub>R</sub> = 3.364 min, m/z [M+H]<sup>+</sup> = 496.1.

**3-(2-Amino-4-oxo-3-(4-(trifluoromethyl)phenyl)-3,4-dihydroquinazolin-6-yl)benzamide (5.8)**

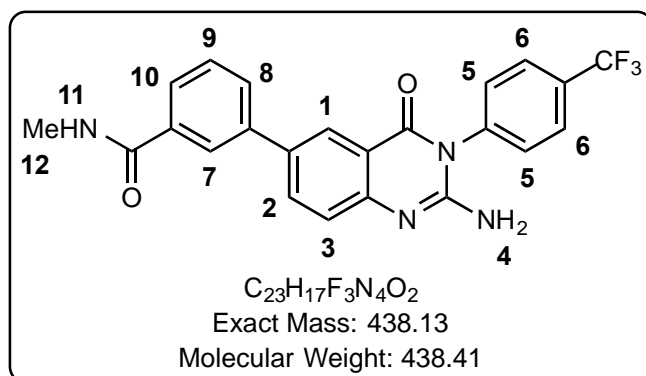


Obtained from **4** (208.1 mg, 0.48 mmol, 1.0 Eq), using 3-aminocarbonylphenyl boronic acid (119.5 mg, 0.72 mmol, 1.5 Eq), as a pale yellow solid (51.6 mg, 25%); m.p 295.5 – 299.9°C; R<sub>f</sub> (5% MeOH in EtOAC) 0.3; <sup>1</sup>H NMR (300 MHz, DMSO-*d*<sub>6</sub>) δ 8.23 (d, *J* = 2.2 Hz, 1H, H<sup>1</sup>), 8.20 (s,

1H, H<sup>7</sup>), 8.16 (s, 2H, H<sup>11</sup>), 8.03 (dd, *J* = 8.6, 2.3 Hz, 1H, H<sup>2</sup>), 7.95 (d, *J* = 8.3 Hz, 2H, H<sup>5</sup>), 7.86 (d, *J* = 7.8 Hz, 1H, H<sup>10</sup>), 7.85 (d, *J* = 7.6 Hz, 1H, H<sup>8</sup>), 7.67 (d, *J* = 8.1 Hz, 2H, H<sup>4</sup>), 7.55 (t, *J* = 6.5 Hz, 1H, H<sup>9</sup>), 7.36 (d, *J* = 4.3 Hz, 1H, H<sup>3</sup>), 6.55 (s, 2H, H<sup>6</sup>); <sup>13</sup>C NMR (101 MHz, DMSO-*d*<sub>6</sub>)

$\delta$  168.26, 162.32, 151.96, 150.44, 139.81, 137.85, 135.52, 133.66, 133.16, 130.67 (2C), 129.51, 129.40, 128.09, 127.56, 126.77, 126.67, 125.68, 125.24, 124.65, 124.54, 117.36; HPLC-MS (APCI/ESI): Purity = 98%,  $t_R$  = 4.263 min,  $m/z$   $[M+H]^+$  = 425.1.

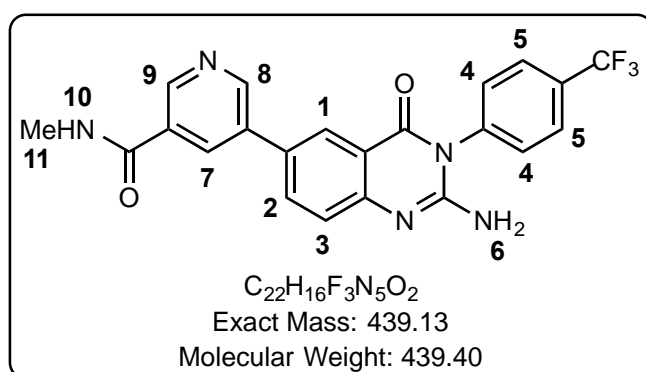
**3-(2-Amino-4-oxo-3-(4-(trifluoromethyl)phenyl)-3,4-dihydroquinazolin-6-yl)-N-methyl benzamide (5.9)**



Obtained from **4** (206.8 mg, 0.48 mmol, 1.0 Eq) using 3-(*N*-methylamino carbonyl) phenylboronic acid (128.8 mg, 0.72 mmol, 1.5 Eq), as a white solid (57.3 mg, 27%); m.p 292.5 – 298.0 °C;  $R_f$  (100% EtOAc) 0.15;  $^1H$  NMR (400 MHz, DMSO- $d_6$ )  $\delta$  8.58 (q,  $J$

= 3.9 Hz, 1H, H<sup>11</sup>), 8.23 (d,  $J$  = 2.2 Hz, 1H, H<sup>1</sup>), 8.16 (t,  $J$  = 1.8 Hz, 1H, H<sup>7</sup>), 8.02 (dd,  $J$  = 8.6, 2.3 Hz, 1H, H<sup>2</sup>), 7.96 (d,  $J$  = 8.2 Hz, 2H, H<sup>6</sup>), 7.84 (m, 1H, H<sup>10</sup>), 7.82 (m, 1H, H<sup>8</sup>), 7.67 (d,  $J$  = 7.8 Hz, 2H, H<sup>5</sup>), 7.56 (t,  $J$  = 7.7 Hz, 1H, H<sup>9</sup>), 7.38 (d,  $J$  = 8.6 Hz, 1H, H<sup>3</sup>), 6.55 (s, 2H, H<sup>4</sup>), 2.83 (d,  $J$  = 4.5 Hz, 3H, H<sup>12</sup>);  $^{13}C$  NMR (101 MHz, DMSO- $d_6$ )  $\delta$  166.93, 162.31, 151.96, 150.44, 139.85, 139.77, 135.72, 133.65, 133.15, 130.66 (2C), 129.56, 129.21, 127.59 (2C), 127.56, 126.42, 125.23 (2C), 125.21, 124.63, 117.36, 26.71; HPLC-MS (APCI/ESI): Purity = 99%,  $t_R$  = 3.778 min,  $m/z$   $[M+H]^+$  = 439.1.

**5-(2-Amino-4-oxo-3-(4-(trifluoromethyl)phenyl)-3,4-dihydroquinazolin-6-yl)-N-methyl nicotinamide (5.10)**

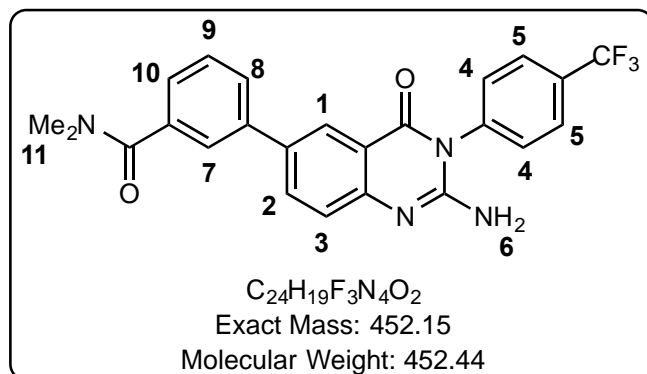


Obtained from **4** (218.7 mg, 0.51 mmol, 1.0 Eq) using 5-(*N*-methylcarbamoyl) pyridine-3-boronic acid, pinacol ester (199.4 mg, 0.77 mmol, 1.5 Eq), as an orange-brown solid (100.1 mg, 45%); m.p 310.5 – 313.5 °C;  $R_f$  (5% MeOH in EtOAc) 0.15;

$^1H$  NMR (400 MHz, DMSO- $d_6$ )  $\delta$  9.05 (d,  $J$  = 2.2 Hz, 1H, H<sup>9</sup>), 8.96 (d,  $J$  = 2.0 Hz, 1H, H<sup>8</sup>), 8.76 (q,  $J$  = 5.8 Hz, 1H, H<sup>10</sup>), 8.47 (t,  $J$  = 2.2 Hz, 1H, H<sup>7</sup>), 8.28 (d,  $J$  = 2.3 Hz, 1H, H<sup>1</sup>), 8.08 (dd,  $J$  = 8.6, 2.3 Hz, 1H, H<sup>2</sup>), 7.96 (d,  $J$  = 8.3 Hz, 2H, H<sup>5</sup>), 7.71 – 7.65 (d,  $J$  = 8.0 Hz, 2H, H<sup>4</sup>), 7.40 (d,  $J$  = 8.6 Hz, 1H, H<sup>3</sup>), 6.61 (s, 2H, H<sup>6</sup>), 2.85 (d,  $J$  = 4.5 Hz, 3H, H<sup>11</sup>);  $^{13}C$  NMR (101

MHz, DMSO-*d*<sub>6</sub>)  $\delta$  172.40, 165.49, 162.20, 152.22, 150.96, 149.69, 147.44, 139.70, 134.90, 133.62, 132.40, 130.64 (2C), 130.16 (q,  $J$  = 32.0 Hz, 1C,  $\underline{C}$ -CF<sub>3</sub>), 127.62 (2C), 125.45, 125.18, 124.92 (q,  $J$  = 272.48 Hz, 1C,  $\underline{C}$ F<sub>3</sub>), 117.52, 26.65, 21.50; HPLC-MS (APCI/ESI): Purity = 98%,  $t_R$  = 3.351 min,  $m/z$  [M+H]<sup>+</sup> = 440.1.

**3-(2-Amino-4-oxo-3-(4-(trifluoromethyl)phenyl)-3,4-dihydroquinazolin-6-yl)-*N,N*-dimethylbenzamide (5.11)**



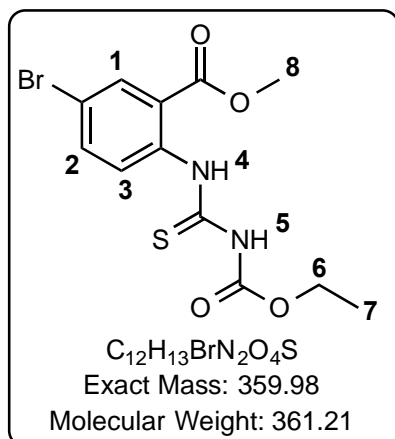
Obtained from **4** (212.6 mg, 0.49 mmol, 1.0 Eq) using 3-(*N,N*-dimethylamino carbonyl)phenylboronic acid (142.7 mg, 0.74 mmol, 1.5 Eq), as a pale yellow solid (100.1 mg, 45%); m.p 286.0 – 288.9 °C;  $R_f$ (5% MeOH in EtOAc) 0.34; <sup>1</sup>H NMR (400 MHz, DMSO-*d*<sub>6</sub>)  $\delta$  8.16 (d,

$J$  = 2.3 Hz, 1H, H<sup>1</sup>), 8.00 (dd,  $J$  = 8.6, 2.4 Hz, 1H, H<sup>2</sup>), 7.95 (d,  $J$  = 8.3 Hz, 2H, H<sup>5</sup>), 7.77 (ddd,  $J$  = 7.9, 1.9, 1.1 Hz, 1H, H<sup>10</sup>), 7.68 (t,  $J$  = 2.0 Hz, 1H, H<sup>7</sup>), 7.66 (d,  $J$  = 8.2 Hz, 2H, H<sup>4</sup>), 7.54 (t,  $J$  = 7.7 Hz, 1H, H<sup>9</sup>), 7.37 (dt,  $J$  = 7.6, 1.2 Hz, 1H, H<sup>8</sup>), 7.36 (d,  $J$  = 8.6 Hz, 1H, H<sup>3</sup>), 6.54 (s, 2H, H<sup>6</sup>), 3.01 (s, 3H, H<sup>11</sup>), 2.97 (s, 3H, H<sup>11</sup>); <sup>13</sup>C NMR (101 MHz, DMSO-*d*<sub>6</sub>)  $\delta$  170.42, 162.27, 151.96, 150.44, 139.85, 139.74, 137.83, 133.59, 133.00, 130.66 (2C), 130.11 (q,  $J$  = 32.0 Hz, 1C,  $\underline{C}$ -CF<sub>3</sub>), 129.53, 127.54 (3C), 126.04, 125.27, 125.08, 124.56 (q,  $J$  = 272.48 Hz, 1C,  $\underline{C}$ F<sub>3</sub>), 124.53, 117.33, 39.43, 35.22; HPLC-MS (APCI/ESI): Purity = 96%,  $t_R$  = 3.890 min,  $m/z$  [M+H]<sup>+</sup> = 453.1.

**6.2.3. GENERAL PROCEDURE FOR THE SYNTHESIS OF INTERMEDIATES 6.1 – 6.3**

The appropriate methyl 2-aminobromobenzoate (1.0 Eq) was dissolved in acetonitrile (10 mL) and the yellow solution was treated with ethoxycarbonyl isothiocyanate (1.2 Eq). After stirring for 10 minutes at room temperature, the precipitate that formed was filtered, the resulting mother liquor was concentrated and solids refiltered to afford the relevant thioureido intermediates **6.1 – 6.3**.

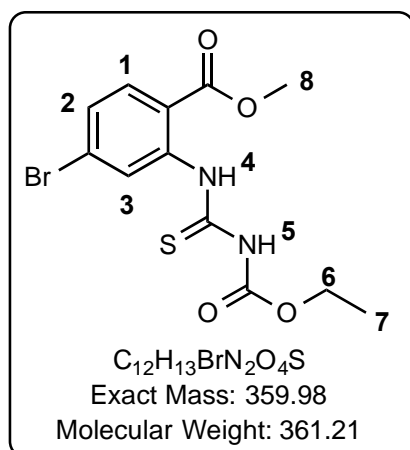
### Methyl 5-bromo-2-(3-(ethoxycarbonyl)thioureido)benzoate (6.1)



Obtained from methyl 2-amino-5-bromobenzoate (3.58 g, 15.57 mmol, 1.0 Eq) to afford **6.1** as a pale yellow solid (5.09 g, 90%); m.p 155.4 – 159.7 °C;  $R_f$  (EtOAc:Hex, 3:7) 0.51;  $^1H$  NMR (400 MHz, Chloroform-*d*)  $\delta$  12.61 (s, 1H, H<sup>4</sup>), 8.47 (d,  $J$  = 8.9 Hz, 1H, H<sup>3</sup>), 8.18 (s, 1H, H<sup>5</sup>), 8.16 (d,  $J$  = 2.4 Hz, 1H, H<sup>1</sup>), 7.68 (dd,  $J$  = 8.8, 2.5 Hz, 1H, H<sup>2</sup>), 4.35 (q,  $J$  = 7.1 Hz, 2H, H<sup>6</sup>), 3.97 (s, 3H, H<sup>8</sup>), 1.37 (t,  $J$  = 7.1 Hz, 3H, H<sup>7</sup>);  $^{13}C$  NMR (101 MHz, Chloroform-*d*)  $\delta$  178.10, 165.46, 151.67, 137.95, 135.35, 133.42, 127.86, 123.54, 118.74,

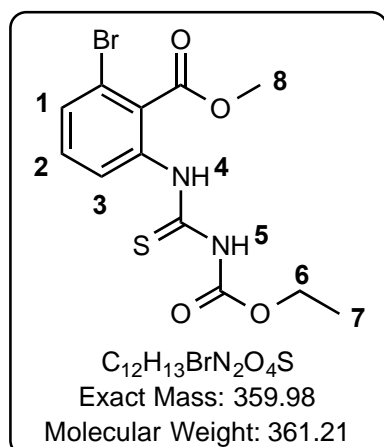
63.07, 52.81, 14.21; HPLC-MS (APCI/ESI): Purity >99%,  $t_R$  = 4.202 min,  $m/z$   $[M+H]^+$  = 360.9, 362.9 (1:1).

### Methyl 4-bromo-2-(3-(ethoxycarbonyl)thioureido)benzoate (6.2)



Obtained from methyl 2-amino-4-bromobenzoate (612.3 mg, 2.66 mmol, 1.0 Eq) to afford **6.2** as a white solid (698 mg, 73%); m.p. 143.3 – 147.1°C;  $R_f$  (5:5 EtOAc:Hexane) 0.57;  $^1H$  NMR (400 MHz, DMSO-*d*<sub>6</sub>)  $\delta$  12.24 (s, 1H, H<sup>4</sup>), 11.37 (s, 1H, H<sup>5</sup>), 8.39 (d,  $J$  = 2.1 Hz, 1H, H<sup>3</sup>), 7.85 (d,  $J$  = 8.5 Hz, 1H, H<sup>1</sup>), 7.58 (dd,  $J$  = 8.5, 2.0 Hz, 1H, H<sup>2</sup>), 4.25 (q,  $J$  = 7.1 Hz, 2H, H<sup>6</sup>), 3.84 (s, 3H, H<sup>8</sup>), 1.28 (t,  $J$  = 7.1 Hz, 3H, 7);  $^{13}C$  NMR (101 MHz, DMSO-*d*<sub>6</sub>)  $\delta$  179.91, 165.66, 153.55, 139.99, 132.41, 130.49, 129.39, 125.78, 123.06, 62.59, 53.06, 14.61; HPLC-MS (APCI/ESI): Purity 95%,  $t_R$  = 4.823 min,  $m/z$   $[M+H]^+$  = 361.0, 363.0 (1:1).

### Methyl 2-bromo-6-(3-(ethoxycarbonyl)thioureido)benzoate (6.3)

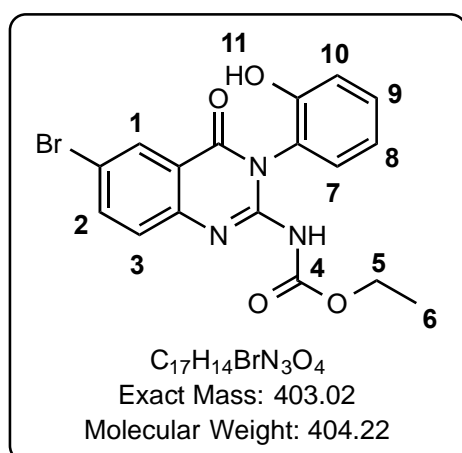


Obtained from methyl 2-amino-6-bromobenzoate (0.35 mL, 2.40 mmol, 1.0 Eq) to afford **6.3** as a light yellow solid (303.6 mg, 35%); m.p. 117.2 – 119.9°C; R<sub>f</sub> (3:7 EtOAc:Hexane) 0.38; <sup>1</sup>H NMR (300 MHz, DMSO-*d*<sub>6</sub>) δ 11.54 (s, 1H, H<sup>4</sup>), 11.48 (s, 1H, H<sup>5</sup>), 7.84 (dd, *J* = 8.1, 1.0 Hz, 1H, H<sup>3</sup>), 7.65 (dd, *J* = 8.1, 1.0 Hz, 1H, H<sup>1</sup>), 7.47 (t, *J* = 8.1 Hz, 1H, H<sup>2</sup>), 4.23 (q, *J* = 7.1 Hz, 2H, H<sup>6</sup>), 3.86 (s, 3H, H<sup>8</sup>), 1.27 (t, *J* = 7.1 Hz, 3H, H<sup>7</sup>); <sup>13</sup>C NMR (101 MHz, DMSO-*d*<sub>6</sub>) δ 180.63, 165.95, 154.23, 137.06, 131.93, 131.64, 131.42, 128.13, 118.68, 62.92, 53.45, 14.50; HPLC-MS (APCI/ESI): Purity >99%, t<sub>R</sub> = 4.453 min, m/z [M+H]<sup>+</sup> = 360.9, 362.9 (1:1).

### 6.2.4. GENERAL PROCEDURE FOR THE SYNTHESIS OF COMPOUNDS 7.1 – 7.9

Compounds **6.1** – **6.3** (1.0 Eq) were dissolved in DCM or DMF and the relative primary cyclic amine (1.5 Eq) and EDCI (2.0 Eq) were successively added to the solution. The solution was allowed to stir at room temperature (21.3–24.9°C) until completion, as per TLC and LCMS monitoring (18-22 hours). Once complete, DMF solutions were diluted with EtOAc and washed with 5% LiCl (5x), thereafter all solutions were washed with 1% of 1M HCl (x2), water, brine (x3) and dried over magnesium sulphate. The solvent was concentrated under reduced pressure to furnish compounds **7.1** – **7.5**.

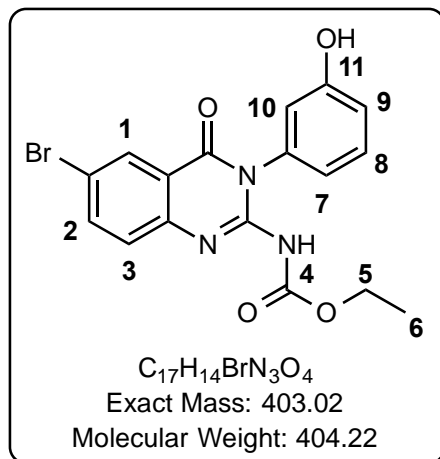
### Ethyl (6-bromo-3-(2-hydroxyphenyl)-4-oxo-3,4-dihydroquinazolin-2-yl)carbamate (7.1)



Obtained from **6.1** (310.6 mg, 0.86 mmol, 1.0 Eq) using 2-aminophenol (140.8 mg, 1.29 mmol, 1.5 Eq), to give a light brown solid (154.6 mg, 38%); m.p. 186.1 – 190.1°C; R<sub>f</sub> (5% MeOH in DCM) 0.48; <sup>1</sup>H NMR (400 MHz, DMSO-*d*<sub>6</sub>) δ 12.35 (s, 1H, H<sup>4</sup>), 9.62 (s, 1H, H<sup>11</sup>), 8.10 (d, *J* = 2.3 Hz, 1H, H<sup>1</sup>), 7.97 (dd, *J* = 8.8, 2.4 Hz, 1H, H<sup>2</sup>), 7.72 (d, *J* = 8.8 Hz, 1H, H<sup>3</sup>), 7.27 (ddd, *J* = 8.1, 7.3, 1.7 Hz, 1H, H<sup>9</sup>), 7.16 (dd, *J* = 7.8, 1.7 Hz, 1H, H<sup>7</sup>), 6.95 (dd, *J* = 8.2, 1.3 Hz, 1H, H<sup>10</sup>), 6.89 (td, *J* = 7.6, 1.4 Hz, 1H, H<sup>8</sup>), 3.99 (q, *J* = 7.1 Hz, 2H, H<sup>5</sup>), 1.13 (t, *J* = 7.1 Hz, 3H, H<sup>6</sup>); <sup>13</sup>C NMR (101 MHz, DMSO-*d*<sub>6</sub>) δ 162.72, 160.11, 153.78, 153.27, 149.92, 138.33, 137.33, 130.46,

130.24, 129.41, 126.78, 123.37, 119.47, 116.98, 113.07, 61.36, 14.71; HPLC-MS (APCI/ESI): Purity 95%,  $t_R = 4.258$  min,  $m/z$   $[M+H]^+ = 404.0, 406.0$  (1:1).

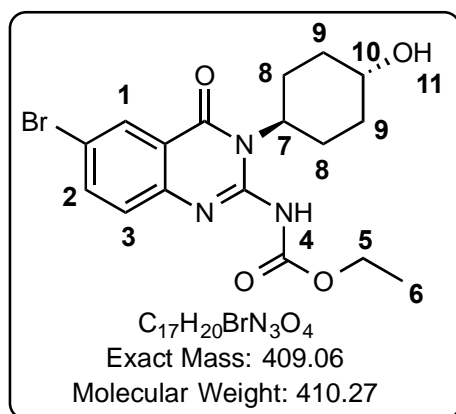
**Ethyl (6-bromo-3-(3-hydroxyphenyl)-4-oxo-3,4-dihydroquinazolin-2-yl)carbamate (7.2)**



Obtained from **6.1** (310.6 mg, 0.86 mmol, 1.0 Eq) using 3-aminophenol (140.8 mg, 1.29 mmol, 1.5 Eq), as a white solid (108.7 mg, 31%); m.p. 350.9 – 356.9°C;  $R_f$  (5% MeOH in DCM) 0.48;  $^1H$  NMR (400 MHz, DMSO- $d_6$ )  $\delta$  12.11 (s, 1H, H<sup>4</sup>), 9.67 (s, 1H, H<sup>11</sup>), 8.10 (d,  $J = 2.3$  Hz, 1H, H<sup>1</sup>), 7.96 (dd,  $J = 8.7, 2.4$  Hz, 1H, H<sup>2</sup>), 7.70 (d,  $J = 8.7$  Hz, 1H, H<sup>3</sup>), 7.28 (t,  $J = 8.3$  Hz, 1H, H<sup>8</sup>), 6.85 (ddd,  $J = 8.2, 2.2, 1.2$  Hz, 1H, H<sup>7</sup>), 6.73 – 6.72 (m, 1H, H<sup>9</sup>), 6.71 – 6.70 (m, 1H, H<sup>10</sup>), 3.99 (q,  $J = 7.1$

Hz, 2H, H<sup>5</sup>), 1.13 (t,  $J = 7.1$  Hz, 3H, H<sup>6</sup>);  $^{13}C$  NMR (101 MHz, DMSO- $d_6$ )  $\delta$  162.72, 160.02, 158.23, 153.85, 138.42, 137.49, 130.04, 129.47, 120.09, 119.70, 118.13, 116.41 (2C), 116.02, 115.88, 61.50, 14.85; HPLC-MS (APCI/ESI): Purity 95%,  $t_R = 4.273$  min,  $m/z$   $[M+H]^+ = 404.0, 406.0$  (1:1).

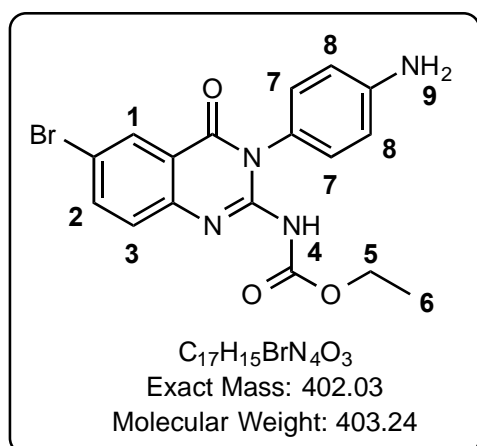
**Ethyl(6-bromo-3-((1*r*,4*r*)-4-hydroxycyclohexyl)-4-oxo-3,4-dihydroquinazolin-2-yl)carbamate (7.3)**



Obtained from **6.1** (307.3 mg, 0.85 mmol, 1.0 Eq) using *trans*-4-aminocyclohexanol (146.9 mg, 1.28 mmol, 1.5 Eq) to afford a white solid (164.3 mg, 47%); m.p. 310.0 – 317.7°C;  $R_f$  (5% MeOH in DCM) 0.41;  $^1H$  NMR (400 MHz, DMSO- $d_6$ )  $\delta$  12.28 (s, 1H, H<sup>4</sup>), 8.05 (d,  $J = 2.3$  Hz, 1H, H<sup>1</sup>), 7.88 (dd,  $J = 8.7, 2.3$  Hz, 1H, H<sup>2</sup>), 7.60 (d,  $J = 8.7$  Hz, 1H, H<sup>3</sup>), 5.00 (m, 1H, H<sup>7</sup>), 4.58 (d,  $J = 4.6$  Hz, 1H, H<sup>11</sup>), 4.16 (q,  $J = 7.1$  Hz,

2H, H<sup>5</sup>), 3.44 (td,  $J = 11.0, 4.5$  Hz, 1H, H<sup>10</sup>), 2.54 (q,  $J = 12.4$  Hz, 2H, H<sup>8ax</sup>), 1.93 (d,  $J = 13.0$  Hz, 2H, H<sup>9eq</sup>), 1.61 (d,  $J = 12.3$  Hz, 2H, H<sup>8eq</sup>), 1.28 (t,  $J = 7.1$  Hz, 4H, H<sup>6</sup>), 1.24 – 1.15 (m, 1H, H<sup>9ax</sup>);  $^{13}C$  NMR (101 MHz, DMSO- $d_6$ )  $\delta$  162.27, 160.36, 152.99, 138.07, 137.05, 129.28, 120.18, 118.41, 116.71, 68.69, 61.55, 55.34, 35.51 (2C), 26.02 (2C), 14.86; HPLC-MS (APCI/ESI): Purity >99%,  $t_R = 4.802$  min,  $m/z$   $[M+H]^+ = 410.0, 412.0$  (1:1).

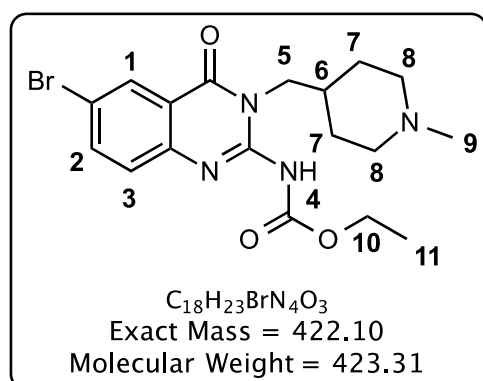
**Ethyl (3-(4-aminophenyl)-6-bromo-4-oxo-3,4-dihydroquinazolin-2-yl)carbamate (7.4)**



Obtained from **6.1** (246.1 mg, 0.68 mmol, 1.0 Eq.) using *p*-phenylenediamine (81.0 mg, 0.75 mmol, 1.1 Eq), as a white solid (222.7 mg, 81%); m.p. 331.2 – 339.4°C;  $R_f$  (100% EtOAc) 0.57;  $^1H$  NMR (400 MHz, DMSO- $d_6$ )  $\delta$  12.15 (s, 1H, H<sup>4</sup>), 8.10 (d,  $J$  = 2.3 Hz, 1H, H<sup>1</sup>), 7.95 (dd,  $J$  = 8.7, 2.4 Hz, 1H, H<sup>2</sup>), 7.65 (d,  $J$  = 8.7 Hz, 1H, H<sup>3</sup>), 6.89 (d,  $J$  = 8.6 Hz, 2H, H<sup>7</sup>), 6.62 (d,  $J$  = 8.6 Hz, 2H, H<sup>8</sup>), 5.29 (s, 2H, H<sup>9</sup>), 3.99 (q,  $J$  = 7.1 Hz, 2H, H<sup>5</sup>), 1.14 (t,  $J$  = 7.1 Hz, 3H, H<sup>6</sup>);  $^{13}C$

NMR (101 MHz, DMSO- $d_6$ )  $\delta$  173.85, 161.96, 161.42, 149.30, 147.10, 138.35 (2C), 129.36 (2C), 124.11, 124.01, 121.45 114.08 (2C), 113.28, 61.37, 14.72; HPLC-MS (APCI/ESI): Purity 95%,  $t_R$  = 4.100 min,  $m/z$   $[M+H]^+$  = 403.0, 405.0 (1:1).

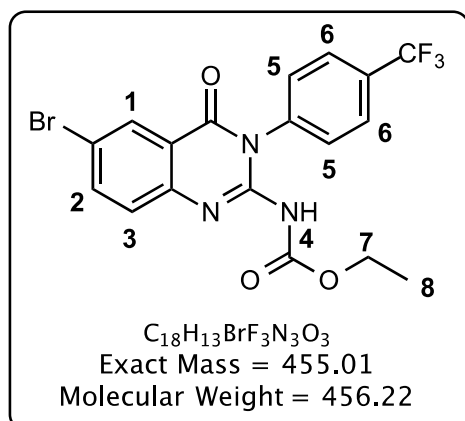
**Ethyl (6-bromo-3-((1-methylpiperidin-4-yl)methyl)-4-oxo-3,4-dihydroquinazolin-2-yl)carbamate (7.5)**



Obtained from **6.1** (546.7 mg, 1.51 mmol, 1.0 Eq) using (1-methyl-4-piperidinyl)methanamine (0.32mL, 2.27 mmol, 1.5 Eq), as a white solid (633.8 mg, 98%); m.p. 174.2 – 180.4°C;  $R_f$  (2 x 10% MeOH in DCM) 0.45;  $^1H$  NMR (400 MHz, DMSO- $d_6$ )  $\delta$  7.95 (d,  $J$  = 2.4 Hz, 1H, H<sup>1</sup>), 7.67 (dd,  $J$  = 8.7, 2.5 Hz, 1H, H<sup>2</sup>), 7.12 (d,  $J$  = 8.8 Hz, 1H, H<sup>3</sup>), 4.32 (s, 1H, H<sup>4</sup>), 4.15 (q,  $J$  = 7.1 Hz, 2H, H<sup>10</sup>), 3.93 (d,  $J$  = 7.5 Hz,

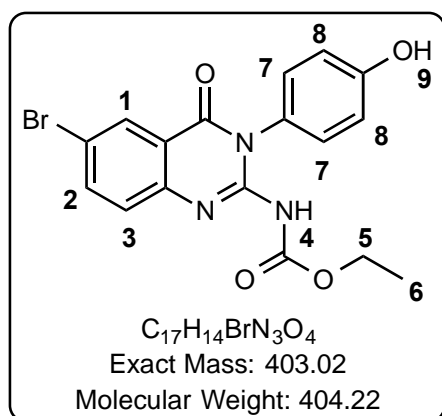
2H, H<sup>5</sup>), 2.73 (d,  $J$  = 11.9 Hz, 2H, H<sup>8eq</sup>), 2.14 (s, 3H, H<sup>9</sup>), 1.72 – 1.82 (m, 2H, H<sup>8ax</sup>), 1.74 – 1.65 (m, 1H, H<sup>6</sup>), 1.51 (m, 2H, H<sup>7eq</sup>), 1.36 – 1.23 (m, 2H, H<sup>7ax</sup>), 1.26 (t,  $J$  = 7.1 Hz, 3H, H<sup>11</sup>);  $^{13}C$  NMR (101 MHz, DMSO- $d_6$ )  $\delta$  152.89, 138.07, 137.17, 128.96, 126.66, 117.97, 113.07, 55.42 (2C), 46.49, 46.20, 45.54, 40.47, 33.99, 29.52 (2C), 19.02, 14.93; HPLC-MS (APCI/ESI): Purity = >99%,  $t_R$  = 3.020 min,  $m/z$   $[M+H]^+$  = 423.1, 425.1 (1:1).

**Ethyl (6-bromo-4-oxo-3-(4-(trifluoromethyl)phenyl)-3,4-dihydroquinazolin-2-yl)carbamate (7.6)**



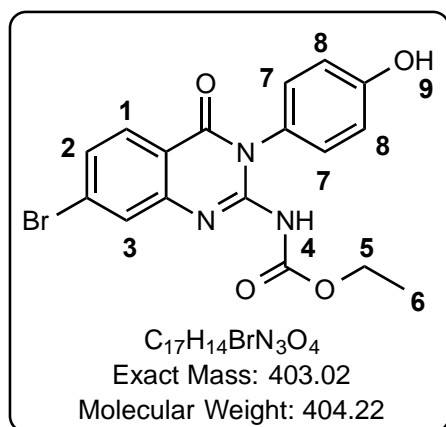
Obtained from **6.1** (4.9402 g, 13.68 mmol, 1.0 Eq) using 4-(trifluoromethyl)aniline (3.31 g, 20.52 mmol, 1.5 Eq), as a pale yellow solid (4.31 g, 69%); m.p 282.7 – 290.5 °C;  $R_f$  (3:7 EtOAc:Hexane) 0.28;  $^1H$  NMR (400 MHz, Chloroform-*d*)  $\delta$  13.00 (s, 1H, H<sup>4</sup>), 8.33 (d,  $J$  = 2.3 Hz, 1H, H<sup>1</sup>), 7.84 (dd,  $J$  = 8.7, 2.3 Hz, 1H, H<sup>2</sup>), 7.81 (d,  $J$  = 8.3 Hz, 2H, H<sup>6</sup>), 7.40 (d,  $J$  = 8.0 Hz, 2H, H<sup>5</sup>), 7.18 (d,  $J$  = 8.4 Hz, 1H, H<sup>3</sup>), 4.12 (q,  $J$  = 7.1 Hz, 2H, H<sup>7</sup>), 1.26 (t,  $J$  = 7.1 Hz, 3H, H<sup>8</sup>);  $^{13}C$  NMR (151 MHz, DMSO-*d*<sub>6</sub>)  $\delta$  162.42, 160.06, 153.63, 140.54, 138.64, 137.71, 130.66, 130.10 (q,  $J$  = 32.00 Hz, 1C, C-CF<sub>3</sub>), 129.48 (2C), 126.61 (2C), 122.37 (q,  $J$  = 161.28 Hz, 1C, C-F<sub>3</sub>), 120.23, 118.09, 116.59, 61.54, 14.81; HPLC-MS (APCI/ESI): Purity = 68%,  $t_R$  = 4.537 min,  $m/z$  [M+H]<sup>+</sup> = 455.9, 457.9 (1:1).

**Ethyl (6-bromo-3-(4-hydroxyphenyl)-4-oxo-3,4-dihydroquinazolin-2-yl)carbamate (7.7)**



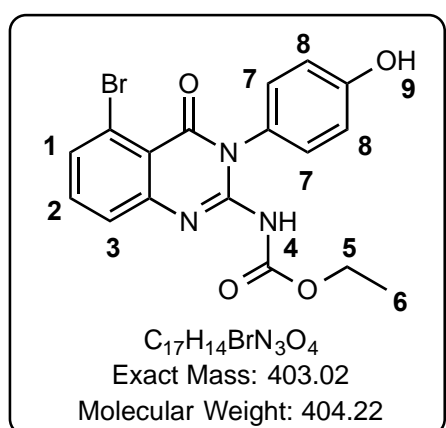
Obtained from **6.1** (1.51 g, 4.17 mmol, 1.0 Eq) using 4-aminophenol (682.2 mg, 6.25 mmol, 1.5 Eq), as a white solid (1.038 g, 62%); m.p. 317.8 – 322.4 °C;  $R_f$  (5:5 EtOAc:Hexane) 0.30;  $^1H$  NMR (400 MHz, DMSO-*d*<sub>6</sub>)  $\delta$  12.12 (s, 1H, H<sup>4</sup>), 9.67 (s, 1H, H<sup>9</sup>), 8.10 (d,  $J$  = 2.3 Hz, 1H, H<sup>1</sup>), 7.96 (dd,  $J$  = 8.7, 2.4 Hz, 1H, H<sup>2</sup>), 7.68 (d,  $J$  = 8.6 Hz, 1H, H<sup>3</sup>), 7.07 (d,  $J$  = 8.7 Hz, 2H, H<sup>7</sup>), 6.84 (d,  $J$  = 8.8 Hz, 2H, H<sup>8</sup>), 3.98 (q,  $J$  = 7.1 Hz, 2H, H<sup>5</sup>), 1.12 (t,  $J$  = 7.1 Hz, 3H, H<sup>6</sup>);  $^{13}C$  NMR (151 MHz, DMSO-*d*<sub>6</sub>)  $\delta$  162.74, 160.96, 160.04, 157.81, 154.08, 145.83, 138.36, 130.15 (2C), 129.45, 127.34, 120.06, 118.08, 115.91 (2C), 61.48, 14.82; HPLC-MS (APCI/ESI): Purity >99%,  $t_R$  = 4.212 min,  $m/z$  [M+H]<sup>+</sup> = 404.0, 406.0 (1:1).

### ***Ethyl (7-bromo-3-(4-hydroxyphenyl)-4-oxo-3,4-dihydroquinazolin-2-yl)carbamate (7.8)***



Obtained from **6.2** (457.2 mg, 1.27 mmol, 1.0 Eq) using 4-aminophenol (207.2 mg, 1.90 mmol, 1.5 Eq) to give a white solid (210.4 mg, 41%); m.p. 193.4 – 200.1°C;  $R_f$  (5:5 EtOAc:Hexane) 0.43;  $^1H$  NMR (300 MHz, DMSO- $d_6$ )  $\delta$  12.26 (s, 1H, H<sup>4</sup>), 9.63 (s, 1H, H<sup>9</sup>), 8.01 (s, 1H, H<sup>3</sup>), 7.93 (d,  $J$  = 8.5 Hz, 1H, H<sup>1</sup>), 7.54 (d,  $J$  = 7.4 Hz, 1H, H<sup>2</sup>), 7.05 (d,  $J$  = 8.7 Hz, 2H, H<sup>7</sup>), 6.83 (d,  $J$  = 8.7 Hz, 2H, H<sup>8</sup>), 3.99 (q,  $J$  = 7.1 Hz, 2H, H<sup>5</sup>), 1.13 (t,  $J$  = 7.1 Hz, 3H, H<sup>6</sup>);  $^{13}C$  NMR (101 MHz, DMSO- $d_6$ )  $\delta$  161.10, 157.61, 153.08, 149.82, 137.95, 130.15 (2C), 129.34, 129.52, 127.55, 125.80, 120.25, 115.85 (2C), 113.02, 61.37, 14.69; HPLC-MS (APCI/ESI): Purity 98%,  $t_R$  = 4.298 min,  $m/z$   $[M+H]^+$  = 404.0, 406.0 (1:1).

### ***Ethyl (5-bromo-3-(4-hydroxyphenyl)-4-oxo-3,4-dihydroquinazolin-2-yl)carbamate (7.9)***



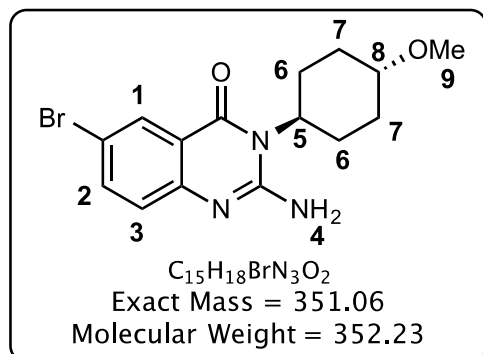
Obtained from **6.3** (248.0 mg, 0.69 mmol, 1.0 Eq) using 4-aminophenol (112.4 mg, 1.03 mmol, 1.5 Eq), as a white solid (142 g, 51%); m.p. 314.8 – 319.9°C;  $R_f$  (7:3 EtOAc:Hexane) 0.56;  $^1H$  NMR (400 MHz, DMSO- $d_6$ )  $\delta$  11.52 (s, 1H, H<sup>4</sup>), 9.70 (s, 1H, H<sup>9</sup>), 7.83 – 7.49 (m, 3H, H<sup>1</sup>, H<sup>2</sup>, H<sup>3</sup>), 7.06 (d,  $J$  = 8.7 Hz, 2H, H<sup>7</sup>), 6.85 (d,  $J$  = 8.8 Hz, 2H, H<sup>8</sup>), 3.98 (q,  $J$  = 7.1 Hz, 2H, H<sup>5</sup>), 1.12 (t,  $J$  = 7.1 Hz, 3H, H<sup>6</sup>);  $^{13}C$  NMR (101 MHz, DMSO- $d_6$ )  $\delta$  162.94, 160.82, 159.89, 157.76, 137.20, 134.61, 132.25, 131.87, 130.18 (2C), 127.53, 121.93, 117.92, 115.85 (2C), 61.34, 14.72; HPLC-MS (APCI/ESI): Purity >99%,  $t_R$  = 4.021 min,  $m/z$   $[M+H]^+$  = 404.0, 406.0.

#### **6.2.5. GENERAL PROCEDURE FOR THE SYNTHESIS OF COMPOUNDS 8.1 – 8.4**

Compound **6.1** (1.0 Eq) was dissolved in DMF (3–6 mL) and the relevant primary amine (1.5 Eq) and EDCI (2.0 Eq) were successively added to the solution. After stirring at room temperature (24 – 26°C) for 5 hours, the solution was heated under pressure at 100°C for 18 - 22 hours. The solution was cooled to room temperature, diluted with EtOAc and washed with 5% LiCl (x5), water and brine. The organic layer was dried over  $MgSO_4$ , concentrated under reduced pressure and the resulting residue was triturated

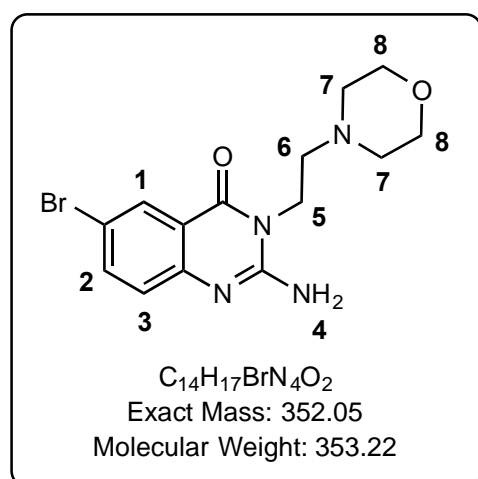
by stirring in Et<sub>2</sub>O to afford the cyclized and deprotected penultimate compounds **8.1** – **8.4**.

**2-Amino-6-bromo-3-((1*r*,4*r*)-4-methoxycyclohexyl)quinazolin-4(3*H*)-one (8.1)**



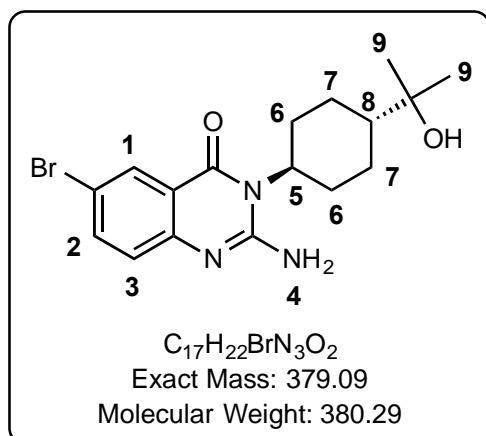
Obtained using 4-methoxycyclohexanamine (0.31 mL, 2.27 mmol, 1.5 Eq.) as a light brown solid (350 mg, 55%); m.p. 241.1 – 243.3°C; *R<sub>f</sub>* (2 x 5% MeOH in DCM) 0.3; <sup>1</sup>H NMR (400 MHz, DMSO-*d*<sub>6</sub>) δ 7.92 (d, *J* = 2.4 Hz, 1H, H<sup>1</sup>), 7.65 (dd, *J* = 8.7, 2.5 Hz, 1H, H<sup>2</sup>), 7.09 (d, *J* = 8.6 Hz, 1H, H<sup>3</sup>), 7.09 (s, 2H, H<sup>4</sup>), 4.20 (m, 1H, H<sup>5</sup>), 3.26 (s, 3H, H<sup>9</sup>), 3.26 – 3.13 (m, 1H, H<sup>8</sup>), 2.59 (qd, *J* = 12.9, 3.4 Hz, 2H, H<sup>6ax</sup>), 2.06 (d, *J* = 12.4 Hz, 2H, H<sup>7eq</sup>), 1.66 (d, *J* = 12.4 Hz, 2H, H<sup>6eq</sup>), 1.31 (qd, *J* = 13.3, 3.7 Hz, 2H, H<sup>7ax</sup>); <sup>13</sup>C NMR (101 MHz, DMSO-*d*<sub>6</sub>) δ 161.92, 153.15, 149.02, 137.08, 128.58, 126.36, 119.38, 113.11, 78.10, 56.40, 55.64, 31.25 (2C), 26.07 (2C); HPLC-MS (APCI/ESI): Purity = >99%, *t<sub>R</sub>* = 4.090 min, *m/z* [M+H]<sup>+</sup> = 350.1, 352.1 (1:1).

**2-Amino-6-bromo-3-(2-morpholinoethyl)quinazolin-4(3*H*)-one (8.2)**



Obtained using 4-(2-aminoethyl)morpholine (0.29 mL, 2.18 mmol, 1.5 Eq) as a light orange solid (354.9 mg, 69%); m.p. 216.5 – 221.0 °C; *R<sub>f</sub>* (5% MeOH in EtOAc) 0.18; <sup>1</sup>H NMR (400 MHz, DMSO-*d*<sub>6</sub>) δ 7.96 (d, *J* = 2.4 Hz, 1H, H<sup>1</sup>), 7.67 (dd, *J* = 8.8, 2.5 Hz, 1H, H<sup>2</sup>), 7.26 (s, 2H, H<sup>4</sup>), 7.13 (d, *J* = 8.8 Hz, 1H, H<sup>3</sup>), 4.15 (t, *J* = 6.2 Hz, 2H, H<sup>5</sup>), 3.55 (t, *J* = 4.6 Hz, 4H, H<sup>8</sup>), 2.58 (t, *J* = 6.2 Hz, 2H, H<sup>6</sup>), 2.49 (t, *J* = 4.8 Hz, 4H, H<sup>7</sup>); <sup>13</sup>C NMR (101 MHz, DMSO-*d*<sub>6</sub>) δ 161.31, 153.24, 149.27, 137.18, 128.84, 126.74, 118.21, 113.22, 66.69 (2C), 56.29, 53.88 (2C), 40.06; HPLC-MS (APCI/ESI): Purity 86%, *t<sub>R</sub>* = 3.533 min, *m/z* [M+H]<sup>+</sup> = 355.1, 353.1 (1:1).

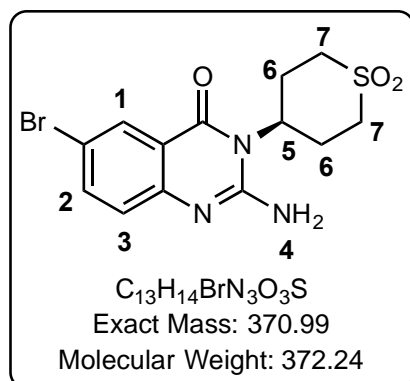
### 2-Amino-6-bromo-3-((1*r*,4*r*)-4-(2-hydroxypropan-2-yl)cyclohexyl)quinazolin-4(3*H*)-one (8.3)



Obtained using *trans*-2-(4-aminocyclohexyl)-2-hydroxy propane (395.6 mg, 2.51 mmol, 1.5 Eq) as a light brown solid (250.9 mg, 40 %); m.p. 248.6 – 255.7°C;  $R_f$  (5% MeOH in DCM) 0.25;  $^1H$  NMR (400 MHz, DMSO- $d_6$ )  $\delta$  7.92 (d,  $J$  = 2.4 Hz, 1H, H<sup>1</sup>), 7.64 (dd,  $J$  = 8.7, 2.5 Hz, 1H, H<sup>2</sup>), 7.09 (d,  $J$  = 8.8 Hz, 1H, H<sup>3</sup>), 7.04 (s, 2H, H<sup>4</sup>), 4.27 – 4.07 (m, 1H, H<sup>5</sup>), 2.60 – 2.44 (m, 2H, H<sup>6ax</sup>), 1.87 (d,  $J$  = 12.0 Hz, 2H, H<sup>7eq</sup>),

1.67 (d,  $J$  = 10.0 Hz, 2H, H<sup>6eq</sup>), 1.35 – 1.25 (m, 2H, H<sup>8</sup>), 1.25 – 1.13 (m, 1H, H<sup>7ax</sup>), 1.07 (s, 6H, H<sup>9</sup>);  $^{13}C$  NMR (101 MHz, DMSO- $d_6$ )  $\delta$  161.92, 153.25, 149.04, 137.01, 128.61, 126.35, 119.46, 113.05, 71.00, 55.35, 47.89, 28.11 (2C), 27.49 (2C), 26.95 (2C); HPLC-MS (APCI/ESI): Purity 96%,  $t_R$  = 4.826 min,  $m/z$  [M+H]<sup>+</sup> = 380.1, 382.1 (1:1).

### 2-Amino-6-bromo-3-(1,1-dioxidotetrahydro-2*H*-thiopyran-4-yl)quinazolin-4(3*H*)-one (8.4)



4-aminotetrahydro-2*H*-thiopyran-1,1-dioxide, HCl (553 mg, 2.98 mmol, 1.5 Eq) was used with the addition of Et<sub>3</sub>N (0.5 mL), since the amine reagent is a salt, to obtain a light brown solid (313 mg, 42%); m.p. 237.2 – 243.4°C;  $R_f$  (5% MeOH in DCM) 0.25;  $^1H$  NMR (400 MHz, DMSO- $d_6$ )  $\delta$  7.94 (d,  $J$  = 2.5 Hz, 1H, H<sup>1</sup>), 7.67 (dd,  $J$  = 8.7, 2.5 Hz, 1H, H<sup>2</sup>), 7.18 (s, 2H, H<sup>4</sup>), 7.11 (d,  $J$  = 8.7 Hz, 1H, H<sup>3</sup>), 4.39

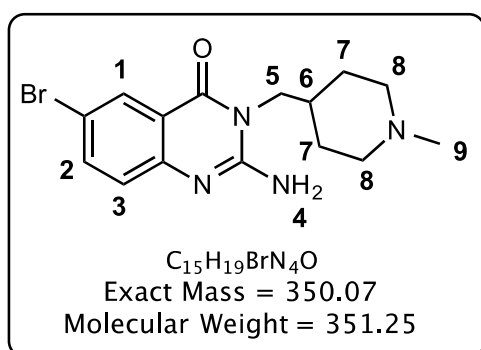
(m, 1H, H<sup>5</sup>), 3.27 – 3.11 (m, 6H, H<sup>7</sup>, H<sup>6ax</sup>), 2.01 (d,  $J$  = 13.5 Hz, 2H, H<sup>6eq</sup>);  $^{13}C$  NMR (101 MHz, DMSO- $d_6$ )  $\delta$  161.96, 152.79, 149.06, 137.31, 128.56, 126.47, 119.37, 113.34, 54.21, 50.89 (2C), 26.32 (2C); HPLC-MS (APCI/ESI): Purity 96%,  $t_R$  = 3.729 min,  $m/z$  [M+H]<sup>+</sup> = 372.0, 374.0 (1:1).

#### 6.2.6. GENERAL PROCEDURE FOR THE SYNTHESIS OF COMPOUNDS 8.5 – 8.7

Compounds 7.1–7.2 (1.0 Eq) were dissolved in TFA (20 Eq) and microwaved at 100°C for 20 minutes. Once complete, the reaction was diluted with methanol and concentrated *in vacuo*. The crude residue was taken up in ethyl acetate, neutralized with saturated sodium bicarbonate and the aqueous layer was extracted with ethyl acetate (x3), dried over magnesium sulphate and concentrated *in vacuo* to yield the

aminoquinazolinone intermediates **8.1 – 8.3**.

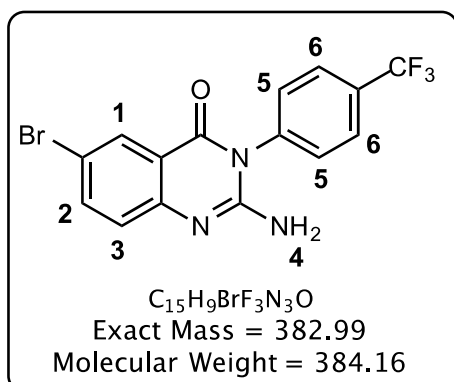
**2-Amino-6-bromo-3-((1-methylpiperidin-4-yl)methyl)quinazolin-4(3H)-one (8.5)**



Obtained using **7.2** (573.8 mg, 1.36 mmol, 1.0 Eq) as an white solid (454.9 mg, 96%); m.p. 224.2 – 228.4°C;  $R_f$  (1 x 10% MeOH in DCM) 0.05;  $^1H$  NMR (400 MHz, DMSO- $d_6$ )  $\delta$  7.95 (d,  $J$  = 2.4 Hz, 1H, H<sup>1</sup>), 7.67 (dd,  $J$  = 8.8, 2.4 Hz, 1H, H<sup>2</sup>), 7.12 (d,  $J$  = 8.9 Hz, 1H, H<sup>3</sup>), 7.10 (s, 2H, H<sup>4</sup>), 3.93 (d,  $J$  = 7.5 Hz, 2H, H<sup>5</sup>), 2.72 (d,  $J$  = 11.7 Hz, 2H, H<sup>8eq</sup>), 2.11 (s, 3H, H<sup>9</sup>), 1.73

(td,  $J$  = 11.4, 2.4 Hz, 2H, H<sup>8ax</sup>), 1.72 – 1.65 (m, 1H, H<sup>6</sup>), 1.48 (d,  $J$  = 12.4 Hz, 2H, H<sup>7eq</sup>), 1.28 (qd,  $J$  = 12.12, 3.8 Hz, 2H, H<sup>7ax</sup>);  $^{13}C$  NMR (101 MHz, DMSO- $d_6$ )  $\delta$  161.51, 152.89, 149.32, 137.18, 128.96, 126.67, 117.96, 113.09, 55.47 (2C), 46.58, 46.23, 34.04, 29.57 (2C); HPLC-MS (APCI/ESI): Purity = >99%,  $t_R$  = 1.385 min,  $m/z$  [M+H]<sup>+</sup> = 351.1, 353.1 (1:1).

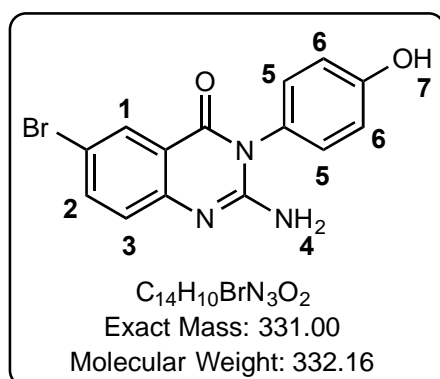
**2-Amino-6-bromo-3-(4-(trifluoromethyl)phenyl)quinazolin-4(3H)-one (8.6)**



Obtained using **7.1** (4.17 g, 9.14 mmol, 1.0 Eq) as an off-white solid (2.90 g, 83%); m.p 302.4 – 306.6 °C;  $R_f$  (3:7 EtOAc:Hexane) 0.08;  $^1H$  NMR (400 MHz, DMSO- $d_6$ )  $\delta$  7.93 (d,  $J$  = 2.4 Hz, 1H, H<sup>1</sup>), 7.91 (d,  $J$  = 8.0 Hz, 2H, H<sup>6</sup>), 7.71 (dd,  $J$  = 8.8, 2.5 Hz, 1H, H<sup>2</sup>), 7.61 (d,  $J$  = 7.8 Hz, 2H, H<sup>5</sup>), 7.18 (d,  $J$  = 8.8 Hz, 1H, H<sup>3</sup>), 6.57 (s, 2H, H<sup>4</sup>);  $^{13}C$  NMR (101 MHz, DMSO- $d_6$ )  $\delta$  161.26,

152.17, 149.89, 139.48, 137.63, 130.59 (2C), 130.19 (q,  $J$  = 32.0 Hz, 1C, C- $CF_3$ ), 128.81, 127.59 (2C), 126.89, 122.37 (q,  $J$  = 161.3 Hz, 1C,  $CF_3$ ) 118.66, 113.29; HPLC-MS (APCI/ESI): Purity = 96%,  $t_R$  = 4.080 min,  $m/z$  [M+H]<sup>+</sup> = 383.9, 385.9 (1:1).

### 2-Amino-6-bromo-3-(4-hydroxyphenyl)quinazolin-4(3H)-one (8.7)

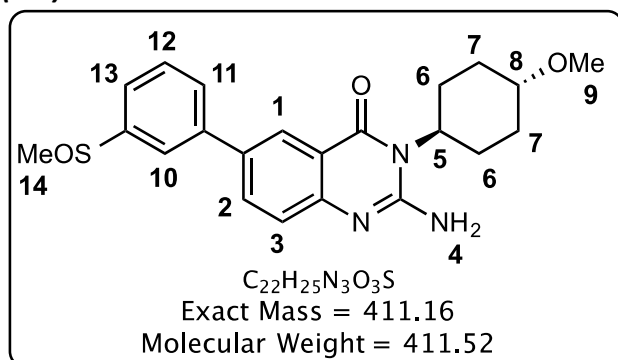


Obtained from **7.4** (980.8 mg, 2.43 mmol, 1.0 Eq.), as a light pink solid (426.4 mg, 53%); m.p. 310.1 – 318.2 °C;  $R_f$ (100% EtOAc) 0.44;  $^1H$  NMR (400 MHz, DMSO- $d_6$ )  $\delta$  9.79 (s, 1H, H<sup>7</sup>), 7.94 (d,  $J$  = 2.5 Hz, 1H, H<sup>1</sup>), 7.71 (dd,  $J$  = 8.8, 2.5 Hz, 1H, H<sup>2</sup>), 7.19 (d,  $J$  = 8.7 Hz, 1H, H<sup>3</sup>), 7.13 (d,  $J$  = 8.7 Hz, 2H, H<sup>5</sup>), 6.92 (d,  $J$  = 8.7 Hz, 2H, H<sup>6</sup>), 6.38 (s, 2H, H<sup>4</sup>);  $^{13}C$  NMR (101 MHz, DMSO- $d_6$ )  $\delta$  161.46, 158.45, 153.13, 149.71, 137.36, 130.12 (2C), 128.85, 126.81, 126.39, 118.87, 117.01 (2C), 113.14; HPLC-MS (APCI/ESI): Purity >99%,  $t_R$  = 3.843 min,  $m/z$   $[M+H]^+$  = 332.0, 334.0 (1:1).

#### 6.2.7. GENERAL PROCEDURE SUZUKI MIYAUURA COUPLING IN THE SYNTHESIS OF THE TARGET COMPOUNDS 9.1 – 9.6

Compounds **8.1** – **8.7** (1.0 Eq) and the appropriate arylboronic acid (1.5 Eq.) were dissolved in 1,4-dioxane or DMF (2 – 4 mL) and the solution was purged with nitrogen.  $PdCl_2(PPh_3)_2$  (0.1 Eq) was added to the solution followed by the addition of potassium carbonate (3.0 Eq) dissolved in water (0.05 Eq). The reaction was heated at 80°C until TLC monitoring showed completion (1-3 hours), allowed to cool to room temperature and diluted with EtOAc to be filtered through Celite. The organic phase was washed with water and brine, dried over magnesium sulphate and concentrated under reduced pressure. The resulting crude residue was purified by silica-gel chromatography using the relevant solvent system, combined pure fractions were concentrated *in vacuo*, triturated with  $Et_2O$ , filtered and dried under vacuum to give the relevant target compounds **9.1** – **9.6**.

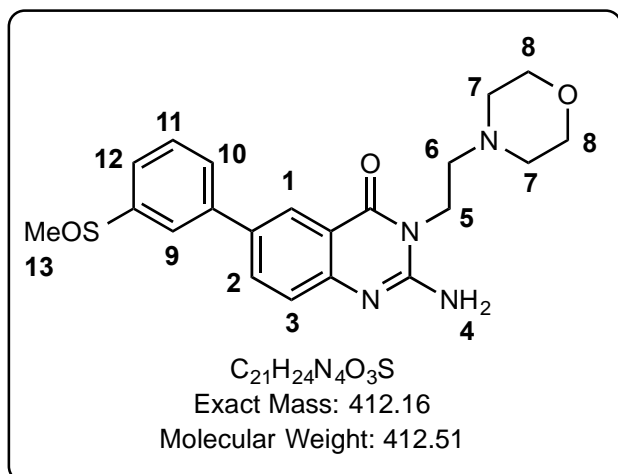
**2-Amino-3-((1*r*,4*r*)-4-methoxycyclohexyl)-6-(3-(methylsulfinyl)phenyl)quinazolin-4(3*H*)-one (9.1)**



Obtained from **8.4** (304.5 mg, 0.86 mmol, 1.0 Eq), using 3-methylsulfinylphenyl boronic acid (256.8 mg, 1.40 mmol, 1.6 Eq), as a brown solid (54 mg, 11%); m.p 221.3 – 223.6 °C; R<sub>f</sub> (1:9, MeOH:DCM) 0.41; <sup>1</sup>H NMR (400 MHz, DMSO-*d*<sub>6</sub>) δ 8.18 (d, *J* =

2.3, 1H, H<sup>1</sup>), 7.96 (t, *J* = 2.1 Hz, 1H, H<sup>10</sup>), 7.94 (dd, *J* = 8.5, 2.3 Hz, 1H, H<sup>2</sup>), 7.84 (dt, *J* = 6.8, 2.0 Hz, 1H, H<sup>11</sup>), 7.69 – 7.63 (m, 2H, H<sup>12</sup>, H<sup>13</sup>), 7.27 (d, *J* = 8.6 Hz, 1H, H<sup>3</sup>), 7.06 (s, 2H, H<sup>4</sup>), 4.24 (m, 1H, H<sup>5</sup>), 3.27 (s, 3H, H<sup>9</sup>), 3.26 – 3.15 (m, 1H, H<sup>8</sup>), 2.82 (s, 3H, H<sup>14</sup>), 2.65 (qd, *J* = 13.6, 3.0 Hz, 2H, H<sup>6ax</sup>), 2.07 (d, *J* = 6.6 Hz, 2H, H<sup>7eq</sup>), 1.69 (d, *J* = 11.4 Hz, 2H, H<sup>6eq</sup>), 1.34 (qd, *J* = 13.1, 3.7 Hz, 2H, H<sup>7ax</sup>); <sup>13</sup>C NMR (101 MHz, DMSO-*d*<sub>6</sub>) δ 163.01, 153.10, 149.83, 147.80, 140.98, 133.05, 132.32, 130.40, 128.79, 124.75, 124.54, 122.49, 121.43, 118.14, 78.17, 56.36, 55.64, 43.73, 31.31 (2C), 26.20 (2C); HPLC-MS (APCI/ESI): Purity = 96%, t<sub>R</sub> = 3.580 min, m/z [M+H]<sup>+</sup> = 412.2.

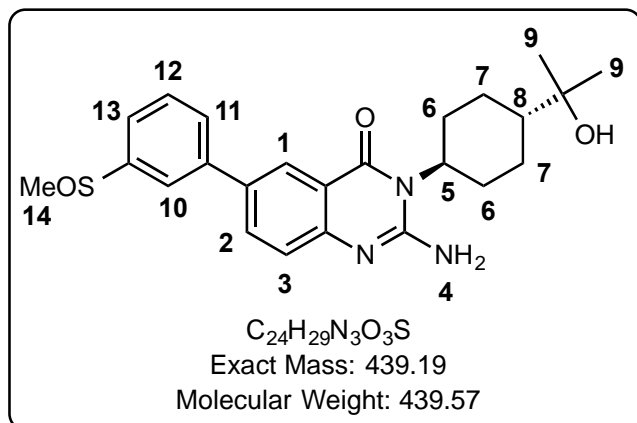
**2-Amino-6-(3-(methylsulfinyl)phenyl)-3-(2-morpholinoethyl)quinazolin-4(3*H*)-one (9.2)**



Obtained from **8.5** (224.5 mg, 0.64 mmol, 1.0 Eq) using 3-methylsulfinylphenyl boronic acid (175.4 mg, 0.95 mmol, 1.5 Eq) as an off-white solid (45 mg, 17 %); m.p. 214.2 – 217.2°C; R<sub>f</sub> (3% MeOH in DCM) 0.1; <sup>1</sup>H NMR (400 MHz, DMSO-*d*<sub>6</sub>) δ 8.23 (d, *J* = 2.4 Hz, 1H, H<sup>1</sup>), 7.97 (t, *J* = 2.1 Hz, 1H, H<sup>9</sup>), 7.96 (dd, *J* = 8.6, 2.3 Hz, 1H, H<sup>2</sup>), 7.85 (dt, *J* = 6.7, 2.0 Hz, 1H, H<sup>10</sup>),

7.70 – 7.64 (m, 2H, H<sup>11</sup>, H<sup>12</sup>), 7.31 (d, *J* = 8.6 Hz, 1H, H<sup>3</sup>), 7.11 (s, 2H, H<sup>4</sup>), 4.20 (t, *J* = 6.2 Hz, 2H, H<sup>5</sup>), 3.64 – 3.51 (m, 4H, H<sup>8</sup>), 2.82 (s, 3H, H<sup>13</sup>), 2.64 (t, *J* = 6.2 Hz, 2H, H<sup>6</sup>), 2.54 – 2.52 (m, 4H, H<sup>7</sup>); <sup>13</sup>C NMR (101 MHz, DMSO-*d*<sub>6</sub>) δ 162.37, 153.13, 150.04, 147.84, 140.87, 133.17, 132.43, 130.42, 128.82, 125.12, 124.79, 122.55, 121.44, 116.94, 66.57 (2C), 56.34, 53.82 (2C), 43.76, 39.48; HPLC-MS (APCI/ESI): Purity 98%, t<sub>R</sub> = 3.126 min, m/z [M+H]<sup>+</sup> = 413.1, 415.1 (1:1).

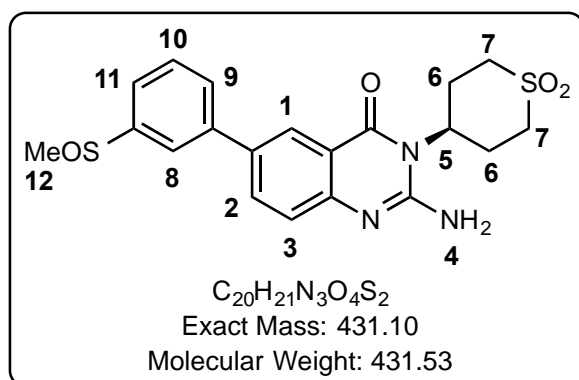
**2-Amino-3-((1*r*,4*r*)-4-(2-hydroxypropan-2-yl)cyclohexyl)-6-(3-(methylsulfinyl)phenyl)quinazolin-4(3*H*)-one (9.3)**



Obtained from **8.6** (220.5 mg, 0.58 mmol, 1.0 Eq) using 3-methylsulfinylphenyl boronic acid (160.0 mg, 0.87 mmol, 1.5 Eq) as an off-white solid (55.1 mg, 22%); m.p. 232.0 – 237.2°C;  $R_f$  (5% MeOH in DCM with 1% Et<sub>3</sub>N) 0.23; <sup>1</sup>H NMR (400 MHz, DMSO-*d*<sub>6</sub>)  $\delta$  8.18 (d,  $J$  = 2.3 Hz, 1H, H<sup>1</sup>),

7.96 (t,  $J$  = 1.8 Hz, 1H, H<sup>10</sup>), 7.94 (dd,  $J$  = 8.6, 2.3 Hz, 1H, H<sup>2</sup>), 7.85 (dt,  $J$  = 6.8, 2.0 Hz, 1H, H<sup>11</sup>), 7.67 (t,  $J$  = 7.7 Hz, 1H, H<sup>12</sup>), 7.68 – 7.63 (m, 1H, H<sup>13</sup>), 7.26 (d,  $J$  = 8.6 Hz, 1H, H<sup>3</sup>), 7.01 (s, 2H, H<sup>4</sup>), 4.21 (m, 1H, H<sup>5</sup>), 2.82 (s, 3H, H<sup>14</sup>), 2.59 (q,  $J$  = 12.0 Hz, 2H, H<sup>6ax</sup>), 1.89 (d,  $J$  = 11.8 Hz, 2H, H<sup>7eq</sup>), 1.71 (d,  $J$  = 12.2 Hz, 2H, H<sup>6eq</sup>), 1.35 – 1.26 (m, 1H, H<sup>8</sup>), 1.26 – 1.20 (m, 2H, H<sup>7ax</sup>), 1.08 (s, 6H, H<sup>9</sup>); <sup>13</sup>C NMR (101 MHz, DMSO-*d*<sub>6</sub>)  $\delta$  163.00, 153.22, 149.87, 147.84, 141.01, 132.97, 132.24, 130.39, 128.78, 124.73, 124.57, 122.46, 121.43, 118.23, 71.03, 57.30, 47.96, 43.75, 28.27 (2C), 27.51 (2C), 27.03 (2C); HPLC-MS (APCI/ESI): Purity 98%,  $t_R$  = 4.266 min,  $m/z$  [M+H]<sup>+</sup> = 440.2, 442.2 (1:1).

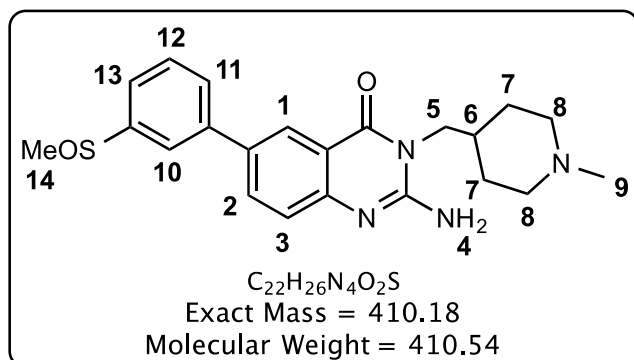
**2-Amino-3-(1,1-dioxidotetrahydro-2*H*-thiopyran-4-yl)-6-(3-(methylsulfinyl)phenyl)quinazolin-4(3*H*)-one (9.4)**



Obtained from **8.7** (274.4 mg, 0.75 mmol, 1.0 Eq) using 3-methylsulfinylphenyl boronic acid (203.5 mg, 1.11 mmol, 1.5 Eq) as a white solid (55.2 mg, 17%); m.p. 328.1 – 333.2°C;  $R_f$  (5% MeOH in DCM) 0.2; <sup>1</sup>H NMR (400 MHz, DMSO-*d*<sub>6</sub>)  $\delta$  8.20 (d,  $J$  = 2.3 Hz, 1H, H<sup>1</sup>), 7.97 (t,  $J$  = 1.8 Hz, 1H, H<sup>8</sup>), 7.97

(dd,  $J$  = 8.6, 2.4 Hz, 1H, H<sup>2</sup>), 7.86 (dt,  $J$  = 6.7, 2.1 Hz, 1H, H<sup>9</sup>), 7.72 – 7.63 (m, 1H, H<sup>10</sup>), 7.66 (m, 1H, H<sup>11</sup>), 7.28 (d,  $J$  = 8.6 Hz, 1H, H<sup>3</sup>), 7.15 (s, 2H, H<sup>4</sup>), 4.41 (m, 1H, H<sup>5</sup>), 3.27 – 3.14 (m, 6H, H<sup>7</sup>, H<sup>6ax</sup>), 2.82 (s, 3H, H<sup>12</sup>), 2.04 (d,  $J$  = 10.1 Hz, 2H, H<sup>6eq</sup>); <sup>13</sup>C NMR (101 MHz, DMSO-*d*<sub>6</sub>)  $\delta$  163.03, 152.72, 149.85, 147.88, 140.87, 133.27, 132.53, 130.42, 128.80, 124.86, 124.51, 122.55, 121.47, 118.13, 54.19, 50.96 (2C), 43.75, 26.45 (2C); HPLC-MS (APCI/ESI): Purity 98 %,  $t_R$  = 3.313 min,  $m/z$  [M+H]<sup>+</sup> = 432.1, 434.1 (1:1).

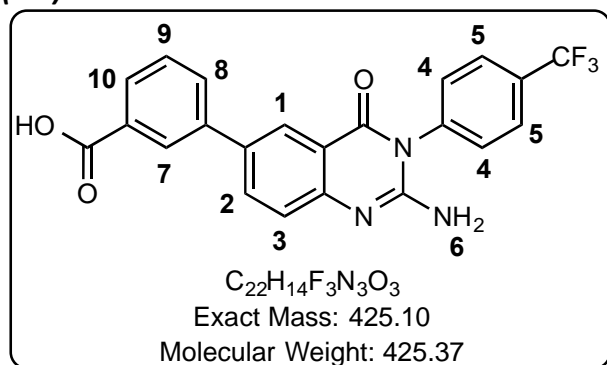
**2-Amino-3-((1-methylpiperidin-4-yl)methyl)-6-(3-(methylsulfinyl)phenyl)quinazolin-4(3H)-one (9.5)**



Obtained from **8.2** (171.4 mg, 0.49 mmol, 1.0 Eq), using 3-methylsulfinylphenyl boronic acid (134.7 mg, 0.73 mmol, 1.5 Eq), as an off-white solid (20.4 mg, 20%); m.p. 235.7 – 237.8°C; R<sub>f</sub> (2:7.9:0.1, MeOH:DCM:Et<sub>3</sub>N) 0.26; <sup>1</sup>H NMR (400

MHz, DMSO-*d*<sub>6</sub>) δ 8.22 (d, *J* = 2.3 Hz, 1H, H<sup>1</sup>), 7.97 (m, 1H, H<sup>10</sup>), 7.96 (dd, *J* = 8.6, 2.3 Hz, 1H, H<sup>2</sup>), 7.86 (d, *J* = 6.8 Hz, 1H, H<sup>11</sup>), 7.68 (t, *J* = 7.4 Hz, 1H, H<sup>12</sup>), 7.66 (m, 1H, H<sup>13</sup>), 7.29 (d, *J* = 8.5 Hz, 1H, H<sup>3</sup>), 7.09 (s, 2H, H<sup>4</sup>), 3.98 (d, *J* = 7.5 Hz, 2H, H<sup>5</sup>), 2.82 (s, 3H, H<sup>14</sup>), 2.79 (d, *J* = 11.9 Hz, 2H, H<sup>8eq</sup>), 2.17 (s, 3H, H<sup>9</sup>), 1.85 (m, 2H, H<sup>8ax</sup>), 1.78 (m, 1H, H<sup>6</sup>), 1.54 (d, *J* = 12.7 Hz, 2H, H<sup>7eq</sup>), 1.33 (qd, *J* = 12.1, 3.8 Hz, 2H, H<sup>7ax</sup>); <sup>13</sup>C NMR (101 MHz, DMSO-*d*<sub>6</sub>) δ 162.55, 152.83, 150.14, 147.80, 140.92, 133.15, 132.31, 130.41, 128.81, 125.07, 124.92, 122.50, 121.45, 116.71, 55.28 (2C), 46.23, 46.02, 43.76, 33.92, 29.37 (2C); HPLC-MS (APCI/ESI): Purity = 98%, t<sub>R</sub> = 1.987 min, m/z [M+H]<sup>+</sup> = 411.1.

**3-(2-Amino-4-oxo-3-(4-(trifluoromethyl)phenyl)-3,4-dihydroquinazolin-6-yl)benzoic acid (9.6)**

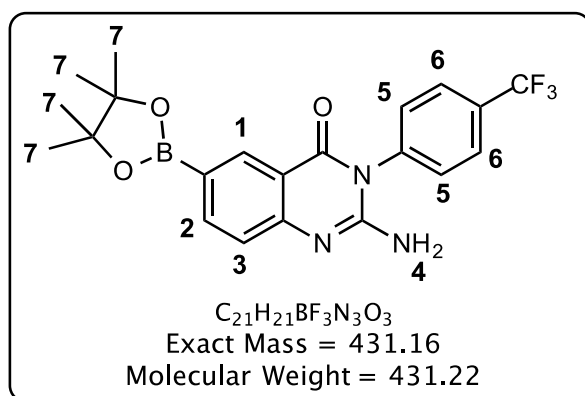


Obtained from **8.1** (250 mg, 0.65 mmol, 1.0 Eq), using 3-carboxyphenylboronic acid (161.9 mg, 0.98 mmol, 1.5 Eq), as a yellow solid (31.6 mg, 11%); m.p. 319.1 – 323.6°C; R<sub>f</sub> (15% MeOH in DCM) 0.41; <sup>1</sup>H NMR (400 MHz, DMSO-*d*<sub>6</sub>) δ 8.21 (t, *J* = 1.9 Hz, 1H, H<sup>7</sup>), 8.17 (d, *J* = 2.3 Hz, 1H, H<sup>1</sup>),

8.01 (dd, *J* = 8.6, 2.3 Hz, 1H, H<sup>2</sup>), 7.95 (d, *J* = 8.4 Hz, 2H, H<sup>5</sup>), 7.95 – 7.93 (m, 1H, H<sup>10</sup>), 7.92 (m, 1H, H<sup>8</sup>), 7.67 (d, *J* = 8.2 Hz, 2H, H<sup>4</sup>), 7.60 (t, *J* = 7.7 Hz, 1H, H<sup>9</sup>), 7.38 (d, *J* = 8.6 Hz, 1H, H<sup>3</sup>), 6.56 (s, 2H, H<sup>6</sup>); <sup>13</sup>C NMR (101 MHz, DMSO-*d*<sub>6</sub>) δ 167.88, 162.30, 151.99, 150.48, 140.03, 139.71, 133.52, 132.84, 132.60, 130.81, 130.65 (2C), 130.12 (q, *J* = 32.0 Hz, 1C, C-CF<sub>3</sub>), 129.85, 128.41, 127.59, 127.55, 127.24, 125.37, 124.55 (q, *J* = 272.3 Hz, 1C, C<sub>F</sub>CF<sub>3</sub>), 124.48, 117.34; HPLC-MS (APCI/ESI): Purity = 97%, t<sub>R</sub> = 3.937 min, m/z [M+H]<sup>+</sup> = 426.1.

**2-Amino-6-(4,4,5,5-tetramethyl-1,3,2-dioxaborolan-2-yl)-3-(4-(trifluoromethyl)phenyl)quinazolin-4(3H)-one (10)**

Compound **8.1** (1.03 g, 2.68 mmol, 1.0 Eq) and bis(pinacolato)diboron (1.23 g, 3.49 mmol, 1.3 Eq) were dissolved in anhydrous 1,4-dioxane (13mL) and flushed with nitrogen. PdCl<sub>2</sub>(dppf)-DCM (219.0 mg, 0.27 mmol, 0.1 Eq) and KOAc (789.7 mg, 8.05 mmol, 3.0 Eq) were added successively and the reaction was heated at 80°C for 2 hours. Once complete, the solution was cooled to room temperature, diluted with EtOAc and filtered through Celite. The filtrate was washed with water, brine and dried over magnesium sulphate with removal of solvent under reduced pressure. The resulting residue was triturated with diethyl ether and filtered to obtain the pinacol ester **10**.



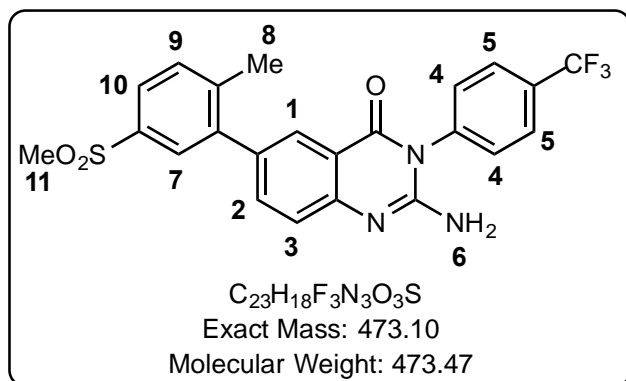
Brown solid (723.8 mg, 63%); m.p 321.2 – 323.5 °C; R<sub>f</sub> (7:3 EtOAc:Hexane) 0.48; <sup>1</sup>H NMR (400 MHz, DMSO-*d*<sub>6</sub>) δ 8.27 (d, *J* = 1.5 Hz, 1H, H<sup>1</sup>), 7.94 (d, *J* = 7.9 Hz, 2H, H<sup>6</sup>), 7.84 (dd, *J* = 8.3, 1.6 Hz, 1H, H<sup>2</sup>), 7.64 (d, *J* = 7.9 Hz, 2H, H<sup>5</sup>), 7.22 (d, *J* = 8.2 Hz, 1H, H<sup>3</sup>), 6.63 (s, 2H, H<sup>4</sup>), 1.31 (s, 12H, H<sup>7</sup>); <sup>13</sup>C NMR (101 MHz, DMSO-*d*<sub>6</sub>) δ 162.23, 153.20, 152.62,

140.03, 139.64, 134.59, 130.65 (2C), 127.58 (2C), 123.82, 116.56, 84.12 (2C), 60.21, 25.15 (4C), 21.22, 14.55; HPLC-MS (APCI/ESI): Purity = 79%, t<sub>R</sub> = 4.417 min, m/z [M+H]<sup>+</sup> = 432.1.

**2-Amino-6-(2-methyl-5-(methylsulfonyl)phenyl)-3-(4-(trifluoromethyl)phenyl)quinazolin-4(3H)-one (11)**

Compound **10** (250.9 mg, 0.58 mol, 1.3 Eq) and 2-bromo-4-(methylsulfinyl) toluene (111.5 mg, 0.45 mmol, 1.0 Eq) were dissolved in anhydrous 1,4-dioxane (2.7mL) and the solution was purged with nitrogen. PdCl<sub>2</sub>(PPh<sub>3</sub>)<sub>2</sub> (31.4mg, 0.045 mmol, 0.1 Eq) was added to the solution followed by the addition of potassium carbonate (185.6 mg, 1.34 mmol, 3.0 Eq) dissolved in water (0.58 mL). The reaction was heated at 80°C for 3 hours, allowed to cool to room temperature and diluted with EtOAc to be filtered through Celite. The organic phase was washed with water and brine, dried over magnesium sulphate and concentrated under reduced pressure. The resulting crude residue was purified by silica gel chromatography (30 – 55% EtOAc/hexane), combined pure

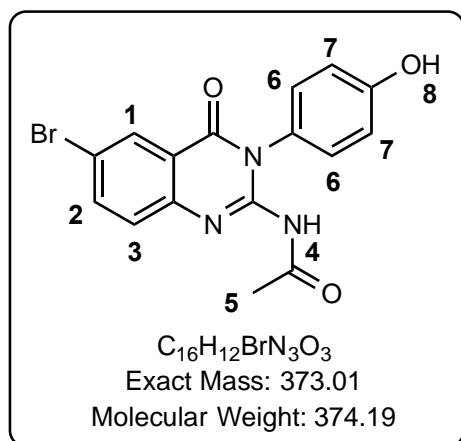
fractions were concentrated *in vacuo*, triturated with Et<sub>2</sub>O, filtered and dried under vacuum to give **11**.



Light brown solid (164.6 mg, 60%); m.p. 278.0 – 282.2°C; R<sub>f</sub> (7:3 EtOAc:Hexane) 0.22; <sup>1</sup>H NMR (400 MHz, DMSO-*d*<sub>6</sub>) δ 7.95 (d, *J* = 8.2 Hz, 2H, H<sup>5</sup>), 7.88 (d, *J* = 2.3 Hz, 1H, H<sup>1</sup>), 7.83 (dd, *J* = 8.0, 2.1 Hz, 1H, H<sup>10</sup>), 7.75 (d, *J* = 2.1 Hz, 1H, H<sup>7</sup>), 7.70 (dd, *J* = 8.5, 2.3 Hz, 1H, H<sup>2</sup>), 7.67 (d, *J* =

8.2 Hz, 2H, H<sup>4</sup>), 7.61 (d, *J* = 8.0 Hz, 1H, H<sup>9</sup>), 7.36 (d, *J* = 8.4 Hz, 1H, H<sup>3</sup>), 6.56 (s, 2H, H<sup>6</sup>), 3.25 (s, 3H, H<sup>11</sup>), 2.37 (s, 3H, H<sup>8</sup>); <sup>13</sup>C NMR (151 MHz, DMSO-*d*<sub>6</sub>) δ 162.23, 160.05, 152.14, 150.28, 141.96, 141.91, 139.74, 139.17, 135.96, 133.09, 132.06, 130.76 (2C), 130.16 (q, *J* = 29.1 Hz, 1C, C-CF<sub>3</sub>) 128.25, 127.69, 127.08, 126.21, 124.67, 124.58 (q, *J* = 272.2 Hz, 1C, CF<sub>3</sub>), 116.96, 44.27, 20.98; HPLC-MS (APCI/ESI): Purity = 97%, t<sub>R</sub> = 3.840 min, m/z [M+H]<sup>+</sup> = 474.0.

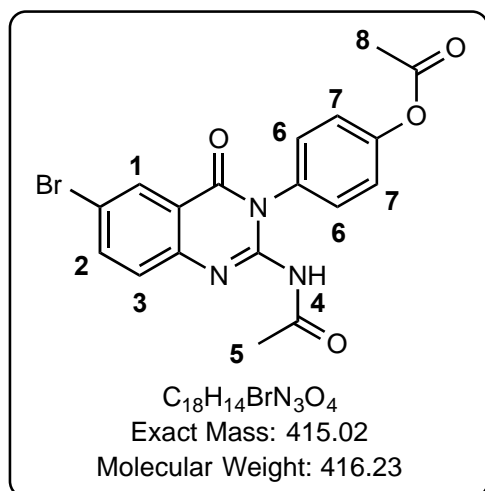
**JA066: N-(6-bromo-3-(4-hydroxyphenyl)-4-oxo-3,4-dihydroquinazolin-2-yl)acetamide (12.1)**



Compound **8.3** (114.5 mg, 0.34 mmol, 1.0 Eq) was heated in acetic anhydride (0.4 mL) at 100°C for 2 hours, diluted with Et<sub>2</sub>O and filtered to afford a white solid (30 mg, 23%); m.p. 231.4 – 234.6°C; R<sub>f</sub> (4% MeOH in DCM) 0.5; <sup>1</sup>H NMR (400 MHz, DMSO-*d*<sub>6</sub>) δ 9.86 (s, 1H, H<sup>4</sup>), 9.76 (s, 1H, H<sup>8</sup>), 8.18 (d, *J* = 2.4 Hz, 1H, H<sup>1</sup>), 8.00 (dd, *J* = 8.7, 2.4 Hz, 1H, H<sup>2</sup>), 7.61 (d, *J* = 8.7 Hz, 1H, H<sup>3</sup>), 7.10 (d, *J* = 8.8 Hz, 2H, H<sup>6</sup>), 6.85 (d,

*J* = 8.7 Hz, 2H, H<sup>7</sup>), 1.87 (s, 3H, H<sup>5</sup>); <sup>13</sup>C NMR (101 MHz, DMSO-*d*<sub>6</sub>) δ 161.41, 158.06, 146.60, 138.10, 130.11, 129.99 (2C), 129.14 (2C), 127.02, 122.18, 119.17, 117.00, 115.77 (2C), 23.36; HPLC-MS (APCI/ESI): Purity 95%, t<sub>R</sub> = 3.669 min, m/z [M+H]<sup>+</sup> = 374.0, 376.0.

#### 4-(2Acetamido-6-bromo-4-oxoquinazolin-3(4H)-yl)phenyl acetate (12.2)



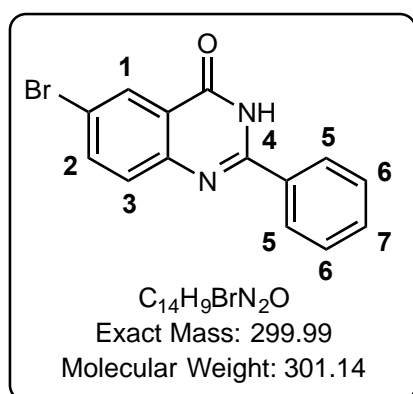
Off-white solid (97.8 mg, 93%); m.p. 228.0 – 234.6°C;  $R_f$  (5:5 EtOAc:Hexane) 0.47;  $^1H$  NMR (400 MHz, DMSO- $d_6$ )  $\delta$  8.31 (d,  $J$  = 2.3 Hz, 1H, H<sup>1</sup>), 8.13 (dd,  $J$  = 8.7, 2.3 Hz, 1H, H<sup>2</sup>), 7.77 (d,  $J$  = 8.7 Hz, 1H, H<sup>3</sup>), 7.34 (d,  $J$  = 2.7 Hz, 4H, H<sup>6</sup>, H<sup>7</sup>), 2.31 (s, 3H, H<sup>8</sup>), 2.20 (s, 3H, H<sup>5</sup>);  $^{13}C$  NMR (101 MHz, DMSO- $d_6$ )  $\delta$  171.63, 169.40, 161.21, 151.56, 145.87, 145.21, 138.62, 132.87, 130.35, 129.56 (2C), 129.40, 123.44 (2C), 123.35, 121.56, 25.72, 21.32; HPLC-

MS (APCI/ESI): Purity 99%,  $t_R$  = 4.000 min,  $m/z$   $[M+H]^+$  = 415.9, 417.9.

#### 6.2.8. GENERAL PROCEDURE FOR THE SYNTHESIS OF COMPOUNDS 12.3 – 12.4

Sodium bisulfate (NaHSO<sub>4</sub>) (2.0 Eq) was added to a solution of 2-amino-5-bromobenzamide (1.0 Eq) and the relevant benzaldehyde (1.0 Eq) in DMF (25 Eq). The mixture was refluxed at 150 °C for 3 hours and poured into ice-water. The precipitate was filtered, washed with water followed by ethanol and dried to form 2-arylquinazolinones 12.3 – 12.4.

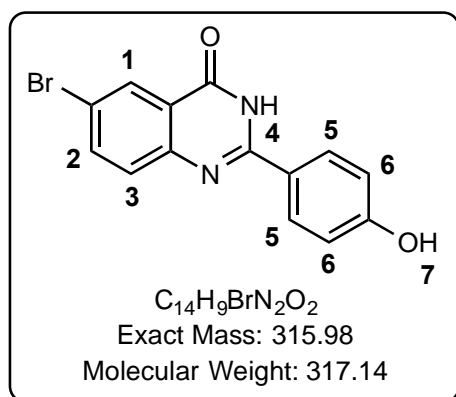
#### JA072: 6-bromo-2-phenylquinazolin-4(3H)-one (12.3)



White crystalline solid (137.9 mg, 69%); m.p. 306.2 – 310.4°C;  $R_f$  (6:4 EtOAc: Hexane) 0.41;  $^1H$  NMR (300 MHz, DMSO- $d_6$ )  $\delta$  12.68 (s, 1H, H<sup>4</sup>), 8.23 (d,  $J$  = 2.3 Hz, 1H, H<sup>1</sup>), 8.18 (dd,  $J$  = 8.1, 1.6 Hz, 2H, H<sup>5</sup>), 7.98 (dd,  $J$  = 8.7, 2.4 Hz, 1H, H<sup>2</sup>), 7.70 (d,  $J$  = 8.7 Hz, 1H, H<sup>3</sup>), 7.64 – 7.53 (m, 3H, H<sup>6</sup>, H<sup>7</sup>);  $^{13}C$  NMR (101 MHz, DMSO- $d_6$ )  $\delta$  161.73, 153.51, 148.18, 137.88, 132.99, 132.08, 130.29, 129.11

(2C), 128.48, 128.33 (2C), 123.08, 119.38; HPLC-MS (APCI/ESI): Purity >99%,  $t_R$  = 4.787 min,  $m/z$   $[M+H]^+$  = 301.0, 303.0 (1:1).

**JA073: 6-bromo-2-(4-hydroxyphenyl)quinazolin-4(3H)-one (12.4)**



Yellow solid (51.3 mg, 17%); m.p. 314.6 – 318.1°C; R<sub>f</sub> (6:4 EtOAc:Hexane) 0.28; <sup>1</sup>H NMR (400 MHz, DMSO-*d*<sub>6</sub>) δ 12.44 (s, 1H, H<sup>4</sup>), 10.17 (s, 1H, H<sup>7</sup>), 8.20 (d, *J* = 2.4 Hz, 1H, H<sup>1</sup>), 8.09 (d, *J* = 8.8 Hz, 2H, H<sup>5</sup>), 7.93 (dd, *J* = 8.7, 2.4 Hz, 1H, H<sup>2</sup>), 7.63 (d, *J* = 8.7 Hz, 1H, H<sup>3</sup>), 6.90 (d, *J* = 8.8 Hz, 2H, H<sup>6</sup>); <sup>13</sup>C NMR (101 MHz, DMSO-*d*<sub>6</sub>) δ 161.68, 161.24, 153.21, 148.55, 137.74, 130.19 (2C), 130.05, 128.41, 123.40, 122.66, 118.58, 115.88

(2C); HPLC-MS (APCI/ESI): Purity >99%, t<sub>R</sub> = 4.448 min, m/z [M+H]<sup>+</sup> = 317.0, 319.0 (1:1).

### 6.3. BIOLOGICAL STUDIES

#### 6.3.1. IN VITRO ANTIMYCOBACTERIAL ASSAY

Antimycobacterial studies were performed by Ronnett Seldon at UCT's Drug Discovery and Development Centre, H3D. The broth microdilution method allows a range of antibiotic concentrations to be tested on a single 96-well microtitre plate in order to determine the minimum inhibitory concentration (MIC).<sup>81,82</sup> Briefly, a 10 ml culture of *Mycobacterium tuberculosis* pMSp12 green fluorescent protein (GFP) strain was grown to an optical density (OD<sub>600</sub>) of 0.6 - 0.7. The culture was then diluted 1:500 in the appropriate medium.<sup>83</sup> In a 96-well microtitre plate, 50 µl of medium was added to all wells from Rows 2-12. The compounds to be tested are added to Row 1 in duplicate, at a final concentration of 640 µM. A two-fold serial dilution was prepared, using a multichannel pipette, by transferring 50 µl of the liquid in Row 1 to Row 2 and aspirating to mix. 50 µl of the liquid in Row 2 was then transferred to Row 3 and aspirated, and so on. This procedure is repeated until Row 12 is reached, from which 50 µl of the liquid was discarded so as to bring the final volume in all wells to 50 µl. Controls included media only, 5% DMSO, Rifampicin and Kanamycin. Finally, 50 µl of the 1:500 diluted *M. tuberculosis* culture was added to all wells in Rows 2-12. Cells were not added to Row 1, as this serves as a contamination control. The microtitre plate was sealed in a secondary container and incubated at 37°C with humidifier to prevent evaporation of liquid. The lowest concentration of drug that inhibits growth of more than 99% of the bacterial population was considered to be the MIC<sub>99</sub>. MIC<sub>99</sub> values were

scored visually at 7-days and 14-days post inoculation, and digital images captured and stored.

#### **6.3.1.1. 7H9 Media Preparation**

Bacto Middlebrook 7H9 (Difco), glycerol and water were combined and autoclaved for 15 mins. The solution was cooled to 55 - 60°C and 100ml ADC Enrichment Media and 0.05% Tween 80 were added. Filter sterilize (0.2µM filter) and store at 37°C.

#### **6.3.1.2. ADC Enrichment Media Preparation**

Sodium chloride, bovine albumin fraction V and D-glucose were dissolved into 1L distilled water. Filter sterilize (0.2µM filter) and store at 4°C.

#### **6.3.1.3. Casitone 7H9-Based Medium (BSA-Free) Preparation**

4.7g Middlebrook 7H9 broth + 900 mL water (double distilled) + 2mL glycerol (add with sterile syringe) + 0.5mL Tween 80 (add with 1mL sterile syringe). Stir until dissolved and filter sterilize (0.2µm filter). Aseptically add 100mL ADC.

### **6.3.2. IN VITRO CYTOTOXICITY ASSAY**

Test samples were screened for in vitro cytotoxicity against a mammalian cell-line, Chinese Hamster ovarian (CHO) using the 3-(4,5-dimethylthiazol-2-yl)-2,5-diphenyltetrazoliumbromide (MTT) assay at the Division of Clinical Pharmacology, University of Cape Town. The MTT-assay is used as a colorimetric assay for cellular growth and survival, and compares well with other available assays.<sup>84,85</sup> The reduction of tetrazolium salt MTT to a formazan salt was used to measure all growth and chemosensitivity. The test samples were tested in triplicate on one occasion.

The test samples were prepared to a 20 mg/ml stock solution in 10% methanol or 10% DMSO and were tested as a suspension if not properly dissolved. Test compounds were stored at -20°C until use. Emetine was used as the reference drug in all experiments. The initial concentration of each compound was 100 µg/ml, which was serially diluted in complete medium with 10-fold dilutions to give 6 concentrations, the lowest being 0.001 µg/ml. The same dilution technique was applied to the all test samples. The highest concentration of solvent to which the cells were exposed to had no measurable effect on the cell viability (data not shown). Plates were developed after 44 hours of exposure to

the drug by the addition of a solution of MTT. After four hours further incubation at 37°, the supernatant was removed from the cells via suction and DMSO was added to each well to dissolve the reduced dye crystals. Plates were analysed at 540nm wavelength using a spectrophotometer to determine the relative amount of formazan in each well.

The 50% inhibitory concentration (IC<sub>50</sub>) values were obtained from full dose-response curves, using a non-linear dose-response curve fitting analysis via GraphPad Prism v.4 software.

### **6.3.3. IN VITRO ANTIPLASMODIAL ASSAY**

*In vitro* activity against the erythrocytic stages NF54 *P. falciparum* strains was determined using a [3H]-hypoxanthine incorporation assay by Sergio Wittlin at the Swiss Tropical and Public Health Institute. Compounds were dissolved in DMSO at 10 mg/mL and added to parasite cultures incubated in RPMI 1640 medium without hypoxanthine, supplemented with HEPES (5.94 g/l), NaHCO<sub>3</sub> (2.1 g/l), neomycin (100 U/mL), AlbumaxR (5 g/l) and washed A+ human red cells at 2.5 % hematocrit (0.3% parasitemia). Serial drug dilutions of eleven three-fold dilution steps covering a range from 100 to 0.002 µg/mL were prepared. The 96-well plates were incubated in a humidified atmosphere at 37 °C; 4 % CO<sub>2</sub>, 3 % O<sub>2</sub> and 93 % N<sub>2</sub>. After 48 h, 50 µL of 3H-hypoxanthine (= 0.5 µCi) was added to each well of the plate. The plates were incubated for a further 24 h under the same conditions. The plates were then harvested with a Betaplate™ cell harvester (Wallac, Zurich, Switzerland), and the red blood cells transferred onto a glass fiber filter then washed with distilled water. The dried filters were inserted into a plastic foil with 10 ml of scintillation fluid, and counted in a Betaplate™ liquid scintillation counter (Wallac, Zurich, Switzerland). IC<sub>50</sub> values were calculated from sigmoidal inhibition curves by linear regression using Microsoft Excel.

### **6.3.4. IN VITRO METABOLIC STABILITY STUDIES**

The metabolic stability of compounds was assessed in mouse, rat and human liver microsomes at the pre-clinical pharmacology laboratory at Groote Schuur Hospital. All compounds were prepared to a 10 mM stock solution in DMSO. The test compound (1 µM) was incubated at 37 °C in a solution containing 0.35 mg/ml microsomes (MLM – male mouse BALB/c, Xenotech; RLM – male rat IGS, Xenotech or HLM – mixed gender, Xenotech) and NADPH (1 mM) in phosphate buffer (100 mM, pH 7.4) for 30 min while

shaking. The samples were then prepared by cold-ice acetonitrile precipitation containing 0.1 $\mu$ M carbamazepine (internal standard), centrifuged and filtered for LC-MS analysis. The incubations were performed in triplicate and three controls (propranolol, midazolam and MMV390048) were also included. Results are reported as percentage remaining unchanged after 30 min incubation and as predicted half-life using Obach's formula.

LC-MS/MS analysis was performed on a 4000 Q-TRAP (AB SCIEX) equipment with a Turbo V<sup>®</sup> ion source coupled to an Agilent 1200 Rapid Resolution (600 bar) HPLC system. Electron spray ionization mode was used for all synthetic compounds. Analyst 1.5.1 software was used for instrument control and data acquisition. Metabolic stability analysis was performed using a Kinetex PFP column, 2.1 mm  $\times$  50 mm, 2.6  $\mu$ m particles (Phenomenex) or a Kinetex C18 column, 2.1 mm  $\times$  50 mm, 2.6  $\mu$ m particles (Phenomenex) with gradient of 0.4 ml/min of the mobile phase constituted of 0.1% formic acid (A) and 0.1% formic acid in acetonitrile (B) at 40  $^{\circ}$ C. Sample tray temperature was 8  $^{\circ}$ C and the injection volume used was 2  $\mu$ L. Multiple reaction monitoring (MRM) mode was used for quantification of parent compound before and after incubation in liver microsomes.

### **6.3.5. HPLC-BASED SOLUBILITY STUDIES**

Kinetic solubility of compounds was performed by Mathew Njoroge at the drug discovery and development centre, H3D. Aqueous solubility was measured using the DMSO-dry down method, adapted from Zhou et al.<sup>69</sup> Briefly, the high and medium calibration standards (220 $\mu$ M, 100 $\mu$ M) in duplicate as well as the samples (200 $\mu$ M) in triplicate were added to a 96-well plate, from a 10mM stock solution in DMSO. DMSO was then evaporated in a MiVac sample concentrator (SP Scientific, Cape Town, South Africa) operated at full vacuum, 37 $^{\circ}$ C, for 2 hours. DMSO was then added to the standards and after vortexing the plate, the high standard was used to prepare a low (11 $\mu$ M) calibration standard in DMSO. Phosphate buffered saline (pH 7.4) was added to the sample wells and the plate was incubated for 24hrs at 25 $^{\circ}$ C with shaking. The plate was then centrifuged at 2500g for 30min and the supernatants transferred to another plate for analysis. Aqueous solubility was determined from UV peak areas of the samples relative to the standards using best-fit calibration curves in Microsoft Excel 2013.

HPLC-DAD analysis was performed using an Agilent 1200 Rapid Resolution HPLC, coupled with an Agilent 1200 diode array detector (ABSciex, Johannesburg, South Africa). For elution, 0.1% formic acid in water and 0.1% formic acid acetonitrile were used as mobile phases A and B respectively. A Kinetex C18 (50mm x 2.1 mm), packed with 2.6  $\mu$ M fused-core particles (Separations, Johannesburg, South Africa) was used for the chromatography. Agilent Chemstation for used for instrument control and data processing.

## CHAPTER 7: REFERENCES

---

- (1) WHO; World Health Organization: Global Tuberculosis Report 2016; **2016**.
- (2) WHO; World Health Organization: Global Tuberculosis Report 2014; **2014**.
- (3) Shrivastava, A.; Shrivastava, A.; Ahirwar, S.; Agarwal, P. Research Article Selected Therapeutic Targets of Tuberculosis: An Overview. *J. Comb. Chem.* **2014**, *29* (49), 258–267.
- (4) Sakamoto, K. The Pathology of Mycobacterium Tuberculosis Infection. *Vet. Pathol.* **2012**, *49*, 423–439.
- (5) Zumla, A.; Nahid, P.; Cole, S. T. Advances in the Development of New Tuberculosis Drugs and Treatment Regimens. *Nat. Rev. Drug Discov.* **2013**, *12* (May), 388–404.
- (6) Diel, R.; Loddenkemper, R.; Zellweger, J. P.; Sotgiu, G.; D’Ambrosio, L.; Centis, R.; Van Der Werf, M. J.; Dara, M.; Detjen, A.; Gondrie, P.; Reichman, L.; Blasi, F.; Migliori, G. B. Old Ideas to Innovate Tuberculosis Control: Preventive Treatment to Achieve Elimination. *Eur. Respir. J.* **2013**, *42*, 785–801.
- (7) Mukadi, Y. D.; Maher, D.; Harries, A. Tuberculosis Case Fatality Rates in High HIV Prevalence Populations in Sub-Saharan Africa. *AIDS* **2001**, *15*, 143–152.
- (8) WHO; *Treatment of Tuberculosis: Guidelines*, 4th ed.; World Health Organization, **2010**.
- (9) Gong, Y.; Somersan Karakaya, S.; Guo, X.; Zheng, P.; Gold, B.; Ma, Y.; Little, D.; Roberts, J.; Warriar, T.; Jiang, X.; Pingle, M.; Nathan, C. F.; Liu, G. Benzimidazole-Based Compounds Kill Mycobacterium Tuberculosis. *Eur. J. Med. Chem.* **2014**, *75*, 336–353.
- (10) Simithy, J.; Reeve, N.; Hobrath, J. V.; Reynolds, R. C.; Calderón, A. I. Identification of Shikimate Kinase Inhibitors among Anti-Mycobacterium Tuberculosis Compounds by LC-MS. *Tuberculosis* **2014**, *94* (2), 152–158.
- (11) Falzon, D.; Jaramillo, E.; Schünemann, H. J.; Arentz, M.; Bauer, M.; Bayona, J.; Blanc, L.; Caminero, J. a.; Daley, C. L.; Duncombe, C.; Fitzpatrick, C.; Gebhard, a.; Getahun, H.; Henkens, M.; Holtz, T. H.; Keravec, J.; Keshavjee, S.; Khan, a. J.; Kulier, R.; Leimane, V.; Lienhardt, C.; Lu, C.; Mariandyshev, a.; Migliori, G. B.; Mirzayev, F.; Mitnick, C. D.; Nunn, P.; Nwagboniwe, G.; Oxlade, O.; Palmero, D.; Pavlinac, P.; Quelapio, M. I.; Raviglione, M. C.; Rich, M. L.; Royce, S.; Rüsç-Gerdes, S.; Salakaia, a.; Sarin, R.; Sculier, D.; Varaine, F.; Vitoria, M.; Walson, J. L.; Wares, F.; Weyer, K.; White, R. a.; Zignol, M. WHO Guidelines for the Programmatic Management of Drug-Resistant Tuberculosis: 2011 Update. *Eur. Respir. J.* **2011**, *38* (3), 516–528.
- (12) Barry, C. E.; Boshoff, H. I.; Dartois, V.; Dick, T.; Ehrt, S.; Flynn, J.; Schnappinger, D.; Wilkinson, R. J.; Young, D. The Spectrum of Latent Tuberculosis: Rethinking the Biology and Intervention Strategies. *Nat. Rev. Microbiol.* **2009**, *7*, 845–855.
- (13) Koul, A.; Arnoult, E.; Lounis, N.; Guillemont, J.; Andries, K. The Challenge of New Drug Discovery for Tuberculosis. *Nature* **2011**, *469*, 483–490.

- (14) Villemagne, B.; Crauste, C.; Flipo, M. European Journal of Medicinal Chemistry Tuberculosis : The Drug Development Pipeline at a Glance. *Eur. J. Med. Chem.* **2012**, *51*, 1–16.
- (15) D’Ambrosio, L.; Centis, R.; Sotgiu, G.; Pontali, E.; Spanevello, A.; Migliori, G. B. New Anti-Tuberculosis Drugs and Regimens: 2015 Update. *ERJ Open Res.* **2015**, *1*, 00010–02015.
- (16) Gualano, G.; Capone, S.; Matteelli, A.; Palmieri, F. New Antituberculosis Drugs: From Clinical Trial to Programmatic Use. *Infect. Dis. Rep.* **2016**, *8*, 6569.
- (17) Diacon, A.; Pym, A.; Grobusch, M.; Patientia, R.; Rustomjee, R.; Page-Shipp, L. The Diarylquinoline TMC207 for Multidrug-Resistant Tuberculosis. *N. Engl. J. Med.* **2009**, *360* (23), 2397–2405.
- (18) TB Alliance, Nix-TB: Testing a New Potential Treatment for XDR-TB. [http://www.tballiance.org/downloads/NixTB/NixTB\\_factsheet.pdf](http://www.tballiance.org/downloads/NixTB/NixTB_factsheet.pdf) (Accessed Oct 27, 2016)
- (19) Saha, K. New Drugs for Treating Tuberculosis. *J. Assoc. Chest Physicians* **2015**, *3*, 1.
- (20) Kerns, E. H.; Di, L. *Drug-like Properties: Concepts, Structure, Design and Methods*, 1st ed.; Elsevier, 2008.
- (21) Lipinski, C. A. Drug-like Properties and the Causes of Poor Solubility and Poor Permeability. *J. Pharmacol. Toxicol. Methods* **2000**, *44*, 235–249.
- (22) Hansch, C.; Leo, A.; Mekapati, S. B.; Kurup, A. QSAR and ADME. *Bioorganic Med. Chem.* **2004**, *12*, 3391–3400.
- (23) Di, L.; Kerns, E. H. Profiling Drug-like Properties in Discovery Research. *Current Opinion in Chemical Biology.* 2003, pp 402–408.
- (24) Lipinski, C. A.; Lombardo, F.; Dominy, B. W.; Feeney, P. J. Experimental and Computational Approaches to Estimate Solubility and Permeability in Drug Discovery and Development Settings I. *Adv. Drug Deliv. Rev.* **2012**, *64*, 4–17.
- (25) Ishikawa, M.; Hashimoto, Y. Improvement in Aqueous Solubility in Small Molecule Drug Discovery Programs by Disruption of Molecular Planarity and Symmetry. *J. Med. Chem.* **2011**, *54*, 1539–1554.
- (26) Savjani, K. T.; Gajjar, A. K.; Savjani, J. K. Drug Solubility: Importance and Enhancement Techniques. *ISRN Pharm.* **2012**, *2012*, 1–10.
- (27) Williams, H. D.; Trevaskis, N. L.; Charman, S. A.; Shanker, R. M.; Charman, W. N.; Pouton, C. W.; Porter, C. J. H. Strategies to Address Low Drug Solubility in Discovery and Development. *Pharmacol. Rev.* **2013**, *65* (1), 315–499.
- (28) Li, Y.; Zhu, Y. M.; Jiang, H. J.; Pan, J. P.; Wu, G. S.; Wu, J. M.; Shi, Y. L.; Yang, J. D.; Wu, B. A. Synthesis and Antimalarial Activity of Artemisinin Derivatives Containing an Amino Group. *J. Med. Chem.* **2000**, *43*, 1635–1640.
- (29) Di, L.; Kerns, E. Application of Physicochemical Data to Support Lead Optimization

- by Discovery Teams. In *Optimizing the "Drug-Like" Properties of Leads in Drug Discovery*; Borchartd, R., Kerns, E., Hageman, M., Thakker, D., Stevens, J., Eds.; 2006; Vol. IV, pp 167–193.
- (30) Le Manach, C.; González Cabrera, D.; Douelle, F.; Nchinda, A. T.; Younis, Y.; Taylor, D.; Wiesner, L.; White, K. L.; Ryan, E.; March, C.; Duffy, S.; Avery, V. M.; Waterson, D.; Witty, M. J.; Wittlin, S.; Charman, S. a.; Street, L. J.; Chibale, K. Medicinal Chemistry Optimization of Antiplasmodial Imidazopyridazine Hits from High Throughput Screening of a SoftFocus Kinase Library: Part 1. *J. Med. Chem.* **2014**, *57*, 2789–2798.
- (31) Wang, H.-L.; Katon, J.; Balan, C.; Bannon, A. W.; Bernard, C.; Doherty, E. M.; Dominguez, C.; Gavva, N. R.; Gore, V.; Ma, V.; Nishimura, N.; Surapaneni, S.; Tang, P.; Tamir, R.; Thiel, O.; Treanor, J. J. S.; Norman, M. H. Novel Vanilloid Receptor-1 Antagonists: 3. The Identification of a Second-Generation Clinical Candidate with Improved Physicochemical and Pharmacokinetic Properties. *J. Med. Chem.* **2007**, *50* (15), 3528–3539.
- (32) Lee, M. C.; Chian, E. S. K.; Griffin, R. A. Solubility of Polychlorinated Biphenyls and Capacitor Fluid in Water. *Water Res.* **1979**, *13* (12), 1249–1258.
- (33) Abdel Gawad, N. M.; Georgey, H. H.; Youssef, R. M.; El-Sayed, N. a. Synthesis and Antitumor Activity of Some 2, 3-Disubstituted Quinazolin-4(3H)-Ones and 4, 6-Disubstituted- 1, 2, 3, 4-Tetrahydroquinazolin-2H-Ones. *Eur. J. Med. Chem.* **2010**, *45* (12), 6058–6067.
- (34) Zhang, J.; Liu, J.; Ma, Y.; Ren, D.; Cheng, P.; Zhao, J.; Zhang, F.; Yao, Y. One-Pot Synthesis and Antifungal Activity against Plant Pathogens of Quinazolinone Derivatives Containing an Amide Moiety. *Bioorg. Med. Chem. Lett.* **2016**, *26* (9), 2273–2277.
- (35) Pandit, U.; Dodiya, A. Synthesis and Antitubercular Activity of Novel Pyrazole-Quinazolinone Hybrid Analogs. *Med. Chem. Res.* **2013**, *22*, 3364–3371.
- (36) Ahmed, M. F.; Youns, M. Synthesis and Biological Evaluation of a Novel Series of 6,8-Dibromo-4(3H)quinazolinone Derivatives as Anticancer Agents. *Arch. Pharm. (Weinheim)*. **2013**, *346*, 610–617.
- (37) Alafeefy, A. M.; Ashour, A. E.; Prasad, O.; Sinha, L.; Pathak, S.; Alasmari, F. a.; Rishi, A. K.; Abdel-Aziz, H. a. Development of Certain Novel N-(2-(2-(2-Oxindolin-3-Ylidene)hydrazinecarbonyl)phenyl)-Benzamides and 3-(2-Oxindolin-3-Ylideneamino)-2-Substituted Quinazolin-4(3H)-Ones as CFM-1 Analogs: Design, Synthesis, QSAR Analysis and Anticancer Activity. *Eur. J. Med. Chem.* **2015**, *92*, 191–201.
- (38) Birhan, Y. S.; Bekhit, A. A.; Hymete, A. In Vivo Antimalarial Evaluation of Some 2,3-Disubstituted-4(3H)-Quinazolinone Derivatives. *BMC Res. Notes* **2015**, *8* (1), 589.
- (39) Zuo, S. J.; Li, S.; Yu, R. H.; Zheng, G. X.; Cao, Y. X.; Zhang, S. Q. Discovery of Novel 3-Benzylquinazolin-4(3H)-Ones as Potent Vasodilative Agents. *Bioorganic Med.*

- Chem. Lett.* **2014**, 24 (24), 5597–5601.
- (40) Rosse, G. Quinalozinones as Inhibitors of Class I PI3K Kinases. **2014**, 15–16.
- (41) Patel, M. B.; Harikrishnan, U.; Valand, N. N.; Modi, N. R.; Menon, S. K. Novel Cationic Quinazolin-4(3H)-One Conjugated Fullerene Nanoparticles as Antimycobacterial and Antimicrobial Agents. *Arch. der Pharm. (Weinheim, Ger.* **2013**, 346 (3), 210–220.
- (42) Khodarahmi, G.; Jafari, E.; Hakimelahi, G.; Abedi, D.; Rahmani Khajouei, M.; Hassanzadeh, F. Synthesis of Some New Quinazolinone Derivatives and Evaluation of Their Antimicrobial Activities. *Iran. J. Pharm. Res. IJPR* **2012**, 11, 789–797.
- (43) Peng, L.-P.; Nagarajan, S.; Rasheed, S.; Zhou, C.-H. Synthesis and Biological Evaluation of a New Class of Quinazolinone Azoles as Potential Antimicrobial Agents and Their Interactions with Calf Thymus DNA and Human Serum Albumin. *Medchemcomm* **2015**, 6 (1), 222–229.
- (44) Wallace & Tiernan Inc. Hydroxy and Alkoxy Aryl Quinazolinones, US3135659A **1964**.
- (45) Leivers, A. L.; Tallant, M.; Shotwell, J. B.; Dickerson, S.; Leivers, M. R.; McDonald, O. B.; Gobel, J.; Creech, K. L.; Strum, S. L.; Mathis, A.; Rogers, S.; Moore, C. B.; Botyanszki, J. Discovery of Selective Small Molecule Type III Phosphatidylinositol 4-Kinase Alpha (PI4KIII $\alpha$ ) Inhibitors as Anti Hepatitis C (HCV) Agents. *J. Med. Chem.* **2014**, 57, 2091–2106.
- (46) Deuschle, U.; Loebbert, R.; Blume, B.; Koegl, M.; Kremoser, C.; Kober, I.; Bauer, U.; Hermann, K.; Albers, M. Novel 2-Amino-4-Quinazolinones and 2-Amino-4-Oxoquinazolones as LXR (Liver X Receptor) Nuclear Receptor Binding Compounds with Partial Agonistic Properties., US20050261319A1, **2005**.
- (47) Latvian Institute Of Organic Synthesis. Preparation of Substituted 2-Aminoquinazolin-4(3H)-One Derivatives as Malarial Aspartic Protease Inhibitors., WO2015063544 A1, **2015**.
- (48) Pattan, S. R.; Reddy, V. V. K.; Manvi, F. V.; Desai, B. G.; Bhat, A. R. Synthesis of N-3(4-(4-Chlorophenyl Thiazole-2-Yl)-(2-(Amino)methyl)-Quinazoline-4(3H)-One and Their Derivatives for Antitubercular Activity. *Indian J. Chem. Sect. B Org. Chem. Incl. Med. Chem.* **2006**, 45B (7), 1778–1781.
- (49) Al-deeb, O. A.; Alafeefy, A. M. Synthesis of Some New 3H-Quinazolin-4-One Derivatives as Potential Antitubercular Agents. *World Appl. Sci. J.* **2008**, 5 (1), 94–99.
- (50) Patel, M. B.; Harikrishnan, U.; Valand, N. N.; Modi, N. R.; Menon, S. K. Novel Cationic Quinazolin-4(3 H)-One Conjugated Fullerene Nanoparticles as Antimycobacterial and Antimicrobial Agents. *Arch. Pharm. (Weinheim).* **2013**, 346, 210–220.
- (51) Reddy, H.; Himabindu, V.; Chakravarthy, K.; Shiradkar, M. Development of New Molecular Entities as Potent Antimycobacterial Agents : Synthesis of Substituted

- Quinazolines. **2012**, 5 (5), 2538–2542.
- (52) Couturier, C.; Lair, C.; Pellet, A.; Upton, A.; Kaneko, T.; Perron, C.; Cogo, E.; Menegotto, J.; Bauer, A.; Scheiper, B.; Lagrange, S.; Bacqué, E. Identification and Optimization of a New Series of Anti-Tubercular Quinazolinones. *Bioorg. Med. Chem. Lett.* **2016**, 26 (21), 5290–5299.
- (53) Chen, J. M.; Alexander, D. C.; Behr, M. A.; Liu, J. Mycobacterium Bovis BCG Vaccines Exhibit Defects in Alanine and Serine Catabolism. *Infect. Immun.* **2003**, 71 (2), 708–716.
- (54) Steenken, W.; Gardner, L. U. History of H37 Strain of Tubercle Bacillus. *Am. Rev. Tuberc.* **1946**, 54, 62–66.
- (55) Younis, Y.; Douelle, F.; Feng, T.-S.; Cabrera, D. G.; Manach, C. Le; Nchinda, A. T.; Duffy, S.; White, K. L.; Shackleford, D. M.; Morizzi, J.; Mannila, J.; Katneni, K.; Bhamidipati, R.; Zabiulla, K. M.; Joseph, J. T.; Bashyam, S.; Waterson, D.; Witty, M. J.; Hardick, D.; Wittlin, S.; Avery, V.; Charman, S. A.; Chibale, K. 3,5-Diaryl-2-Aminopyridines as a Novel Class of Orally Active Antimalarials Demonstrating Single Dose Cure in Mice and Clinical Candidate Potential. *J. Med. Chem.* **2012**, 55 (7), 3479–3487.
- (56) Connolly, D. J.; Cusack, D.; O'Sullivan, T. P.; Guiry, P. J. Synthesis of Quinazolinones and Quinazolines. *Tetrahedron* **2005**, 61 (43), 10153–10202.
- (57) Asif, M. Chemical Characteristics , Synthetic Methods , and Biological Potential of Quinazoline and Quinazolinone Derivatives. *Int. J. Med. Chem.* **2014**, 2014, 1–27.
- (58) Suzuki, A. Organoboron Compounds in New Synthetic Reactions. *Pure Appl. Chem.* **1985**, 57 (12), 1749–1758.
- (59) Lecoutey, C.; Fossey, C.; Rault, S.; Fabis, F. Efficient Room-Temperature One-Pot Synthesis of 2-Amino-3-alkyl(3-Aryl)quinazolin-4(3H)-Ones. *European J. Org. Chem.* **2011**, 2011, 2785–2788.
- (60) Marrero, J.; Rhee, K. Y.; Schnappinger, D.; Pethe, K.; Ehrt, S. Gluconeogenic Carbon Flow of Tricarboxylic Acid Cycle Intermediates Is Critical for Mycobacterium Tuberculosis to Establish and Maintain Infection. *Proc. Natl. Acad. Sci.* **2010**, 107 (21), 9819–9824.
- (61) Pethe, K.; Sequeira, P. C.; Agarwalla, S.; Rhee, K.; Kuhen, K.; Phong, W. Y.; Patel, V.; Beer, D.; Walker, J. R.; Duraiswamy, J.; Jiricek, J.; Keller, T. H.; Chatterjee, A.; Tan, M. P.; Ujjini, M.; Rao, S. P. S.; Camacho, L.; Bifani, P.; Mak, P. A.; Ma, I.; Barnes, S. W.; Chen, Z.; Plouffe, D.; Thayalan, P.; Ng, S. H.; Au, M.; Lee, B. H.; Tan, B. H.; Ravindran, S.; Nanjundappa, M.; Lin, X.; Goh, A.; Lakshminarayana, S. B.; Shoen, C.; Cynamon, M.; Kreiswirth, B.; Dartois, V.; Peters, E. C.; Glynne, R.; Brenner, S.; Dick, T. A Chemical Genetic Screen in Mycobacterium Tuberculosis Identifies Carbon-Source-Dependent Growth Inhibitors Devoid of in Vivo Efficacy. *Nat. Commun.* **2010**, 1, 57.
- (62) Ujjini, M. H.; Paul W, S. Perspective: Challenges and Opportunities in TB Drug

- Discovery from Phenotypic Screening. *Bioorg. Med. Chem.* **2015**, *23* (16), 5087–5097.
- (63) Stanley, S. A.; Grant, S. S.; Kawate, T.; Iwase, N.; Shimizu, M.; Wivagg, C.; Silvis, M.; Kazyanskaya, E.; Aquadro, J.; Golas, A.; Fitzgerald, M.; Dai, H.; Zhang, L.; Hung, D. T. Identification of Novel Inhibitors of M. Tuberculosis Growth Using Whole Cell Based High-Throughput Screening. *ACS Chem. Biol.* **2012**, *7* (8), 1377–1384.
- (64) Khadka, D. B.; Tran, G. H.; Shin, S.; Nguyen, H. T. M.; Cao, H. T.; Zhao, C.; Jin, Y.; Van, H. T. M.; Chau, M. Van; Kwon, Y.; Le, T. N.; Cho, W.-J. Substituted 2-Arylquinazolinones: Design, Synthesis, and Evaluation of Cytotoxicity and Inhibition of Topoisomerases. *Eur. J. Med. Chem.* **2015**, *103*, 69–79.
- (65) O'Neill, P. M.; Mukhtar, A.; Stocks, P. A.; Randle, L. E.; Hindley, S.; Ward, S. A.; Storr, R. C.; Bickley, J. F.; O'Neil, I. A.; Maggs, J. L.; Hughes, R. H.; Winstanley, P. A.; Bray, P. G.; Park, B. K. Isoquine and Related Amodiaquine Analogues: A New Generation of Improved 4-Aminoquinoline Antimalarials. *J. Med. Chem.* **2003**, *46* (23), 4933–4945.
- (66) Fischer, V.; West, P. R.; Harman, L. S.; Mason, R. P. Free-Radical Metabolites of Acetaminophen and a Dimethylated Derivative. *Environ. Health Perspect.* **1985**, *64*, 127–137.
- (67) Harrison, A. C.; Kitteringham, N. R.; Clarke, J. B.; Park, B. K. The Mechanism of Bioactivation and Antigen Formation of Amodiaquine in the Rat. *Biochem. Pharmacol.* **1992**, *43* (7), 1421–1430.
- (68) Kerns, E.; Di, L.; Carter, G. In Vitro Solubility Assays in Drug Discovery. *Curr. Drug Metab.* **2008**, *9* (9), 879–885.
- (69) Zhou, L.; Yang, L.; Tilton, S.; Wang, J. Development of a High Throughput Equilibrium Solubility Assay Using Miniaturized Shake-flask Method in Early Drug Discovery. *J. Pharm. Sci.* **2007**, *96* (11), 3052–3071.
- (70) Alsenz, J.; Kansy, M. High Throughput Solubility Measurement in Drug Discovery and Development. *Adv. Drug Deliv. Rev.* **2007**, *59* (7), 546–567.
- (71) Avdeef, A. Solubility of Sparingly-Soluble Ionizable Drugs. *Adv. Drug Deliv. Rev.* **2007**, *59* (7), 568–590.
- (72) Saal, C.; Petereit, A. C. Optimizing Solubility: Kinetic versus Thermodynamic Solubility Temptations and Risks. *Eur. J. Pharm. Sci.* **2012**, *47* (3), 589–595.
- (73) Tan, H.; Semin, D.; Wacker, M.; Cheetham, J. An Automated Screening Assay for Determination of Aqueous Equilibrium Solubility Enabling SPR Study During Drug Lead Optimization. *J. Assoc. Lab. Autom.* **2005**, *10* (6), 364–373.
- (74) Lipinski, C. A.; Lombardo, F.; Dominy, B. W.; Feeney, P. J. Experimental and Computational Approaches to Estimate Solubility and Permeability in Drug Discovery and Development Settings. *Adv. Drug Deliv. Rev.* **2012**, *64*, 4–17.
- (75) Bevan, C. D.; Lloyd, R. S. A High-Throughput Screening Method for the

- Determination of Aqueous Drug Solubility Using Laser Nephelometry in Microtiter Plates. *Anal. Chem.* **2000**, *72* (8), 1781–1787.
- (76) Ertl, P.; Rohde, B.; Selzer, P. Fast Calculation of Molecular Polar Surface Area as a Sum of Fragment-Based Contributions and Its Application to the Prediction of Drug Transport Properties. *J. Med. Chem.* **2000**, *43* (20), 3714–3717.
- (77) Evans, J. D. *Straightforward Statistics for the Behavioral Sciences*; Brooks/Cole Pub Co., 1995.
- (78) Kasuga, J.; Ishikawa, M.; Yonehara, M.; Makishima, M.; Hashimoto, Y.; Miyachi, H. Improvement of Water-Solubility of Biarylcarboxylic Acid Peroxisome Proliferator-Activated Receptor (PPAR)  $\delta$ -Selective Partial Agonists by Disruption of Molecular Planarity/symmetry. *Bioorg. Med. Chem.* **2010**, *18* (20), 7164–7173.
- (79) Fujita, Y.; Yonehara, M.; Tetsuhashi, M.; Noguchi-Yachide, T.; Hashimoto, Y.; Ishikawa, M.  $\beta$ -Naphthoflavone Analogs as Potent and Soluble Aryl Hydrocarbon Receptor Agonists: Improvement of Solubility by Disruption of Molecular Planarity. *Bioorg. Med. Chem.* **2010**, *18* (3), 1194–1203.
- (80) Wenglowisky, S.; Moreno, D.; Rudolph, J.; Ran, Y.; Ahrendt, K. A.; Arrigo, A.; Colson, B.; Gloor, S. L.; Hastings, G. Pyrazolopyridine Inhibitors of B-RafV600E. Part 3: An Increase in Aqueous Solubility via the Disruption of Crystal Packing. *Bioorg. Med. Chem. Lett.* **2012**, *22* (2), 912–915.
- (81) Collins, L. A.; Torrero, M. N.; Franzblau, S. G. Green Fluorescent Protein Reporter Microplate Assay for High-Throughput Screening of Compounds against Mycobacterium Tuberculosis. *Antimicrob. Agents Chemother.* **1998**, *42*, 344–347.
- (82) Collins, L. A.; Franzblau, S. G. Microplate Alamar Blue Assay versus BACTEC 460 System for High- Throughput Screening of Compounds against Mycobacterium Tuberculosis and Mycobacterium Avium. *Antimicrob. Agents Chemother.* **1997**, *41*, 1004–1009.
- (83) Ioerger, T. R.; Feng, Y.; Ganesula, K.; Chen, X.; Dobos, K. M.; Fortune, S.; Jacobs, W. R.; Mizrahi, V.; Parish, T.; Rubin, E.; Sasseti, C.; Sacchetti, J. C. Variation among Genome Sequences of H37Rv Strains of Mycobacterium Tuberculosis from Multiple Laboratories. *J. Bacteriol.* **2010**, *192*, 3645–3653.
- (84) Mosmann, T. Rapid Colorimetric Assay for Cellular Growth and Survival: Application to Proliferation and Cytotoxicity Assays. *J. Immunol. Methods* **1983**, *65*, 55–63.
- (85) Rubinstein, L. V.; Shoemaker, R. H.; Paull, K. D.; Simon, R. M.; Tosini, S.; Skehan, P.; Scudiero, D. A.; Monks, A.; Boyd, M. R. Comparison of in Vitro Anticancer-Drug-Screening Data Generated with a Tetrazolium Assay versus a Protein Assay against a Diverse Panel of Human Tumor Cell Lines. *J. Natl. Cancer Inst.* **1990**, *82*, 1113–1117.